CONF-920905--

U.S. Department of Energy
Office of Environmental Restoration and Waste Management
Office of Special Programs
Transportation Management Division

Papers Presented by

Sandia National Laboratories

at

PATRAM '92

10th International Symposium on the Packaging and Transportation of Radioactive Materials

September 13-18, 1992
Yokohama City, Japan

Sandia National Laboratories

ttd
transportation technology development program

MASTER

DISCLAIMER

CONTENTS

CONTENTS (Continued)

CONTENTS (Concluded)

*Received PATRAM '92 Award of Excellence

Hazardous and Mixed Waste Transportation Program*

G. F. Hohnstreiter, R. E. Glass, M. E. McAllaster, P. J. Nigrey, A. J. Trennel, and H. R. Yoshimura

Transportation Systems Technology Division, Sandia National Laboratories**
Albuquerque, New Mexico, United States of America

INTRODUCTION

Sandia National Laboratories (SNL) has developed a program to address the packaging needs associated with the transport of hazardous and mixed waste during the United States' Department of Energy (DOE) remediation efforts. The program addresses the technology needs associated with the transport of materials which have components that are radioactive and chemically hazardous.

The mixed waste transportation activities focus on on-site specific applications of technology to the transport of hazardous and mixed wastes. These activities were identified at a series of DOE-sponsored workshops. These activities will be composed of the following: (1) packaging concepts, (2) chemical compatibility studies, and (3) systems studies. This paper will address activities in each of these areas.

BACKGROUND

The basic motivation for hazardous and mixed waste transportation derives from the DOE-sponsored Transportation Assessment and Integration (TRAIN) final report. This document outlines the approach to the DOE transportation needs for the 1990s. In this document, it is clear that transportation will play an integrating role in the environmental restoration activities being undertaken by the DOE. Further, as is shown in Figure 1, the research and development activities for transportation play an integrating role for transportation. This figure shows the interface between the research and development function and seven major elements of transportation. These elements are: (1) institutional and outreach programs, (2) regulatory development and impacts, (3) emergency preparedness, (4) training, (5) operations, (6) the definition of transportation and packaging needs, and (7) the role of the DOE's Transportation Management Program.

---

*This work was performed at Sandia National Laboratories, Albuquerque, New Mexico, supported by the United States Department of Energy under Contract DE-AC04-76DP00789.

**A United States Department of Energy Facility.

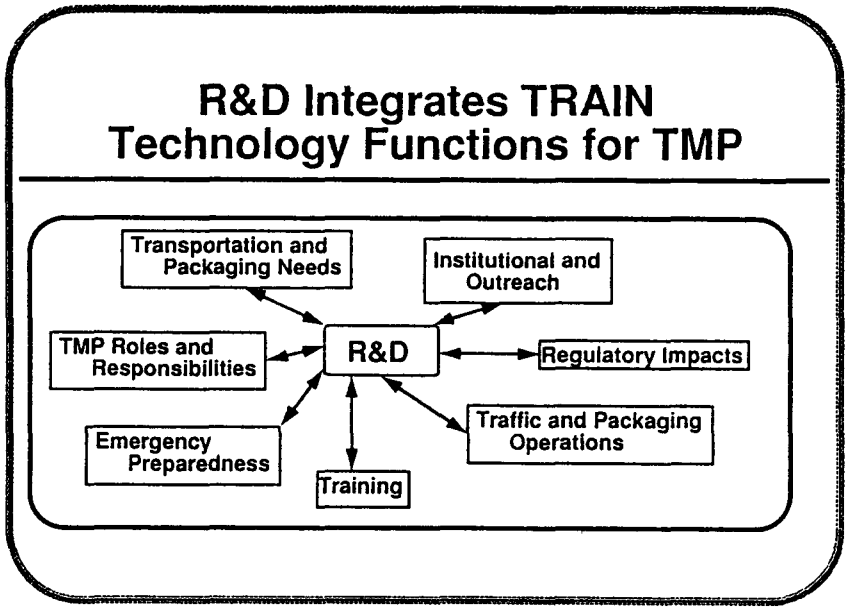

Figure 1. The Integrating Role of Research and Development in Transportation Functions

The research and development activities are divided into the seven tasks shown in Figure 2. These include: (1) packaging development, (2) engineering analysis, (3) testing, (4) advanced technology development, (5) certification support, (6) regulatory development support, and (7) systems and safety assessments. The focus of the hazardous and mixed waste transportation program is the development of packagings for sample transport. The success of the hazardous and mixed waste activity requires each of the seven elements of research and development to be applied. For example, the development of a packaging is undertaken due to a need identified during a systems analysis. The development of that packaging requires engineering analysis of preliminary designs, testing development models and prototypes to demonstrate compliance with the regulatory requirements in the development of the Safety Analysis Report for Packagings.

PACKAGING CONCEPTS

The purpose of this activity is to provide conceptual designs that meet the needs of the DOE and its contractors for packagings to transport hazardous and radioactive materials. This activity is done in parallel with the chemical compatibility activities and systems studies to ensure that (1) the conceptual designs meet a projected need and (2) the systems engineering studies are based on manufacturable packaging designs.

The short term goal of this project is to produce a family of conceptual designs that meets the requirements of the Westinghouse Hanford Company Sample Packaging criteria. A conceptual design will be completed in 1993 for a chilled sample packaging. The preliminary design for the chilled sample container is shown in Figure 3. The intent of this package is to transport chemically hazardous, radioactive, or mixed waste samples. This goal is achieved with a modular package. The interior of the package contains a teflon insert that can be machined to hold sample sizes of up to 1 liter. It is anticipated that the samples will be transported in glass vials. Hence the teflon insert will be lined with a low durometer elastomeric material to provide shock attenuation. Containing the samples and the insert is the internal containment vessel which is being designed to meet the requirements of the United States Department of

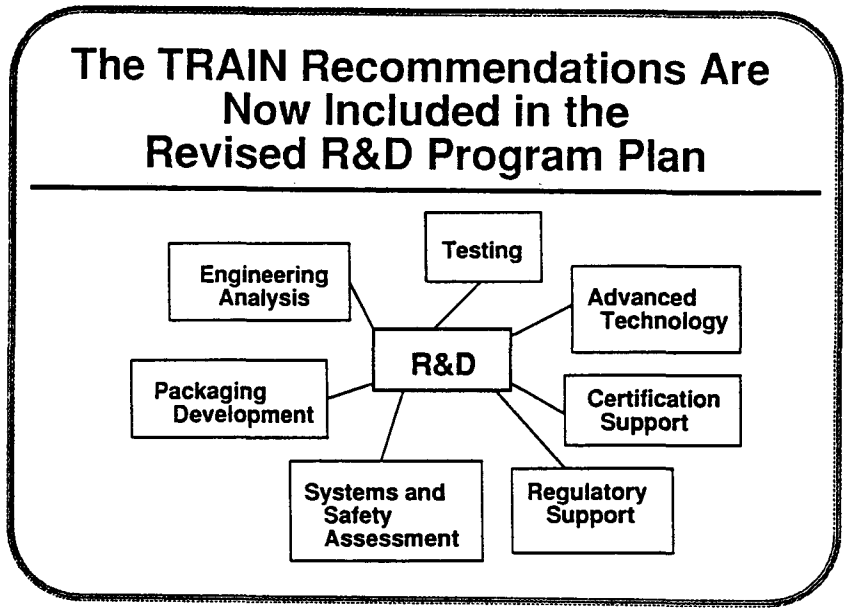

Figure 2. The Elements of a Research and Development Program

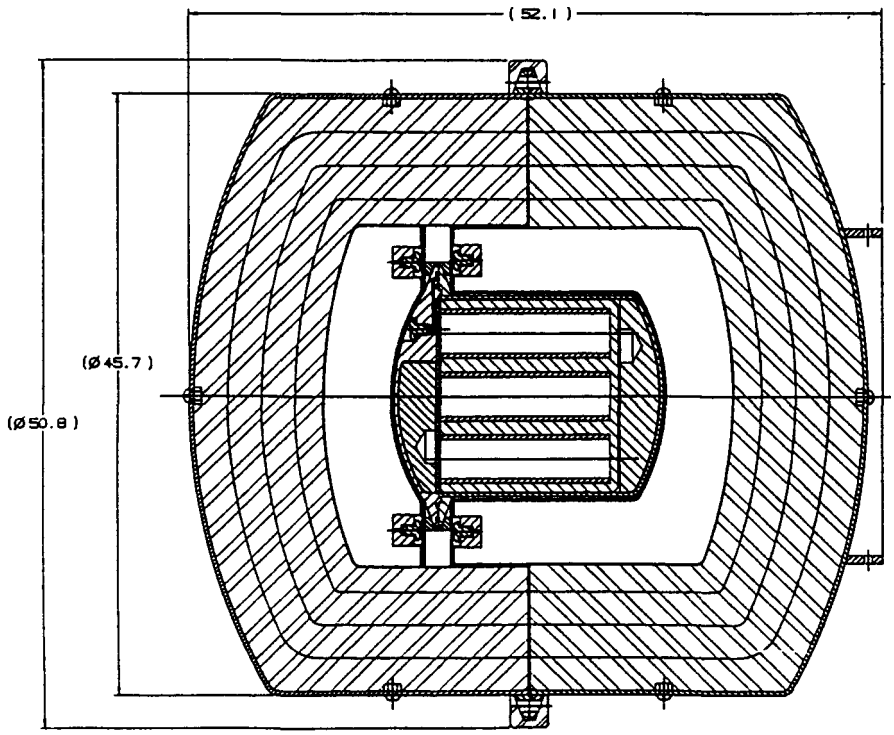

Figure 3. Chilled Sample Container Preliminary Conceptual Design

Transportation Packaging Group I criteria. This internal package is then surrounded with a bladder which contains a high heat of fusion material with the requisite melting point (usually ice). This module is the basic chilled sample container. For the package to also be capable of transporting type B quantities of radioactive materials, a sacrificial outer shell is included that provides the impact, puncture, and thermal protection required of a Type B packaging. It is anticipated that the requirement for chilling will not occur concurrently with the requirement for a Type B packaging. In that case, the bladder will not be included in a Type B packaging design with the resulting reduction in packaging size and weight.

The intermediate goal is to complete the engineering development required to move from concept to completed design. This goal will encompass prototype fabrication, testing, and analysis. It is anticipated that this task will be completed for the chilled sample container and for the Type B sample packaging in 1995. The Packaging Group I tests will also be completed to certify the packagings for transport of hazardous materials.

The long-term goals are focused on developing packaging designs based on the results of the systems studies. The developments will be coordinated with the packaging users. In all packaging development activities, SNL will support the certification process through completion.

CHEMICAL COMPATIBILITY

The DOE-sponsored TRAIN Report identified a need for a program that will involve chemical compatibility testing and research on materials used in transportation packagings. The short-term goal for the activities carried out in this task will be to experimentally evaluate the behavior of simulated mixed wastes with transportation packaging materials and to provide significant chemical compatibility data for package design and certification. The chemical compatibility testing will initially focus on seals, liners, and sample ports. The preliminary testing will be done with simulated mixed waste chemicals. The long-term goals are to select specific mixed wastes and perform similar compatibility testing. Both of these goals are intended to provide an understanding of the effects of hazardous and mixed-waste substances on packaging materials. This understanding will provide valuable engineering input to packaging design and certification.

The specific data required will be obtained in an experimental program. This experimental testing program will determine the effects of selected chemicals on various packaging materials by measuring the degree of swelling/softening (dimensional changes, hardness changes), surface cracking/crazing (appearance changes), plasticizer extraction (weight changes), effects (physical property changes), and physical property deterioration (physical property changes). These physical property changes will be measured using static and dynamic mechanical methods and thermal methods of analysis. Specifically, durometer range, tensile strength, elongation, compression set, and glass transition temperature data will provide additional data to evaluate the compatibility of packaging components with simulated mixed waste. As can be seen, the testing program will rely on traditional analytical chemistry methods and on methods more common to the area of material science. In addition, while the above methods are particularly useful for evaluating the environmental response of plastics, some of these methods are equally applicable to the packaging materials. Furthermore, while the previously discussed methods provide fundamental material response data, applied component data, such as leak rate measurement for seals under simulated closure conditions, will also be acquired.

Currently, test plans and procedures for the chemical compatibility studies are being developed. This documentation will provide the necessary details on how the experimental testing program will be conducted. For example, this documentation will give the sample

dimensions, the exposure protocol (i.e., the length of time that the sample will be exposed to the waste), and the sequence of physical measurements to be performed. It will also include the criteria that will be used to establish whether the material has been affected by exposure to the waste. Most importantly, this documentation will address any quality assurance and environmental, safety, and health issues that must be addressed to perform this work. Upon completion (and DOE acceptance) of the test plans and procedures, compatibility testing will begin in October 1993. Before work can begin, several simulated mixed wastes will be selected. The simulated waste chosen will most closely resemble actual waste streams. The experimental evaluation ~~will begin in the March~~ 1994 and ~~be completed by~~ the end of September 1995. With the completion of the simulated waste testing, a performance report will be issued by September 1996. Since the transportation packagings to be designed will contain mixed wastes, test plans and procedures for chemical compatibility studies with actual mixed wastes will be initiated in 1997 and compatibility testing on these wastes can begin in 1998.

SYSTEMS STUDIES

The systems studies effort at SNL focuses on four areas. These are: (1) sample packagings, (2) Greater-Than-Class C materials (GTCC), (3) other packagings, and (4) engineering systems analysis of technology needs. The systems engineering analysis of sample packages will ensure that efficient and cost-effective packagings are available to support the DOE's Environmental Restoration and Waste Management laboratory sample analysis program. The systems engineering analysis will analyze and integrate the transportation elements in the GTCC program to ensure that safe, timely, and cost-effective packagings are available to meet the storage and disposal needs for GTCC wastes as mandated by United States Federal law. A systems engineering analysis for other material and waste packages will ensure that efficient and cost-effective packagings are available to support DOE's transportation needs on a timely basis. The purpose of the systems engineering analysis of technology needs is to identify what technologies will be required for future USDOE packaging development activities. Assessments will be made together with others in the Transportation Management Division to address how well current technology development is addressing DOE's needs as well as to identify technology gaps.

Laboratory sampling requirements to support materials characterization for the Office of Environmental Restoration and Waste Management (EM) wastes are expected to increase dramatically. Examples of waste requiring characterization includes drums of buried and stored high-level and low-level wastes; transuranic wastes; uncontained low-level wastes; materials from hazardous, radioactive, and mixed-waste sites; mill tailings sites; and materials at facilities scheduled for decommissioning and decontamination. These wastes must be characterized before clean-up operations become effective. The Analytical Services Program (ASP) will make maximum use of U.S. laboratory capability in order to meet waste characterization schedules. The analysis of DOE waste samples will be performed using a mix of commercial laboratories, DOE laboratories, and site field tests including those that can be best accomplished by a mobile laboratory. This effort will result in the need for a significant and responsive transportation network to feed the analytical laboratories. Thus transportation will be a critical component in assuring maximum efficiency in processing on- and off-site laboratory samples.

United States Public Law 99-240 (the Low-Level Radioactive Waste Policy Amendments Act of 1985) requires the Federal government (DOE) to provide technical and other assistance to the States in their efforts to meet responsibility under the law and for the Federal government to dispose of GTCC low-level waste. In response to the legislative requirement for the DOE to dispose of these wastes, the DOE has developed a three-phase strategy to provide safe and effective management of commercially generated GTCC waste. The first phase is to provide for interim storage of limited amounts of GTCC waste that pose a potential threat to public health

and safety. Selection of a specific DOE facility for interim storage is in process. The second phase of the strategy provides for a centralized dedicated storage facility for all commercial GTCC wastes until a U.S. Nuclear Regulatory Commission- (NRC-) licensed disposal facility becomes available. The third phase provides for the disposal of GTCC waste, either by storage in conjunction with a high-level waste repository or at a separate GTCC disposal facility.

SNL will perform systems engineering analysis of technology needs to identify what technologies will be required for future EM packaging development activities. Assessments will be made together with others in the Transportation Management Division to address how well current technology development is addressing EM's needs as well as to identify technology gaps. The full range of analysis and testing disciplines will be addressed: structural, thermal, criticality, shielding, containment, optimization, testing methodologies and facility requirements, new package concepts, advanced technology development, standards development and regulatory support, normal environments and severe accident studies, and risk and systems engineering analysis techniques. The packaging needs will be addressed and the results will provide input into the technology assessments.

Roadmapping

A specific example of a systems study methodology embraced by SNL is the Roadmap. Roadmapping is a process used by the DOE EM to show issue-based planning activities necessary for achieving final waste disposal, completing site remediation, and bringing waste operations into compliance. Roadmaps are developed at both the headquarters and installation levels by following a systematic planning process that largely focuses on issue identification, root-cause analysis, and issue resolution. The Roadmap methodology sets the course of events necessary to complete a mission.

The Roadmap methodology includes nine steps that are grouped into three phases: assessment, analysis, and issue resolution. The Assessment phase defines the current status and background of the organization. Planning assumptions are identified and documented. Regulatory drivers are cataloged, and schedules of commitments are determined. It is during this phase that logic diagrams are constructed to show the sequence of events necessary to achieve a particular goal and to indicate interface requirements.

A logic diagram has been developed (Figure 4) that, in general, shows the steps necessary to begin development of a Roadmap for Transportation of Hazardous and Mixed Waste. Certain activities and decisions delineated in the diagram may be accomplished in parallel to shorten the time required to complete a program. The diagram becomes the backbone to which the remaining Roadmap steps may be added as deemed necessary. For instance, assumptions, issues, and milestones (these steps may be accomplished prior to logic diagram development) leading to activities and issue resolution steps can be developed with the logic diagram acting as a core project reference tool. Upon completion of the Roadmap steps deemed necessary, activities can be planned to accomplish the transportation mission with a high degree of confidence that all requirements have been met.

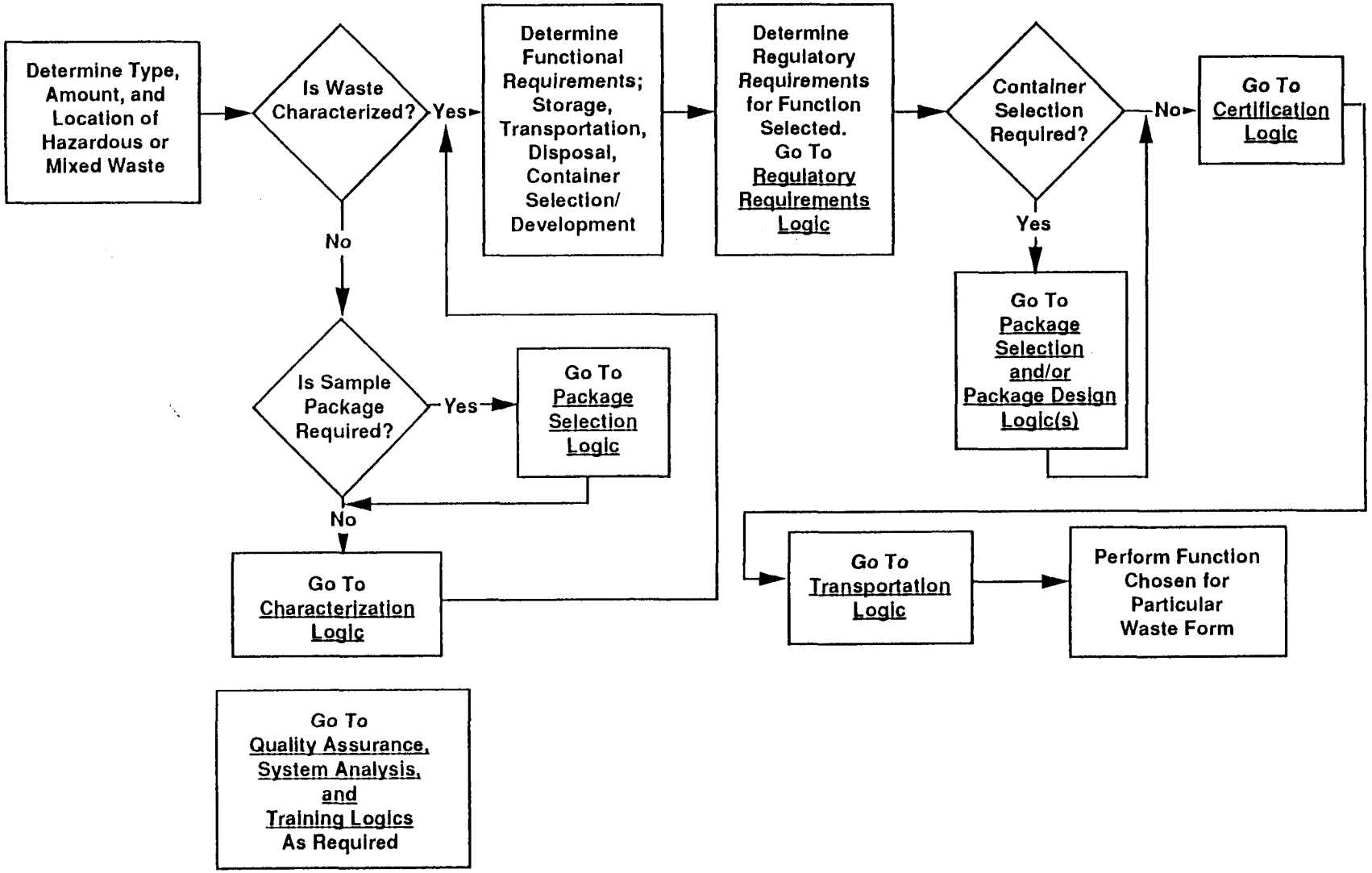

Figure 4. Hazardous and Mixed Waste Transportation Logic Diagram

REFERENCES

USDOE Office of Environmental Restoration and Waste Management, Transportation Assessment and Integration (TRAIN), A Basis for Planning DOE Transportation in the 1990s, Final Report, July 1992, DOE/EM-0075.

System Certification: An Alternative to Package Certification?*

Robert E. Luna [1] *and Robert J. Jefferson* [2]

[1] *Sandia National Laboratories, Albuquerque, New Mexico*
[2] *Consultant, Albuquerque, New Mexico*

One precept of the current radioactive material transportation regulations is that the package is the primary protection for the public. A packaging is chosen to provide containment, shielding, and criticality control suitable to the quantity and characteristics of the radionuclide being transported. Occasionally, radioactive materials requiring transport are not of a mass or size that would allow the materials to be shipped in an appropriate packaging. This is a particular problem for materials that should be shipped in a Type B package, but because such packages are designed and certified for specific contents, the package is usually fairly expensive, available in relatively small numbers, and often requires a fairly long period to achieve certification or amended certification for new contents. Where the shipment to be made is relatively infrequent, there may be economic and time penalties that may hamper shipment or force the shipper into uneconomic or high risk options. However, there is recognition of such situations in the International Atomic Energy Agency (IAEA) regulations under the provisions for Special Arrangement.

The principal paragraphs defining Special Arrangement in Regulations for the Safe Transport of Radioactive Material; Safety Series 6 (SS6) [IAEA, 1990a] are 141, 211, 720, and 727. Many national regulations contain similar provisions, but under a variety of terms. For instance, in the US regulations the applicable term is "Exemption." An exemption is obtained from either the United States Department of Transportation (USDOT) or the United States Nuclear Regulatory Commission (USNRC) depending on the character of the needed exemption. The applicable paragraphs are 10CFR71.7 and .41 for the USNRC and 49CFR107 Part B for the USDOT. The essential concept is that some requirements of the regulations that apply in a given situation are not required if the shipment is subjected to other operational controls that provide an equivalent level of risk to that attained if the regulations were observed fully. This paper deals primarily with changing of packaging requirements in Special Arrangements, but it is also true that operational requirements also may be changed as a result of an Exemption or Special Arrangement approval by a regulatory authority.

One problem with Special Arrangement is that not everyone may agree that it is a legitimate application of regulation in the same way that the Competent Authority usually does. The fact that it is a "Special Arrangement" or "Exemption" means that shipments under such arrangements may be looked upon as a risky deal between the regulator and the applicant. This impression is furthered by the fact that little public involvement is sought or required prior to granting the requested Special Arrangement or Exemption. This perception is generally incorrect; Competent Authorities evaluate each exemption application on its face and confirm an appropriate level of safety before granting the request.

*This work performed at Sandia National Laboratories, Albuquerque, New Mexico, supported by the United States Department of Energy under Contract DE-AC04-76DP00789

A change in the IAEA's regulations currently being discussed is to institute a process referred to here as System Certification (SC). While the concept has been discussed in transportation regulatory circles for some time, a proposal for SC seemed to arise as a result of a 1989 action at an IAEA meeting to amend the 1985 edition of SS6 to improve the new Low Specific Activity and Low Contamination Object requirements with a SC concept [Petterson, 1989]. Because the proposal was seen as leading to a major regulation change, it was determined to be outside the scope of that meeting. A meeting of the Standing Advisory Group on the Safety of Radioactive Materials in transport (SAGSTRAM) in 1990[Rolland, 1990] debated the issues without resolution and decided to convene a Consultant Services Meeting (CSM) to consider the issues broadly prior to the 1992 SAGSTRAM meeting in October. The CSM was not funded in 1992, but the 1991 meeting of the first revision panel for the 1995 edition of SS6 was provided information that the CSM would occur in 1993 to provide data for the 1995 Revision Panel meeting [Petterson, 1991].

If it is assumed that SC were to come into wide use, what methods could be used by the Competent Authority (CA) to assess the advisability of certifying the system operation? To a large extent the assessment would be keyed to the content of the application; where there was significant quantitative data offered, confirmation of the information offered and consideration of other features not covered in the application would go forward. Where there was qualitative argument the assessment would, of necessity be qualitative. In such a mode the skill of the applicant to argue the case becomes very important to success. This sets up the opportunity for the CA to be questioned concerning the basis for a decision and makes the proceeding subject to appeal. Note that the system in place for package certification is set within a largely quantitative framework with a binary result. You meet specific design and performance criteria or not. This is not to say that the yes or no is not decided with some measure of subjectivity in some situations, but the result is not often decided by the presentation skills of the applicant. It seems clear that a workable and reliable system certification process must be undertaken with a well defined quantitative framework for application and demonstration of equivalent safety.

The basic precept of SC is similar to Special Arrangement, but differs conceptually in that a set of relatively clear-cut rules would be put into place in order to remove the appearance of an arbitrary decision based on a negotiation outside of public scrutiny. Under SC, the packaging and conveyance as well as all of the operations undertaken to ship a given material in a shipping campaign are evaluated in terms of risk to the public and are approved if the risk measures calculated were within specific acceptable limits. The real difference between the present certification approach and SC would be the consideration of all features of the transport system in addition to the packaging in limiting public risk during safety evaluation of a transportation operation.

As indicated above, exemptions are permitted under USNRC and USDOT regulations. Some exemptions granted by DOT were the following:

- Use of the ATMX railcar for the movement of TRU waste material from Rocky Flats to temporary storage in Idaho [USDOT, 1990].
- Carriage of up to 1000 TI (Transport Index) in radiopharmaceuticals in a single conveyance [USDOT, 1989 & 1990].
- Approval for the DOE and EPA (in separate programs) to transport mill tailings in bulk loads without detailed identification of the nuclide content of each load [USDOT, 1992a] [USDOT, 1992b].

In the first case the special arrangement was a package tradeoff. The ATMX railcar is not a Type B package, but a semi-quantitative risk assessment of the transportation showed sufficiently equivalent risk for approval. In the second case, the usual 50 TI limit per conveyance was waived because the controls put on dose to crew and the low dose to other exposed employees and public resulting from air mode transport, automated handlings and careful controls of proximity of persons to the conveyance. The third case was a waiver of the requirement to fully characterize each shipment since each was a part of a large and relatively homogeneous volume. The first example relates to the type of package/procedure tradeoffs of special interest to this paper. The remaining items relate almost exclusively to operational tradeoffs, but would also need to fit within the guidelines of a viable SC process.

System Certification – What could it include?

It must be noted that the current version of SS6 and the advisory and explanatory information contained, respectively in SS7[IAEA, 1990b] and SS37[IAEA, 1990c] directly or indirectly validate the concept of SC within the existing framework of Special Arrangement. In fact, the explanatory material for paragraph 211 on Special Arrangement indicates that justification of a Special Arrangement request "ranges from considered judgment ... to probabilistic risk assessment" [IAEA, 1990c]. It is the spectre of defending a decision based on "considered judgment" that makes the need for a new and quantitative method of evaluating Special Arrangement or SC decisions important in the current and growing atmosphere of questioning Competent Authority decisions.

The problem of defending a decision (among others) has caused the IAEA to defer the concept of System Certification until it can be studied by consultants. At the Senior Advisory Group on Safe Transport of RAM (SAGSTRAM) Meeting in June of 1991[Petterson, 1991], it was "envisioned that the 1993 Revision Panel will consider this issue before a final Consultant Service meeting to be held before the 1995 Revision Panel."

While the impression from the USNRC and USDOT regulations is that any Exemption or SC would include both the package and the conveyance, it is mentioned (and confirmed by the cases cited above) that operational controls are also to be included. If operational controls are included, the possibilities are broadened considerably. For example, in the United States there has been considerable pressure from the railroads to ship spent fuel in "Special Trains" operating under more conservative rules than ordinary freight trains. These "Special Trains" are limited to speeds under 35 mph (56 kph), must yield right of way to all other trains, and must be standing still when being passed in either direction by another train. From the railroad's perspective, these "Special Train" shipments are subject to far lower accident forces than regular train service. Could the accident resistance of the package therefore be reduced or be less well characterized for such shipments without sacrificing overall safety?

Since the risk of shipping high level radioactive materials is at least partially dependent upon the total population along the route, might it be possible to route the shipment to reduce total population exposed along the path and use that reduced risk to offset the added risk of using a packaging that does not fully meet the external dose rate requirements? In a similar way, might shipments be required to be made during low traffic density times of the day so as to reduce the public involvement? For years the City of New York insisted that spent fuel shipments transit Manhattan Island at night while the streets were empty of other vehicles. Routing of shipments of large quantities of radioactive materials over the best available and shortest highways is already a requirement of the DOT in the U.S.

Some states in the United States have insisted on notification of shipments of high level radioactive materials. A communication and tracking system called TRANSCOM allows real time tracking of each such shipment. The TRANSCOM data is available to the states so they may know the exact location of each shipment on a real time basis. In principle, this allows better emergency response and thus lowers risk. Is this reduction of risk available to be applied to the level of competency of the packaging?

Another factor in reducing risk envisioned by most of the public in the U.S. is the state of readiness and competence of the Emergency Response capabilities along the route. If training were instituted (as is being done in the case of the WIPP facility) for fire and police personnel along the transportation routes, could the reduced risk generated by this activity be applied to a reduction in the severity of the regulatory requirements for the packaging?

Before application of SC to situations such as those indicated above, a risk based regulatory concept must be fully defined and accepted. One such concept is that of equivalent safety which might be defined as keeping risk constant by shifting risk between various regulatory control concepts.

System Certification - How might it be used?

It is rather simple to envision, from an operational standpoint, instances where System Certification could be used to great advantage. For example, the regulator might certify the system of shipments for a limited campaign involving a specific package, specific routing, and specific operational controls. The packaging may not be certified for the specific contents involved except for the limited campaign, the routing might be unique to the campaign and the operational controls might be used to attain the level of risk deemed acceptable by the regulators. Included in such a system certification might be requirements for additional Quality Assurance (QA) measures or Compliance Assessment (CoA) inspections by the shipper, the carrier, the States or some independent reviewer acceptable to all three.

Similarly, System Certification might be used to approve a specific package and conveyance for a fixed period irrespective of the number of shipments. This approach might be used to provide an evaluation period of the adequacy of the System Certification before the regulator issued an unlimited System Certification. Alternately, this approach could be used for very short campaigns where time is deemed to be a dominate risk factor.

One possibility that might arise in the U.S.A. and elsewhere involves shipment of storage casks to a repository. Regulators are likely to be uneasy about allowing a cask used to store spent fuel for 20 or more years to then be used for transport with only a relatively simple inspection to find serious problems. System Certification might be used to allow a single trip by such a cask, without inspection. Of course, this assumes that easily obtained measurements confirmed no obvious problems. Certainly the early shipments, if the fuel is unloaded from the cask at the repository, could be used as the basis to confirm satisfactory long term cask behavior thus giving the regulator more data upon which to continue the System Certification, to certify the casks under normal rules, or to discontinue the practice.

If a System Certification is to include a large number of variables, then the regulator must regulate all these variables as well. When training is used as a component of SC, then training must be a regulated component. This would include training covering the QA and CoA requirements applicable to the SC, training covering the operational controls, and training specific to any special conditions involved.

In the United States the most common use of System Certification could be in the movement of materials within the boundaries of a large research site. Most of these sites are several thousand square miles (several thousand square kilometers) and frequently are traversed by public highways. Agreements with the States allow blockage of these highways and the establishment of at least some control over the public at risk. Still, special needs arise that could be quite amenable to SC approaches. SC should not be viewed as an "easy out" somehow relieving the shipper of responsibility. But, if it is to be a viable method of achieving solutions to special problems, it cannot be practically impossible either. To be effective, SC must meet the needs of both the applicant and the regulator while not introducing either significant risk to the public nor spawning widespread public reaction.

Demonstrating Equivalent Safety

A safe activity is one which is perceived as being relatively free of hazard or danger to the person or public affected. Because it includes perception, achieving safety involves more than achieving acceptably low risk. As a result, any SC scheme must preserve the current perception that the regulations provide safety while allowing some risk tradeoff.

Achieving "equivalent safety" would seem to demand specific guides for the protection of the public. Limitation of dose to the public controls consequence; preventing occurrence of an event limits the probability. Since risk is the summation over all events of the products of frequency and consequence of each event,

limiting both is a control on risk. All three measures represent the potential output of risk assessment. Control of risk or achieving "equivalent risk" lays the groundwork for using risk assessment methods and imposing specific risk criteria.

A way of demonstrating equivalent safety is based on the concept of maintaining an equivalent level of risk between the fully regulated activity and that occurring under system certification. The result of such a requirement puts heavy emphasis on being able to calculate risks under both options and being able to show equivalence. Alternately, it would be necessary to meet some absolute risk acceptance criterion that is generally accepted as describing an "acceptable risk." Neither of these options is particularly straightforward given the quality of the data needed to perform risk assessments. Moreover, public experience in interpreting risk assessments is very limited. This means that there might not be high public confidence in risk assessment and its practitioners.

When a decision to use risk criteria in evaluating whether a proposal represents equivalent safety is made, there are several additional problems that become important which relate to using relative or absolute risk criteria, how to handle uncertainty in the basic data needed in each case, and how to handle needed data that may not exist.

Relative vs Absolute Risk - Risk is the summation over all events of the product of an event's frequency and its consequence. Frequency is expressed in terms of expected events per year, events per trip, or events over the duration of a project. Consequence is the outcome from an event in terms of individual dose, population dose, cost or any other quantifiable result of the event. From the definition it is seen that risk is the expected value (or average value) of consequence for the activity. An event tree is usually used to represent the various sequences of events that lead to radiological risks and to guide the risk calculations.

To utilize relative or absolute risk assessment to support an application for system certification requires an event tree(s) that describes the sequences of all possible events affecting the system's risk profile. For relative risks two event trees are constructed; one is for the operation for which a system certificate is desired, the second is for a "reference system" that meets all regulatory requirements. Only the parts of the two event trees which differ between the regulatory and proposed system approval applications need be detailed, since the goal of the calculations is to demonstrate that the ratio of the risk from the proposed operation to what would occur if all regulatory requirements were met is less than unity.

For absolute risk an event tree that describes the sequences of all possible events is constructed, filled in with frequencies and consequences, and evaluated. If one value is used for each parameter in the analysis (a "point estimate"), what results is one numerical estimate of the risk, or one set of points that represents the cumulative probability of exceeding a given consequence level (abscissa) and consequence (ordinate). When plotted, these points become a complementary cumulative density function (CCDF) curve. If each of the parameters in the analysis may have a distribution of values which are selected in a random manner, then many point estimates and a family of CCDF curves will result. These risk assessment results make up the information which can be the basis of all or a part of a decision to certify a system. Finding a criterion on which the CA can accept these risks may have several kinds of formats. Two examples may be instructive:

NRC Reactor Risk Goal - The USNRC has indicated a set of "goals" [USNRC, 1990] for individual reactor risk based on different measures of consequence. One of the goals is that for the population from the reactor fence to a distance of 50 miles, the operation of the reactor should cause no more than a 0.1% increase in individual mortality. This and the other goals were arrived at as a result of a very long process involving much public interaction and staff/consultant effort.

CCDF Goal - A risk limiting goal that was being considered for specific transport operations appears as shown in Figure 1. On the CCDF field, a risk profile that fell below the line would be acceptable. The lines were arrived at in the following way: 1. events that produced or had potential to produce any consequence should not

occur more frequently than 0.001/year; 2. events that could result in 1 latent cancer fatality (LCF) or more should have a probability less than 1 in a million per year; and 3. from the point (1 LCF,10-6) a line of constant risk (probability times consequence) connects to the 0.001 line.

To use these or other absolute risk criteria, the CA must be able to demonstrate that the criterion being used limits the risk for the transportation situation under consideration to that which would occur if conducted under the regulations that are normally in force. This would not be a trivial undertaking for the CA given the number of situations for which system certification is sought. Of course, the CA could require the applicant to provide the comparative estimate of absolute risk under normal regulation events.

Choosing between these two possible absolute risk criteria, the easiest to use is the point estimate (NRC). This is particularly true if variations of parameters or uncertainty analysis is included in the calculations. The CA might require that none, or no more than 5% or as many as 50% of the set of estimated risk values exceed the criterion so long as the median or mean risk is below the criterion line. To use the CCDF criterion will require examining a family of curves for conformance to the requirements and developing a method to determine whether a few exceedences in a small area of the plot disqualifies the applicant.

Data Limitations to the Use of SC

Whether an applicant for SC must meet relative, absolute or even qualitative risk equivalence demonstration, there will be a heavy load of data gathering that must occur. Tradeoffs of package certification for package and conveyance certification or reliance on operational controls implies that the behavior of the containment systems in either case must be known, identical, or reliably estimated in environments below and above the performance limits for the package. Otherwise there is no method for calculating risks for comparison of risk associated with different packaging concepts. Since most packages are not tested to failure above the performance standards, such data tends to be scarce.

Where there is a tradeoff that involves operational restrictions or modifications, the same problem indicated above occurs; the applicant must present data that suggests a quantified difference in probability or consequence between two operational procedures. Usually such information is not available or is gained only by examining accident records and recalculating rates after accidents caused by specific behaviors and processes are excluded. Where the data does not provide a record that can be so analyzed there is little but qualitative arguments to be used. For example, if transport is restricted to daylight hours, it is relatively easy to find tabulated accident rates for day and night and establish the advantage of daylight travel. To gauge the effect of special driver training or maintenance, however, is a much more difficult restriction to define quantitatively.

Future

The IAEA will examine the issues associated with System Certification in order to determine whether there can be a meaningful elaboration of the SC concept for the 1995 version of SS6. To produce a change which truly embraces the SC concept will take significant effort in resolving the role of risk assessment, the criterion for equivalent risk, and how to account for uncertainty among others. These are non-trivial issues and suggest to the authors that SC inclusion in the 1995 version of SS6 is unlikely. However, there is time to develop the concept for the 2005 version of SS6 if a well conceived plan is put in place soon to develop consensus on need and technical bases for the concept.

A danger in the SC concept is that the process of developing quantitative understanding of the effects of special operational controls will generate a demand for their incorporation in the regulations without specific tradeoff goals. An aligned but slightly different feature of SC is that it represents a change from the current process which states that when you meet the requirements you can proceed with transportation without any additional

permission or approval. Under SC an applicant potentially must demonstrate need and safety for every shipment and incur the possibility of protracted delay.

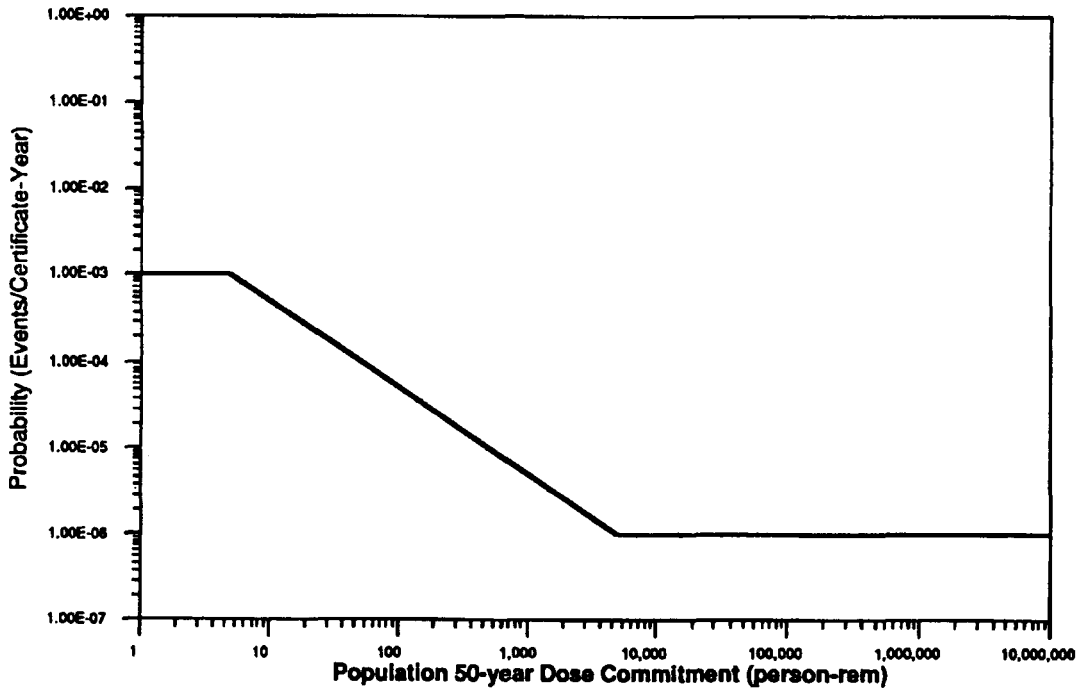

References

IAEA, 1990a; "Regulations for the Safe Transport of Radioactive Materials (1985 Edition)," (as amended 1990), IAEA Safety Series 6, 1990.

IAEA, 1990b; "Exploratory Material for the IAEA Regulations for The Safe Transport of Radioactive Material (1985 Edition), Second Edition (as amended 1990), IAEA Safety Series 7, 1990.

IAEA, 1990c; "Advisory Material for the IAEA Regulations for The Safe Transport of Radioactive Materials (1985 Edition)," Third Edition (as amended 1990), IAEA Safety Series 37, 1990.

Petterson, 1989; "Chairman's Report on the Technical Committee Meeting on the Continuous Review of the IAEA Regulations for the Safe Transport of Radioactive Materials," TC 405.3, 10-14 July 1989, Vienna, Austria.

Petterson, 1991; "Chairman's Report on Meeting of The Advisory Group on The Revision of SS6," AG 550.2, 10-14 June 1991, Vienna, Austria.

Rolland, 1990; "Chairman's Report on the 8th Meeting of the Standing Advisory Group on The Safe Transport of Radioactive Material (SAGSTRAM), TC 407.6, December 1990, Vienna, Austria

USDOT, 1989 & 1990; DOT Exemptions (DOT-E7060 & DOT-E 10045) 1989 & 1990.

USDOT, 1990; DOT Exemption (DOT-E5948), Sixth Revision, November 1990.

USDOT, 1992a; DOT Exemption (DOT-E10594), First Revision, May 1992.

USDOT, 1992b; DOT Exemption (DOT-10727), September 1992.

USNRC, 1990; NUREG 1150, "Severe Accident Risks: An Assessment for Five U. S. Nuclear Power Plants," Volumes 1-3, U. S. Nuclear Regulatory Commission, Office of Nuclear Regulatory Research, 1990.

IAEA Regulatory Initiatives for the Air Transport of Large Quantities of Radioactive Materials*

Robert E. Luna [1], Michael W. Wangler [2] and Hendrik A. Selling [3]

[1] Sandia National Laboratories, Albuquerque, NM 87185, USA
[2] U. S. Department of Energy, Washington, DC, USA
[3] International Atomic Energy Agency, Vienna, Austria

Introduction

The International Atomic Energy Agency (IAEA) has been laboring since 1988 over a far reaching change to its model regulations (IAEA, 1990) for the transport of radioactive materials (RAM). This change could impact the manner in which certain classes of radioactive materials are shipped by air and change some of the basic tenets of radioactive material transport regulations around the world.

The impetus for this effort was spawned in part by the decision of the Japanese government to move large quantities of reprocessed plutonium by air from France to Japan. The exploration of options for overflights of United States and Canadian airspace (among others) and landings in Anchorage, Alaska, generated intense debate in the USA and countries that might have been overflown. The debate centered on general questions of the need to air transport plutonium in large quantities, package survival in an accident, prenotification, emergency response, routing, safeguards and other facets of the proposed operations.

In the USA, which already had the most stringent regulations for packaging of plutonium shipped by air (NUREG-0360), there was immediate additional legislative action to increase the stringency by requiring demonstration that an aircraft carrying plutonium in certified packagings could undergo a severe crash without release of plutonium (the Murkowski amendment). In the United Kingdom there was an official inquiry that resulted in a high visibility report (ACTRAM, 88) and a conclusion that the IAEA should examine regulatory needs in the general area of air transport.

The Japanese program to return plutonium was a triggering event leading to the current IAEA initiative, but, in fact, there had been discussion at many earlier meetings of IAEA's Standing Advisory Group for Safe Transport of Radioactive Materials (SAGSTRAM) concerning the need for specific package qualification standards for the air mode. These discussions stemmed both from unilateral action in the US in the mid-seventies driven by a Congressional requirement and from the realization that the air mode does have the potential to impose more severe accident environments than the truck, rail and water modes for which the IAEA package performance requirements are demonstrably adequate. The main arguments to retain the existing regulatory structure were:

1. the fact that, on a risk per trip basis, air transport was about equivalent to surface modes;

*This work was performed at Sandia National Laboratories, Albuquerque, New Mexico, supported by the United States Department of Energy under Contract DE-AC04-76DP00789.

2. there were relatively few shipments of large quantities of RAM by air; and
3. there was a desire to maintain a relatively simple regulatory structure that was independent transport mode.

Regulatory Process

The ongoing effort to modify the air transport aspects of the IAEA regulations that started in 1988 is scheduled in such a way that if regulation formation is successful, the 1995 edition of the IAEA's "Regulations for the Safe Transport of Radioactive Materials" (also known as Safety Series 6 or SS6) (IAEA, 1990) will include specific provisions for air transport of large quantities of radioactive material. Figure 1 shows the progress and potential result of the regulatory effort.

The December 1991 Technical Committee Meeting (TCM) generated a technical report (IAEA, 92) that contains an account of the work done at the meeting as well as a complete account of the proposed changes to the regulations and their justification as derived from discussions that date to the first SAGSTRAM meeting on the subject.

Regulatory Changes Proposed

The proposed changes to the regulations (see Figure 2) fall into four main categories: Exemption Limits Package Test Standards, Design Requirements, Post-Test Acceptance Standards, and Regulatory Accommodations. All of the first three items engendered significant technical discussion in the process of coming to a decision on the specific features to be sent forward to the Revision panels. Technical data and analyses were provided and argued by a number of member states for the consideration of the TCM's, SAGSTRAM and Consultant Services Meetings. Some continued discussion of technical points is expected to occur in the Revision Panel Working Groups that are charged with the process of integrating realistic changes into the 1995 edition of SS 6

The most visible change to the regulations is in the creation of a new packaging type, termed the Type C package. This is the designator for the package that meets the performance criteria for air shipment of large quantity or high activity RAM. The Type C package must first be shown to meet the requirements of a Type B (u) package including the sequential impact/crush, puncture, fire and immersion tests. Then there are additional design and performance requirements described below that must be met.

Exemption Limits The types and quantities of RAM affected by the change are normal and special forms and fissile materials.

Normal Form - The exemption limit was set at 3000A2, that is, shipments of RAM in quantities less than 3000A2 and more than 1 A2 continue to be allowed to be shipped in a Type B package in the air mode. The decision to set the limit at 3000 A2 was based on two arguments. The first was that it was a level at which shipment notification to competent authorities was required in IAEA rules. In addition, it is a significant level in the US regulations in that it is the lower limit for a Highway Route Controlled Quantity which requires specific routes to be used. Thus there was some recognition that 3000A2 represents a boundary between ordinary shipment operations and large quantities. The second argument was based on some US data (IAEA, 92) that suggested that the release fraction for some Type B packages tested to destruction at typical aircraft crash speeds was in the range of 0.3% to 3%. With 3000A2 in a package this would indicate a release of perhaps 10-100A2 which most participants agreed was a reasonable threshold between serious consequence and high consequence events.

Special Form - Invoking the parallelism between special form and normal forms derived from the Q-system (IAEA, 90a), the exemption level for Special Forms was set at 3000A1, but, because some special form

materials contain nuclides with very small A2's , it was decided to limit the total activity content of a Special Form to less than 100,000A2. This value was set under the assumption that the special form encapsulation would limit the release of RAM to the inside of the package to less than 3% as was assumed to be provided by a Type B; so the resultant equivalent normal form content of the package would be 3000A2.

Fissile Materials - Fissile materials presented a particular problem because many fissile materials have large A2 values and as a result shipments would not be affected by the exemption limits indicated above. However, the possibility of a criticality event might be enhanced if ordinary fissile packagings were subjected to an aircraft accident where more massive damage than is ordinarily accounted for in fissile package certification occurred. A special Consultant Services Meeting (Collin, 88) considered the issue. They recommended that existing exemption limits in the regulations also hold for air shipments, but that fissile packages for use in air transport be evaluated in their damaged state as though they had been subjected to the performance tests for a Type C package and that features that would ordinarily be expected to prevent water in-leakage be assumed not to function.

Package Test Standards - It was recognized in defining these standards that there were existing packaging performance standards in place in the US regulations for one specific element, plutonium. It was also recognized that a more general regulatory framework based on the Q-system, was required for fitting all elements and isotopes into a coherent radiological protection scheme. It was also recognized that performance tests must be set to protect against most, not all, possible accident environments. The definition of "most" is that level at which increased capability of the package to resist accident forces would result in little or no increase in the probability of the package remaining competent to retain its contents during an accident. Much effort was expended to determine where the "knee of the curve" is that defines the point of diminishing returns for the impact and fire test requirements. Figure 3 illustrates this point.

Impact - After extensive and largely independent work by several nations, it was clear that the knee of the curve for impact speed was at or about 85m/s. A package built to withstand impacts at higher speeds was likely to be heavier and bulkier and more costly, but provides little additional decrease in risk to the public. As a result the recommended test is specified in the same manner as the existing Type B test, except at a speed of 85m/s into an unyielding target.

Fire - Fire data is notoriously poor with regard to duration and intensity of direct fire exposure over an area which might contain a package (Clarke, 76). The data seemed to suggest that 1 hr duration was about at the knee of the curve (See Fig. 4). In low speed crashes and ground accidents impact damage will not be great, but the fuel is concentrated around the aircraft and can produce a long and intense fire. This situation is the target of the 1 hour fire test for Type C packages. The specification for intensity of fire currently contained in SS6 was adopted for the test because it is judged to be a severe environment that is unlikely to be surpassed in a actual fire event. This is the same intensity and duration required in the US tests.

Puncture - Because it seemed likely that a package in a real accident would encounter a potential puncture probe during an accident's early phases and before any fire had broken out, it was judged necessary to inflict a puncture environment on the package prior to fire exposure. Since the Type B test regime puncture probe seemed untypical of the air mode, the NUREG-0360 (NRC, 1978) puncture test was evaluated and adopted. A 250 kg conical penetrator with 2.5 cm diameter frustum is dropped from a height of 3 metres onto a package with mass less than 250 kg. For package mass greater than 250 kg the package is dropped from 3m onto the probe.

Crush - Dynamic crush is an environment that is likely to occur in aircraft accidents. The intensity of the crush environment was subject to discussion that involved considerations of potential mass and stiffness of other cargo and impact angles that control the severity of crush. Since it was impossible to define the crush environment in a meaningful test but possible to control it with stowage requirements, and since it was clear that the structural capability built into a package to meet the impact test was considerable, it was decided that

the existing crush test in the Type B test sequence was appropriate for all Type C packagings (not just those with density less than 1000 Kg/m3 and mass less than 500 Kg).

Immersion - Since the air mode is frequently used for intercontinental movements of RAM, it was judged necessary to impose a 200m immersion requirement that reflected the possibility of accidents that resulted in packages submerged in the ocean. To facilitate recovery and to safeguard coastal populations from exposure to released radionuclides, a 200 metre submersion test would be imposed. Using 200 m essentially covers the continental shelf areas where recovery is fairly certain and where there is little opportunity for dilution to minimize impacts on food products from the sea. This requirement parallels current requirements in SS 6 for spent fuel casks.

Sequence of Tests - In the Type B package performance demonstrations the tests are sequential in their application to the same package. The concept behind the sequence of tests is to compound damage as it might occur in actual accident events which could include mechanical insults followed by fire. For Type C testing, only the puncture and fire tests are sequential on the same package. The concept behind this apparent lack of parallelism with the Type B tests results from the fact that high speed aircraft crashes disperse fuel widely such that the fire environment that follows the crash is not extreme. As a result there was no need to concatenate the 85m/s impact and 1 hr fire.

Design Requirements - There was discussion of the need to include specific tests for exposure to fireball environment, burial in near-adiabatic conditions and terminal velocity impacts. It was finally determined that these conditions needed to be brought to the attention of packaging designers in an explicit manner to assure that weaknesses for these mode particular environments don't creep into a design. No tests were proposed in these areas.

Post-Test Acceptance Standards - Considerable discussion of this topic occurred during the Technical Committee Meetings and SAGSTRAM. Two basic positions were taken. The first was that there were existing post-test performance requirements for leakage and radiation levels for Type B packagings that ought to be carried over directly to the new Type C package qualification testing. Consistency and the comfort of not having to justify different values were primary considerations. The second position supported more lenient requirements than the A2/week leakage and 1 rem/hr at 1 metre radiation level post-test currently used for Type B. The basis for the relaxation of requirements was based on two arguments; 1. that the test environments were so much more severe than Type B that using the same requirements would make the packages very expensive or perhaps impossible to build; and, 2. that ICRP guidelines for allowed dose during accident recovery procedures were such that much higher releases and dose rates were justifiable. The result of the Technical Committee activities was to adopt the existing criteria and to note that the position concerning ICRP allowances was a generic problem and could be taken up as part of the overall revision process and apply to all packagings alike.

Regulatory Accommodations - Many modifications in the regulations will need to be evaluated and accommodated in order to bring these changes for the air mode about. Aside from the purely mechanical steps of changing paragraph sequences etc., there are significant issues in marking and labeling packagings to assure that appropriate air packages are identifiable from those not air mode qualified.

Other Issues

Affects on Other Modes - There was significant concern about the effect of these changes on the perception that performance tests for other modes are inadequate. While this is always a danger, the same analysis methods that allowed the lengthy IAEA regulatory process to converge to these proposals fully support the current Type B performance test regime. In fact, the 10 m drop and 30 minute fire are quite representative of the knee of the curve for these same environments in the surface modes (truck, rail, ship/barge). As a result, there should be little impact on other modes from these decisions.

Additional Data Needs- It became clear in the deliberations that there are problems associated with data needed to support these kinds of regulatory decisions. Of particular importance here were data for fire and crush environments. Fire data is rather poorly reported and is confused regarding total duration and duration of involvement of aircraft structure or cargo. Improved standard forms for reporting and training of responders in observing and reporting of accident events will provide a much more useful and reliable database. From the standpoint of crush environments, data needs relate to surveys of cargo and interactions of packagings and aircraft structure as a function of impact angle and speed. There is a need for data on mass and stiffness of cargo in typical cargo flights and those that might contain large quantity RAM shipments. Many such shipments occur in Exclusive Use where loading and other cargo are controlled, but surveys could provide useful information for the design of a relevant crush test. Some additional detail on aircraft crash phenomenology may indicate the relative importance of impact and crush environments and allow some fine tuning and, perhaps, liberalization of these requirements.

Implementation - When there is a change in regulations affecting packagings, there is usually a period of 2 to 5 years in which use of old designs are "grandfathered." Because this change puts an entirely new type of packaging in the regulations, the TCM's have taken the position that the only time needed is that to design and build a package. It was believed that, given the duration of the studies reported here, the short time before requiring use of the Type C package should be (1 or 2 years).

Conclusion

Few technical issues remain in determining the shape of the IAEA's revision of its regulations to accommodate air transport of large quantities of radioactive material. In the next two years the detailed wording of the regulations will be fully worked out and proposed for inclusion in SS 6. Considering the breadth of the member state participation in the process, it seems likely that the approved version of the 1995 revision of SS 6 will contain air mode revisions that move away from the predominantly mode independent character that characterized their first 30 years.

References

(ACTRAM, 88), Advisory Committee on the Safe Transport of Radioactive Materials, "The Transport of Civil Plutonium by Air", Her Majesty's Stationary Office, London, 1988.

(Clarke, 76), Clarke, R. K., et al, "Severities of Transportation Accidents: Volume II - Cargo Aircraft", SAND74-0001, Sandia National Laboratories, July 1976.

(Collin, 88), Collin, F. W., "Technical Committee Meeting on Mode-related Aspects of the Regulations for the Safe Transport of Radioactive Materials: Vienna,5-9 December 1988 - Chairman's Report", TC-675.

(Degrange, 89), Degrange, J. P., Hubert, P., and Pages, P., "The Transport of Plutonium Oxide: A Study of Air and Road Accidents," Report 138, IPSN/DAS/SAET, CEA-France, July 1989.

(NRC, 78), NUREG-0360,"Qualification Criteria to Certify a Package for Air Transport of Plutonium", USNRC Report, 1976

(IAEA, 90), "Regulation for the Safe Transport of Radioactive Materials," Safety Series 6, 1985 edition (1990 revision).

(IAEA, 90a), "Exploratory Materials for the IAEA Regulations for The Safe Transport of RAM" (1985) Edition), IAEA, 2nd ed. 1990.

(IAEA, 92), "The Air Transport of Radioactive Material (in Large Quantities or with High Activity", TECDOC-xxxxxx, IAEA, Vienna, Austria, 1992.

Figure 1: IAEA Air Transport Regulation Development Process

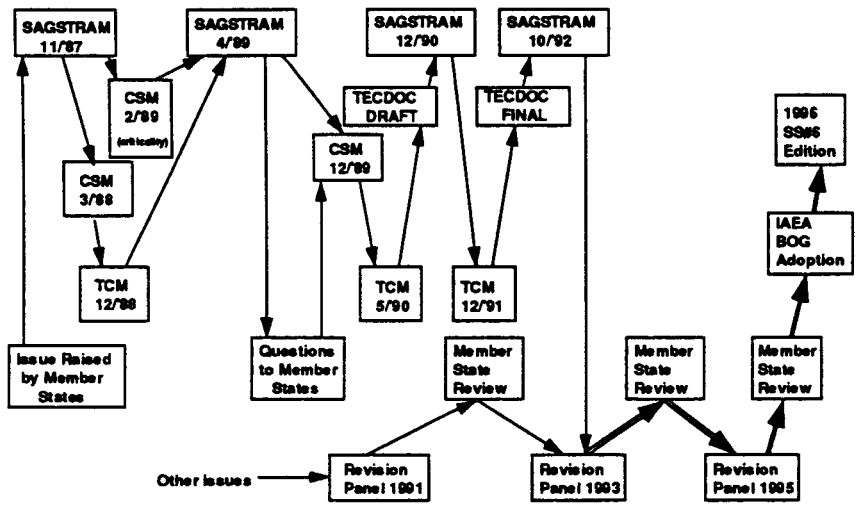

Figure 2: Issues Considered in New Air Transport Regulations

- Nuclide / Isotope Application
- Exemption Levels
  - Normal Form
  - Special Form
- Candidate Performance Requirements
- Test Pass Criteria
- Non-Dispersible Forms
- Fissile Materials
- Operational Features
- Applicability of Risk Assessment
- Bleed Over into Other Mode Requirements
- Phase in Period

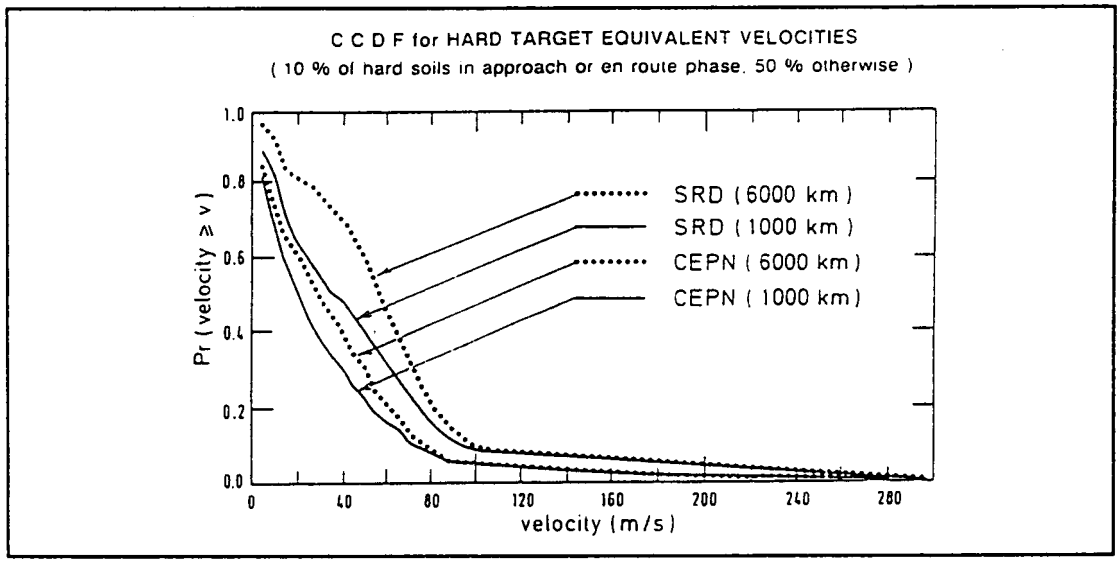

Figure 3: CCDF for Aircraft Hard Target Impact Velocity from (Degrange, 89)

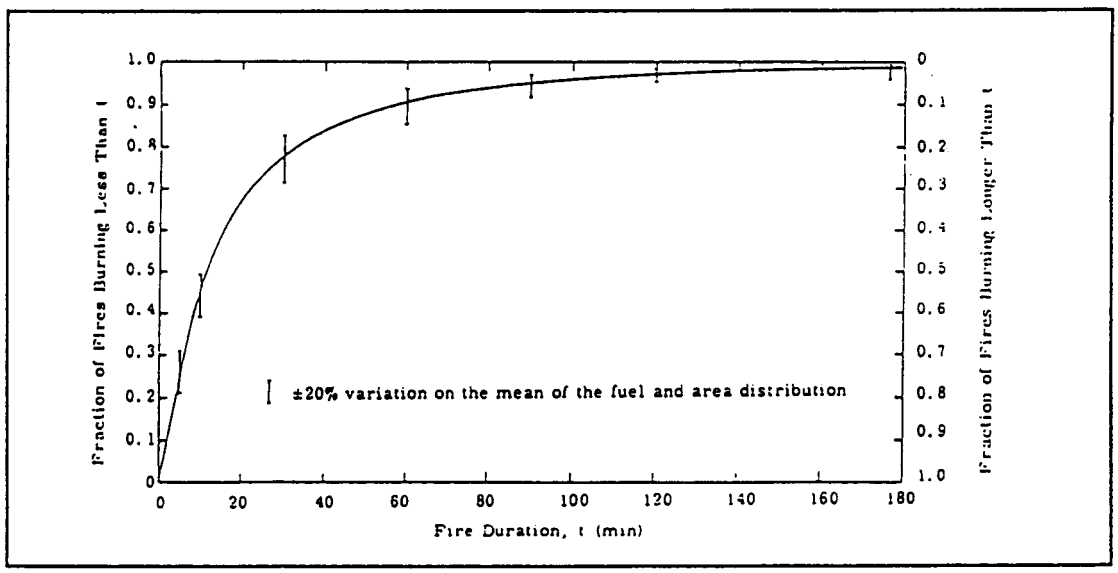

Figure 4: CDF for Aircraft Fire Duration from (Clarke, 76)

Emergency Response Packaging: A Conceptual Outline*

R. E. Luna, J. D. McClure, P. C. Bennett, T. A. Wheeler

Sandia National Laboratories**, Albuquerque, New Mexico, 87185, U.S.A.

INTRODUCTION

The Packaging and Transportation Needs in the 1990's (PATN) component of the Transportation Assessment and Integration (TRAIN) program (DOE Nov. 1991) was designed to survey United States Department of Energy programs, both ongoing and planned, to identify needs for packaging and transportation services over the next decade. PATN also identified transportation elements that should be developed by the DOE Office of Environmental Restoration and Waste Management (DOE EM) Transportation Management Program (TMP). As a result of the predominant involvement of the TMP in radioactive material shipment issues and DOE EM's involvement with waste management issues, the primary focus of PATN was on waste packaging issues. However, contacts in other programs not related to waste and radioactive material shipments were also made.

Pending DOE regulations will formalize federal guidelines and regulations for transportation of hazardous and radioactive materials within the boundaries of DOE reservations and facilities. The pending requirements reflect a growing awareness of concern regarding safety environmental responsibility activities on DOE reservations. Future practices involving the transportation of radioactive material within DOE reservations will closely parallel those used for commercial and governmental transportation across the United States. This has added to the perceived need for emergency recovery packaging and emergency response features on primary packaging, for both on-site shipments and shipments between DOE facilities (off-site).

Historically, emergency response and recovery functions of packaging have not been adequately considered in packaging design and construction concepts. This paper develops the rationale for emergency response packaging, including both overpack concepts for repackaging compromised packaging and primary packaging redesign to facilitate the recovery of packages via mobile remote handling equipment. The rationale will examine concepts for determination of likely use patterns to identify types of shipments where recovery packaging may have the most favorable payoff. These concepts can lead to likely configurations of recovery packaging and their physical attributes to facilitate remote recovery and handling, as needed.

*This work performed at Sandia National Laboratories, Albuquerque, New Mexico, supported by the United States Department of Energy under Contract No. DE-AC04-76DP00789

**A United States Department of Energy facility

CHARACTERISTICS OF RADIOACTIVE MATERIAL PACKAGING

According to the most recent estimate (Javitz et al., 1985), approximately 2.8 million packages of radioactive material (RAM) are transported annually in the U.S.A. The movement of RAM on this order of magnitude has been characteristic of the past several years in the U.S. The characteristics of these shipments can be evaluated in a number of ways, one of which would be from the viewpoint of what types of packaging are transported. Table 1 describes typical packages and their capabilities. Small or limited quantities, low specific activity (LSA), and Type A package shipments account for approximately 96 percent of the packages shipped in the U.S. In another view, approximately 90 percent of the commercial (non-government) packages transported contain 1 Curie or less of activity. With this information, it is possible to make a judgment that a significant number of low activity shipments are made and are made in packages that are not required to withstand the accident conditions of transport. When greater severity accidents occur, there can be releases from Type A or industrial packages. It is unlikely that such accidents can cause releases from Type B packages. Based on the analysis (Cashwell, 1992) of actual transport accidents, it has been observed that even Type A packages can withstand more than modest accident conditions in transport without releasing their contents. With this as a background, it is possible to determine that the most likely accident during which a release of radioactive contents might occur will involve a package that is not designed to resist accident conditions; in addition, if such an accident occurs, it is likely to be a small quantity of radioactive material in the package, namely less than an A1 or A2 amount. Therefore, the design of a recovery package to aid in the response to transport accidents involving radioactive materials should deal with the most likely situations to occur where radioactive material is released, namely Type A and lesser types of packaging.

TABLE 1

PACKAGING TYPES AND CHARACTERISTICS

Package Type	Package Tests	Package Uses
Industrial (Strong & Tight)	Performance tested	Limited quantities, LSA materials, radiopharmaceuticals in small amounts, instruments and articles, low-level waste
Type A	Performance tested for "normal" transport or median accident	Radiopharmaceuticals, low level waste, industrial sources
Type B	Performance tested for severe accidents	Spent fuel, TRU waste, low level waste, irradiator sources

THE CHARACTERISTICS OF U.S. SHIPMENTS OF RAM

The most recent estimate of U.S. RAM shipments stated the shipping volume as being made up of two principal components: all U.S. shipments (other than DOE shipments) and DOE shipments (Javitz et al., 1985). The U.S. shipments (other than DOE) totaled approximately 2 million annual shipments, 2.8 million packages, and involved approximately 9 million curies of RAM. The DOE shipments and packages shipped involved only a small segment of the total 5090 annual shipments and 31800 packages shipped, but the total activity transported included 27.3 million curies. This means that the total of all U.S. shipments involved approximately 36.3 million curies of RAM, and DOE accounted for approximately 75 percent of this amount. This establishes USDOE as a major transporter in the U.S. on a national basis.

During FY 1990, DOE performed approximately 23460 hazardous material shipments for all classes of hazmat (DOE May 1991). On a shipment basis, DOE performed 10681 shipments of RAM involving 116,622 tons of RAM. Other hazmat shipments involved approximately 12779 shipments and 53740 tons. This means that the total of 23460 hazmat shipments involved 170362 tons of hazmat. On a percentage basis, radioactive material accounted for 45.5 percent of the USDOE hazmat shipments and 68.4 percent of the tons of USDOE hazmat transported.

TABLE 2

U.S. DOE RAM SHIPMENTS BY CATEGORY (FY 1990)

Category	Number of Shipments	Percent of RAM Shipments
Irradiated Fuel	28	0.3
Medical Research	2014	19.1
Unirradiated Fissile Material	611	5.8
Uranium Compounds	2968	28.2
Waste	859	8.1
Reactor Core Debris	6	0.1
Empty Containers	2510	23.9
Miscellaneous	1525	14.5

Table 2 displays the categories of US DOE RAM shipments. A significant number of the shipments indicated in Table 2 could involve Type B accident resistant packages. While recovery packages could be developed to support the possibility that a Type B accident resistant packaging could be involved in a release of contents, an analysis of actual RAM transport history has shown that the most likely event where a recovery packaging is needed is not for the Type B package but for the

less robust class of package, the Type A or industrial package. Table 3 displays this experience for U.S. RAM transport operations. What can be observed is that the accident resistant Type B packages perform very well and have, under accident conditions in transport, released none of their contents. A total of 2030 Type A packages have been exposed to transport accident conditions: 62 of these have been damaged without release of contents and 51 sustained such damage that they released their radioactive contents. Similar experience was noted from industrial packages where a total of 1340 packages were exposed to accident conditions: 18 of these packages sustained damage due to accident conditions, and 65 of the industrial packages received sufficient damage from the accidents that they released their contents. It should be re-emphasized that Type A (or lesser quality) packages are not designed to withstand accident conditions. The question might correctly be raised as to where the radioactive protection comes from under such circumstances. The answer is that, in general, there is a very severe restriction on the magnitude of radioactive material contained in Type A or industrial packages. This limit is the A1 or A2 amount (IAEA 1990) except for LSA materials.

The category of shipments involving LSA can result in quantities of RAM in excess of A1 or A2 being in a Type A or industrial package. This occurs because LSA is limited to a specific number of curies per gram of material. The safety concept involved for LSA is that the material is so diluted in inert material that it cannot present an inhalation/ingestion problem. An evaluation was performed of the potential consequences of a severe highway transport accident involving low specific activity waste (Ostmeyer et al., 1988). The analysis involved the development of a shipment scenario which contained unconsolidated spent ion-exchange resin from a nuclear reactor facility. The scenario assumed the overturning of a trailer carrying a shipment of LSA material with spillage of 100 percent of the material. The scenario was considered to represent a credible worst case for the shipment of LSA material. Of all the LSA wastes, spent ion-exchange from nuclear facilities contains the highest activity and is the most likely to be near the specific activity limit for LSA materials in the U.S.A. The analysis reflected current shipping practice. It should be mentioned that in actual transport accidents the likely releases of radioactive materials would be orders of magnitude less than those assumed in the analysis and further, that a 100 percent release of contents would be unlikely. From (Javitz et al., 1985) it can be determined that on a package basis, approximately 96 percent of the packages transported involve Type A or lesser magnitudes of RAM.

EMERGENCY RECOVERY OF RAM PACKAGING

A fundamental question is which segment of the shipment population would public safety benefit most from development of a recovery package. Every Member State of the IAEA has its own experience to draw upon; but based on U.S. experience as shown in Table 3, it can be seen that the package classes damaged with and without release of RAM most frequently were Type A and industrial packages. There is potential for large consequence involving the public if a Type B package is involved in a transport accident. Actual experience in the U.S.A. indicates that damage requiring control and retrieval of spilled RAM has not occurred for Type B packages involved in transport accidents.

Each country can survey its own accident experience to determine what the possibility for package recovery and clean-up is. If similar to U.S. experience, it appears that clean-up and recovery operations could involve either single or multiple Type A or lesser quality packages. Larger releases would probably come from shipments of multiple Type A packages. National assessments could evaluate the forms and radionuclides involved in the accidents, but it must be recognized that it would be difficult to generalize from historical experience to predict the potential for future recovery and clean-up operations.

RECOVERY PACKAGE NEEDS

Table 4 carries the analysis of actual transport accident experience a step further and categorizes the relative need for recovery packages. The last column indicates a qualitative judgment of the need for a recovery package which emphasizes those packages which are shipped most frequently, fail most frequently and pose significant, hazards.

TABLE 3

PACKAGE BEHAVIOR DURING TRANSPORTATION ACCIDENTS
(U.S. EXPERIENCE 1971-1990)

Package Category	No. of Accidents	No. of Packages in Accidents	No. of Packages Damaged	No. of Packages Failed
Industrial (Strong-Tight)	43	1340	18	65
Type A	159	2030	62	51
Type B	50	84	2	0
Totals	252	3454	82	116

TABLE 4

RELATIVE IMPORTANCE OF RECOVERY PACKAGES

RAM Material Type	Pkg. Type	Direct Radiation Hazard/if released	Ingestion/ Inhalation Hazard/if released	Likelihood of Pkg. Failure in Accident	No. of Shipments	Recovery package Importance
Limited Quantities	Industrial	None	Low to none	High	High	Low
Radiopharm.	Type A	Low/Mod.	Low to mod.	Medium	High	High
Industrial Use	Type A	Moderate	Low	Medium	Modest	Medium
Industrial Use	Type B	High	Low	Low	Many	Medium
LSA	Type A+	Moderate	Low	Low	Modest	Medium
Irradiators or Spent Fuel or HLW	Type B	High	High	Very low	Few	Low

CONCEPTS FOR RECOVERY PACKAGES

Based on the actual transport accident experience cited in Table 3, it appears that some simple approaches to providing a recovery package are called for. An example might be a set of nesting metal drums and bags of lead shot/polyethylene beads and packaging materials. The released RAM

or damaged package could be inserted into the smallest possible interior drum, and the granular shielding material would be used to shield and pack the drum interior to meet safety requirements as required.

If able to be contact handled, the released RAM could be wrapped in a plastic wrapping such as a plastic bag and placed in the interior of the drum. Further confinement of the contents, however deformed they might be, could be accomplished by the use of lead pellets (shot) which could form a flexible shielding blanket (or polyethylene beads for neutron sources which would fill all of the interstices of the drum interior). In Table 4, a qualitative matrix of the relative importance of several radiation safety and transportation parameters is presented. The recovery package concept seems most important when hazards are high, package failure is likely, and the number of shipments (and opportunities for package use) is high.

Because of the likelihood that the released radioactive material would be able to be contact handled, the procedures outlined above would cover a large number of actual transport accident conditions. However, recovery operations would require that some regionally located stockpiles of recovery supplies and drums be established.

If remote handling should be required, it is important that recovery packages be designed such that handling lugs (or other handling attachments) be attached to facilitate the movement of the recovery package about the accident scene. Such considerations would include the loading of the radioactive material into the recovery packages in a remote manner to reduce radiation exposures to the recovery personnel.

CONCEPTS FOR RECOVERY DESIGN

For massive packages, greater than 500 kg, Type A and Type B packages are designed to maintain their shielding capabilities, and based on experience, a release of contents is unlikely. However, the handling of such a cask in the post accident condition may be difficult if the normal handling points are not accessible. To expedite the recovery and post accident handling of such packages, it is suggested that multiple sets of handling lugs be designed into the cask during packaging development. The incorporation of multiple (redundant) sets of lugs would facilitate the handling of a cask in an unorthodox position that might occur in its post accident orientation.

AUTHORIZED CONTENTS OF RECOVERY PACKAGING

The format of most national certificates of compliance is that they include a list of authorized contents to be placed in the package. One of the considerations that would have to be made in the case of recovery packaging would be whether or not the recovery package is to be a certified packaging. Since it is anticipated that there would be a limited number of recovery packaging to deal with a broad class of packaging, such as Type A or industrial packaging, that have the potential for being involved in a transport accident, some type of special arrangements would have to be agreed upon prior to recovery package development and procurement. This is because it would be very difficult to anticipate the actual contents to be placed into a recovery package and have these contents listed on the certificate of compliance in the usual manner.

Based on the experience cited above in actual transport accidents, it appears most likely that the recovery of released radioactive materials from packages involved in transport accidents will be for Type A packages. An additional possibility is for low specific activity packages involving greater than A1 or A2 amounts and, in effect, the recovery package would be an LSA package. There has

been no experience dealing with the release of contents from Type B packaging due to transport accident conditions.

CONCLUDING REMARKS

The main thrust of this paper has been to put forth the idea of developing a package for the recovery and retrieval of released radioactive material contents from RAM packaging involved in transport accidents. Prior to the development of such a package, some additional studies might be performed which would confirm the general type of candidate materials which might have to be recovered. This would require a detailed inventory of U.S. packages that have released their contents due to transport accidents. The main issue is one of preparedness which would allow the U.S. Department of Energy to respond to accidents for DOE shipments and to respond nationally for shipments outside the normal jurisdiction of U.S. DOE shipments.

REFERENCES

Cashwell, C. and J. D. McClure, *Transportation Accidents Involving Radioactive Materials (1971-1991)*, Proceedings of PATRAM-92, to be published.

IAEA Safety Standards, Safety Series No. 6, (as amended 1990), International Atomic Energy Agency, Vienna, Austria, 1990.

Javitz, H. S., et al., *Transport of Racioactive Material in the United States: Results of a Survey to Determine the Magnitude and Characteristics of Domestic, Unclassified Shipments of Radioactive Materials*, Contractor Report, SAND84-7174, Menlo Park, CA, April 1985.

Ostmeyer, R. M., et al, *The Potential Consequences and Risks of Highway Accidents Involving Gamma-Emitting Low Specific Activity (LSA) Waste*, SAND87-2808, Sandia National Laboratories, August 1988.

U. S. Department of Energy Draft Report, Transportation Assessment and Integration (TRAIN), November 6, 1991.

U. S. Department of Energy Transportation Information Systems, Shipment Mobility/Accountability Collection Summary Report: Fiscal Year 1990, A Summary of DOE Commercial Transportation Activity, May 1991.

Information Management and Collection for U. S. DOE's Packaging and Transportation Needs in the '90's *

T.A. Wheeler, R.E. Luna, J.D. McClure[1], and Geoffrey Quinn[2]

[1]Sandia National Laboratories**, Albuquerque, New Mexico, United States of America
[2]WASTREN, Inc., Germantown, Maryland, United States of America

INTRODUCTION

The Transportation Assessment and Integration (TRAIN) Project (US DOE 1992) was established to provide a systematic approach to identify the problems and needs that will affect the capability of the United States Department of Energy (US DOE) to provide itself with cost-effective, efficient, and coordinated transportation services during the 1990s. Eight issue areas were identified to be included in the TRAIN Project, with one principal investigator assigned to each. The eight areas are as follows:

> 1) Packaging and Transportation Needs (PATN) in the 1990s; 2) Institutional and Outreach Programs; 3) Regulatory Impacts on Transportation Management; 4) Traffic and Packaging Operations; 5) Research and Development Requirements; 6) Training Support; 7) Emergency Preparedness Requirements; and 8) US DOE-EM 561 Roles and Responsibilities.

This paper focuses on the results of the PATN activity of TRAIN. The objective of PATN is to prepare the US DOE, in general, and US DOE-EM 561 (Environmental Restoration and Waste Management (EM), Office of Technology Development, Transportation) in particular, to respond to the transportation needs of program elements in the Department. One of the first tasks in evaluating these needs was to formulate the potential for transportation of radioactive materials in the next decade.

The US DOE is responsible for a relatively small fraction of the national shipments of radioactive material. Nevertheless, the assessment of its packaging and transportation needs presents a problem of wide scope. Large quantities of material are shipped each year throughout the US DOE establishment as a result of its work in the various field offices, national laboratories, and contractor facilities which carry out its programs.

* This work was performed under the auspices of the U.S. Department of Energy by Sandia National Laboratories under Contract DE-AC04-76-DP00789.
** A United States Department of Energy facility.

OBJECTIVE OF PATN TASK

The objective of the PATN component of TRAIN was to survey ongoing and planned US DOE programs. Needs for packaging and transportation services over the next decade were identified. Those needs which are critical will be targeted for resolution by US DOE-EM 561 through its own efforts or together with national laboratories and contractors.

SUMMARY OF ACTIVITIES

The following activities were undertaken as a first phase of the investigation:

- Workshops involving participants from all eight TRAIN issue areas
- Review of major US DOE transportation data bases for information on projected shipments
- Assessment of waste management data bases for information relevant to packaging
- Survey of program planning documents for projects potentially in need of packaging development
- Development of a network of program and site contacts through out the US DOE Complex to facilitate identification of packaging and transportation issues
- Packaging needs questionnaires sent to specific field staff and contractor contacts.

The primary focus of these activities was on issues relevant to the packaging and transportation of radioactive waste. However, some contacts with programs responsible for shipping radioactive products were made.

SUMMARY OF FINDINGS

Information Management and Collection

The results of these activities represent a preliminary survey of the US DOE complex to identify how, where, and by whom information necessary for transportation planning is collected and processed. However, some general conclusions can be made on the basis of the current level of effort.

Three major US DOE data bases were reviewed; the Shipment Mobility and Accountability Collection (SMAC), the Waste Management Information System (WMIS),

and the Integrated Data Base (IDB). Review of these data bases indicates that transportation and packaging issues have not been considered sufficiently in the design and implementation of the data bases, and in the collection and analysis of data. SMAC is a data management system that is used to collect and process detailed information on all US DOE commercial transportation shipments. SMAC contains significant information on actual shipments, including limited descriptions of the material and the packaging used. The IDB is a compilation of data on current inventories of US DOE-owned radioactive wastes and commercial spent fuel. The data base receives information from all of the field offices regarding both quantities and certain characteristics of the waste stored throughout the US DOE complex. The WMIS is being developed as part of the Waste Information Network (WIN) for the US DOE by HAZWRAP (Hazardous Waste Remedial Action Program). This data system is still in a developmental stage. It is intended to provide the US DOE with a comprehensive and consistent tracking of waste stream storage, treatment, and disposal throughout its complex. None of these data bases were designed with the perspective of evaluating packaging needs for future transportation.

The identification and assessment of packaging needs throughout the US DOE complex is not a simple task. Uncertainties exist with respect to the accuracy of waste characterization, the location, and the format in which information relevant to packaging needs is maintained. Often, information is not maintained in a useful format at all. This uncertain environment stems from a tendency to not incorporate packaging and transportation as an integral part of overall strategic planning. The root cause of this is a failure to recognize the need for transportation planning in the US DOE program planning process. This lapse in planning is pervasive throughout the US DOE complex.

The current method of collecting and managing information in the US DOE does not adequately encompass packaging issues as a constituent aspect of the data to be collected. Historically, data bases have not been designed to adequately address waste characteristics and other information necessary to track packaging needs.

Strategic Planning and Documentation

Planning documentation from US DOE headquarters and the US DOE field sites (US DOE 1990, US DOE 1989) is limited with respect to packaging and transportation issues. Some notable exceptions where such issues have been addressed as a fundamental component of the program plans are the Waste Isolation Pilot Plant (WIPP) (US DOE 1991, US DOE 1990, US DOE 1990), the Defense High Level Waste (DHLW) management program (US DOE 1983), the Office of Civilian Radioactive Waste Management (OCRWM) spent fuel repository program (OTA 1985), and the Three Mile Island 2 cleanup program (Vigil et al. 1981). However, the inclusion of packaging issues in strategic planning (e.g., roadmapping) is not typical in the US DOE's planning process. This situation is exacerbated by the current organizational relationships between US DOE-EM 561 and other US DOE offices. US DOE-EM 561 does not have sufficient influence to ensure the inclusion of packaging and transportation in overall program planning.

STRATEGIES TO ADDRESS NEEDS

Strategies which meet the packaging and transportation needs of the 1990s are proposed in three categories, near-term, long term, and overarching. The near-term strategies involve actions that can be taken in the next one to two years. Long-term strategies involve actions that can be undertaken within the next two to ten years. Overarching strategies address issues whose resolutions must span the entire time horizon of the US DOE's activities. Recommended strategies are listed below by category (i.e., near-term, long-term, and overarching).

Near-Term Strategies:

1. Continue and improve the needs assessment.

2. Commence a comprehensive process of conducting US DOE on-site interviews with project managers and back-up mail surveys of US DOE packaging and transportation needs.

3. Develop a generic response form for on-site surveys to define packaging needs. The form should address the following important waste stream characteristics and information for packaging needs assessment:

    a. Quantity of Waste Stream or Products

    b. Redemption/Processing Plans for Waste (e.g., Incineration followed by grouting, vitrification)

    c. Chemical Description of Waste, for example:
        (1). Corrosivity - Acidic or Alkaline
        (2). Ignitability - Ignitability Group
        (3). Reactivity - Reactive Group
        (4). Thermal Energy Generation Rates

    d. Physical Description of Waste (e.g.; Solid, liquid, or gas; sludge, metal, rubber; absorbents, labpack, equipment)

    e. Cask/Packaging Status for Waste or Product

    f. Packaging and Transportation Plans for Waste or Product:
        (1). On-site
        (2). Off-site
        (3). Estimate Time Frame of Shipping Campaign

4. Perform detailed studies to assess applicability of existing US DOE data bases to packaging needs assessment.

5. Include US DOE-EM 561 and contractor staff in US DOE roadmapping exercises for overall program planning.

6. Improve tradeoffs between optimizing waste form for compatibility with transportation and disposal criteria.

7. Improve relationship between the field office and contractor traffic managers.

Long-Term Strategies:

1. Develop a detailed transportation plan for each US DOE radioactive material category or waste form that would provide a strategic framework upon which other program elements can be attached.

2. Promote the centralized, professional services of US DOE-EM 561 program.

3. Consider the promulgation of a US DOE Order that requires US DOE-EM 561 sign-off of program plans that include major transportation operations.

4. Consider offering transportation planning services from US DOE-EM 561.

5. Examine transportation activities to eliminate duplication of activities at multiple US DOE sites.

6. Develop the capability for offering turn-key transportation services at reasonable and competitive cost.

7. Educate project officers to consult US DOE-EM 561 professionals early in project planning activities.

Overarching Strategies:

1. Develop documentation of transportation plans that explicitly state the assumptions for transportation of the product or item produced.

2. Provide US DOE-EM 561 support to the EM Assistant Secretary's Office so that the US DOE-EM 561 will have input into EM program planning at the formative stage.

CURRENT ACTIVITIES

Roadmapping

Roadmapping is a process used by the US DOE-EM to show issue-based planning activities necessary for achieving final waste disposal, completing site remediation, and bringing waste operations into compliance with all pertinent regulations (US DOE 1991). Roadmaps are developed by a systematic process that focuses on issue identification, root-cause analysis, and issue resolution.

The roadmap methodology includes nine steps that are grouped into three phases:

- Assessment Phase
  - Establish Assumptions
  - Establish Regulatory Requirements
  - Establish Committed Milestones
  - Depict Logic and Planned Activities
- Analysis Phase
  - Define Issues
  - Perform Root-Cause Analysis
  - Translate Issues into Activities
  - Develop Issue Resolution Schedules
- Issue Resolution Phase
  - Integrate Issue Resolution Activities with Planned Activities

The roadmap process is being applied to the US DOE Headquarters and field offices to identify specific issues and programs which will form a context for developing programs to implement the strategies identified above (US DOE 1992). As an example, the US DOE headquarters' comprehensive Roadmap identified **Packaging Selection** as one of the US DOE's functional activities. Figure 1 is the logic diagram for the Depict Logic and Planned Activities step of the Assessment Phase of the Roadmap being developed for package selection. This logic was developed based on information and insights gained in the previous steps of the process, and it will provide guidance and input to the next phase of the roadmap process, the Analysis Phase. Issues will be defined and analyzed, and activities to address and resolve these issues in the Analysis and Issue Resolution Phases of the Roadmap process.

SUMMARY

The US DOE accounts for a relatively small fraction of the U.S. national shipments of radioactive material. Yet defining packaging and transportation needs for the US DOE presents a problem which has very wide scope because of the breadth of the US DOE's activities. Enormous quantities of material are shipped each year throughout the US DOE establishment to carry on the work of the Department in the field offices, national laboratories, and contractors. Departmental programs which involve the movement of

radioactive material include naval reactors, fossil energy, waste management, weapon production, and other areas vital to the U.S. national interest.

The PATN activity of TRAIN indicates that there are specific needs that currently exist for packaging and transportation services. In addition, it is clear that there is also a pressing need for a more global and strategic view of transportation and packaging needs in the overall US DOE strategic planning efforts.

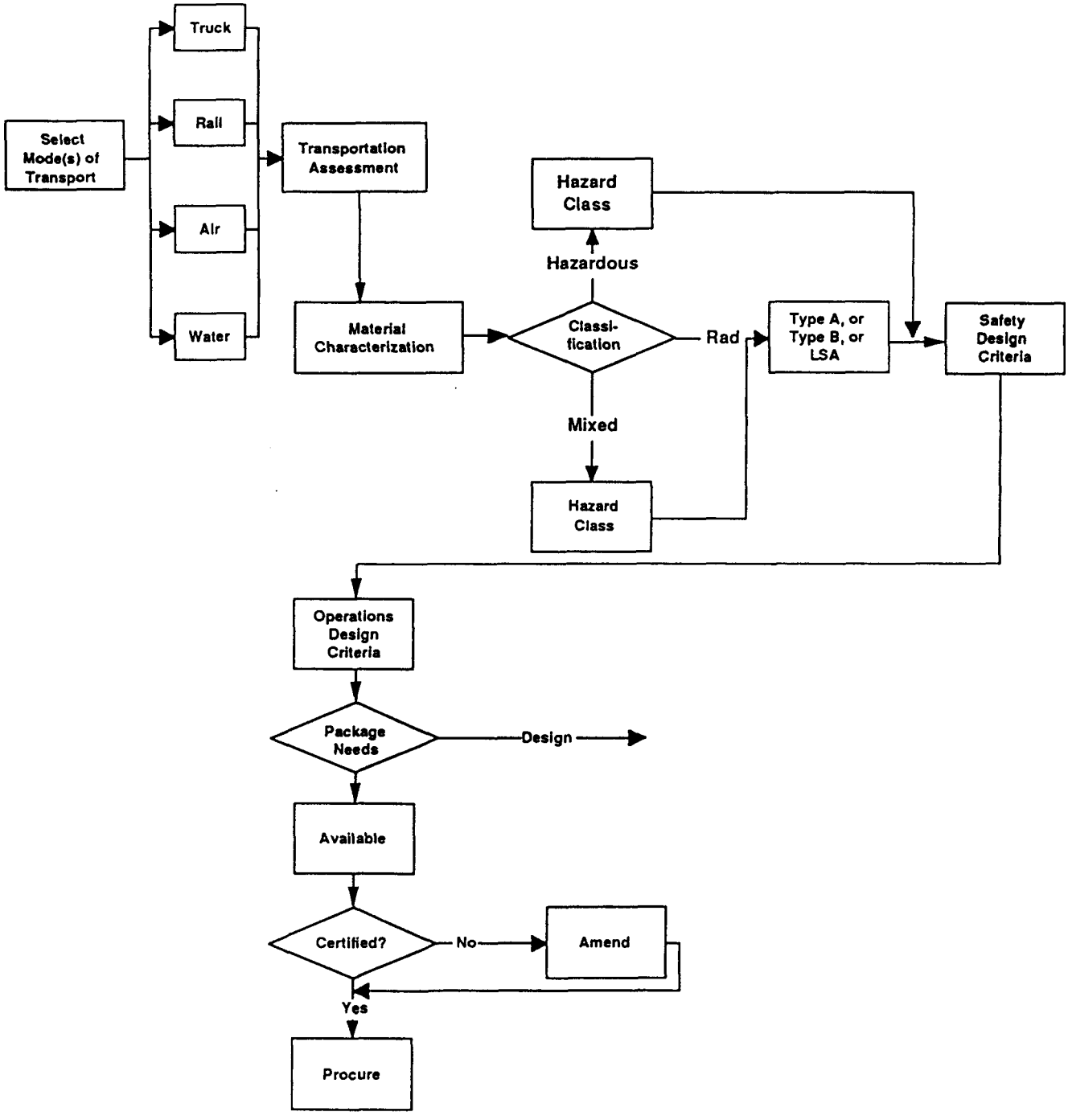

Figure 1. Packaging Selection Logic

REFERENCES

Office of Technology Assessment, Congress of the United States, Managing the Nation's Commercial High-Level Radioactive Waste, March 1985.

United States Department of Energy, Headquarter's Transportation Roadmap, May 1992.

United States Department of Energy, Transportation Assessment And Integration (TRAIN), August, 1992.

United States Department of Energy WIPP Project Office, Long-Range Master Plan for Defense Transuranic Waste Program, DOE/WIPP 88-028, May 1991.

United States Department of Energy, Roadmap Methodology Document, May 1991.

United States Department of Energy, Environmental Restoration and Waste Management Five-Year Plan, Fiscal Years 1992-1996, DOE/S-0078P, June 1990.

United States Department of Energy, Final Supplement, Environmental Impact Statement, Waste Isolation Pilot Plant, DOE/EIS-0026-FS, January 1990.

United States Department of Energy, Waste Isolation Pilot Plant Final Safety Analysis Report, WP 02-9, May 1990.

United States Department of Energy, Draft Applied Research, Development, Demonstration, Testing and Evaluation Plan, November 1989.

United States Department of Energy, The Defense Waste Management Plan, DOE/DP-0015, June 1983.

Vigil M. G. et al., Proposed Design Requirements for High Integrity Containers Used to store, Transport, and Dispose of High Specific-Activity, Low Level Radioactive Waste From Three Mile Island Unit II, SAND81-0567, Sandia National Laboratories, Albuquerque, New Mexico, April 1981.

Impact-Limiting Materials Characterization*

R. E. Glass
Transportation Systems Technology Department
Sandia National Laboratories, Albuquerque, New Mexico, United States of America**

T. A. Duffey
Spectra Research Institute, Albuquerque, New Mexico, United States of America

P. McConnell
GRAM, Inc., Albuquerque, New Mexico, United States of America

INTRODUCTION

Packagings for the shipment of radioactive materials are required to survive a sequence of hypothetical accident conditions. Regulatory requirements for Type B packages are specified in the United States Code of Federal Regulations (10 CFR 71, "Packaging and Transportation of Radioactive Materials"). The regulatory sequence consists of a free drop onto an unyielding target followed by a puncture and then a fire. Impact limiters are often used in packages designed to survive this hypothetical accident sequence.

The primary goal in the design of an impact limiter is to minimize the deceleration loads that the package and contents experience during the drop. Minimizing the decelerations enhances packaging performance by reducing loads in critical areas such as the closures, containment boundaries, and shielding. A secondary goal for impact limiter design is to reduce the thermal assault on the package due to the regulatory thermal event. A final objective in impact limiter design is to minimize the weight or size of the impact limiter consistent with the other design constraints. This requires materials, such as foams and honeycombs, which have a high energy absorption per unit weight or per unit volume. Characterization of the responses of the impact-limiting materials to the impact and fire events provides the design parameters required for selection of materials for the impact limiter.

Historically, there have been substantial efforts in identifying materials for use in impact limiters for specific packaging designs. These efforts include screening processes (Hill and Joseph, 1974), evaluation of materials for specific accident-resistant containers (Hill and Joseph, 1974), static and dynamic tests of foams (Berry et al., 1975) and modeling of cellular products (Neilsen et al., 1989). These references provide a basis of data and test methods. However, testing of the materials has been done for a variety of specific applications. In particular, much of the data in these references are for low-density crushable materials with structural testing performed at design-specific strain rates and with no corresponding thermal response.

Sandia National Laboratories (SNL) is developing inexpensive methods for selecting impact-limiting materials for use in radioactive materials packagings for the United States Department of Energy (DOE). Figures of merit have been developed for screening both structural and thermal response. These methods have been applied to two types of impact-limiting materials: aluminum honeycombs and polyurethane foams.

---

*This work was performed at Sandia National Laboratories, Albuquerque, New Mexico, supported by the United States Department of Energy under Contract DE-AC04-76DP00789.

**A United States Department of Energy Facility.

The development of the figures of merit examined the response of the materials to the impact event with the intent of maximizing the energy absorption of the materials with respect to either the volume or mass of the materials. Three figures of merit will be presented for the structural response. The figure of merit for the thermal event is based on minimizing the heat flux due to the regulatory thermal event into the containment boundary.

STRUCTURAL TESTS

The structural tests were designed to simulate the conditions enveloped by the hypothetical free drop accident. The 9-m drop determines the initial impact velocity and, hence, for a given material thickness determines the initial crush rate. For example, the velocity at impact is 13.3 m/s. For an initial thickness of impact-limiting material of 0.3 m, the initial strain rate is 44 s^{-1}. To determine the effects of this strain rate, testing was performed at quasi-static ($<10^{-2}$ s^{-1}) and dynamic ($>10^{1}$ s^{-1}) initial strain rates. Since the length of the impact-limiting sample was fixed, the impact velocity was selected to obtain the desired initial strain rate. The dynamic testing was done with an instrumented drop weight machine. The static load tests were accomplished with a screw driven quasi-static test machine.

Figure 1 shows an idealized load-deflection curve for crushable materials. The test was designed to ensure that the materials were taken to lock-up. This required that the product of the drop height and drop weight was greater than or equal to the area under the load-deflection curve to the lock-up deflection. For the static tests, displacements exceeded those associated with lock-up.

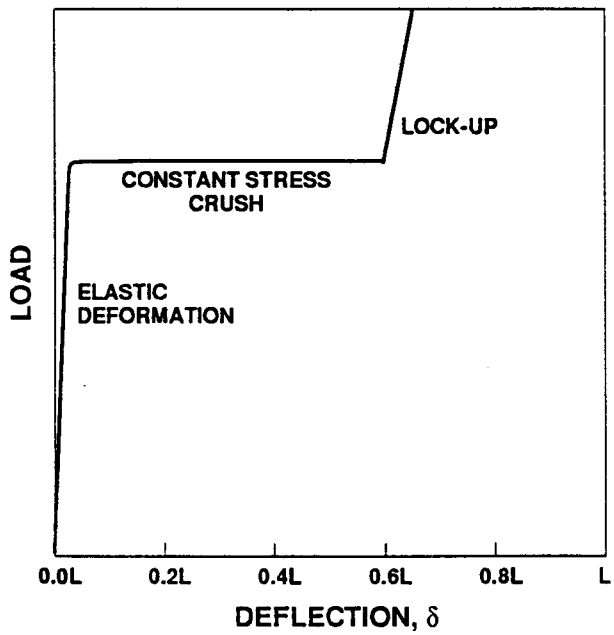

Figure 1. Idealized Crush Load-Deflection Curve

The test also simulated the lateral confinement experienced by impact-limiting materials during impact due to either the impact limiter skin or the surrounding impact-limiting materials. The lateral confinement was simulated by placing the 7.5-cm-long by 9.82-cm-diameter impact-limiting material samples in a 10-cm inside diameter steel pipe. The outside of the pipe was instrumented with strain gages to determine whether significant hoop or axial stresses were generated during the impact. No significant strains were measured.

STRUCTURAL TEST RESULTS

A series of seventeen structural tests was performed for SNL by General Research Corporation (McConnell et al., 1986). The results indicate the effects of initial strain rate and density for each of

the materials. The materials tested were corrosion resistant aluminum honeycombs, supplied by HEXCEL, with nominal densities of 91 kg/m^3 and 147 kg/m^3 and char forming polyurethane foams, supplied by General Plastics (FR9900 series), with densities of 168 kg/m^3 and 288 kg/m^3. The complete results are contained in Reference (Duffey, 1992).

The data are presented in terms of the engineering stress-strain curves. Engineering stress is defined as the measured load divided by the initial cross-sectional area. Engineering strain is defined by the measured deflection divided by the initial length of the specimen. The energy dissipated by an impact-limiting material is equal to the area under the load-deflection curve and hence is proportional to the area under the stress-strain curve. For this discussion, lock-up is defined as 125% of crush strength where the crush strength is defined as the engineering stress at 0.3 strain.

The aluminum honeycomb composite results are shown in Figure 2. These curves have an initial linear portion representing the elastic deformation. As the load increases, the peak or buckling strength of the honeycomb is reached. The peak occurs at small deformation and hence represents limited energy dissipation. The peak stress is followed by a reduction in stress to a constant stress plateau representing the crush strength of the material. This plateau lasts until lock-up is initiated at 70 to 80% strain. During this crush to lock-up, most of the energy is dissipated. Past lock-up energy dissipation results in significantly larger and increasing stresses.

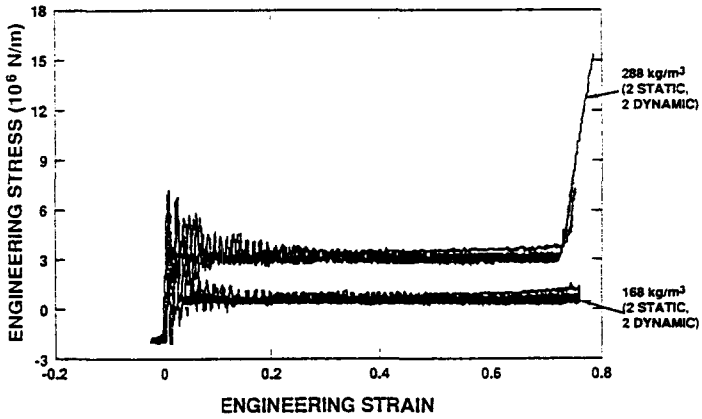

Figure 2. Aluminum Honeycomb Composite Results

The polyurethane foam results are shown in Figure 3. These curves show an initial low energy dissipation elastic response which transitions into a plateau region representing the crush of the foam. As the foam crushes, it hardens as represented by the upward slope of the plateau. Unlike the honeycomb, there is no sharp transition at lock-up. Instead, the slope of the curve continues to increase resulting in a smooth transition to the higher decelerations resulting from increasing stress. Another foam characteristic is the significant increase in strength at dynamic versus quasi-static load rates. In particular, the low-density foams experienced an approximately 40% increase in crush strength at dynamic rates and the high-density foams experienced an approximately 50% increase in dynamic crush strength.

THERMAL TESTS

The thermal tests subjected the materials to a 30-min exposure to a radiant heat environment. The radiating surface was controlled to 800°C (+30°C/-0°C) with an emissivity greater than 0.9. The intent of the thermal tests was to provide a comparison of the ability of the materials to limit the heat flux into the packaging.

The samples consisted of cylinders of crushable material that were 12.7 cm in diameter and 7.6 cm thick. Thermocouples were placed in the samples as shown in Figure 4. Data were acquired every 10 s during the heating and every minute for 90 min during cool-down. The circumference of each sample was wrapped with a ceramic fiber insulation to provide a radial adiabatic boundary. The back

face of each sample was also insulated with a 5-cm-thick section of insulation. Two samples were tested simultaneously as shown in Figure 4.

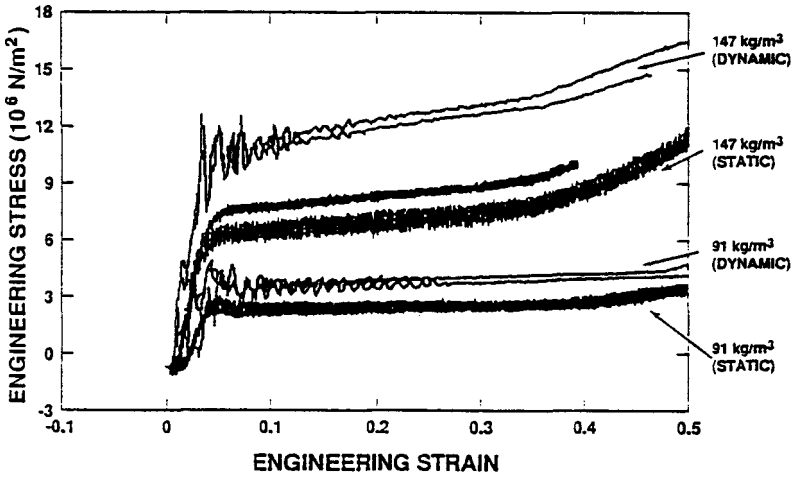

Figure 3. Polyurethane Foams Composite Results

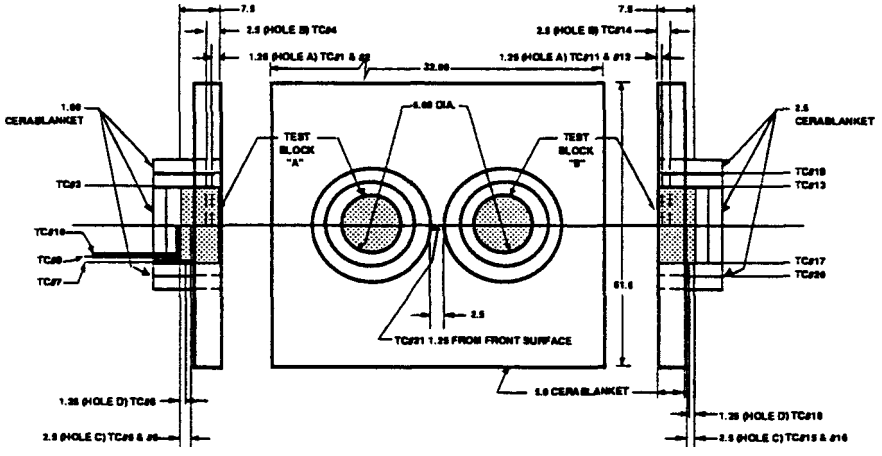

Figure 4. Thermal Test Setup

Two independent tests of each of the four different materials were performed. Each test consisted of two identical samples. The responses of 16 samples were recorded. The data are in the form of temperature histories at each location.

THERMAL TEST RESULTS

The radial data for a given axial location were used to demonstrate that the heat transfer was essentially one-dimensional. This section will discuss the results of the axial temperature distributions.

The axial temperature distribution for a low-density aluminum honeycomb is shown in Figure 5. This figure is representative of both honeycomb densities. The axial gradients through the honeycombs are small. These results indicate that the open-celled honeycomb provides minimal thermal protection.

The low-density polyurethane foam material samples experienced substantial burning during radiant heat testing. Representative data for the behavior of this material are given in Figure 6. These data

indicate that once the foam was ignited, the burning and associated charring continued until the back-face temperatures were as great as that of the incident radiant environment. This was supported by the posttest material that showed the sample had been reduced to a small amount of residual char.

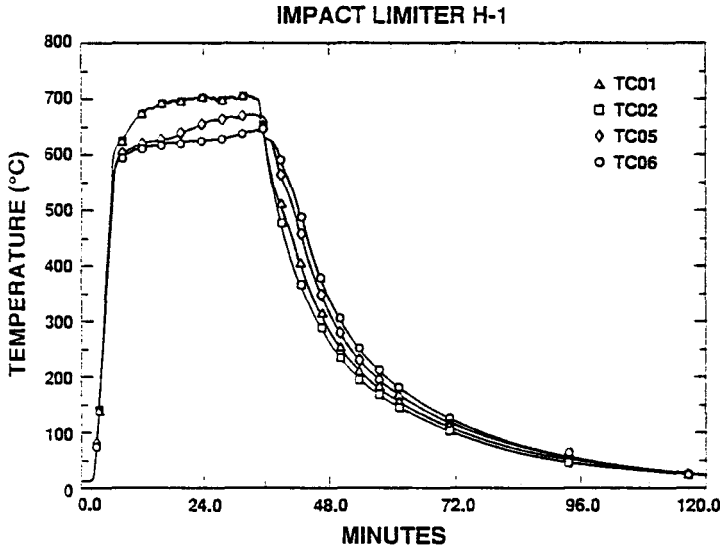

Figure 5. Axial Temperature Distribution for Aluminum Honeycomb

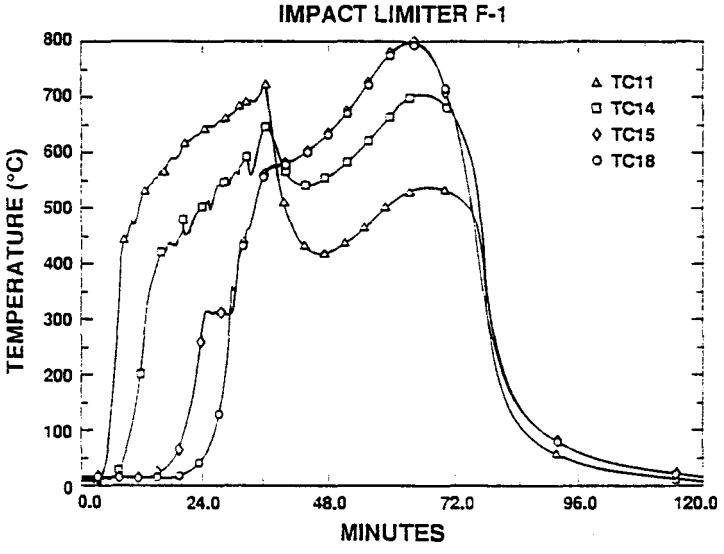

Figure 6. Axial Temperature Distribution for Low-Density Polyurethane Foam

The data for the high-density foam illustrated significantly different results as shown in Figure 7. These curves indicate good insulating capability. The back face temperature is less than 260°C. The posttest examination showed charring only of the front half of the materials, indicating that a self-sustaining charring front could not form as it did in the low-density material. These results indicate that the high-density foam can provide a good thermal resistance even in the presence of air.

FIGURES OF MERIT

In order to select materials for use in impact limiters, simple methods for screening those materials are needed. Three methods for evaluating structural response and one method for evaluating thermal response were used.

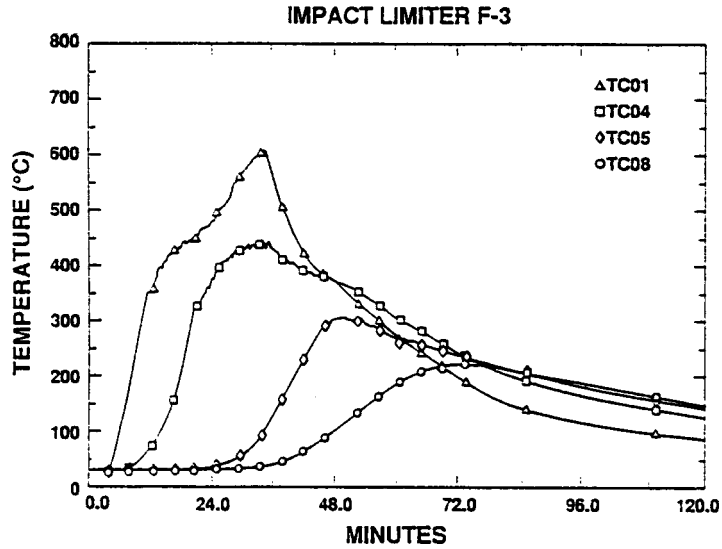

Figure 7. Axial Temperature Distribution for High-Density Polyurethane Foam

The structural figures of merit focus on the energy absorbed. These are discussed in detail in Duffey et al., 1992. The first structural figure of merit is the energy absorbed per unit mass of sample. This figure of merit should be used where weight of the packaging is a critical parameter. The energy is obtained by integrating the area under the load-deflection curves. The mass of the sample is known. The results are shown in Figure 8. The dynamic case is of most interest. For that case, while the aluminum honeycomb has the highest figure of merit, the high-density polyurethane foam is comparable without the need to control the crush direction inherent when using honeycomb.

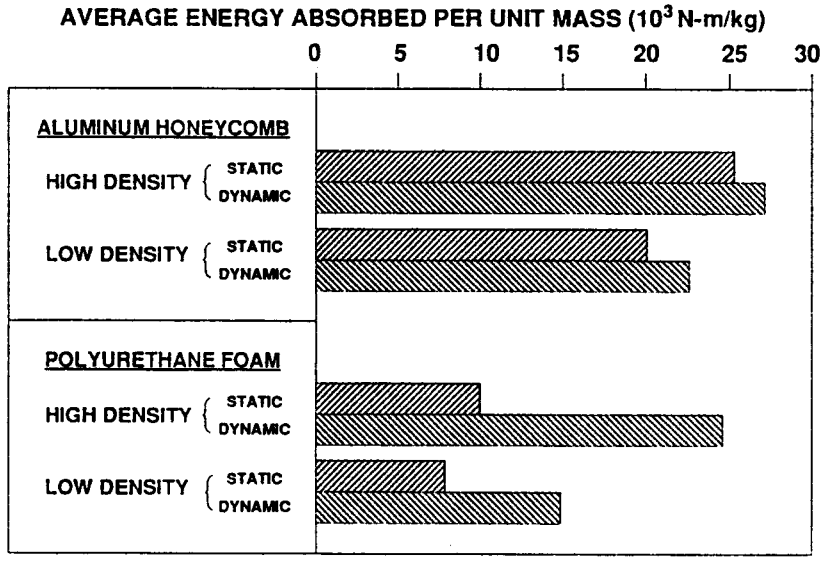

Figure 8. Energy Absorbed per Unit Mass

The second structural figure of merit is the energy absorbed per unit volume of sample. This figure of merit should be used where the size of the impact limiter is the controlling parameter. In this case, shown in Figure 9, the high-density polyurethane foam under dynamic loading is clearly the preferred material. This indicates that for a volumetrically constrained design, the polyurethane foam would be selected.

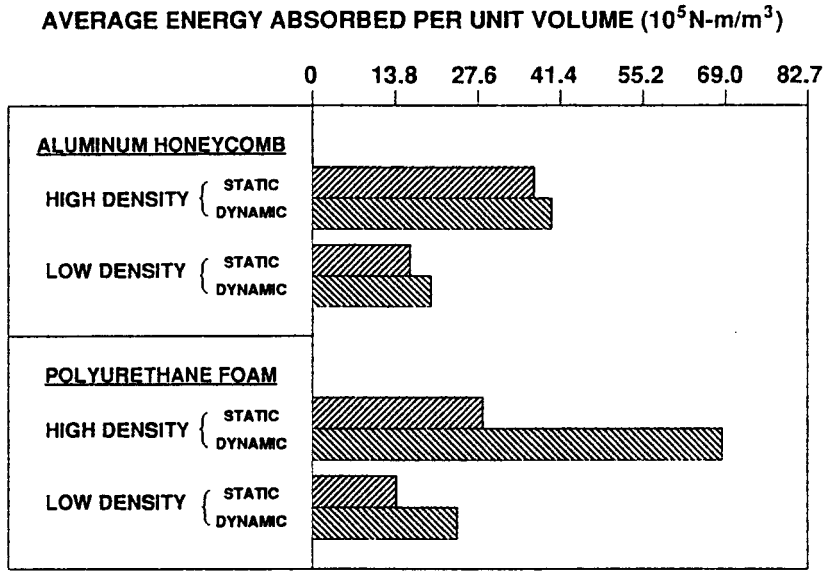

Figure 9. Energy Absorbed per Unit Volume

A third structural figure of merit uses the Janssen factor to determine the optimal strain. The optimal strain is then used to determine the energy absorbed per unit volume. The Janssen factor can be defined as the ratio of the peak acceleration observed with the sample to that which would be produced by an ideal material (one which is capable of crushing at constant crush stress to zero volume). To use this method, the optimal strain is determined from the stress-strain curve. The optimal strain occurs where a line from the origin is tangent to the stress-strain curve (see Duffey et al., 1992 for detailed discussion). The energy absorbed is determined by integrating the area under the curve to that optimal strain. The energy absorbed per unit volume is then plotted as in Figure 10. This procedure, while providing similar results for these materials as for the energy absorbed per unit volume based on lock-up, provides a more rigorous method of obtaining the maximum strain instead of relying upon an arbitrary selection of the lock-up point.

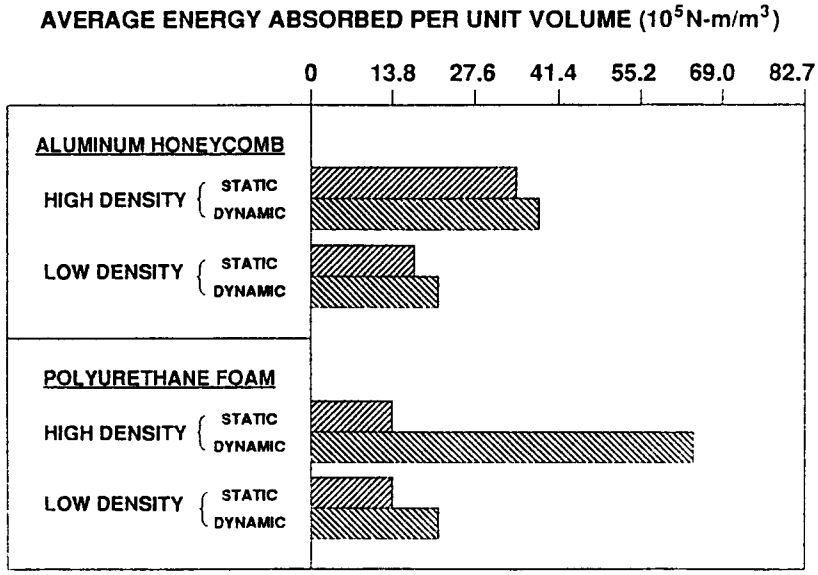

Figure 10. Energy Absorbed per Unit Volume Using Janssen Factor

The thermal figure of merit is based on treating the heat transfer through the impact-limiting material as a transient heat conduction problem. This simplification of the heat transfer phenomenon allows comparison of an "effective" thermal diffusivity. This "effective" thermal diffusivity is approximated by:

$$\frac{T(0,30) - T(0, 0)}{T(1,30) - T(0,30)}$$

where T(l,t) is the temperature as a function of the distance, l, from the insulated back-face and the time, t, in minutes from start of heating. This diffusivity includes the effects of the heat transfer by conduction, convection, and radiation and the effects of heat storage and/or generation. Using this "effective" thermal diffusivity as the thermal figure of merit produces the results shown in Figure 11. In this graph, the smaller the figure of merit, the more appropriate the material for limiting the thermal flux. In this case, the high-density char forming polyurethane foam is the most appropriate material.

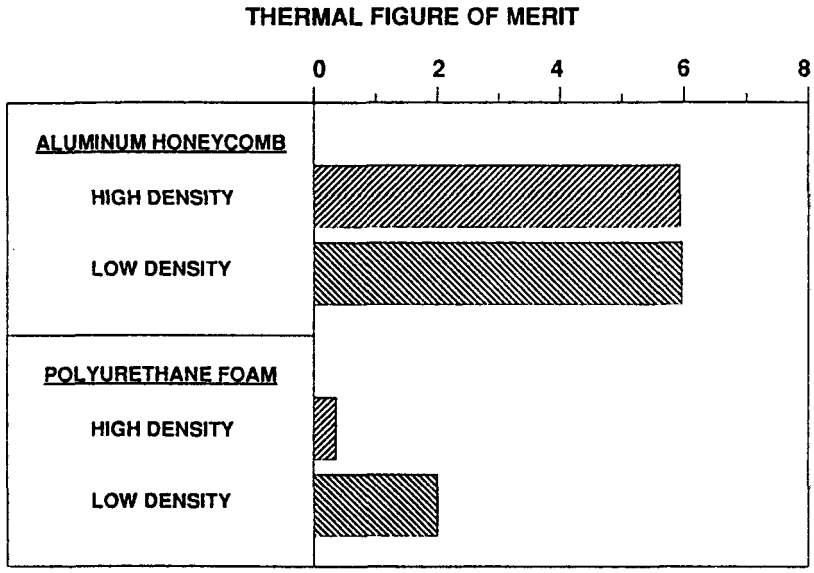

Figure 11. "Effective" Thermal Diffusivity

CONCLUSIONS

In this paper we have presented methods for characterizing impact-limiting materials, representative data obtained in materials characterization and figures of merit which can be used for selection among available materials. The figures of merit have been developed to address specific needs of the packaging design community such as minimizing the weight of the impact limiter for a given weight of packaging and protecting against the fire environment.

REFERENCES

Berry, R. E., Hill, T. K., Joseph, W. W., and Clarke, R. K., "Accident Resistant Container: Materials and Structures Evolution," SAND74-0010, Sandia National Laboratories, Albuquerque, NM, August 1975.

Duffey, T. A., Glass, R. E., and McConnell, P., "Characterization of Impact-Limiting Material," SAND92-0773/TTC-1207, Sandia National Laboratories, Albuquerque, NM, May 1992.

Hill, T. K. and Joseph, W. W., "Energy-Absorbing Characteristics of Materials," SLA74-0159, Sandia National Laboratories, Albuquerque, NM, May 1974.

McConnell, P., Ritchey, G., and Adler, W., "Effects of Loading Rate on the Compressive Strength of Constrained Impact Limiter Materials," CR-86-1063, General Research Corporation, Santa Barbara, CA, July 1986.

Neilsen, M. K., Morgan, H. S., Krieg, R. D., and Yoshimura, H. R., "Development of a Phenomenological Constitutive Model for Polyurethane Foams," PATRAM'89 Proceedings, pp. 79-86.

Title 10, Code of Federal Regulations, Part 71, Nuclear Regulatory Commission, Washington, D.C., 1 January 1988.

Over-the-Road Testing of Radioactive Materials Packagings*

R. E. Glass and K. W. Gwinn

Sandia National Laboratories, Albuquerque, New Mexico, United States of America**

INTRODUCTION

Sandia National Laboratories has an ongoing program to characterize the environments encountered during normal surface transport of radioactive materials. This effort consists of obtaining experimental data from both road simulator and over-the-road tests and of analyzing the data to obtain numerical models to simulate those environments (Glass and Gwinn, 1986, 1987, 1989; Gwinn et al., 1991).

These data and models have been used to define the design basis for resistance to shock and vibration and the requirements for tiedowns of truck-transported radioactive materials. This work is in conjunction with the American National Standards Institute (ANSI) standards development for radioactive materials transport.

This paper summarizes the data (Gwinn et al., 1991) from a series of over-the-road tests performed with Chem-Nuclear Systems, Inc. equipment near Barnwell, South Carolina. The data include packaging responses to driving over various road types as well as measurements of packaging and trailer responses to hard braking and turning events. The data also include the responses of both flexible and rigid tiedown systems. The results indicate that the tiedown forces for these tests were less than 0.06 g based on packaging weight.

EVENTS

Each test consisted of a trailer and packaging being subjected to nine separate events to determine both the acceleration and tiedown loads experienced during normal transport. Five types of roads (Gwinn et al., 1991) were used: (1) smooth asphalt primary, (2) rough asphalt primary, (3) rough concrete primary, (4) rough asphalt secondary, and (5) spalled asphalt secondary. The roads provided a vibrational environment for the packaging. To subject the packaging to shock environments, a railroad crossing and bridge approach were selected. Finally, to determine the package's response to maneuvering, a hard turn and hard stop were executed. The speed driven for each event was the lesser of either the posted legal speed limit or the fastest speed consistent with the safe operation of the tractor. The events for each packaging test are given in Table 1.

---

*This work was performed at Sandia National Laboratories, Albuquerque, New Mexico, supported by the United States Department of Energy under Contract DE-AC04-76DP00789.

**A United States Department of Energy Facility.

Table 1. Events

Event	Primary Load Type	Description
1	Vibration	Smooth Asphalt Primary
2	Shock	Railroad Grade Crossing
3	Vibration	Rough Asphalt Primary
4	Shock	Bridge Approach
5	Vibration	Rough Concrete Primary
6	Rigid Body	Hard Turn
7	Rigid Body	Hard Stop
8	Vibration	Rough Asphalt Secondary
9	Vibration	Spalled Asphalt Secondary

PACKAGINGS

Two test packagings, the CNS 14-170 and CNS 3-55, were selected based on the weight and tiedown type. Test 1 used the CNS 14-170, a lead and steel Type A package used to ship dewatered or solidified waste materials. The package has an empty weight of 15,330 kg and a payload of 6350 kg. It is transported vertically and has a flexible tiedown system.

Test 2 used the CNS 3-55, a steel-encased lead-shielded Type B package. The packaging weight is 28,800 kg with a payload capacity of 4180 kg. The package is transported horizontally in a cradle representative of a rigid tiedown system.

INSTRUMENTATION

The primary roles of the instrumentation were to obtain the acceleration at various points on the trailer and package, and to either directly measure forces in the flexible tiedown, or to measure strains in the cradle which can be used to determine forces acting on the cradle tiedown. The locations and measurements obtained from each instrument are given in Table 2. Nine instruments were used in each test.

Table 2. Instrumentation Locations

Instrument	Test	Location	Measurement
1	1,2	Package Top	Transverse Acceleration
2	1,2	Package Top	Vertical Acceleration
3	1,2	Package Top	Longitudinal Acceleration
4	1,2	Trailer Center	Vertical Acceleration
5	1,2	Trailer Rear	Vertical Acceleration
6	1,2	Trailer Rear	Longitudinal Acceleration
7	1,2	Trailer Front	Vertical Acceleration
8	1	Front Tiedown	Separation Force
8	1	Rear Tiedown	Separation Force
9	2	Front Tiedown Strap	Vertical Strain
9	2	Rear Tiedown Strap	Vertical Strain

A triaxial accelerometer was placed on the package's center top to measure the package response along each axis. The package stiffness made this measurement representative of the entire package. At the same longitudinal location, an accelerometer measured the trailer's vertical acceleration. Longitudinal and vertical accelerometers were placed on the trailer bed over the rear axle, and a vertical accelerometer was placed on the trailer over the kingpin. The combination of vertical accelerometers at these three trailer locations allowed the bounce, pitch, and bending modes (Glass and Gwinn, 1986) to be detected. The longitudinal and transverse accelerometers were used to detect the effects of braking and turning.

The response of the tiedowns was determined from load cells in the links between attachment points on the CNS 14-170 and with strain gages mounted on the cradle straps for the CNS 3-55. The load cell was zeroed after preloading so that only transport-induced loads were measured. The strain gages were arranged in a bridge to remove the bending effects and hence measure only the strain in the direction of the strap.

TEST RESULTS

This section summarizes the results of the over-the-road tests. The complete data set is included in Gwinn et al., 1991. The data were obtained in the form of time histories which provide the mean-to-peak response at different locations. From these time histories, the auto spectral density (PSD) was generated for vibrational events. The PSD transforms the time history data into the frequency domain to relate how the response energy varies as a function of frequency. From this data, the vibration modes contributing to the overall response were determined, and the root-mean square (RMS) response was calculated. Figure 1 shows representative samples of time histories and the corresponding PSDs.

The railroad grade crossing and bridge approach shock events were not vibrational events and hence PSD calculations were not appropriate. Rigid body events, such as the hard turn and hard stop, were performed to determine the response magnitude only.

The time history shown in Figure 1a is the measured vertical acceleration of the rear trailer bed in response to the spalled asphalt event for Test 1. This figure shows a fairly severe vibrational environment, with two large transient events occurring 3 and 9 seconds into the run. Figure 1b shows the PSD of the same response in the frequency domain. The larger response at 1.5 Hz is due to the first bounce mode of the tractor/trailer combination (Glass and Gwinn, 1986). This vehicle bounce mode was caused by the structure bouncing in unison with the suspension system of the trailer. The next response at 4 Hz is the frequency of the vehicle's first pitching mode (Glass and Gwinn, 1986). This was caused by the kingpin/rear tractor front suspension deflecting. The high-frequency modes from 10 to 20 Hz are combinations of the trailer bending with the tractor pitching and bending.

Figures 1c and 1d show the comparable responses for the vertical accelerations at the top of the packaging. Note that the acceleration levels for the top of the packagings are approximately an order of magnitude smaller than those at the rear of the trailer. Also of note is that the first bounce mode dominated the packaging response whereas the response at the rear of the trailer was dominated by higher frequency modes.

Table 3 summarizes the peak acceleration results for each test. The RMS responses are presented in Table 4 and the tiedown responses are given in Table 5.

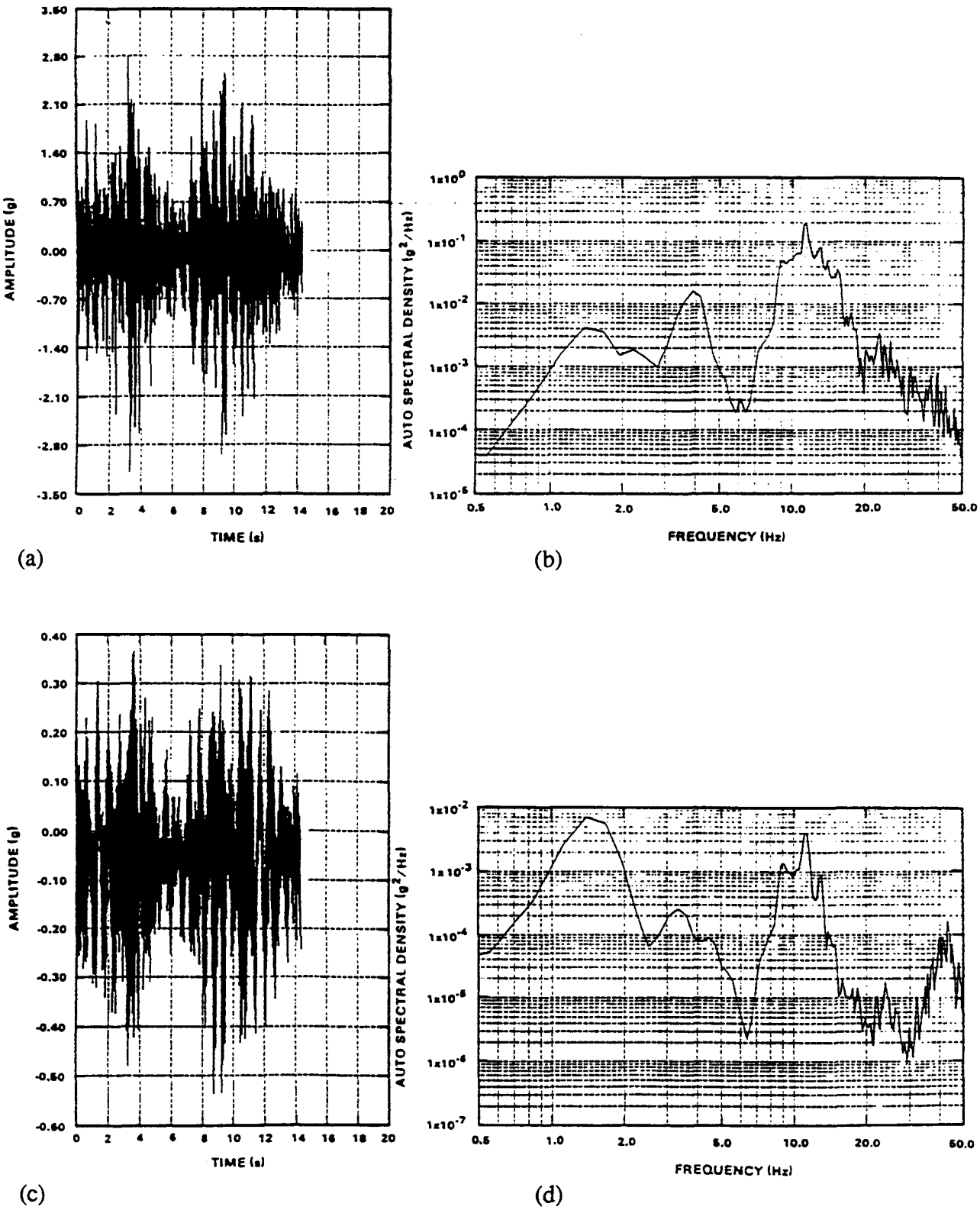

Figure 1. Comparative time histories and PSDs for the CNS 14-170 test of the spalled asphalt event: (a) time history, vertical acceleration, rear trailer bed; (b) PSD equivalent of (a); (c) time history, vertical acceleration, package top; and (d) PSD equivalent of (c).

Table 3. Peak Accelerations (g) for Shock and Vibration Events

Test/Accelerometer	Event - CNS 14-170						
	1	2	3	4	5	8	9
1/1	0.17	0.16	0.21	0.28	0.12	0.13	0.22
1/2	0.23	0.62	0.32	0.45	0.20	0.35	0.58
1/3	0.17	0.90	0.38	0.63	0.22	0.64	0.88
1/4	0.21	2.30	0.37	0.85	0.07	0.07	0.08
1/5	0.46	5.30	1.40	4.60	0.95	1.68	3.10
1/6	0.14	2.80	0.37	1.65	0.22	0.43	0.85
1/7	0.73	4.50	1.70	3.40	1.30	2.70	4.50
	Event - CNS 3-55						
	1	2	3	4	5	8	9
2/1	0.10	0.14	0.13	0.11	--	0.34	--
2/2	0.12	0.47	0.25	0.23	0.12	0.37	0.20
2/3	0.12	0.50	0.15	0.45	--	0.38	0.28
2/4	0.09	0.80	0.25	0.32	0.17	0.35	0.22
2/5	0.55	5.90	1.40	2.40	1.00	2.70	1.95
2/6	0.13	3.00	0.21	0.47	0.30	0.81	0.40
2/7	0.85	6.50	1.10	3.40	1.20	3.40	2.65

Table 4. RMS Acceleration (g) for Vibration Events

Test/Accelerometer	Event - CNS 14-170				
	1	3	5	8	9
1/1	0.042	0.043	0.025	0.027	0.054
1/2	0.041	0.096	0.050	0.066	0.125
1/3	0.041	0.057	0.055	0.143	0.227
1/4	0.040	0.093	0.010	0.011	0.011
1/5	0.135	0.211	0.233	0.401	0.718
1/6	0.030	0.042	0.059	0.088	0.180
1/7	0.201	0.294	0.403	0.571	1.030
	Event - CNS 3-55				
	1	3	5	8	9
2/1	0.020	0.032	--	0.042	--
2/2	0.027	0.072	0.024	0.075	0.043
2/3	0.023	0.035	--	0.097	0.075
2/4	0.027	0.069	0.028	0.078	0.048
2/5	0.280	0.230	0.240	0.650	0.530
2/6	0.028	0.042	0.058	0.110	0.096
2/7	0.102	0.220	0.320	0.770	0.630

Table 5. Peak Tiedown Loads (kg)

Test/Accelerometer	Event - CNS 14-170								
	1	2	3	4	5	6	7	8	9
1/8	195	317	263	180	99	360	284	158	207
1/9	99	293	162	135	68	248	216	126	293
	Event - CNS 3-55								
	1	2	3	4	5	6	7	8	9
2/8	855	--	918	--	509	432	--	927	756
2/9	1139	--	1058	918	702	648	--	1404	990

The test results can be normalized to indicate the dependence of the accelerometer response amplitude on both the type of event and the accelerometer location. The normalized vertical accelerations measured during the CNS 3-55 test at four locations for the shock and vibration events are given in Table 6. The data are normalized to the rail crossing acceleration at each accelerometer location. This approach to the data results in a comparison of relative severity of the events. The rail crossing responses are the most severe at each of the accelerometer locations. The secondary asphalt produces accelerations that range from 40 to 80% of the rail crossing results and the least severe event, the smooth asphalt, produces accelerations ranging from 10 to 26% of the rail crossing results. These results indicate that events that include vertical discontinuities in the road surface lead to the largest vertical accelerations.

Table 6. Event Dependence of Vertical Accelerometer Response Normalized with Respect to the Rail Crossing Response

	Trailer Rear	Package Top	Trailer Middle	Trailer Front
Smooth Asphalt	0.093	0.26	0.11	0.13
Rail Crossing	1.00	1.00	1.00	1.00
Rough Asphalt	0.24	0.53	0.31	0.16
Bridge Approach	0.41	0.49	0.40	0.52
Rough Concrete	0.17	0.26	0.21	0.18
Secondary Asphalt	0.46	0.79	0.44	0.52
Spalled Asphalt	0.33	0.43	0.28	0.41

The variation of the response as a function of accelerometer location is shown in Table 7. This table gives the data for the CNS 3-55 test normalized to the response of the trailer front. In all cases, the greatest response, even for this uniformly distributed load, is at the trailer front or trailer rear. The response on the package at the mid-point of the trailer is less than 20% of the peak response. These results indicate that care must be taken in evaluating the packaging response based on the trailer response.

Table 7. Spatial Dependence of Vertical Accelerometer Normalized with Respect to the Trailer Bed Front Response

	Trailer Rear	Package Top	Trailer Middle	Trailer Front
Smooth Asphalt	0.65	0.14	0.11	1.0
Rail Crossing	0.91	0.072	0.12	1.0
Rough Asphalt	1.33	0.24	0.24	1.0
Bridge Approach	0.71	0.068	0.094	1.0
Rough Concrete	0.83	0.10	0.14	1.0
Secondary Asphalt	0.79	0.11	0.10	1.0
Spalled Asphalt	0.74	0.075	0.083	1.0

The data also provide insight on the relative response of tiedown systems. Current regulations (49 CFR 393, "Parts and Accessories Necessary for Safe Operation") and the draft ANSI tiedown standard (ANSI, 1992) both relate the design of tiedowns to 1.5 times the weight of the packaging. To determine how the tiedowns responded with respect to these values, Table 8 presents the tiedown load divided by the weight of the packaging. The loads range from 0.004 to 0.024 of the weight of the packaging. The results for the CNS 3-55 range up to 0.055. These loads are far less than those derived from either the regulatory requirements or the draft ANSI standard.

Table 8. Tiedown Loads Divided by Packaging Weight

CNS 14-170	Front Tiedown	Rear Tiedown
Smooth Asphalt	0.013	0.007
Rail Crossing	0.021	0.019
Rough Asphalt	0.017	0.011
Bridge Approach	0.012	0.009
Rough Concrete	0.007	0.004
Hard Turn	0.024	0.016
Hard Stop	0.019	0.014
Secondary Asphalt	0.010	0.008
Spalled Asphalt	0.014	0.019

CONCLUSIONS

The data show the dependence of the accelerometer responses on both the type of event and location of the accelerometer. In particular, the greatest peak accelerations result from events that have surface discontinuities, such as the rail crossing and bridge approach.

The dependence of the accelerometer responses on accelerometer location shows that only select locations on the trailer correspond to packaging response. The center of the trailer, for example, corresponds reasonably well with the packaging response, but the extremities of the trailer experience much higher accelerations than the packaging. This indicates that the packaging

response should be measured directly, if possible, and only extrapolated from trailer response where the correlation is well known.

Finally, the tiedown response data demonstrate that current regulations and proposed standards require tiedowns that are capable of withstanding much greater loads than those observed during these normal condition tests. This indicates that the current design standards are adequate to ensure that the package is retained on the trailer during normal transport.

REFERENCES

ANSI (American National Standards Institute), "Proposed American National Standard: Tiedowns for Truck Transport of Radioactive Materials," July 1992.

Glass, R. E. and Gwinn, K. W., "Shock and Vibration Environments: Test and Analysis," Institute of Nuclear Materials Management, 27th Annual Meeting, June 1986.

Glass, R. E. and Gwinn, K. W., "TRUPACT-I Over-the-Road Test," SAND87-0513, Sandia National Laboratories, Albuquerque, NM, 1987.

Glass, R. E. and Gwinn, K. W., "Design Basis for the Resistance to Shock and Vibration," 9th International Symposium on the Packaging and Transport of Radioactive Materials, June 1989.

Gwinn, K. W., Glass, R. E., and Edwards, K. R., "Over-the-Road Tests of Nuclear Materials Package Response to Normal Environments," SAND91-0079, Sandia National Laboratories, Albuquerque, NM, December 1991.

Title 49, Code of Federal Regulations, Part 393 Nuclear Regulatory Commission, Washington, D.C., December 31, 1991.

The Development of an On-Site Container*

R. E. Glass, M. E. McAllaster, and P. L. Jones

Transportation Systems Technology Department, Sandia National Laboratories,**
Albuquerque, New Mexico, United States of America

A. L. McKinney

U.S. Army Chemical Materials Destruction Agency, Aberdeen Proving Ground, Maryland,
United States of America

INTRODUCTION

Sandia National Laboratories (SNL) has developed a package for the on-site transport of chemical munitions for the U.S. Army. This package was designed to prevent the release of lethal quantities of chemical agents during transportation of munitions to the demilitarization facilities on-site. The packaging prevents auto-ignition of the munitions by limiting the thermal and structural assault on the munitions during an accident. This package, with some modifications to account for contents, may be suitable for the on-site transport of mixed wastes at United States Department of Energy facilities. This paper discusses the design and verification testing of the package.

The safety criteria for the package were modeled after the International Atomic Energy Agency (IAEA) hypothetical accident sequence and modified to take credit for operational controls. The modified accident sequence consisted of drop, puncture, and thermal events. The post-accident leak rate was established to prevent harm to an exposed worker.

The packaging has a mass of 8600 kg and can accommodate up to 3600 kg of contents. The interior of the package is 188 cm in diameter and 232 cm long. Two sample ports can be used to sample the interior of the package prior to opening the closure and an o-ring test port can be used to determine the leak rates prior to and after transport.

DESIGN CRITERIA

The objectives of the design criteria (Klevans, 1988) were to produce a packaging design that was safe, operationally efficient, and provided appropriate interfaces with loading and unloading facilities. The safety of the packaging was assured by designing the package to meet specific performance criteria that consisted of a set of hypothetical accident conditions including drop, puncture, crush, and fire after which the leak rate was not to exceed 1×10^{-1} std cc/s. Normal conditions specify a leak rate not to exceed 1×10^{-3} std cc/s (ANSI, 1987).

---

*This work was performed at Sandia National Laboratories, Albuquerque, New Mexico, supported by the United States Department of Energy under Contract DE-AC04-76DP00789.

**A United States Department of Energy Facility.

The hypothetical accident sequence included crush, drop, puncture, and burn tests. The crush test consisted of subjecting the package to a compressive load of 22,700 kg applied to the top of the package. The drop test consisted of a 3-m free drop of the package onto a flat, essentially unyielding surface. The drop height was based on a maximum convoy velocity of 28 km/hr during munitions transport. The puncture test consisted of a 1-m free drop of the package onto a 15.2-cm-diameter mild steel bar. The drop and puncture tests were required to be performed with the package orientation such that maximum damage would occur. To prevent auto-ignition, the maximum rigid body deceleration of the containment vessel during the drop and puncture testing could not exceed 300 g.

The fire test consisted of fully engulfing the package in a JP-4 fuel/air fire for a period of 15 min. The 15-min fire is consistent with the maximum amount of fuel that will be available to fuel a fire during the munitions transport. The fuel source was to extend horizontally at least 1 m beyond any external surface of the package, and the package was positioned 1 m above the surface of the fuel source. The package was not to be artificially cooled following the 15-min exposure. To prevent auto-ignition, the inner wall of the vessel was not to exceed 120°C.

The criteria imposed logistics requirements on the package design. These included: (1) the maximum exterior envelope of the package was 2.6 m wide x 2.6 m tall x 3.66 m long, (2) the interior vessel was 1.88 m in diameter and 2.32 m in length, (3) the package was to contain a sample port to allow routine monitoring of the containment vessel for agent, (4) the sample was to be obtained prior to opening the door, (5) the package was to incorporate a leak-testable seal design to allow periodic testing of the closure seals, and (6) the package was to incorporate ISO corners to facilitate package handling and transport.

DESIGN

The package design criteria resulted in several features that will be discussed in this section. Figure 1 shows the side view of the packaging. The packaging is 3.57 m long and 2.59 m on a side. The left side of the figure shows the closure. It consists of a commercially available 1.27-cm-thick stainless steel pressure vessel head. The pressure vessel head is welded to a flange that transitions from 1.27 to 10.8 cm thick. This flange contains the modular swing bolts, sample ports, o-ring test ports, and o-ring seals. The closure is hung on a hinge that provides smooth operation of the closure. On the body side of the package is the mating flange that transitions back to the 1.27-cm-thick stainless steel cylindrical shell. The right end uses the same pressure vessel head. For ease of handling, there are eight ISO corners attached to the package via stainless steel tubing in a tripod arrangement. The tubing allows loads on the ISO corners to be transmitted directly to the cylindrical portion of the package which provides a strong, integrated response to lifting loads.

A cross-sectional view through the flange of the packaging is shown in Figure 2. This figure shows the ISO corners at the top and bottom, the hinge on the right-hand side, and the cylindrical vessel. The closure is secured with seventeen swing bolts. In the lower half of the view, two sample ports are shown on the left- and right-hand sides. The munitions that are loaded in the package are placed on aluminum trays. The trays are placed on a honeycomb insert which rests on a rail in the bottom of the package. The rail prevents the insert from rotating in the package during transport. The trays are guided by a guide rail into the packaging to ensure that the munitions fit.

A cross-sectional view through the longitudinal axis of the package is shown in Figure 3. From outside to inside, the features of the wall include a 1.27-cm-thick cylindrical, stainless steel containment vessel; a 7.5-cm-thick ceramic fiber insulating layer; 10.5 cm of polyurethane foam; and a 0.48-cm-thick stainless steel inner shell. The outer stainless steel containment

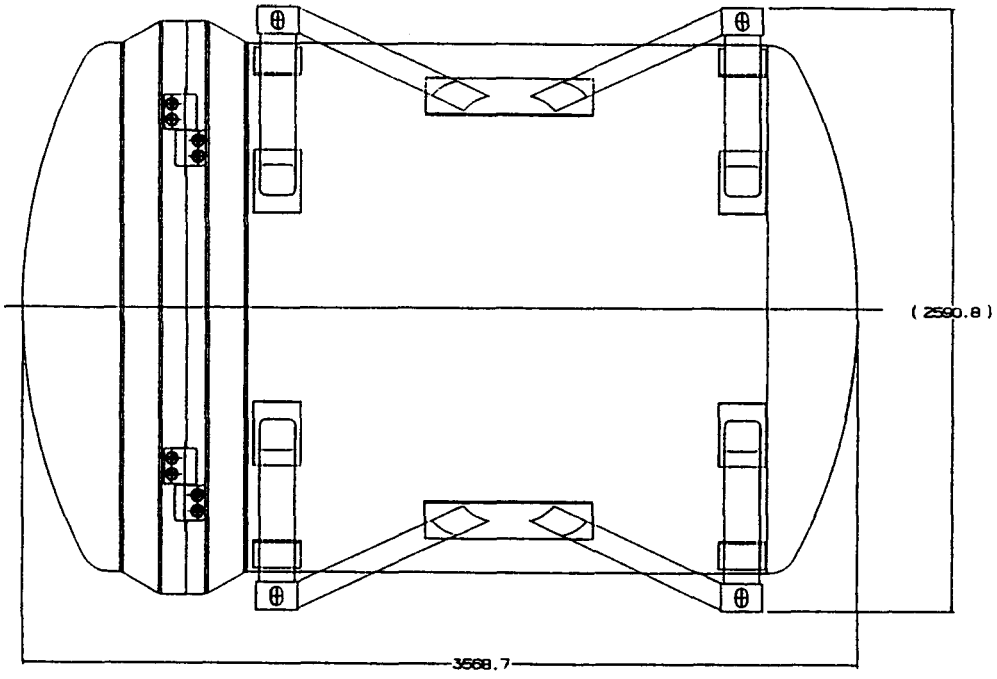

Figure 1. Side View of the On-Site Container

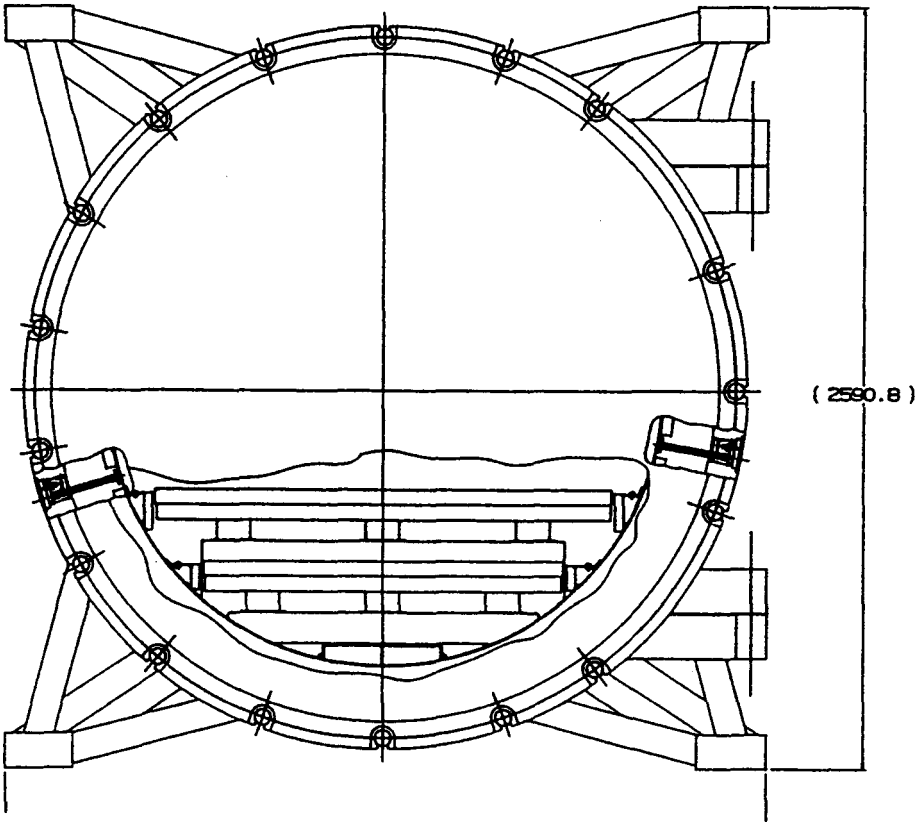

Figure 2. Cross-Sectional View Through the Closure Joint of the On-Site Container

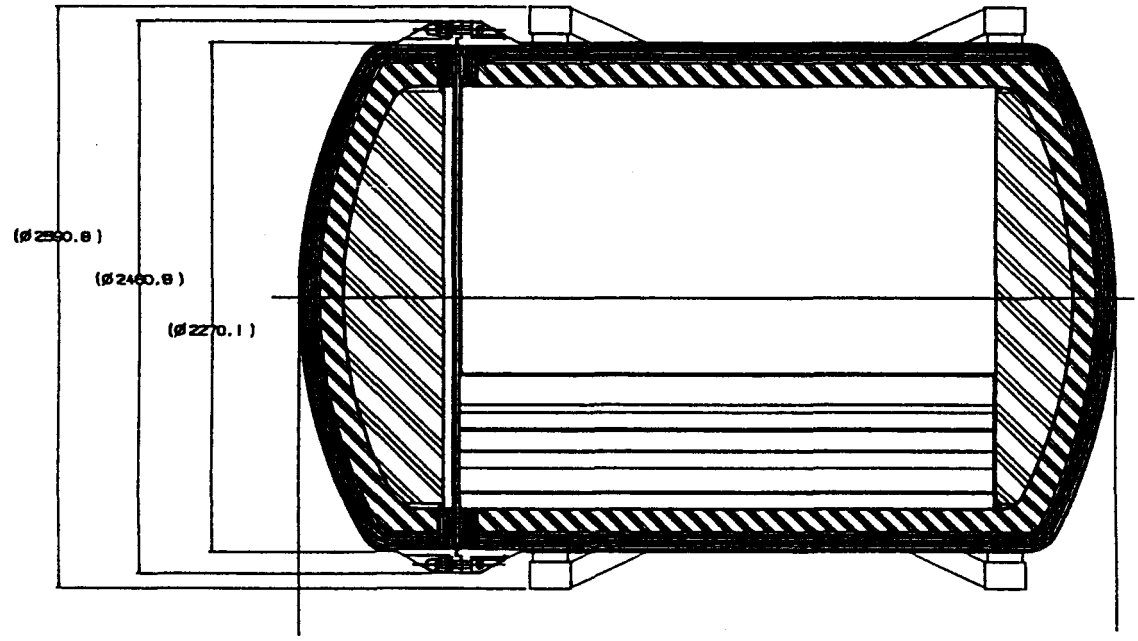

Figure 3. Longitudinal Cross-Sectional View of the On-Site Container

vessel provides puncture protection and impact resistance. The ceramic fiber limits the heat input to the package's contents during the fire and in particular keeps the fiber/foam interface temperature below 175°C. The foam provides both internal and external impact-limiting features and thermal protection that keeps the interior of the vessel below 120°C during the fire test. The inner shell provides an easily decontaminated and impact-limiting surface for the contents. The interior front and rear of the package contain foam-filled, steel clad internal impact limiters that limit the deceleration of the munitions during accident conditions.

VERIFICATION TESTING

A prototype packaging was fabricated for SNL at Gregory Enterprises, Inc. in Carlsbad, New Mexico. This packaging was subjected sequentially to (1) a 22,700-kg static crush test, (2) three 3-m free-drop tests, (3) three 1-m puncture tests, and (4) an all-engulfing JP-4 pool-fire test. The swing bolt assemblies failed during the fire test due to liquid metal embrittlement of the cadmium-plated 4340 bolt material (Robino and Van Den Avyle, 1992). Following the pool-fire test, the bolts were redesigned to use A286 steel which does not require plating for this application and which has stable structural response up to 650°C. The prototype was rebuilt by replacing the fiber insulation, foam, and interior shell. During the rebuild, it was determined that there was no thermal degradation of the foam. Following the rebuild, the prototype was again subjected to a pool-fire test. The results of this test included a package leak rate of 8.9×10^{-2} std cc/s and thus successful completion of the design phase of the project.

The static crush test consisted of placing a concrete slab weighing 22,750 kg on the four upper ISO corners. The slab was left in place for 5 min and then removed. No visible damage resulted from this test.

The setup for the free-drop tests is shown in Figure 4. This photograph shows the package suspended above the target. The distance from the target to the lowest point on the packaging was measured and recorded. Photographic coverage included video and still photography with 400 frame/s and 2000 frame/s cameras. The package was dropped using explosive cable

cutters. The trigger for the explosive cable cutters also initiated the Mobile Instrumentation Data Acquisition System (MIDAS) (Uncapher, 1990).

Figure 4. On-Site Container Suspended 3 m Over the Unyielding Target

The design criteria required that the free-drop test of the packaging occur in the most damaging orientation. To ensure that the drop test sequence met this requirement, the package, loaded with 155-mm projectiles, was dropped in three orientations. These orientations included a: (1) flat side, (2) center-of-gravity over corner, and (3) flat end drop. The criteria also required that the containment vessel's rigid body decelerations be less than 300 g. The flat side drop generated the largest decelerations. Figure 5a shows the wide band data for the accelerometer that measured the vertical deceleration through the center-of-gravity. This accelerometer was mounted on the outside of the containment vessel. The wide band data show total accelerometer peak response of approximately 800 g. The wide band data also show the package's primary and secondary impacts on the target at 0, 60, 310, and 350 ms. Figure 5b shows the accelerometer data filtered at 500 Hz. The data show the package's rigid body deceleration of 240 g. Comparing the rigid body responses for the three drop events, the center-of-gravity over corner drop had a rigid body deceleration of 70 g and the flat end drop had a deceleration of 80 g. The lower decelerations for these two events were expected due to the larger deformations that occurred in those tests.

The setup for the puncture tests was similar to that shown in Figure 4 for the free-drop tests. The setup for the center-of-gravity over the closure joint test is shown in Figure 6. This figure shows the test article just after release from the explosive cable cutters. Note the smoke drifting away from the severed cables. Data acquisition and photometric coverage was identical to that of the free-drop tests.

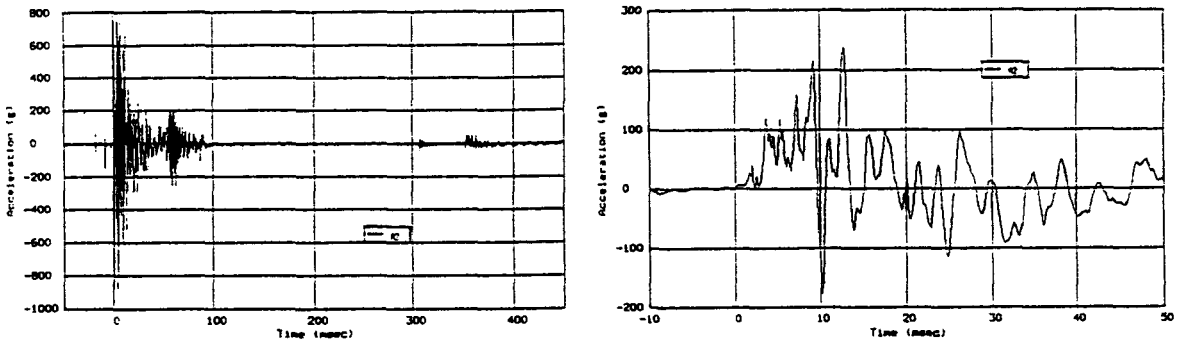

Figure 5. Accelerometer Data for the Flat Side Drop: (a) wide band data and (b) data filtered with a cut-off frequency of 500 Hz

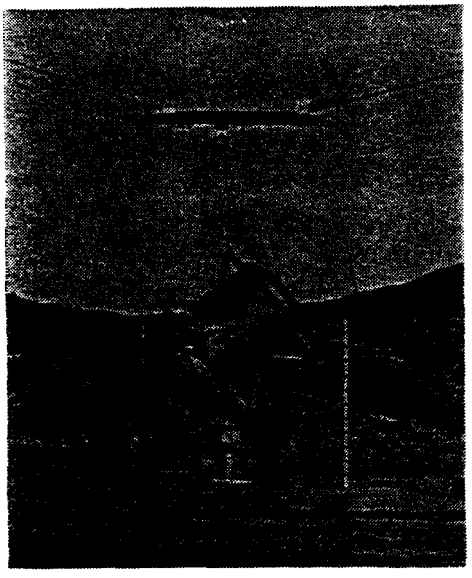

Figure 6. On-Site Container at Release for the Center-of-Gravity Over Closure Joint Puncture Test

As in the drop tests, the requirement to test the package in the most damaging orientation resulted in multiple puncture tests. These included a: (1) center-of-gravity over closure joint test, (2) center-of-gravity over sample port test, and (3) flat bottom puncture. The purpose of the center-of-gravity over closure joint test was to attempt to create a gap in the closure joint resulting in loss of containment. The center-of-gravity over sample port test similarly was intended to attempt to damage the sample port with a resulting loss of containment. The bottom end puncture was an attempt to damage the wall by tearing the containment boundary. None of these tests resulted in loss of containment. The results from the puncture events indicated rigid body decelerations of less than 20 g. The response of the center-of-gravity over closure joint test from the accelerometer mounted to measure the decelerations through the center-of-gravity are given in Figure 7. The wide band data (Figure 7a) indicate that the total decelerations were less than 50 g. The corresponding data for the rigid body decelerations (Figure 7b) indicate

decelerations of less than 20 g. The corresponding rigid body deceleration values for the other puncture tests are 15 g for the center-of-gravity over sample port and 14 g for the flat bottom end drop. These decelerations corresponded well with the force measurements from the instrumented puncture spike.

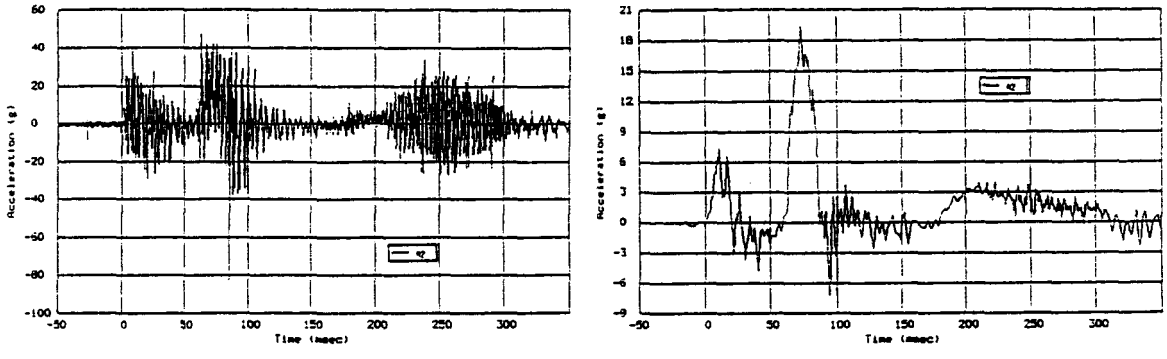

Figure 7. Accelerometer Data for the Center-of-Gravity Over Closure Joint Puncture Test: (a) wide band data and (b) data filtered with a cut-off frequency of 100 Hz

The final test in the sequence was the pool-fire test. The first pool-fire test resulted in loss of containment due to the liquid metal embrittlement of the cadmium-plated 4340 steel bolts. This resulted in the previously mentioned rebuild of the package. The bolt material was replaced with A286 steel and the second pool-fire test was performed. The package was placed on the support as shown in Figure 8. The pool was partially filled with water and a layer of JP-4 fuel was floated on the top. The fire (Figure 9) was ignited and burned for 22.5 min. Thermocouples were used to monitor the external and internal temperatures of the packaging and passive thermal indicators were used as back-up for the internal temperature readings. The interior shell remained below 85°C even though the fire exceeded the design criteria requirement of 15 min by 50%.

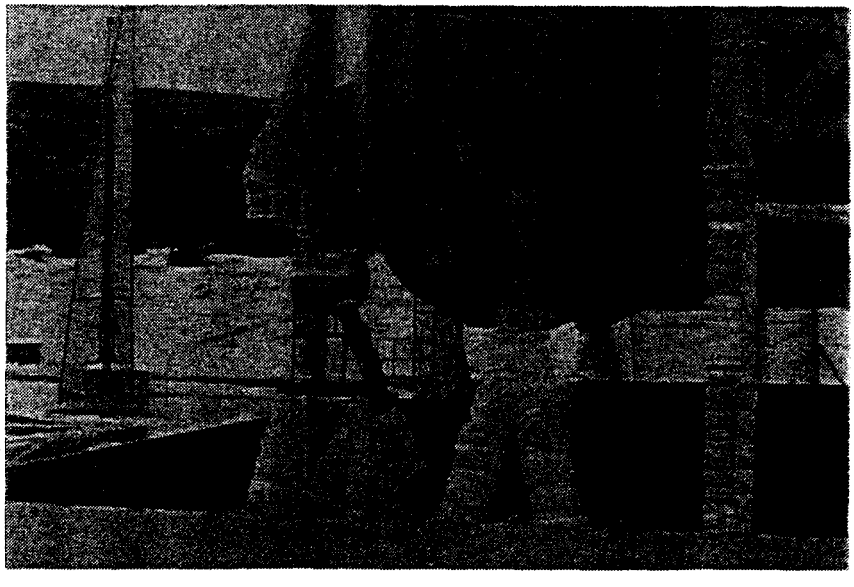

Figure 8. Pool-Fire Test Setup

Figure 9. All-Engulfing JP-4 Fuel Pool-Fire Test

The results of the second fire leak test indicated a packaging leak rate of 8.9×10^{-2} std cc/s. The successful completion of the test sequence resulted in completion of the design phase of the project.

CONCLUSIONS

This paper describes the results of the development of a packaging designed for on-site transportation of chemical munitions. The criteria for the package were patterned after the requirements for Type B packagings, but were modified to take credit for the operational controls that could be applied on-site. The design phase has been completed and a contract has been placed for fabrication of 165 units. In addition to the tests completed during the design phase, a complete sequence of verification tests will be performed on the first fleet unit. This sequence will consist of: (1) a 22,700-kg load placed on the packaging for 24 hours, (2) the flat side free drop, (3) the center-of-gravity over closure joint puncture test, and (4) a 15-min all-engulfing JP-4 pool-fire test. At the completion of the test sequence, the package will be required to meet the less than 1×10^{-1} std cc/s leak test.

REFERENCES

ANSI (American National Standards Institute), "Radioactive Materials - Leakage Tests on Packages for Shipment," ANSI N14.5, 1987.

Klevans, L. M. "Chemical Weapons On-Site Shipping Containers (ONC) Performance Criteria," August 15, 1988.

Robino, C. V. and Van Den Avyle J. A., "Failure Analysis of the On-Site Container Flange Bolts," memo dated May 11, 1992.

Uncapher, W. L., "The Mobile Instrumentation Data Acquisition System (MIDAS)," SAND90-2916, Sandia National Laboratories, Albuquerque, NM, 1990.

The Development of a Type B Sample Container*

R. E. Glass

Transportation Systems Technology Division, Sandia National Laboratories**
Albuquerque, New Mexico, United States of America

INTRODUCTION

Sandia National Laboratories is developing a Protective Sample Container to support chemical agent sampling requirements of the multilateral Chemical Weapons Convention. This work is sponsored by the U.S. Army Chemical Research, Development, and Engineering Center. The Protective Sample Container is designed to prevent the release of lethal chemical agents during international air transport of chemical agents by meeting International Atomic Energy Agency (IAEA) requirements for a Type B container and by incorporating features specific to the Chemical Weapons Convention such as tamper protection, interior sampling, and decontamination.

The current package design includes a removable insert that can be used to support the transport of a range of sample sizes from adsorption tubes to 2 l bulk samples. This package may be applicable to the analytical sampling needs of the U.S. Department of Energy Office of Environmental Restoration and Waste Management.

This paper discusses the design and engineering development tests performed for the Protective Sample Container.

DESIGN

The recommended design criteria (Glass and Gough, 1992) for the Protective Sample Container include the IAEA Type B packaging requirements (IAEA, 1985) and the American National Standards Institute (ANSI) N14.5 leak tight requirement (ANSI, 1987) during both normal transport and following the hypothetical accident sequence. The leak tight requirement eliminates the need for content-specific release rates similar to the A1 and A2 quantities of radioactive materials.

In addition to meeting the Type B design criteria, the Protective Sample Container includes a containment vessel designed to meet the requirements of the International Civil Aviation

---

*This work was performed at Sandia National Laboratories, Albuquerque, New Mexico, supported by the United States Department of Energy under Contract DE-AC04-76DP00789.

**A United States Department of Energy Facility.

Organization's (ICAO)Class 6, Division 6.1 Packaging Group I criteria (ICAO, 1992) for toxic materials. This will provide for operational flexibility in transporting toxic samples .

The Protective Sample Container is 40.6 cm in diameter and 40.8 cm long. The internal cavity is 15 cm in diameter and 14 cm long. An insert can be machined to accept multiple samples of any configuration up to 2 l in volume. The configuration of the packaging shown in Figure 1 includes the insert for 137 adsorption tubes.

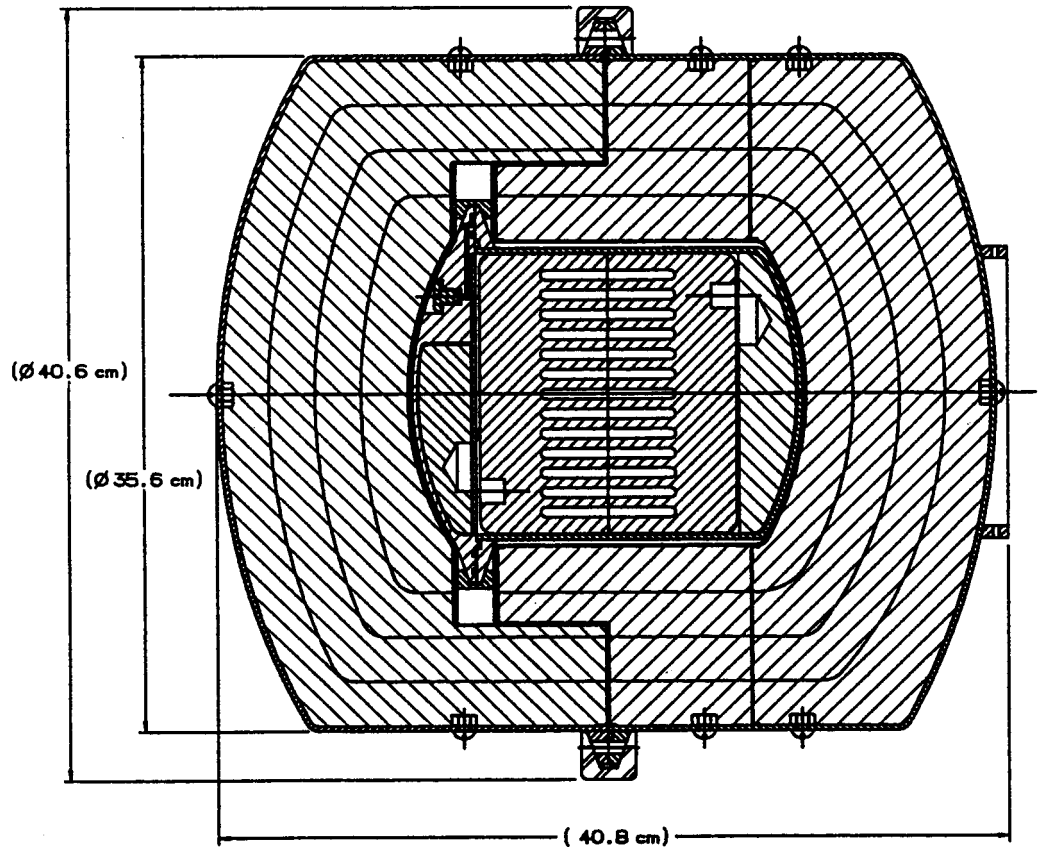

Figure 1. Protective Sample Container Design

The packaging consists of a protective overpack, removable containment vessel, and removable insert for holding contents. The protective overpack provides protection against the thermal and structural assaults of the hypothetical accident sequence. For ease of decontamination, all exposed surfaces are stainless steel. The protective overpack consists of a 2.67 mm stainless-steel cylindrical shell with standard flanged commercial pressure vessel heads, thermal insulation and an inner stainless-steel skin. The stainless-steel shell deforms to absorb most of the impact energy during the drop test and to provide protection from puncture. Internal to this shell is 10 cm of ceramic fiber insulation that limits the thermal input to the containment vessel. The ceramic fiber insulation is enveloped by a stainless-steel skin that can be readily decontaminated in the event of a leaking sample vial. The outer shell and inner skin are connected with a z-ring that limits heat conduction to the containment vessel. The protective overpack is closed with a stainless-steel v-clamp.

The containment vessel is designed to meet the vibration, drop, stacking, leakproof, and hydraulic tests specified for Class 6, Division 6.1 toxic substances by ICAO. The containment vessel is a 2.67-mm stainless-steel cylindrical shell with flanged pressure vessel heads at each end. The containment vessel from the engineering development model is shown in Figure 2 and is identical to the Protective Sample Container. The photograph shows the assembly with the protective overpack lid removed. This model did not include the z-ring between shells. The containment vessel closure is provided by a v-clamp. The containment vessel includes an o-ring test port, shown in upper left, to perform operational leak rate testing of the elastomeric double o-ring seal. The containment vessel also has a sample port that allows the interior of the package to be sampled without release of contents.

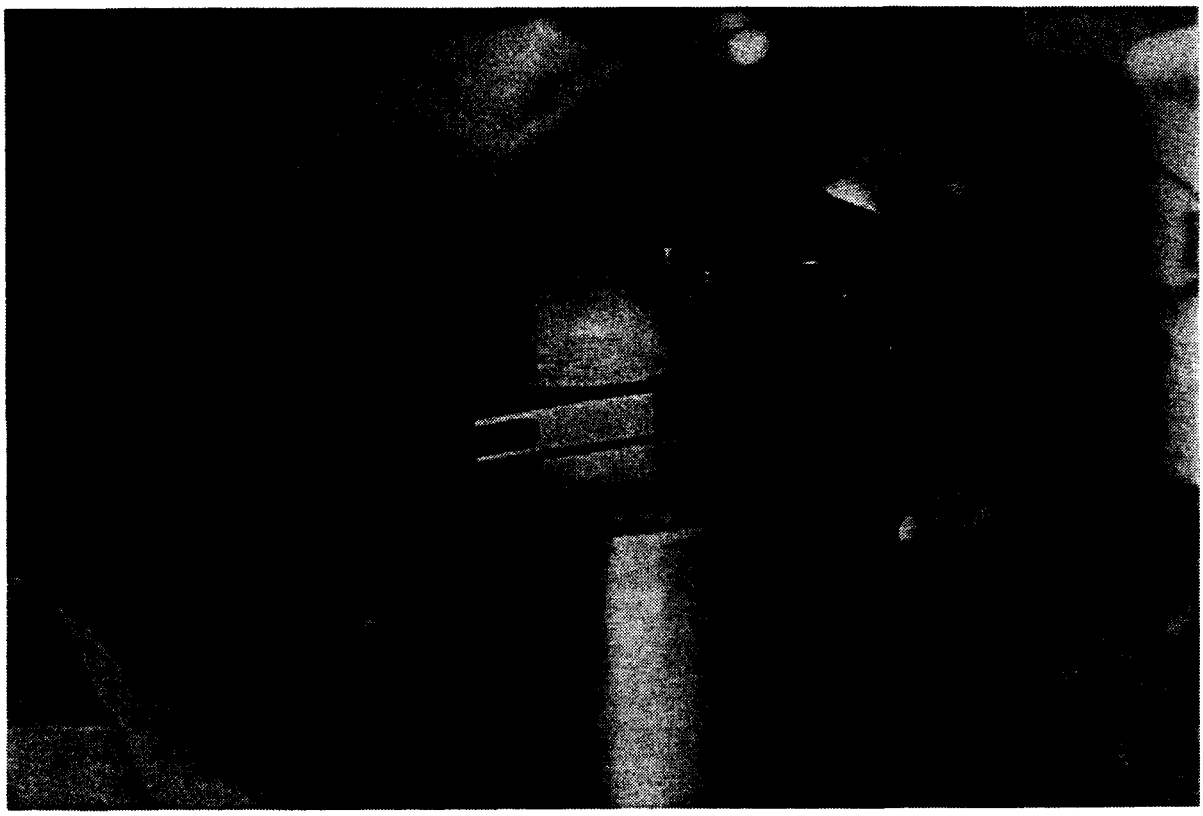

Figure 2. Engineering Development Model with Outer Lid Removed

A removable insert for 10 ml sample vials is shown in Figure 3. The insert consists of a teflon cylinder machined for specific sample vial sizes. The machined slots are lined with a low durometer butyl to attenuate shock. The vials are then placed in the insert slots and packed with an absorbent material.

ENGINEERING DEVELOPMENT MODEL TESTING

A series of drop, puncture and fire tests have been performed on an engineering development model for the Protective Sample Container. The model differed from the current design in that the fiber insulation was only 7.5 cm thick and the protective overpack outer shell and inner skin were connected with a straight ring instead of the current z-ring design. These changes were incorporated due to the response of the development model during the all-engulfing fire test.

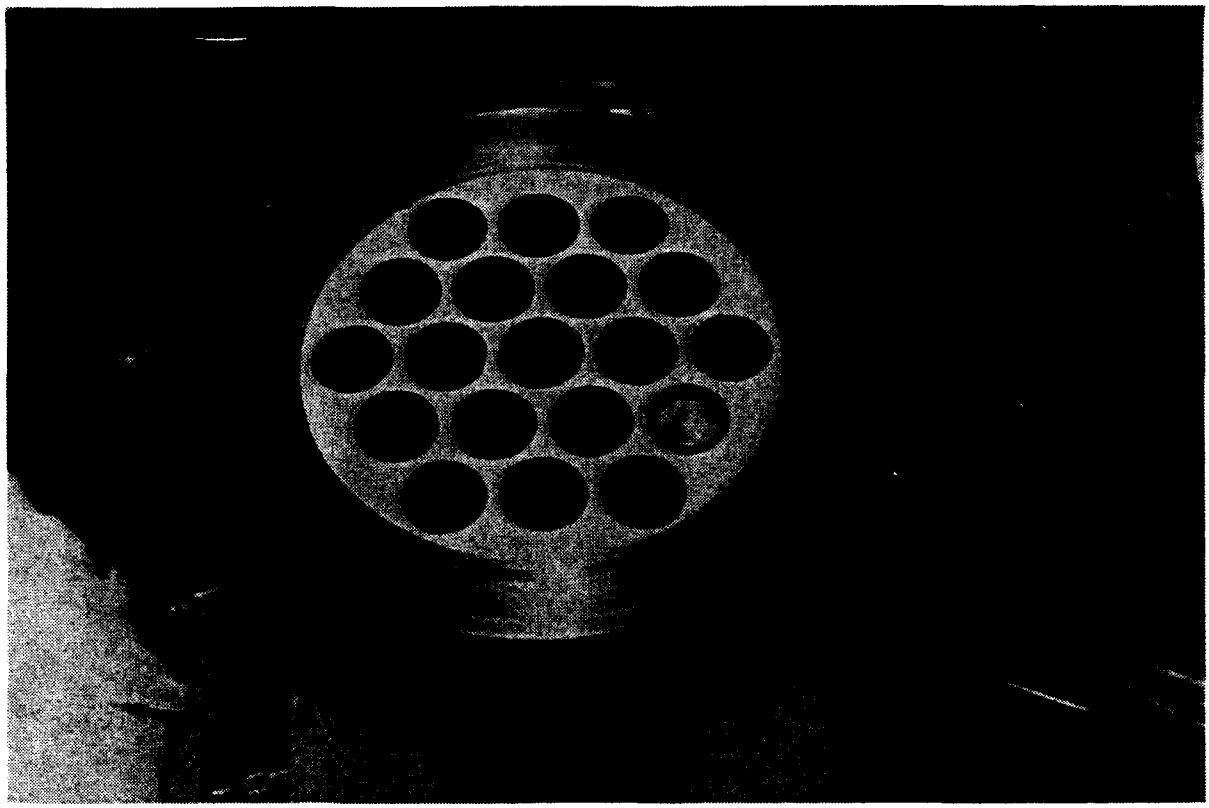

Figure 3. Engineering Development Model Interior

The development model was subjected to the following sequence of tests: three 10-m free drops, one 1-m puncture test, and an all-engulfing JP-4 fuel fire test. This test sequence resulted in an unacceptable leak rate due to excessive temperatures experienced by the o-rings during the fire test.

The intended drop test orientations were flat side drop, center-of-gravity over corner drop, and flat top drop. The instrumentation for each of these drops consisted of two accelerometers. The x accelerometer was oriented to provide the acceleration through the center-of-gravity and the impact point. The y accelerometer measured the accelerations perpendicular to that line. The data presented in subsequent figures are from the flat top drop.

The flat top drop resulted in the lowest accelerations and the largest deformations. Conversely, the highest accelerations occurred during the flat side drop and were due to the impact on the relatively rigid v-clamp. The results of this flat top test are shown in Figure 4. The data show the vertical acceleration obtained using the Mobile Instrumentation Data Acquisition System (Uncapher, 1990). The data show the primary impact at time 0 and three subsequent impacts.

The primary impact had the highest accelerations. The wide band data for the primary impact are shown in Figure 5. These data indicate an impact duration of between 2 and 4 msec which

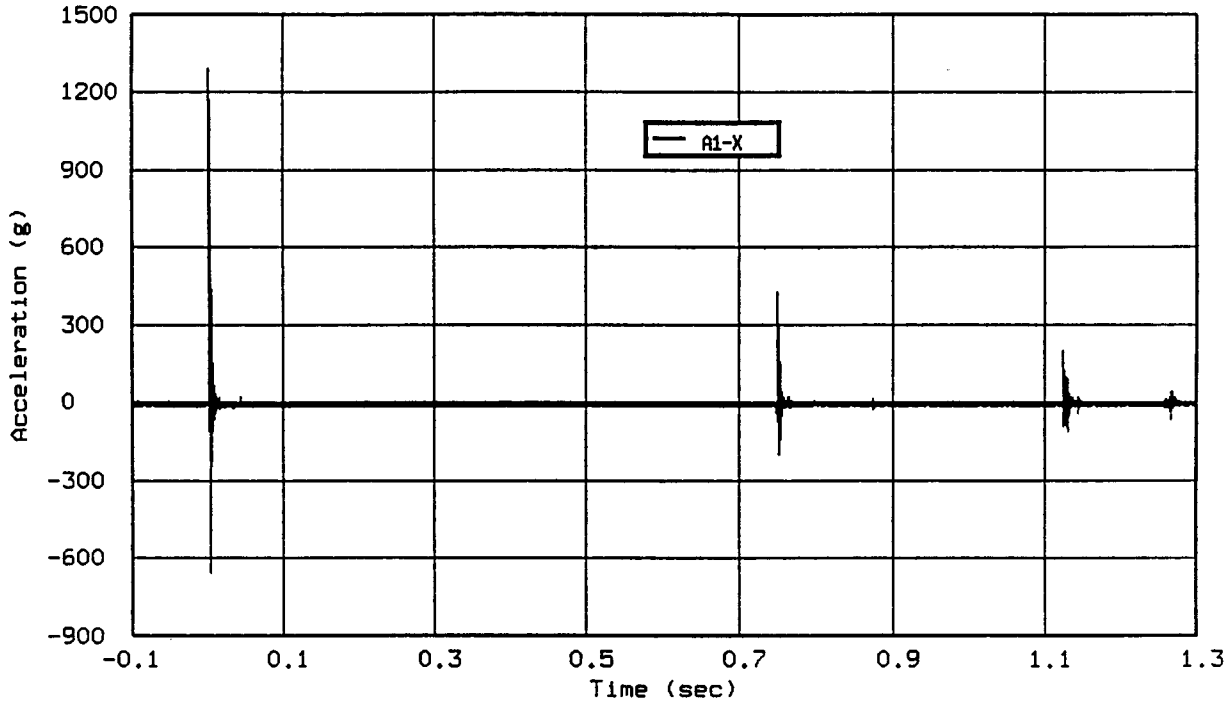

Figure 4. Flat Top Drop Vertical Acceleration Data

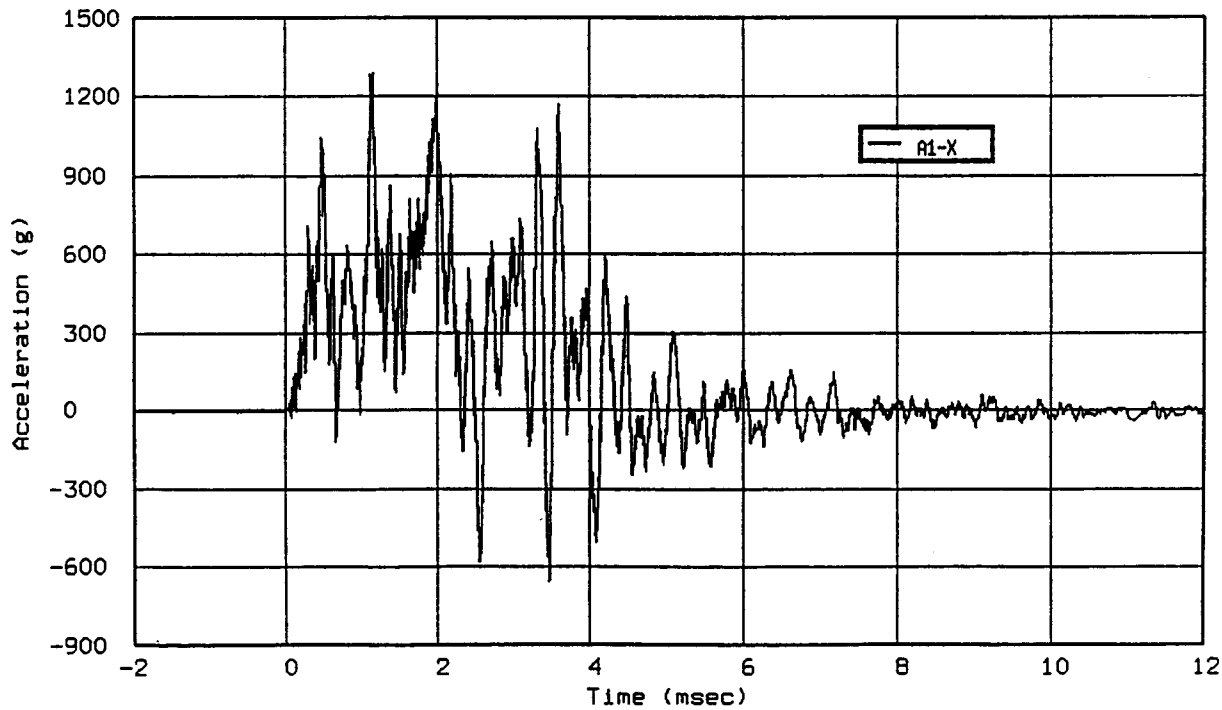

Figure 5. Flat Top Drop Primary Impact Acceleration Data

is an order of magnitude greater than the 0.3-msec impact duration predicted by elastic only response. This long duration agrees with the substantial inelastic deformation observed after the test. Data filtered with a cut-off frequency of 3300 Hz are shown in Figure 6. These data still include a significant contribution from a vibration mode of 3200 Hz and hence produce an upper bound on the rigid body deceleration of the packaging of 1100 g.

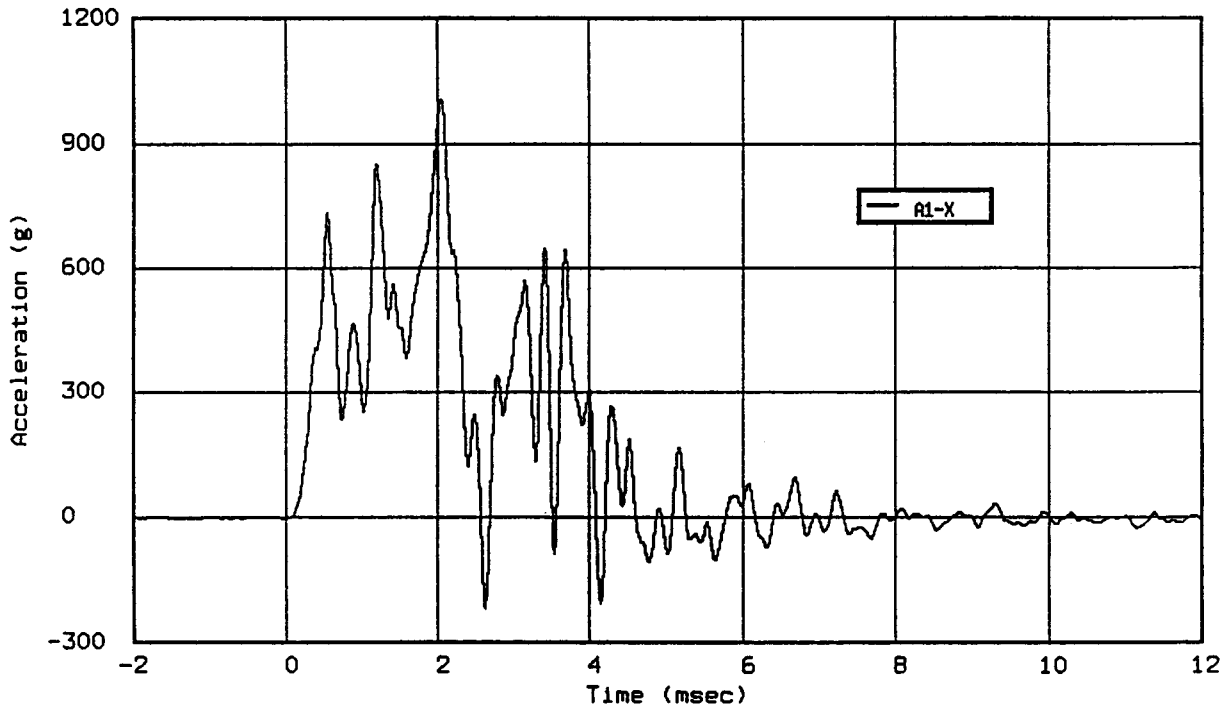

Figure 6. Flat Top Drop Primary Impact Filtered Data

The center-of-gravity over corner test resulted in similar decelerations and deformations. The flat side drop impacted the v-clamp and hence resulted in higher decelerations. The impact drove the v-clamp into the stiff flange and hence very little deformation was observed. The flat top and center-of-gravity over corner drops were considered the most damaging, since they resulted in compression of the insulation layer, whereas impacting the v-clamp did not threaten the closure.

Following the free drop tests, the packaging was subjected to a flat top puncture test. Since the engineering development model's lid diameter was only twice the diameter of the punch, this test was essentially a less severe version of the flat top free drop test. The rigid body deceleration for this test was approximately 95 g and no additional damage was observed as a result of this test.

The test sequence was completed with an all-engulfing fire test. During this test, the package was placed in a JP-4 fuel fire. The instrumentation consisted of thermocouples placed on the exterior of the package and passive thermal indicators placed inside the package. The exterior thermocouples were used to determine the external boundary condition in the event that

additional thermal analyses needed to be performed following the test. The internal thermocouples monitored the packaging response. They were placed along the ring connecting the outer shell and inner skin, along the bottom of the inner skin, and on the exterior of the containment vessel. The actual exposure of the package exceeded the regulatory 30-min, all-engulfing fire. The regulatory test was followed by a 90-min exposure to a wall of flame. The additional exposure was the result of a failure in a mechanism used to shield the test article from the fire. Figure 7 shows the package while still exposed to the ongoing pool fire. The results from this test indicated that temperatures exceeded the maximum passive thermal indicator temperature of 400°C at the o-ring seal location. The bottom of the containment vessel reached temperatures of approximately 200°C.

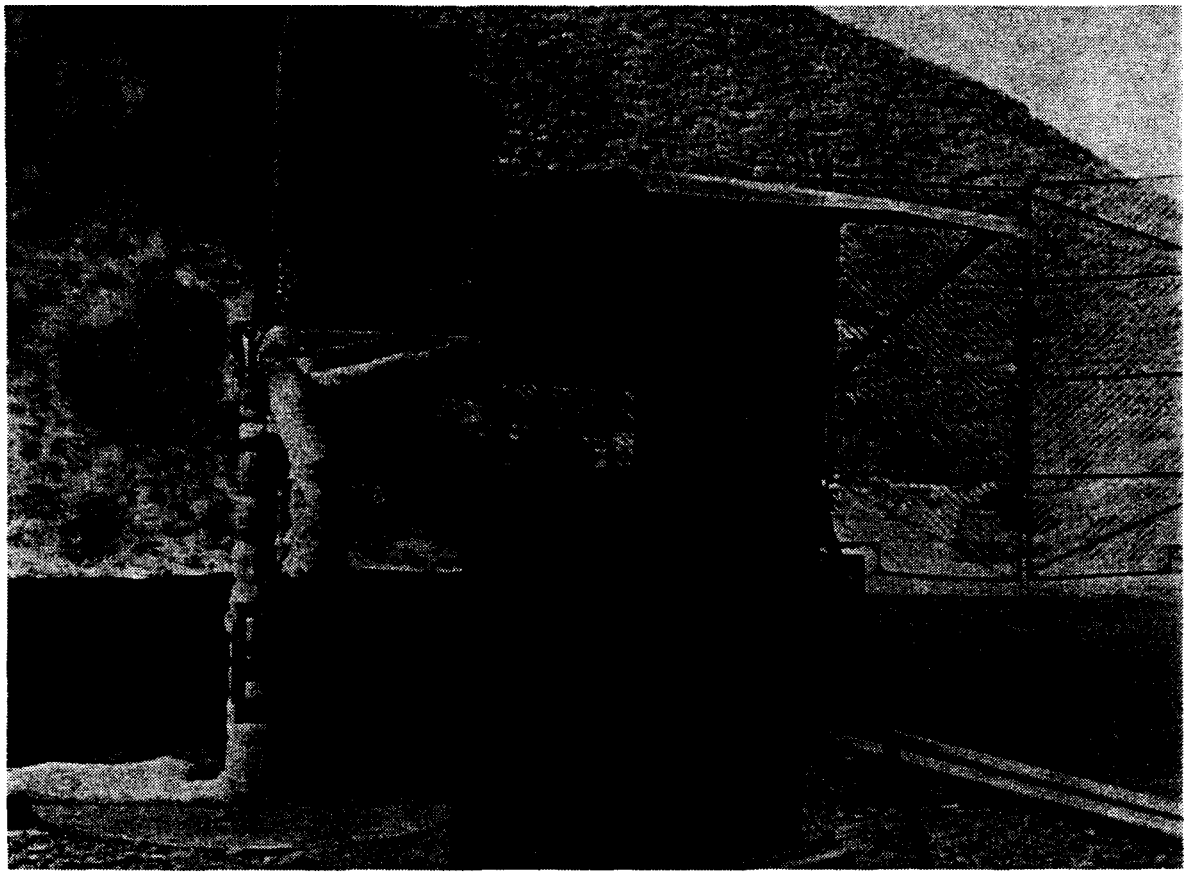

Figure 7. Protective Sample Container Exposed to Ongoing JP-4 Fuel Fire Test

Thermal analyses compared the actual thermal event with the regulatory 30-min all-engulfing fire. These analyses indicated that the peak temperatures at the o-ring surface would have been 480°C (Sisson, 1992) for the regulatory event and 760°C for the actual event. Since the predicted regulatory event o-ring temperature exceeds the manufacturer's continuous operating

temperatures for standard materials such as viton and butyl, the package was redesigned as discussed in the DESIGN section.

CONCLUSIONS

The Protective Sample Container has been designed to remain leak tight following the hypothetical accident sequence of drop, puncture and fire specified in the IAEA regulations. The containment vessel has been designed to meet the requirements of the ICAO for Class 6, Division 6.1 toxic materials transport.

An engineering development model was tested to meet the IAEA requirements. These tests resulted in a redesign of the packaging to incorporate greater thermal resistance. A prototype is being fabricated and verification testing will be completed in October 1992.

REFERENCES

ANSI (American National Standards Institute), "Radioactive Materials - Leakage Tests on Packages for Shipment," ANSI N14.5, 1987.

Glass, R. E. and Gough, R. G., "Considerations for an Air-Transportable Protective Sample Container for the Chemical Weapons Convention," VST-030/TTC-1175, Sandia National Laboratories, Albuquerque, NM, January 1992.

IAEA (International Atomic Energy Agency), "Safety Series No. 6 Regulations for the Safe Transport of Radioactive Material," 1985 Edition.

ICAO (International Civil Aviation Organization), "Technical Instructions for the Safe Transport of Dangerous Goods by Air," Doc 9284-AN/905, 1991-1992 Edition.

Sisson, C. E., Private communication, April 1992.

Uncapher, W. L., "The Mobile Instrumentation Data Acquisition System (MIDAS)," SAND90-2916, Sandia National Laboratories, Albuquerque, NM, 1990.

Comparison of Elastic and Inelastic Analyses*

D. J. Ammerman, M. W. Heinstein, and G. W. Wellman

Sandia National Laboratories, Albuquerque New Mexico, United States of America**

INTRODUCTION

The use of inelastic analysis methods instead of the traditional elastic analysis methods in the design of radioactive material (RAM) transport packagings leads to a better understanding of the response of the package to mechanical loadings. Thus, better assessment of the containment, thermal protection, and shielding integrity of the package after a structural accident event can be made. A more accurate prediction of the package response can lead to enhanced safety and also allow for a more efficient use of materials, possibly leading to a package with higher capacity or lower weight. This paper will discuss the advantages and disadvantages of using inelastic analysis in the design of RAM shipping packages.

The use of inelastic analysis presents several problems to the package designer. When using inelastic analysis the entire nonlinear response of the material must be known, including the effects of temperature changes and strain rate. Another problem is that there currently is not an acceptance criteria for this type of analysis that is approved by regulatory agencies. Inelastic analysis acceptance criteria based on failure stress, failure strain, or plastic energy density could be developed. For both elastic and inelastic analyses it is also important to include other sources of stress in the analyses, such as fabrication stresses, thermal stresses, stresses from bolt preloading, and contact stresses at material interfaces.

Offsetting these added difficulties is the improved knowledge of the package behavior. This allows for incorporation of a more uniform margin of safety, which can result in weight savings and a higher level of confidence in the post-accident configuration of the package. In this paper, comparisons between elastic and inelastic analyses are made for a simple ring structure and for a package to transport a large quantity of RAM by rail (rail cask) with lead gamma shielding to illustrate the differences in the two analysis techniques.

ANALYSIS OF A SIMPLE RING STRUCTURE

A very simple structure (a ring impacting a block of foam) was chosen to illustrate the differences between elastic and inelastic analyses and between equivalent static and dynamic analyses. This simple ring structure is shown in Figure 1. Material properties consistent with actual tensile test results of an A516-Gr60 pressure vessel steel were chosen for the ring. This material has a clearly defined yield plateau with significant strain hardening. Because the purpose of this study was to determine the differences between elastic and inelastic analysis methods, the actual yield (268 MPa) and ultimate stress (465 Mpa) values from the tensile test were used rather than the tabulated minimum

* This work performed at Sandia National Laboratories, Albuquerque, New Mexico, supported by the United States Department of Energy under Contract DE-AC04-76DP00789.

** A United States Department of Energy Facility.

values that would normally be used in design. The allowable stress using the elastic criterion of Regulatory Guide 7.6 (U.S. NRC 1978) is 419 MPa. Similarly, the allowable stress using the inelastic criterion from the ASME Boiler and Pressure Vessel Code (ASME 1983) is 326 MPa.

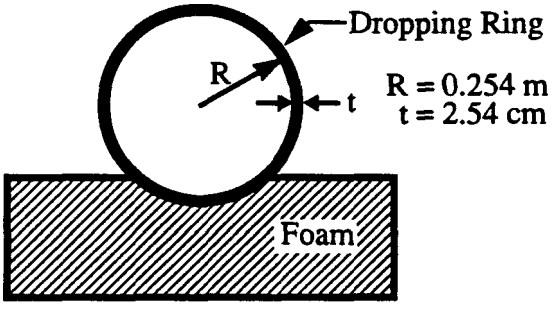

Figure 1. Simple Ring Structure

Five different analyses were performed on this structure. First, an equivalent static handbook (Roark and Young 1975) analysis was performed. In this analysis, an energy balance between the potential energy of the ring before it was dropped from a 9 m height and the strain energy of the foam was used to determine the maximum foam crush. To calculate the stress in the ring, two primary assumptions were made: (1) the foam provides a uniform pressure equal to its crush strength over the area of contact with the ring and (2) the force in the foam is in equilibrium with the inertia of the ring. Multiplying the ring's maximum footprint in the foam (easily computed from the depth of crush above) by the crush strength of the foam gives a maximum applied force of 29.2 kN. This maximum force generates a peak deceleration of 3827 m/s^2 or 390 g's. The crush depth, the footprint in the foam, and the maximum stress in the ring are all shown in Table 1.

The next two analyses were performed with the finite element program SANTOS (Stone 1992), which computes the nonlinear quasistatic response of solids by the dynamic relaxation method. The same problem as described above for the handbook solution was solved using SANTOS. The foam was not modelled, but was replaced by a pressure over the same area as for the handbook solution above. One analysis utilized a linear elastic material response for the ring and the other an inelastic response, where the strain hardening was characterized by the plastic strain raised to a fractional power (Stone et al. 1990). The maximum stresses computed are again shown in Table 1.

The final two analyses employed a nonlinear transient-dynamic finite element program, PRONTO2D (Taylor and Flanagan 1987). As above, the ring was modelled as an elastic material in one analysis and as an inelastic material in the other. The foam was modelled using a recently developed phenomenological plasticity theory (Neilsen et al. 1986). The analyses commenced with the ring just in contact with the foam block. The ring was given an initial velocity consistent with a 9 m drop (13.4 m/s). The analysis was carried out past minimum kinetic energy; the ring had started to rebound from the foam. The maximum depth of foam crush, the ring footprint in the foam, the maximum stress in the ring, and the maximum net force during the impact are shown in Table 1.

Table 1. Results from the Analysis of a Ring Dropping onto Foam

	Depth of Crush	Footprint in Foam	Max Stress in Ring	Maximum Force
Closed Form	4.83 cm	21.06 cm	419 MPa	29.2 kN
Static Elastic	n. a.	n. a.	423 MPa	29.2 kN
Static Inelastic	n. a.	n. a.	310 MPa	29.2 kN
Dynamic Elastic	3.73 cm	28.96 cm	427 MPa	21.8 kN
Dynamic Inelastic	3.68 cm	28.96 cm	309 MPa	21.8 kN

The stresses computed for the elastic analyses were very similar to each other, as were the stresses for the inelastic analyses. The elastically computed stresses were within two percent of the elastic stress criterion of Regulatory Guide 7.6, as expected. The stresses computed using inelastic material response were approximately 5 percent below

the ASME Boiler and Pressure Vessel criteria. The major difference in stress values between the static and the dynamic analyses was that the maximum stress occurred at the maximum foam crush for the static analyses while the maximum stress occurred at about half the time to minimum kinetic energy or half the time to maximum foam crush for the dynamic analyses. For the dynamic analyses the maximum stress in the ring occurred at an earlier time than the maximum load. The dynamic analyses developed a larger footprint with a corresponding lesser depth of crush for approximately the same energy absorbed in the foam. Much of this difference is due to the dynamic analysis taking into account the deformation of the ring, while the static analyses assumed the foam loaded an undeformed ring.

ANALYSIS OF A RAIL CASK WITH LEAD GAMMA SHIELDING

In this section the problems and benefits of using elastic and inelastic analysis in the design of RAM transportation packages are explored via a design for shipping a bulk quantity high level RAM waste. The waste is assumed to have very little strength but high volumetric stiffness and a specific weight of 1.7. It is assumed that the shielding requirements for the package are similar to those for spent fuel. The package is a rail cask that utilizes lead for its gamma shielding, 304 stainless steel shells on the inside and outside of the gamma shielding, and solid stainless steel ends as shown in Figure 2. In addition, the package is encased in neutron shielding, a 304 stainless steel neutron shielding shell and 0.32 g/cm^3 polyurethane foam impact limiters. The dimensions and material properties for the rail cask can be found in prior work by the authors (Heinstein and Ammerman 1992). This reference has detailed analyses for the rail cask as well as a smaller package for transporting RAM by truck (truck cask).

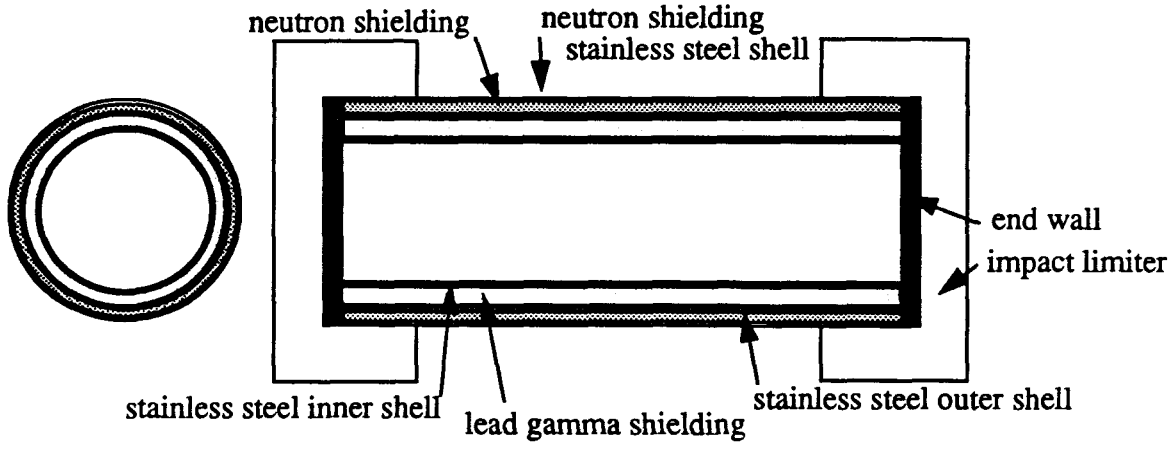

Figure 2. Rail RAM transportation package construction

Depending on whether an elastic design criteria or an inelastic design criteria was used, a different material model was used for the 304 stainless steel inner shell, outer shell, and end walls. A linear elastic material model was used for these components with the elastic design criteria, whereas an elastic-plastic material model with linear hardening was used with the inelastic design criteria.The energy absorbing impact limiter was a 0.32 g/cm^3 polyurethane foam, and its model included the effects of volumetric crush and lock-up (Neilsen et al. 1986). When a change in the wall thickness was required, a replacement ratio of 1 part lead to 1.75 parts stainless steel was used such that the shielding effectiveness was unchanged.

The maximum allowable stresses are computed by the formulas specified in the NRC Regulatory Guide 7.6 (U.S. NRC 1978) for the elastic analysis, and in the ASME Boiler and Pressure Vessel Code, Section III, Appendix F (ASME 1983) for the inelastic analysis. For the stainless steel material, the maximum allowable membrane plus bending stress was 482 MPa for the elastic analysis, and 465 MPa for the inelastic analysis. No design changes were made in the elastic analyses based on buckling according to the ASME Boiler and Pressure Vessel Code, Case N-284 (ASME 1980).

The finite element model for the rail RAM transportation package 9 m corner drop scenarios consisted of a total of 31,960 elements with two elements through the thickness of the inner shell and two elements through the thickness of the outer shell. All analyses for the corner drop impact scenario were performed with a transient dynamic analysis code PRONTO3D (Taylor and Flanagan 1989). This code calculates stresses/strains based on the deformed geometry. The criterion of NRC Regulatory Guide 7.6 (U.S. NRC 1978) and ASME Boiler and Pressure Vessel Code, Section III, Appendix F (ASME 1983) are based on stresses computed using the undeformed geometry (engineering stress). Therefore the computed von Mises stresses were converted to engineering stresses by conservatively assuming that all strains were uniaxial compression by the equation:

$$\sigma_{eng} = \frac{\sigma_{mises}}{1 - \varepsilon}$$

where σ_{eng} is the engineering stress, σ_{mises} is the computed von Mises stress, and ε is the computed strain.

The 9 m center-of-gravity-over-corner drop impact was modelled as a dynamic event with initial velocity of 13.4 m/s. Figure 3 shows the deformed shape of the rail cask for the inelastic analysis.

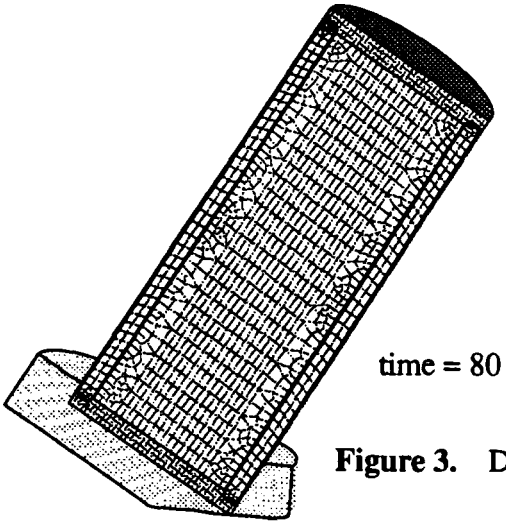

Figure 3. Deformed rail cask after 9 m corner drop

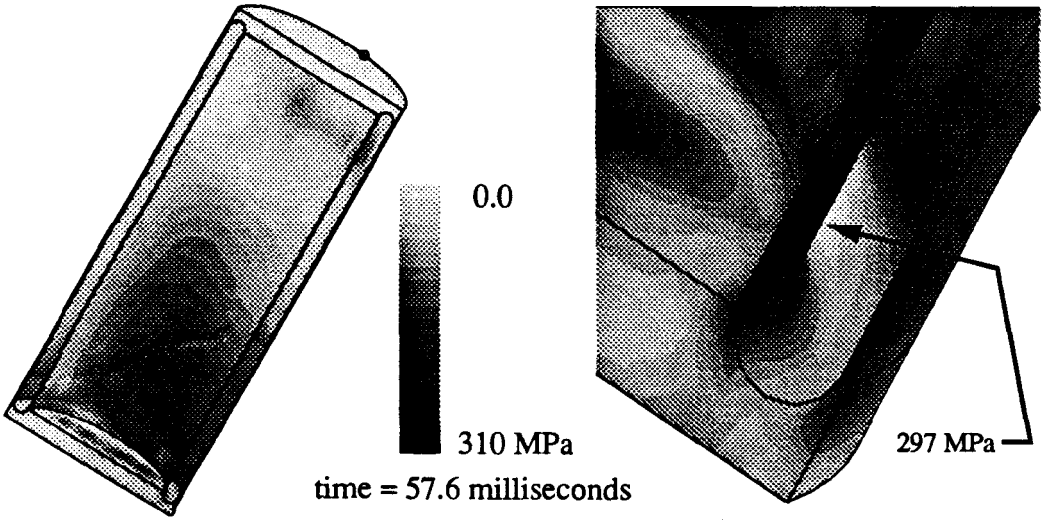

Figure 4. Maximum von Mises stress during the 9 m corner drop of inelastic rail cask

In the inelastic analysis, the von Mises stress increases in the outer shell as the cask is loaded to the maximum g-load. Because the stainless steel is allowed to yield, part of the load is transferred to the shielding and inner wall. The maximum von Mises stress during the corner drop event, was 297 MPa (engineering stress of 308 MPa) at 57.6 milliseconds. The location of this maximum stress, as shown in Figure 4, was in the inner shell. For the inelastic analysis, a plastic strain of 0.063 for the 304 stainless steel was observed in the inner shell of the cask.

Figure 5 shows a series of deformed shapes (with displacements magnified by 5x) of the outer shell (for a cask design with outer shell thickness 1.52 cm) at 40 msec, 48 msec, and 56 msec for an elastic analysis. The high stresses are due to a combination of the endwall bending the shell and the impact limiter pushing inward on the outer shell. Note that the outer shell thickness of 1.52 cm is the same used in the inelastic analysis. The outer shell thickness was significantly increased in the redesigns (to 8.89 cm), yet the maximum stress still exceeded the allowable stress. With the outer shell thickness of 8.89 cm the maximum von Mises stress was 598 MPa (engineering stress of 599 MPa) at 59.2 milliseconds which corresponds to the maximum g-loading on the cask. The location of this maximum stress was in the outer shell as shown in Figure 6. Because of the relatively small stiffness of the lead shielding, practically none of the load on the outer shell is transferred to the inner shell. The maximum von Mises stress of 598 MPa *exceeds* the maximum allowable membrane plus bending stress of 482 MPa specified by the NRC Regulatory Guide 7.6. The outer shell wall thickness was increased from an initial thickness of 1.52 cm to a point where it was felt that the design was no longer realistic and, therefore, no further redesign was attempted.

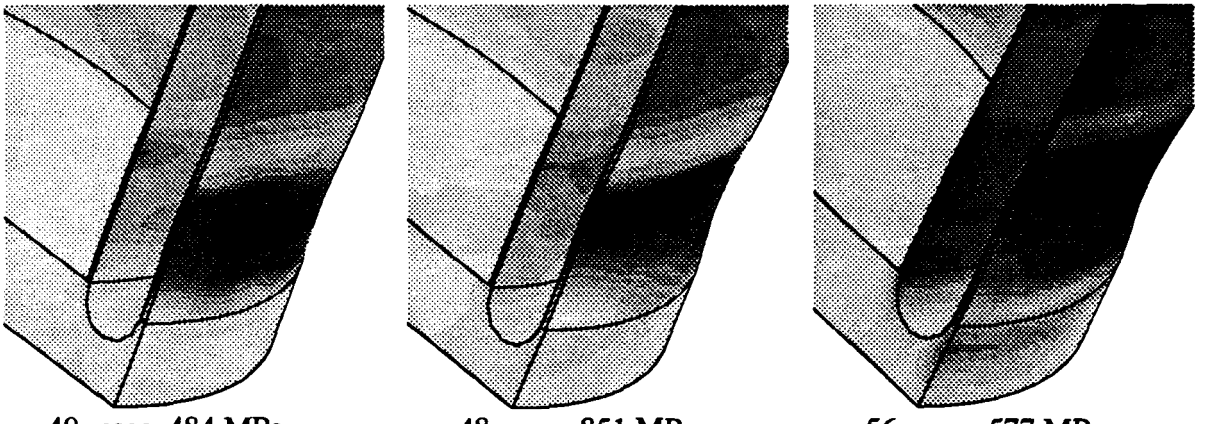

Figure 5. Von Mises stress history in the outer shell (for 1.52 cm thickness) of the elastic rail cask. Displacements are magnified by 5x

The center-of-gravity-over-corner impact scenario modelled above with a transient dynamic analysis technique provided a foundation for comparing elastic and inelastic design methodologies. There are a few issues in this study that have not been resolved and require further study. However, even with these limitations, the use of inelastic analysis technique for radioactive material transportation container design seems to have an advantage over elastic analysis. Based on the impact scenarios of a rail and truck RAM package studied in Heinstein and Ammerman and summarized here, an improved knowledge of the behavior of the cask is obtained by using the inelastic analysis. This can lead to a better overall design in the following ways.

First, elastic analysis may underpredict maximum stress at a particular location, resulting in inappropriately sized wall sections. Elastic analysis does not properly account for the decrease in stiffness resulting from yielding in part of the structure and does not show the redistribution of load caused by this yielding. This was found to be the case in the 9 m end drop impact of the rail cask. The maximum stress predicted in the elastic analysis was 276 MPa whereas the maximum stress in the inelastic analysis was 496 MPa. This was a result of the outer shell yielding and redistributing the load to the gamma shielding and inner shell. It was also observed in the inelastic analysis that significant plastic straining can occur through the thickness in several areas. This may indicate that the elastic analysis is neglecting significant physical features of the impact scenario.

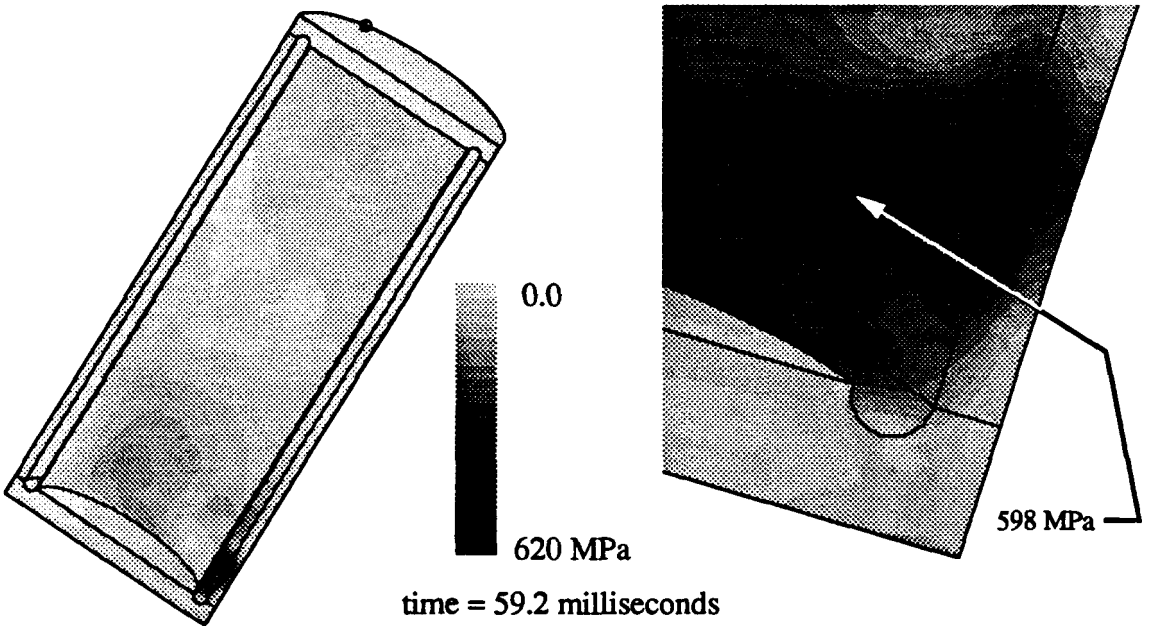

Figure 6. Maximum von Mises stress during the 9 m corner drop of elastic rail cask (for 8.89 cm outer shell thickness)

Second, elastic analysis may overpredict the maximum stress. The inelastic shells can yield and redistribute the loading to other less loaded parts of the structure, whereas the elastic shells cannot predict this behavior. This was shown in the 9 m center-of-gravity-over-corner drop of the rail cask. Based on the elastic analysis of the impact event, an outer shell thickness of over 8.89 cm would be required to meet the design criteria. With the same impact limiter, the inelastic analysis suggested that the loading on the outer shell causes it to yield and redistribute the load to the gamma shielding and inner shell requiring an outer shell thickness of only 1.52 cm. Furthermore, it was observed in the truck cask analyses that the amount of stress redistribution can be small and still influence the location, and time of occurrence of the maximum stress. Therefore, the inelastic analysis may also allow for a better distribution of structural material - which can lead to weight savings. The weight savings can increase the capacity of the package, thereby decreasing the number of shipments required to transport a given quantity of material, which increases the overall shipping program safety. The use of inelastic analysis may also decrease the overall cost of a transportation package, especially for designs where multiple packages will be constructed.

ISSUES INVOLVED IN CONDUCTING ACCURATE ANALYSES

The use of inelastic analysis for RAM transportation containers potentially has several advantages over the currently used elastic analysis. The most prominent of these is that the analysis method models the behavior of the package more closely which leads to a better understanding of the response of the container to the loads applied to it. The transient dynamic analysis technique utilized in this study provides improved knowledge of the structural integrity of the cask, but with additional cost. The computer cost for one center-of-gravity-over-corner impact scenario summarized here involved approximately 25 cpu-hours on a Cray YMP. This cost should be added to the time spent by an experienced user in constructing the finite element model. Such a model typically includes a variety of material models and nonlinear material behavior.

Some additional material properties required include strain rate and temperature dependent stress-strain curves. In the examples considered in (Heinstein and Ammerman 1992) and summarized here, the strain rates can typically range from 10^{-1} s^{-1} to 10^{3} s^{-1}. The fact that the contents will have a temperature higher than the outside ambient

means there will be a temperature gradient through the wall of the cask. For certain materials, especially the lead shielding used in the cask, the effects of temperature and strain rate on the material behavior can be significant and should be considered in the analysis.

An improved understanding of the response of the container depends on how accurately the loading history is predicted. The transient dynamic analysis technique can more accurately predict the load history if all sources of nonlinearity are considered. That includes the nonlinear thermo-mechanical behavior of the cask materials, i.e. shielding, contents, and impact limiters, and the nonlinearities arising from fabrication, i.e. initial stresses, geometric imperfections, and fastener details.

There are also several modelling issues that have not been resolved and require further study. During some impact scenarios stress waves in the shell walls resulted in localized buckling of the inner shell. The buckling events occur over a few microseconds and, to some degree, depend on the finite element model, i.e. finite element size, solution time step and material model. The extent to which the results presented here are influenced by modelling issues have not yet been investigated.

SUMMARY

The design criteria currently used in the design of RAM transportation containers are taken from the ASME Boiler and Pressure Vessel Code. These load based criteria are ideally suited for pressure vessels where the loading is quasistatic and all stresses are in equilibrium with externally applied loads. For impact events, the use of load based criteria is less supportable. Impact events tend to be energy controlled, and thus, energy based criteria would appear to be more appropriate. Determination of an ideal design criteria depends on what behavior is desired. If the intent is that there will be no yielding in the package, an elastic analysis with an allowable stress less than the yield point stress is sufficient. This type of acceptance criteria will lead designers to using materials with the highest possible yield stress, and perhaps a lower margin of safety against gross rupture. However, if the goal is to prevent release of radioactive material, some amount of inelastic deformation is acceptable. In this case, the acceptance criteria should limit through wall tearing and keep deformations to an acceptably small amount. An elastic analysis cannot predict the margin of safety against through wall tearing and the deformations associated with an impact event nearly as well as an inelastic analysis. For the simple ring structure studied here, there is only about a 5 percent difference between the use of linear-elastic criteria versus inelastic criteria. Even the introduction of dynamics does not appreciably affect the stresses in the ring. However, the deformations in the foam (impact limiter) are different between the quasistatic and the dynamic analyses. For more complicated structures, such as the rail cask, the use of an equivalent uniform acceleration over the structure is difficult to justify. More importantly, equivalent static analysis is incapable of resolving the magnitudes and distributions of the load transfer between the impact limiter and the structure, where both strength and inertia are important. The overwhelming advantage of nonlinear dynamic analysis techniques is a better understanding of the response of the structure to the imposed environment. A better understanding of package behavior during impact events should lead to a safer package.

REFERENCES

ASME, Boiler and Pressure Vessel Code, *Case N-284 Metal Containment Shell Buckling Design Methods*, Section III, Division I, Class MC, August 1980.

ASME, *Boiler and Pressure Vessel Code*, Section III, Division I - Appendix F, 1983.

Heinstein, M.W. and Ammerman, D.J., *Use of Inelastic Design for Radioactive Material Transportation Packages*, SAND92-1842, Sandia National Laboratories, Albuquerque, NM (in preparation).

Neilsen, M.K., H.S. Morgan, and R.D. Krieg, *A Phenomenological Material Model for Low Density Polyurethane Foams*, SAND86-2927, Sandia National Laboratories, Albuquerque, NM, 1986.

Roark, R. J., and Young, W. C., *Formulas for Stress and Strain*, fifth edition, McGraw-Hill Book Co., New York, N. Y., 1975, pp230-231.

Stone, C. M., Wellman, G. W., and Krieg, R. D., *A Vectorized Elastic/Plastic Power Law Hardening Material Model Including Lüders Strain*, SAND90-0153, Sandia National Laboratories, Albuquerque, NM, 1990.

Stone, C. M., *SANTOS - A Two-Dimensional Finite Element Program for the Quasistatic Large Deformation, Inelastic Response of Solids*, SAND90-0543, Sandia National Laboratories, Albuquerque, NM (in preparation).

Taylor, L. M. and Flanagan, D. P., *PRONTO 2D - A Two-Dimensional Transient Solid Dynamics Program*, SAND86-0594, Sandia National Laboratories, Albuquerque, NM, 1987.

Taylor, L.M. and Flanagan, D.P., *PRONTO3D: A Three-Dimensional Transient Solid Dynamics Program*, SAND89-1912, Sandia National Laboratories, Albuquerque, NM, 1989.

U.S. Nuclear Regulatory Commission Regulatory Guide 7.6, *Design Criteria for the Structural Analysis of Shipping Cask Containment Vessels*, Revision 1, March 1978.

A Method for Comparing Impacts with Real Targets to Impacts onto the IAEA Unyielding Target*

D. J. Ammerman

Sandia National Laboratories, Albuquerque, New Mexico, United States of America**

INTRODUCTION

The severity of the IAEA accident conditions test requirement (IAEA 1990) of an impact onto an essentially unyielding target from a drop height of 9 meters encompasses a large fraction of all real world impacts. This is true, in part, because of the unyielding nature of the impact target. Impacts onto the unyielding target have severities equivalent to higher velocity impacts onto real targets which are not unyielding. The severity of impacts with yielding targets is decreased by the amount of the impact energy absorbed in damaging the target. In demonstrating the severity of the regulatory impact event it is advantageous to be able to relate this impact onto an essentially unyielding target to impacts with yielding targets.

BACKGROUND

There are several reasons for wanting to relate the severity of impacts with yielding targets to that of impacts with an unyielding target. The motivation for making the comparison will somewhat dictate the way the comparison is made. In the Final Environmental Statement on the Transportation of Radioactive Material by Air and Other Modes (US NRC 1977), which is a risk assessment for the shipment of all types of radioactive material, the properties of the packaging were not known. This forces the relationship between impact velocities for yielding and unyielding surfaces to be independent of package stiffness. For this reason a method was developed that compared the penetration of a rigid sphere into different surfaces, with steel considered to be the unyielding target. Velocities resulting in equal penetration depth were considered to be equivalent. This led to the following relationship for determining equivalent impact velocities:

$$\frac{V_{yielding}}{V_{steel}} = \left[\frac{1-\nu_y^2}{1-\nu_s^2}\right]\left[\frac{E_s}{E_y}\right]^{1/3} \qquad \text{(EQ 1)}$$

where $V_{yielding}$ is the velocity for impact onto a yielding surface, V_{steel} is the velocity for impact onto an unyielding surface, ν_y and E_y are Poisson's ratio and Young's modulus for the yielding surface material, and ν_s and E_s are Poison's ratio and Young's modulus for steel. This method was only applied to aircraft accident scenarios and the distribution of target hardness was determined by the ground surface composition along airline flight paths.

---

* This work performed at Sandia National Laboratories, Albuquerque, New Mexico, supported by the United States Department of Energy under Contract DE-AC04-76DP00789.

** A United States Department of Energy Facility.

In the Modal Study (Fischer et al. 1987), a risk assessment for the transport of spent fuel, the properties of the package were known. This allows the relationship between yielding and unyielding targets to depend on package characteristics. To determine equivalent impact velocities an equivalent damage technique was used. This technique resulted in a relationship for velocities of:

$$\frac{V_{yielding}}{V_{unyielding}} = \sqrt{1 + \frac{d_s}{d_c}} \qquad \text{(EQ 2)}$$

where $V_{unyielding}$ is the impact velocity for impacts onto an unyielding surface, d_s is the deformation of the yielding target caused by an impact of a rigid package at a velocity such that the impact force is the same as for the impact of the package on an unyielding target, and d_c is the deformation of the package caused by impact on an unyielding target.

METHOD

The method discussed in this paper for relating impacts with yielding targets to an impact with an unyielding target will apply the principle of conservation of energy. Immediately before the impact the energy of the package and target is equal to the kinetic energy of the package. At the point of maximum deformation of the package and the target the velocity is zero, so all of the energy in the system is strain energy. For impacts onto a rigid target the strain energy of the system is all in the package. During an impact with a real target the strain energy of the system is in both the package and the target. For casks, the strain energy in the package is typically divided into strain energy in the impact limiter and strain energy in the cask body, with the strain energy in the impact limiter typically being orders of magnitude larger than the strain energy in the cask body. If inertial effects are ignored the force acting on the cask body is the same as the force acting on the impact limiter and target for any time during the impact event. This condition can be viewed as a spring-mass system with a set of three massless nonlinear springs acting in series. Figure 1 shows this simplification of the impact event. Notice in this figure that the impact limiter target springs are treated as massless. For the impact limiter this assumption is generally quite accurate because its mass is usually much less than the mass of the cask. Neglecting the mass of the target in most cases does not introduce a large error in the analysis because the velocity, and therefore kinetic energy, of this mass is usually very small.

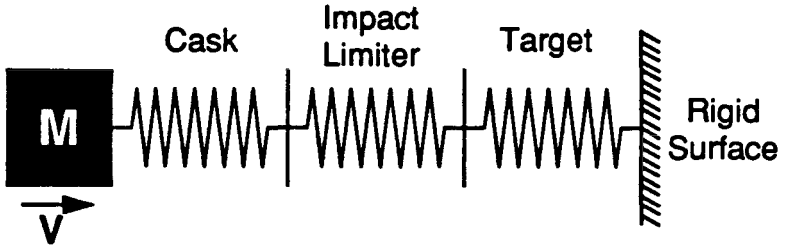

Figure 1 - Simplified spring model for impacts.

The strain energy in each of the springs for a given displacement is equal to the area under the force-deflection curve up to that displacement. For a linear spring this results in the familiar equation $E = 1/2K\delta^2$, where E is the strain energy in the spring, K is the linear spring constant, and δ is the displacement of the spring. For a non-linear spring with a force-deflection relationship defined by F(x), equation 3 shows the mathematical expression for the strain energy:

$$E = \int_0^{\delta} F(x)\,dx \qquad \text{(EQ 3)}$$

Where:

E = The strain energy in the spring.
F(x) = The force in the spring as a function of displacement.
x = The displacement of the spring.
δ = The displacement of the spring at the force level of interest.

In the system depicted in Figure 1, the total strain energy of the three springs must be equal to the kinetic energy of the mass at impact, and the force in the three springs is equal. These two conditions are the constraints on the problem and may be expressed mathematically as:

$$\frac{1}{2}MV_{yielding}^2 = E_c + E_i + E_t \qquad \text{(EQ 4)}$$

and

$$F_c = F_i = F_t \qquad \text{(EQ 5)}$$

where M is the mass of the cask and impact limiter, $V_{yielding}$ is the impact velocity onto a yielding target, E_c, E_i, and E_t are the strain energies in the springs representing the cask body, impact limiter, and target, and F_c, F_i, and F_t are the instantaneous forces in these springs.

For impacts onto an unyielding target the entire kinetic energy of the mass must be converted into strain energy of the cask and impact limiter. This implies that the strain energy in the springs representing the cask and impact limiter is equal to the kinetic energy of the mass for an impact onto an unyielding target. Expressing this mathematically:

$$E_c + E_i = \frac{1}{2}MV_{unyielding}^2 \qquad \text{(EQ 6)}$$

where $V_{unyielding}$ is the impact velocity onto an unyielding target. Equations 4 and 6 can be combined to provide a relationship for velocities of:

$$\frac{V_{yielding}}{V_{unyielidng}} = \sqrt{1 + \frac{E_t}{E_c + E_i}} \qquad \text{(EQ 7)}$$

EXAMPLE PROBLEM

The method described above will be demonstrated with the following example problem. A 90,700 kg (100 ton) rail cask impacts a hard soil with a velocity of 26.8 m/s (60 MPH). The impact limiter for this cask is designed using simplified relationships to limit the deceleration from the regulatory drop to 40 g with a crush of 0.23 m, which is below the lock-up deflection of the impact limiting material. This impact limiter is within the normal range used for this type of package, but it is softer than most. In the regulatory 9 meter drop the cask has an actual acceleration of 43.5 g and there is 0.236 m of crush in the impact limiter. The force deflection curve for the impact limiter is shown in Figure 2, along with force deflection curves for the cask body and the hard soil target. For this case the force displacement relationship for the cask body is:

$$F_c = A(1 - e^{-Bx_c} + Cx_c) \qquad \text{(EQ 8)}$$

the force displacement relationship for the impact limiter is given by:

$$F_i = D[1 - e^{-Ex_i} + F(e^{G(x_i - H)} - e^{-GH})] \qquad \text{(EQ 9)}$$

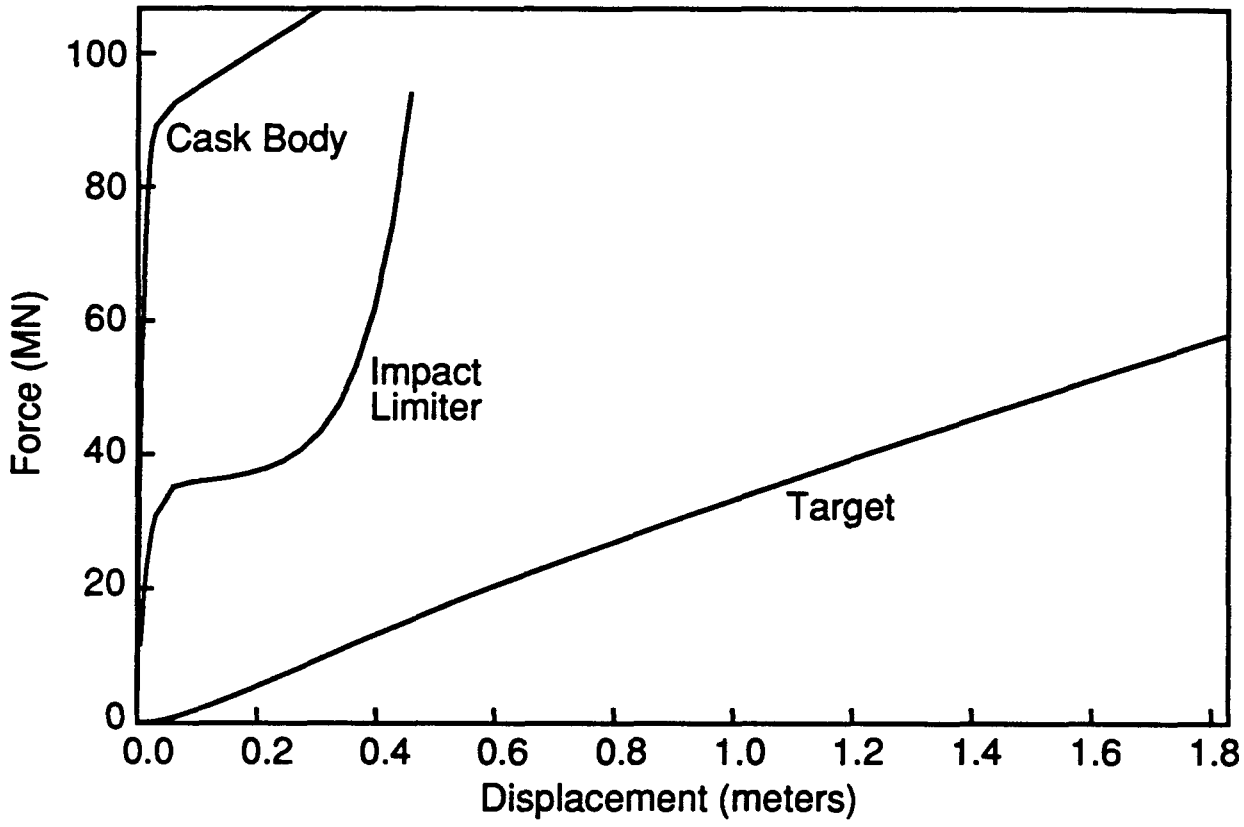

Figure 2 - Force-displacement curves for a rail cask body, its impact limiter, and a hard soil target.

and the force displacement curve for the hard soil target is given by:

$$F_t = K\left[JLx_t^{L-1} - P\left(e^{-Px_t} - e^{-Nx_t}\right)\right] \qquad \text{(EQ 10)}$$

In these equations A-P are constants that define the curves with the values listed below, x_c, x_i, and x_t are expressed in meters and the forces F_c, F_i, and F_t are expressed in Newtons:

A = 89.0×10^6 N
B = 131 m^{-1}
C = 0.656 m^{-1}
D = 35.6×10^6 N
E = 98.4 m^{-1}
F = 0.1
G = 13.12 m^{-1}
H = 0.244 m
J = 9.81 $m^{-1.922}$
K = 1.76×10^6 N.m
L = 1.922
N = 9.84 m^{-1}
P = 4.92 m^{-1}

These equations were developed by fitting experimental (Bonzon and Schamaun 1976, Gonzales 1987, and Waddoups 1975) and analytical data. It would also be possible to use experimental data directly and express the relationships between force and displacement in tabular form. This method will require numerical integration of the force-displacement curves to calculate the strain energy associated with each spring. For the equations above it is possible to integrate explicitly, resulting in the expressions below for strain energy.

$$E_c = \int_0^{\delta_c} F_c dx_c = A\left[\delta_c + \frac{1}{B}e^{-B\delta_c} - \frac{1}{B} + \frac{C}{2}\delta_c^2\right] \quad \text{(EQ 11)}$$

$$E_i = \int_0^{\delta_i} F_i dx_i$$

$$= D\left[\delta_i + \frac{1}{E}(e^{-E\delta_i} - 1) + \frac{F}{G}e^{-GH}(e^{G\delta_i} - 1 - G\delta_i)\right] \quad \text{(EQ 12)}$$

$$E_t = \int_0^{\delta_t} F_t dx_t = K\left[J\delta_t^L + e^{-P\delta_t} - 1 - \frac{P}{N}(e^{-N\delta_t} - 1)\right] \quad \text{(EQ 13)}$$

The sum of the strain energies for the three springs must be equal to the kinetic energy at impact, which is equal to $1/2MV_1^2$, where V_1 is equal to 26.8 m/s and M is equal to 90,700 kg. This gives a value for the kinetic energy of 32.6×10^6 N·m. To determine how this energy is distributed between the cask body, the impact limiter, and the target a complex system of non-linear equations must be solved. Generally for problems of this nature it is easier to solve them numerically with the aid of a computer, but it is possible to use a trial and error method for the solution. Solving this system of equations for this problem yields the following results. The strain energy in the cask body is 0.09×10^6 N·m, the strain energy in the impact limiter is 8.69×10^6 N·m, and the strain energy in the target is 23.82×10^6 N·m. The force acting on the three springs is 39.4×10^6 N (equivalent to 44.3 g acceleration). The elastic displacement of the cask body spring is 4.4 mm, the displacement of the impact limiter spring is 0.252 m, and the displacement of the target spring is 1.20 m. The sum of the energy in the cask and impact limiter springs is 8.78×10^6 N·m, which is the kinetic energy for a 13.9 m/s impact onto an unyielding target, using Eq. 6.

If we consider a 26.8 m/s impact of this cask onto the yielding target without its impact limiter the force in the cask and target springs is 45.5×10^6 N (equivalent to 51.1 g acceleration), the strain energy in the cask body spring is 0.14×10^6 N·m, and the strain energy in the target spring is 32.5×10^6 N·m. The elastic displacement of the cask body spring is 5.4 mm and the displacement of the target spring is 1.41 m. The equivalent velocity for an impact onto an unyielding target is 1.74 m/s (3.9 MPH). In the two cases the damage to the cask body is likely to be very small or non-existent. This is indicated by the lack of inelastic deformation in the cask body springs. (Note from Figure 2 that a force of 45.5×10^6 N is still well within the linear portion of the force-displacement curve for the cask body spring.)

This example demonstrates an important fact concerning target hardness. A target that is hard for one package may be soft for another package. The package system with an impact limiter is not as stiff as the package without the impact limiter. In the case of the package with the impact limiter a significant amount of the impact energy is absorbed by the impact limiter, which is only slightly stiffer than the target for this level of loading. For the package without an impact limiter almost all of the impact energy is absorbed by the target because the cask body is much stiffer than the target.

EFFECT OF PACKAGE AND TARGET STIFFNESS

The effect of package and target stiffness on the relative damage, as measured by deformation, caused by impacts onto yielding targets can be demonstrated by varying the impact limiter and target stiffnesses. For this exercise the energy absorbed by the package itself is ignored because it is insignificant compared to the amount absorbed by the impact limiter and target. The target is considered to be a linear spring with variable stiffness and the impact limiter is considered to be a bi-linear spring with nearly constant crush force. The crush force for the impact limiter depends on the g level desired for the impact. For each impact limiter and target stiffness the impact velocity required to produce the same amount of damage as that from a 9 m free fall (13.4 m/s impact velocity) onto an unyielding target is calculated. Two packages are considered, a 90,700 kg rail cask and a 23,000 kg truck cask. For the rail cask three different impact limiters are used, one resulting in approximately 40 g acceleration, one with approximately 60 g acceleration, and one with approximately 80 g acceleration. For the truck cask four impact limiters are considered, with approximate accelerations of 40, 60, 80, and 100 g. Figure 3 shows the resulting equivalent impact velocities required for the three rail casks and Figure 4 shows the equivalent velocities for the four truck casks. The linear stiffness that approximates the force deflection curve for the hard soil target in the preceding example is 3.3×10^7 N/m. From these two figures it can be seen that targets with stiffness greater than about 1×10^9 N/m can be treated as essentially unyielding and targets with stiffness less than about 1×10^6 N/m cause very little damage to the package. This result is very package specific and should not be thought of as globally applicable. For smaller, less stiff packages targets with stiffnesses in the range of 1×10^6 N/m may appear to be essentially unyielding. For these smaller packages it is less likely to have targets with these high stiffness levels because the contact area between the package and the target is also smaller.

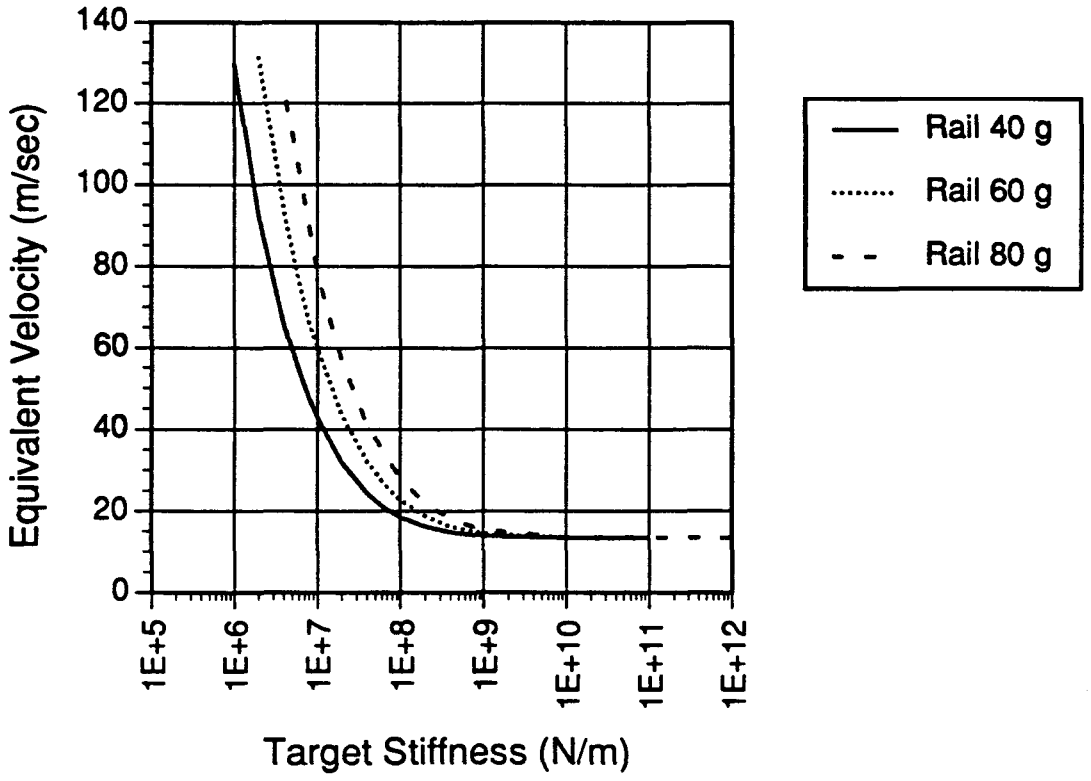

Figure 3 - Impact velocity onto a yielding target that causes the same damage as a 9 m impact onto an unyielding target for a 90,700 kg rail cask.

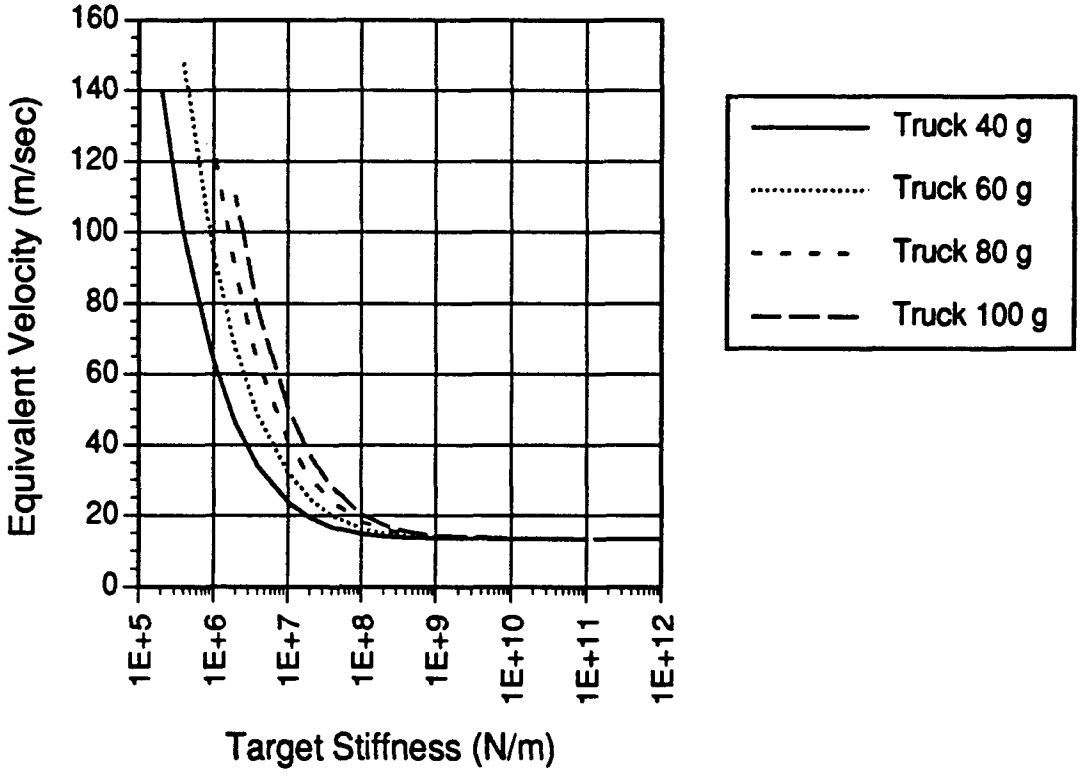

Figure 4 - Impact velocity onto a yielding target that causes the same damage as a 9 m impact onto an unyielding target for a 23,000 kg truck cask.

LIMITATIONS

To apply the method described in this paper for relating impacts with yielding targets to impacts with an unyielding target the user must know the load-displacement properties of the target as well as the cask body and impact limiter. For most radioactive material shipping packages the cask body is much more rigid than the impact limiter, and a close approximation to the solution can be obtained by assuming the cask is rigid. This reduces the spring system to two springs: one representing the impact limiter and one representing the target. For many targets, such as vehicles and posts, the amount of energy they can absorb before failing is finite. In these cases, if the impact energy is greater than the energy absorbed by the cask body, impact limiter, and target at the time the target fails, the package will not be stopped by the impact and will have a residual kinetic energy.

Modelling the cask body, the impact limiter, and the target as massless springs implies that the impact event is one-dimensional and quasistatic. That is, there is no load transmitted normal to the direction of motion, the forces are applied as distributed loads, and there are no inertial or strain rate effects. For packages such as the one in the example, where the cask body is much stiffer than the impact limiter, loads at this interface that are normal to the direction of motion have little significance and point loads are unlikely so the one dimensional crush is an accurate approximation. At the interface between the impact limiter and the target it is quite likely that loads in the transverse direction will cause crushing of either the impact limiter or the target, which will result in some energy absorption. This fact will tend to reduce the severity of the impact on the yielding target compared to the impact modelled as one dimensional crush. Severe impact tests on small packages (Bonzon and Schamaun 1976) showed this result by differences in failure mode. Impacts onto soil targets that had deformations of the cask body similar to lower velocity impacts onto an unyielding target did not result in gross failure of the containment boundary, while the impacts on the unyielding target did. This result could also be caused by higher strain rates for the impacts onto the unyielding

target. The change in failure mode caused by transverse forces or strain rate effects is impossible to model as an impact onto an unyielding target at a lower velocity. The method of this paper considers the impact onto the yielding target to be more severe than it actually is. For the purpose of risk assessments or hazard communications this result is conservative.

CONCLUSIONS

A mathematically rigorous method is developed for relating impacts with yielding targets to lower velocity impacts with unyielding targets. The method correctly models the mechanics of the impact and the conversion of kinetic energy to strain energy. An important result shown by the example problem is that apparent target hardness depends on the stiffness of the impacting package. For a cask with impact limiters a 26.8 m/s impact onto hard soil results in equivalent forces as a 13.9 m/s impact onto an unyielding target. For the same cask without the impact limiters a 26.8 m/s impact onto hard soil is equivalent to a 1.74 m/s impact onto an unyielding target. This is one reason why non-technical members of the public often have difficulty realizing the severity of the regulatory impact. For most people, objects such as trucks and bridge columns appear to be very hard, but to many radioactive material shipping packages these objects are relatively soft.

The method discussed in this paper for relating impacts with yielding targets to lower velocity impacts with unyielding targets helps to explain how the regulatory impact accident provides a high degree of safety to the public. This methodology is relatively simple to use, and can be applied to the "What if" scenarios brought up by interveners.

REFERENCES

L. L. Bonzon. and J. T. Schamaun, *Container Damage Correlation with Impact Velocity and Target Hardness*, IAEA-SR-10/21, Transport Packaging for Radioactive Materials, IAEA, Vienna, Austria, 1976.

L. E. Fischer, et.al., *Shipping Container Response to Severe Highway and Railway Accident Conditions*, NUREG/CR-4829, February 1987.

A. Gonzales, *Target Effects on Package Response: An Experimental and Analytical Evaluation*, SAND86-2275, Sandia National Laboratories, Albuquerque, NM, 1987.

IAEA, *Regulations for the Safe Transport of Radioactive Materials* 1985 Edition (As Amended 1990), IAEA Safety Series No. 6, International Atomic Energy Agency, Vienna, 1990.

U.S. Nuclear Regulatory Commission, *Final Environmental Statement on the Transportation of Radioactive Material by Air and Other Modes*, NUREG-0170, Washington, DC, December 1977.

I. G. Waddoups, *Air Drop Test of Shielded Radioactive Material Containers*, SAND75-0276, Sandia National Laboratories, Albuquerque, NM, 1975.

Results of the Sandia National Laboratories MOSAIK Cask Drop Test Program*

Ken Sorenson, Richard Salzbrenner, Gerald Wellman and Jeffrey Bobbe

Sandia National Laboratories,** Albuquerque, New Mexico, United States of America

Introduction

There has been a significant international effort over the past ten years to qualify structural materials for construction of radioactive material (RAM) transportation casks. As *total life cycle cost* analyses argue the necessity for more efficient casks, new candidate structural materials are evaluated relative to the historically accepted austenitic stainless steels. New candidate cask containment materials include ferritic steels, ductile iron, depleted uranium, and titanium. Another material, borated stainless steel is being considered for structural cask internals because of its neutron absorption properties. The mechanical performance of the borated stainless steels is a function of the boron content and metallurgical processing conditions. A separate paper in this symposium (Stephens et al. 1992) deals with the properties of a range of borated stainless steels. A major technical issue involved with the qualification of all these candidate materials is that they may, under certain combinations of mechanical and environmental loading, fail in a brittle fashion. Such a failure would of course not be acceptable for a RAM transport cask involved in an accident. The cask designer must assure cask owners, regulators as well as the general public that the cask will not undergo brittle fracture for all regulatory loading conditions.

Qualification of ferritic metals, and in particular ductile iron, has progressed on a number of fronts. Standards development and analyses and testing programs have been pursued through a number of international organizations. Two companion papers are also being presented at PATRAM '92; the first paper (Sorenson et al. 1992) deals with developing a brittle fracture evaluation criterion through the IAEA and the second paper (Salzbrenner et al. 1992) describes the materials characterization program for the MOSAIK casks.

This paper summarizes the drop tests that were conducted using the MOSAIK casks to verify the fracture mechanics cask design approach and to demonstrate that ductile iron could be subjected to severe loading conditions without failing in a brittle manner.

Engineering Basis

The fundamental engineering discipline of linear-elastic fracture mechanics (LEFM) is being applied to the qualification of ferritic materials for structural components in RAM transport casks. The basic formulas that describe material behavior are;

$$K_I = C\sigma(\pi a)^{1/2} \qquad \text{Equation 1}$$

* This work performed at Sandia National Laboratories supported by the U. S. Department of Energy under contract number DE-AC04-76DP00789.

** A U. S. Department of Energy Facility.

where,

K_I = applied stress intensity {MPa-$m^{1/2}$}
C = geometric constant
σ = maximum applied tensile stress {MPa}
a = depth of flaw at location of maximum applied tensile stress {m}

Further, to preclude brittle fracture behavior, the materials fracture toughness value, K_{Ic}, must be greater than the applied stress intensity value, K_I;

$$K_{Ic} > K_I \qquad \text{Equation 2}$$

Equations (1) and (2) can be used to predict the critical flaw depth, a_{CT}, at which brittle fracture is imminent for the set of design conditions under consideration;

$$a_{CT} = \pi^{-1}(K_{Ic}/C\sigma)^2 \qquad \text{Equation 3}$$

This set of equations allows the cask designer to adjust the design parameters (i.e. applied stress, material properties, and inspection procedure) in order to satisfy Equation (2). Applying these equations to cask design, the potential for brittle fracture is precluded.

The above Equations 1-3 assume the cask will behave in a linear elastic manner. Under linear elastic conditions, the applied stress causes negligible plastic deformation, and all of the applied energy is available to extend the flaw. This is a conservative assumption, in actuality plastic deformation in the vicinity of the flaw will often occur. Extensive plastic deformation has at least two effects: the first is that the crack tip is blunted and thereby becomes less potent; the second is that since some of the "energy" from the applied stress has been "absorbed" by the plastic deformation processes, that less is available to propagate the flaw.

The situation in which significant plastic deformation precedes (or accompanies) flaw extension is appropriately treated by elastic-plastic fracture mechanics (EPFM). The engineering application of EPFM is somewhat more complex, but its basic steps are comparable to those described above for LEFM. The applied driving force to extend the flaw is designated J_I, which is a measure of the elastic-plastic stress-strain field ahead of the flaw tip. This can be calculated (using finite element methods for complex geometries) as the path-independent line or surface integral that encloses the crack front from one crack surface to the other. A method for doing this is described elsewhere (Wellman, 1990). The applied J_I is compared to the material's inherent resistance to crack initiation, called J_{Ic}. J_{Ic} is a material property which can be measured in the laboratory (and can be related to K_{Ic} which is the material's resistance to crack initiation in linear elastic terms). When J_I is less than J_{Ic} no crack initiation from the flaw will occur. When J_I is greater than J_{Ic}, at least some crack initiation from the flaw will occur.

While the methods of LEFM may be applied via a straightforward hand calculation, the EPFM procedure in most cases requires finite element analysis (using a material model which accurately captures the plastic regime of the stress-strain behavior) performed on large computers. While the EPFM methods describe the structural response more accurately, the LEFM method can be used as a conservative, easy-to-apply approximation. The MOSAIK cask drop tests were analyzed using both the LEFM approximation and the more exact EPFM procedure. The MOSAIK cask test program was used to demonstrate the validity of this approach and to quantify the factor of safety that can be expected when designing casks using LEFM.

Physical Description of the Test Casks

Two casks were used in this test program; the MOSAIK KfK and the MOSAIK I. These casks were donated to Sandia National Laboratories by Gesselschaft für Nuklearservice (GNS) of Germany. The casks were constructed of ductile iron and are currently used in Europe to transport low-level radioactive wastes. The MOSAIK KfK was the cask that was used for the rigorous testing. The MOSAIK I was used primarily as a device to verify test conditions, rigging procedures, instrumentation, etc., prior to a drop of the MOSAIK KfK. Table 1 details the main physical features for each cask.

The primary test variable in sequential drop tests was the depth of the artificially induced flaw. Successive tests were performed with deeper flaws in order to increase the applied (LEFM) stress intensity in the cask wall as shown in Equation 1. Flaws were introduced by radial cuts from the cask exterior; all flaw tips were subsequently sharpened either by machine or laser techniques. The machine sharpening technique produced flaw tips with a root radius smaller than 0.08 mm. The laser sharpening method produced a small region of remelted material in which small cracks (with a tip radius <0.01 mm) were formed during resolidification. Laboratory tests (room temperature, static loading rate) showed that the measured fracture toughness of ductile iron specimens with the laser induced flaw decreased from the values measured on fatigue precracked specimens. In linear elastic fracture toughness units, the fatigue precracked specimens produced an average value of 120 MPa-$m^{1/2}$ while the laser flawed specimen yielded a value of 78 MPa-$m^{1/2}$. The laser technique was successful in producing an artificial flaw which is more severe than the crack induced by fatigue-type loading.

Figure 1 shows a photograph of a laser-sharpened flaw. This micrograph highlights the graphite nodules imbedded in the ferritic matrix, and also shows the cracks formed during solidification. High carbon martensite is formed in the remelted zone, and possesses a very low toughness. A small volume of embrittled material is thereby placed at the tip of the artificial flaw. The induced cracks and the zone of embrittled material are both effective in lowering the resistance to cracking during an impact loading event. This laser flaw is much more severe than naturally occurring flaws formed by casting defects.

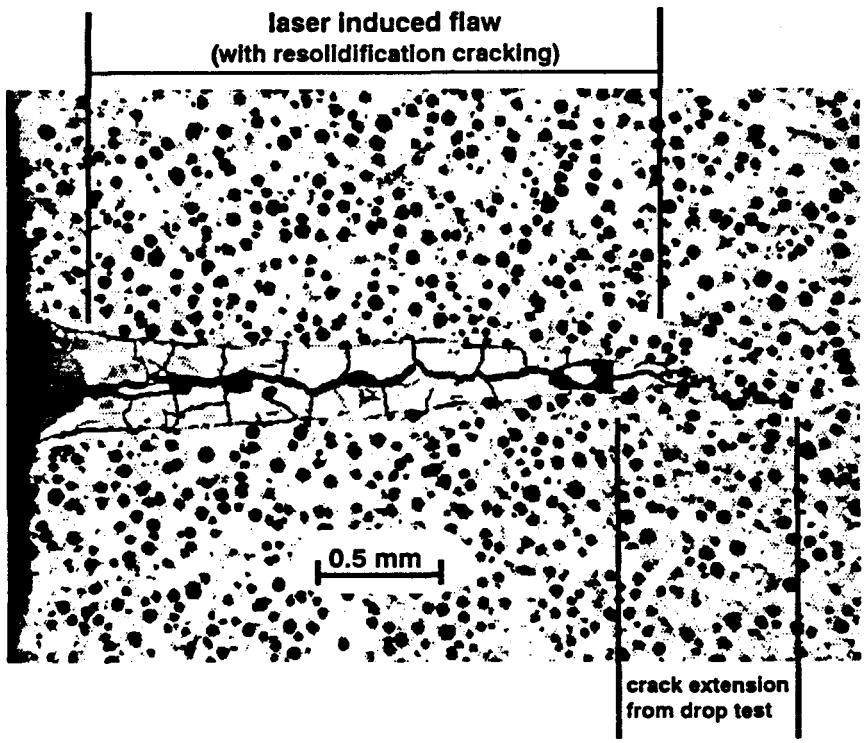

Figure 1. Micrograph of the laser sharpened flaw removed from the MOSAIK KfK cask after the 5th drop test. A small amount (<1 millimeter) of ductile crack extension occurred. A length of approximately 137 mm of uncracked material remained from the furthest extent of crack extension to the inner cask wall.

Table 1. Mass and dimensions of the two MOSAIK casks used in the Sandia National Laboratories MOSAIK Drop Test Program.

Cask	Mass (Kg)	Height (mm)	Outside Ø (mm)	Inside Ø (mm)	Wall Thick, (mm)
MOSAIK KfK	5402	1365	1060	632	214
MOSAIK I	2960	1150	900	600	150

Material Description of the Test Casks

Both the MOSAIK I and the MOSAIK KfK casks were manufactured in the early 1980's and utilize a ductile iron that is not as advanced as the materials currently produced by GNS (and others) using the most recent casting procedures. More advanced, later generation materials generally possess higher ductility and have a lower variation in mechanical properties through the wall thickness. The ductile iron used in the casks tested in this program does not meet the ASTM A-874 specification on ductile iron for composition. Therefore, these casks tests can be considered as lower bound test case for ductile iron. A complete description of materials testing and properties (material composition and microstructure) is provided in another PATRAM '92 paper (Salzbrenner et al. 1992).

The testing revealed that the cask material had the following "average" (Salzbrenner et al. 1992) characteristics:

* Young's Modulus = 24.1 x 10^5 MPa
* Yield Strength = 243 MPa
* Ultimate Strength = 378 MPa
* Tensile Elongation = 24.3% (25mm gage)
* Reduction in Area = 20.6%
* Static Rate Frac. Toughness @–29°C = 95.3 MPa-$m^{1/2}$ (LEFM) ↔ 54.4 kJ/m^2 (EPFM)
* Dynamic Rate Frac. Tough. @–29°C = 74.7 MPa-$m^{1/2}$ (LEFM) ↔ 33.1 kJ/m^2 (EPFM)
* Microstructure — High nodularity of the graphite (>95% Types I & II)
  — Low pearlite (<5%)

Nondestructive Examination Procedures

Before the drop tests were conducted, a comprehensive set of nondestructive examination tests were performed to fully characterize the soundness of the casks. The casks were inspected using dye penetrant, ultra-sonic, and radiographic examinations. The dye penetrant and ultra-sonic testing procedures were performed in accordance with ASTM and ASME standards. The radiography testing was performed in accordance with ASME procedures. No flaws were detected in the castings. These three independent procedures provided a high probability of identifying all material flaws (e.g., casting voids, cracks, and other defects) large enough to constitute a flaw size approaching a_{cr}.

Test Parameters

The drop test program used the hypothetical accident conditions specified by US regulations (10CFR71 1984) as a basis for drop criteria. Parameters that were held constant for each drop were:

1. a 9 meter cask drop height (with one exception),
2. a drop onto an unyielding surface,
3. the cask was dropped without impact limiters (steel rails on the cask ends were used to increase the tensile component of the applied stress in the vicinity of the artificial flaw),
4. the cask metal temperature was = –29°C, and
5. an artificial flaw was placed in the cask wall in the location of the highest applied tensile stress.

Figure 2 depicts the drop test set-up. The casks were dropped with two steel rails attached to the ends to produce through-wall tensile stresses in the proximity of the artificial flaw. The laser flaw in combination with the steel rails on the ends of the cask provides favorable conditions to reveal whether brittle fracture can be induced (at –29°C) in the cask material. The test conditions used for the drop tests of the MOSAIK casks are significantly more severe than those required by the U. S. regulations (in which potential consequences of flaws are not treated). Figure 3 shows the generalized instrumentation employed during the MOSAIK KfK drop tests. Instrumentation included accelerometers, strain gages, and thermocouples (two thermocouples were located in small diameter (~1.6 mm) holes at 2.5 and 10 cm wall depths). The accelerometer and strain gage results are used to benchmark the finite element analyses.

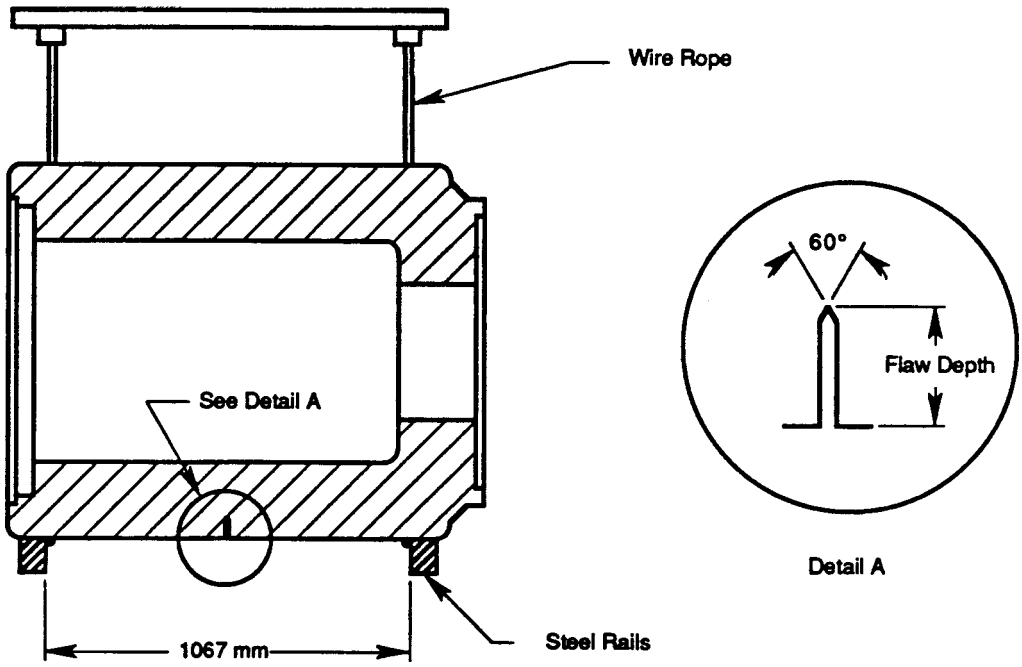

Figure 2. MOSAIK KfK Drop Test Set-up.

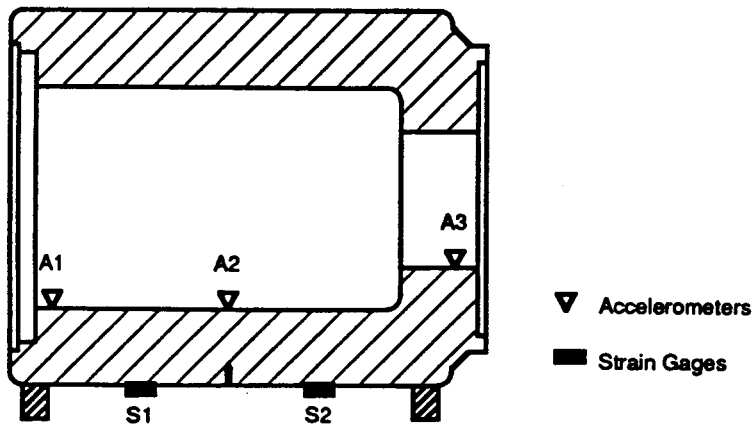

Figure 3. Instrumentation for MOSAIK KfK.

All MOSAIK drop tests were conducted with the parameters shown above, with one exception: in a single drop test, the drop height was increased from 9 to 18 meters. This test was performed to dramatize the integrity of the ductile iron cask when subjected to (extreme) extra-regulatory testing. The drop test was also performed in order to increase the applied tensile stresses, thereby increasing the driving force on the artificial flaw above initiation levels. This test was designed to cause crack propagation from the laser flaw.

Results and Discussion of the Drop Tests

Table 2 shows the results of the drop tests for both the MOSAIK I and the MOSAIK KfK casks. Instrumentation and structural analyses were not performed for the MOSAIK I drop tests. The MOSAIK I drop tests were "break / no break" observations of cask performance. The drop tests of the MOSAIK I casks resulted only in "no break" observations. This was despite an increase in the artificial flaw depth from ~12% to greater than 75% of the thickness of the cask wall for the sequential drops listed in Table 2 as 1 through 6 for MOSAIK I.

For the MOSAIK KfK, Drop Tests 1 through 4 represented essentially constant drop test conditions with successively deeper flaws. The simplified LEFM calculations suggested that the increasingly deep flaws would increase the linear elastic driving force for crack extension (i.e., brittle fracture). Experimental results demonstrated that no brittle crack extension occurred during these tests. The LEFM calculations were conservative for the MOSAIK KfK cask drop tests. LEFM predicted that brittle fracture should occur (if linear elastic conditions could be maintained during these drops), but brittle fracture was not observed. LEFM methods are conservative because they do not account for plastic deformation which effectively lowers the driving force on the artificial flaw. The gross flaws which were used in these tests are much larger than the largest flaw that could be missed (with greater than 99% reliability) during NDE inspections listed as routine (Urabe and Harada, 1989).

The finite element analyses of Drop Tests 1 through 4, showed that even with extremely large flaw depths – up 76.2 mm (36% of the wall thickness) – tensile stresses were still below yield stress levels for the material. The MOSAIK drop tests provide a specific demonstration of the difficulty of obtaining yield level (tensile) stresses in thick-walled casks even when impact limiters are not attached. Calculation (based on the finite element analyses) of the EPFM driving force on the flaws for Drop Tests 1 through 4 showed it to be below the elastic-plastic fracture toughness of the cask material (measured at –29°C and dynamic loading rates). The factors of safety against (ductile) fracture for these drop tests are listed in Table 2, and averaged approximately 1.3. The tip of the artificial flaw was removed after the drop tests and examined for evidence of crack initiation. No crack initiation was found for the MOSAIK KfK Drop Tests 1 through 4.

In order to achieve yield level stresses and increase the applied J_I above the level of J_{Ic} (the material's fracture toughness), the fifth KfK drop test was performed from a height of 18 meters. The experimental results showed that this drop did cause the applied stress to exceed the yield strength of the material. The calculated value of the EPFM driving force exceeded the laboratory measurement (Salzbrenner et. al. 1992) of elastic-plastic fracture toughness. The factor of safety was computed as 0.9 (i.e., the flaw depth was greater than the calculated critical flaw depth). Metallographic examination of the flaw tip region confirmed that crack initiation did in fact, occur. A crack extended from the tip of the remelted zone of the laser flaw into the cask matrix. Approximately 0.25 – 0.31 mm of cracking into the matrix occurred; the growing crack was arrested by the matrix material after this small amount of growth.

The results of the fifth MOSAIK KfK drop test are especially significant. The cask was dropped from a height of 18 meters onto an unyielding surface (without impact limiters). Steel rails were employed to enhance the through-wall driving force near the flaw, and the cask metal temperature was below –29°C. Crack initiation did occur, as was predicted from the EPFM analysis, (the conservative LEFM calculations predicted brittle fracture), but the crack growth arrested after less than a millimeter of growth. That is, only stable ductile tearing occurred. This test verified that the material did indeed behave as an elastic-plastic material, in a manner consistent with that demonstrated by laboratory specimens of the same material. For this material and design configuration, the test parameters could not induce a change in the fracture behavior from ductile tearing to brittle cleavage even when crack initiation (ductile) is intentionally introduced. The entire MOSAIK Drop Test Program on the MOSAIK KfK and the MOSAIK I demonstrate that brittle fracture will not occur for accelerations up to 1150 *gs* at a temperature of –29°C.

Table 2. Test conditions and measured values for the Sandia National Laboratories MOSAIK Drop Test Program of the MOSAIK I and the MOSAIK KfK ductile iron casks (FS = Factor of Safety).

		date	drop hght. (m)	metal temp. (°C)	flaw depth (mm)	flaw tip radius (mm)	flaw aspect ratio	strain⁺ (10^{-6})	tensile stress# (MPa)	fracture toughness K_{Ic}++ (MPa-$m^{1/2}$)	LEFM applied K_I (MPa-$m^{1/2}$)	estimated LEFM FS (K_{Ic}/K_I)	F.E. applied K_I# (MPa-$m^{1/2}$)	FS# (K_{Ic}/K_I)	max. gs⁺ [at 1 kHz]
MOSAIK I															
(2960 Kg	#1	3/14/90	9	-26	25.4	laser	4.5 : 1								
150 mm	#2	3/21/90	9	-31	45.2	laser	3.1 : 1								
wall	#3	5/23/90	9	-32	76.2	.0762	3.2 : 1								
thickness)	#4	8/29/90	9	-32	76.2	laser	3.1 : 1								
	#5	7/10/91	9	-31	101.6	laser	4.0 : 1								
	#6	7/12/91	9	-31	127.0	laser	3.2 : 1								
MOSAIK KfK															
(5402 Kg	#1	6/25/90	9	-26	19.1	.0762	6.8 : 1	1100	179	74.8	51	1.5	50.6	1.5	950
214 mm	#2	2/2/91	9	-29	50.4	.0762	6.0 : 1	750	124	74.8	70	1.1	62.3	1.2	600
wall	#3	8/1/91	9	-29	57.1	laser	6.2 : 1	1100	179	74.8	78	<1	53.9	1.4	800
thickness)	#4	9/5/91	9	-31	76.2	laser	6.0 : 1	900	179	74.8	102	0.7	58.7	1.3	710
	#5	11/14/91	18	-31	57.1	laser	6.2 : 1	1850	**	74.8	**	**	83.6	0.9	1150

Not Determined

⁺ by field measurements
by finite element (elastic-plastic) calculation
++ by laboratory measurement
** not determined

Conclusions

The MOSAIK Drop Test Program at Sandia National Laboratories provides a rigorous demonstration that an LEFM approach to cask design is conservative. Further, it shows that ductile iron is an appropriate material of construction for structural components of RAM transport casks. Results of this test should be used in a complementary fashion with programs from other organizations to provide a background of engineering data that will assure cask owners and regulators alike that LEFM is an appropriately conservative method for designing casks and evaluating cask structural components for the risk of brittle fracture.

References

10CFR71, *Title 10, Code of Federal Regulations, Part 71*, Office of the Federal Register, Washington, DC, (1984).

Sorenson et al., "Development of a Brittle Fracture Acceptance Criterion for the International Atomic Energy Agency," *The 10th International Symposium of the Packaging and Transportation of Radioactive Materials, PATRAM '92* Yokohama, Japan, September 13-18, (1992).

Salzbrenner, R., et al., "Mechanical Properties Used for the Qualification of Transport Casks: Prototype Development and Extension of Serial Production," *The 10th International Symposium of the Packaging and Transportation of Radioactive Materials, PATRAM '92*; Yokohama, Japan, September 13-18, 1992.

Stephens, J. J. et al., "Elevated Temperature Tensile Properties of Borated 304 Stainless Steels: Effect of Boride Dispersion on Strength and Ductility," *The 10th International Symposium of the Packaging and Transportation of Radioactive Materials, PATRAM '92*; Yokohama, Japan, September 13-18, 1992.

Urabe, N., and Harada, Y., "Fracture Toughness of Heavy Section Ductile Iron Castings and Safety Assessment of Cast Casks," Proceedings of *The 9th International Symposium of the Packaging and Transportation of Radioactive Materials, PATRAM '92*; Washington, D.C., June 11-16, 1989, pp. 743-752.

Wellman, G.W., "First Drop of the MOSAIK Cask," *Sandia National Laboratories Memo* to K. B. Sorenson, March 19, 1990.

Development of a Brittle Fracture Acceptance Criterion for the International Atomic Energy Agency (IAEA)*

Ken B. Sorenson, Richard Salzbrenner, and Robert E. Nickell

Sandia National Laboratories, Albuquerque NM Applied Science & Technology, Poway CA, USA

Introduction

Radioactive material (RAM) shipments are increasing in importance because of heightened level of awareness by the general public. Public scrutiny of RAM shipments demands that meticulous attention be given to compliance to all rules and regulations that may apply to a specific payload and shipment. The appearance of any impropriety, or incompleteness in meeting both the letter and the spirit of the rules and regulations must be avoided if public acceptance is to be gained. Regulators that certify transport casks also require exacting verification of compliance with all pertinent rules and regulations. At times, a particular regulator may require demonstration of package integrity above and beyond the regulatory requirements to assure that the transport package is safe.

Given the volume of shipments crossing international boundaries, the plethora of rules and regulations that a transport package must comply with, and the certification philosophy of individual regulators, it is imperative that uniform, consensus regulations be developed and adopted to assure that RAM transport operations can continue in an efficient and safe manner. This philosophy is embodied in the International Atomic Energy Agency (IAEA) regulations in the form of the Type B(U) certification. The "U" stands for unilateral certification. This certification is given by the competent authority in the country of origin. Separate transport certification from each country that a particular cask may enter is not required since the Type B(U) certification is a verification that the cask has met all IAEA rules and regulations. This process obviates the need for redundant (and expensive) certification from each country that a cask is transported through during a RAM shipment.

Although the Type B(U) certification is designed to allow transport of RAM materials in certified casks across international boundaries of IAEA signatory countries, individual competent authorities may still deny entry due to misgivings about the integrity of a particular cask. Such misgivings may arise from gaps in the IAEA regulations, or may be due to differences in the level of risk accepted by separate competent authorities. The methods by which competent authorities evaluate cask designs for susceptibility to brittle fracture of the containment boundary provides a relevant example in which Type B(U) certification is not uniformly applied or accepted. The existing guidance in the IAEA, as provided for in Appendix IX of Safety Series #37, is limited and dated. Several nations involved in the transport of RAM have individually developed criteria to meet specific needs. However, the lack of an international consensus criterion limits the applicability of these criteria.

An effort is underway to develop a consensus brittle fracture evaluation criterion that would have international technical consensus and that would be adopted into the IAEA Safety Series. This criterion would provide a clear and consistent approach to evaluating the potential for brittle fracture of a wide range of structural materials for cask construction.

---

* This work performed at Sandia National Laboratories supported by the U. S. Department of Energy under contract number DE-AC04-76DP00789.

The Issue

New candidate materials are being proposed for the construction of the structural components of RAM transport casks. Candidate materials include ferritic steel, ductile iron, borated stainless steel, titanium, and depleted uranium. The motivations for proposing new materials over more traditional metals such as austenitic stainless steel include lower cost and greater ease of fabrication. The main structural issue associated with these materials is that they may, under certain combinations of mechanical and environmental loading, fail in a brittle fashion. Clearly, this is not acceptable for a RAM transport cask. Design criteria must be established that assure the cask owner, the regulator, and the public that brittle fracture is not a possibility with a particular cask material and design.

Existing brittle fracture criteria in general, cannot be applied to a wide range of structural materials and do not enjoy international consensus. As an example, the brittle fracture criteria which have been proposed in the U. S. for ferritic steels (1) cannot be extended to the full range of structural materials and are not accepted internationally. These U.S. criteria are empirically based, and are not directly associated with fundamental (inherent) materials properties. Their use is suitable only for a restricted range of composition and thickness of ferritic steels; the margin of safety against brittle fracture cannot be quantified by this approach. Such technical limitations (within individual countries) coupled with country-to-country variations, underscore the need to develop a brittle fracture criterion through an international consensus standards body. Given the advancements in fracture mechanics analysis in recent years, such a criterion can be written that will be applicable to a wide range of structural materials. It is most appropriate to write this criterion under the aegis of the IAEA in order to achieve international technical consensus.

IAEA Charter

A proposal was submitted by the U.S. Department of Transportation (DOT) to the IAEA in 1989 to develop a brittle fracture acceptance criterion. The IAEA Continuous Review Committee officially responded through action TC-405.3, which recommended that a Consultant's Services Meeting be convened to expand IAEA regulations to include brittle fracture evaluation criteria. Action TC-405.3 provided five specific instructions;

1. Review the paper by Sorenson, et. al.; "A Proposal for an International Brittle Fracture Acceptance Criterion for Nuclear Material Transport Cask Applications" (2).

2. Consider all packaging materials with "brittle" characteristics.

3. Address issues of "catastrophic flaw, failure prediction and NDT methods for significant flaws."

4. Prepare proposed advisory material for inclusion in Safety Series #37.

5. Submit a Consultant's Report to the Agency.

These recommendations were forwarded to the Standing Advisory Group on the Safe Transport of Radioactive Materials (SAGSTRAM) for implementation. At its December 1990 meeting, SAGSTRAM voted to convene a group of international experts for a Consultant's Services Meeting (CSM) to address the five issues of TC-405.3.

The nine delegates that comprised the Consultant's Services Meeting (CSM) represented transportation and fracture mechanics experts from IAEA-member countries France (L. Tanguy and D. Moulin), Germany (K. Wieser), Japan (N. Urabe and C. Ito), the Confederation of Independent States (V. Ershov), the United Kingdom (T. Webster), and the United States (R. Nickell and K. Sorenson).

The CSM has met two times: Oct 9-11, 1991 and April 1-3, 1992. The focus of these meetings has been to revise Appendix IX of Safety Series #37 (Appendix IX provides guidance on brittle fracture evaluation). Technical consensus has been achieved using a fracture mechanics methodology. An IAEA Technical Document (TECDEC) has also been written by the delegates that provides technical justification for the positions adopted in revised Appendix IX.

Brittle Fracture Evaluation Criteria

The basis for the brittle fracture evaluation criterion in revised Appendix IX is linear-elastic fracture mechanics (LEFM). The fundamental equation that defines LEFM is;

$$K_I = C\sigma(\pi a)^{1/2} \qquad \text{Equation 1}$$

where,

K_I = stress intensity factor (units: MPa $\sqrt{m}$)
C = geometric constant
σ = maximum nominal tensile stress (units: MPa)
a = depth of an existing flaw (units: m)

Further, in order to prevent crack initiation (or extension) from the existing flaw;

$$K_I < K_{Ic} \qquad \text{Equation 2}$$

where,

K_{Ic} = fracture toughness material property (units: MPa $\sqrt{m}$).

Equation 1 computes the stress intensity factor that results from mechanical loads at the location of an existing flaw. Equation 2 ensures that if the applied stress intensity factor is less than the material's fracture toughness, that brittle fracture will not occur. Crack initiation and/or brittle fracture become imminent when a flaw reaches a critical size for a specific cask design, material, and loading. Combining Equations 1 and 2 allows the critical flaw size (a_{cr}) to be estimated.

$$a_{cr} = (K_{Ic}/\pi C\sigma)^2 \qquad \text{Equation 3}$$

Applying Equation 1 to a transportation cask requires the calculation of stress intensity for a specific cask design subjected to regulatory loading at the location of an existing flaw (e.g., slag inclusion, porosity, cold shut, etc.). For conservatism of design, an existing flaw is assumed to be at the location of highest stress and in most damaging orientation. Application of LEFM through Equation 1 may further require that a nondestructive examination (NDE) of the cask be performed to assure that all flaws are less than the critical flaw size calculated in Equation 3 (in some cases however, the critical flaw size is so large that requirements concerning NDE may be greatly relaxed).

Independent mechanical testing is generally required in order to determine that the fracture toughness of the structural component is greater than the applied stress intensity (Equation 2). Therefore, it can be seen that the LEFM methodology involves a combination of engineering analysis, cask inspection and materials testing. Results of the evaluation are specific to the cask geometry, the loading criteria, and the structural material. A full LEFM approach allows the cask designer the latitude to appropriately adjust the design parameters (e.g., applied stress, allowed flaw size, material fracture toughness) to maintain the relationship required by Equation 2. Specifically, abnormally high material properties need not required to compensate for unrealistic expectations for applied stresses or flaw dimensions.

Application of LEFM in Appendix IX

The criterion in revised Appendix IX allows for three approaches to satisfying Equation 2. These approaches are based on different methods for determining the value of K_{Ic} to be used in Equation 2. Approaches 1 through 3 sequentially increase the conservatism of the value of fracture toughness that is used (in Equation 2), as the complexity and requirements associated with the direct determination of the material's fracture toughness decrease.

K_{Ic}, as shown in Equations 2 and 3, is the fracture toughness value that represents the linear-elastic fracture behavior of a material tested at a static loading rate. For many cask applications, the structural material will behave in an elastic-plastic fashion. This may require the measurement of an elastic-plastic fracture toughness parameter, such as

J, which can (under certain circumstances (3)) be used to determine an equivalent K_{Ic} value. In addition, during accident scenarios, cask loading conditions are dynamic, not static. The dynamic fracture toughness may thus be required (and is designated as K_{Id} or J_{Id}). The full range of conditions results in four test measurements which could be required to define a material's fracture toughness; K_{Ic},.K_{Id}, J_{Ic}, and J_{Id}. Depending on which of the three approaches is selected for evaluating brittle fracture, one or more of these measurements may be required. To avoid confusion, revised Appendix IX refers to all four of these parameters as $K_{I(material)}$. The selection of structural material and the approach in Appendix IX will dictate the type of fracture toughness testing that will be required.

Approach 1

Approach 1 requires that the actual fracture toughness of the structural material be determined for the most severe loading and environmental conditions. These conditions are defined by regulatory requirements that a cask must demonstrate an ability to withstand specified (hypothetical) accident scenarios. This generally requires that the fracture toughness be determined for elevated loading rates at –40°C. This value of fracture toughness is then chosen for $K_{I(material)}$ and is compared with the maximum applied stress intensity for a specific cask design/material/flaw (see Equation 2). The ratio of the fracture toughness to the (maximum) applied stress intensity allows a brittle fracture safety margin to be quantified.

Approach 1 demands the least conservatism in terms of selecting the fracture toughness behavior to be used in Equation 2. The rigorously determined fracture toughness is measured and applied in Equation 2. Since the relevant fracture toughness is directly determined, there is no need to add indirect levels of conservatism by assuming a lower-than-actual fracture toughness for the material. A direct control over the level of conservatism is afforded through application of Equations 1 through 3. The appropriate safety margin (level of conservatism) against brittle fracture that is agreed upon by the competent authorities and designers/manufacturers can then be explicitly demonstrated. Approach 1, in which the most rigorously determined fracture toughness is directly determined and compared to the (maximum) applied stress intensity, allows the most precise determination of the actual margin of safety. A cask designer can employ changes in material, design (to control applied stress), and NDE (to limit the maximum flaw size) to meet a specified margin of safety.

Approach 1 is (potentially) the least conservative of the three approaches in terms of the material's fracture toughness which must be used in calculations, but this is compensated for with an increase in the requirements for determining the fracture toughness. As the requirements and confidence in the fracture toughness test measurements increase, the absolute level of conservatism in choosing $K_{I(material)}$ can be reduced. For Approach 1, the fracture toughness parameter must be measured for the specific structural material at the most severe design temperature and loading rate. These test data must be demonstrated as being statistically significant, and must be proven to be representative of production material (for all serially produced casks).

Approach 2

The $K_{I(material)}$ that is allowed for Approach 2 is the lowest bound value from a statistically significant set of data for a specific class of material. These data may, for example, be comprised of static, dynamic, and fracture arrest measurements as a function of temperature. The most important characteristic of the data is that they must be demonstrated as enveloping the fracture behavior for the material of interest. The data set may be pre- existing for a well-characterized material or may need to be generated (through data gathered from manufacturers, and the literature and/or from direct measurement) by the cask designer. The $K_{I(materials)}$ value selected must be the lowest-bound toughness value at the -40°C design temperature. The use of this $K_{I(material)}$ over the direct measurement in Approach 1 will normally yield a lower, more conservative, estimate of the fracture toughness of the material.

The "design margin of safety" against brittle fracture remains defined as the $K_{I(material)}$ divided by the (maximum) applied stress intensity (from Equation 1). The "actual margin of safety" (as opposed to the "design margin of safety") cannot be determined as accurately (as for Approach 1) since there is increased uncertainty in the real behavior of the material (i.e., its real fracture toughness may fall in a range from the lower-bound to values significantly higher). The difference between the lowest bound fracture toughness and the real fracture toughness adds to the "actual margin of safety," but this increase cannot be quantified nor credited to the design. The designer must meet the requisite "design margin of safety" by controlling the applied stress intensity (by limiting the applied stress through design considerations, and/or limiting the flaw sizes through NDE requirements) to remain below a specified fraction of the lowest bound fracture toughness (at -40°C). The designer is not allowed credit (in this approach) for improved material behavior brought about by advances in fabrication, processing, etc. The benefit of Approach 2 lies

in the (potentially) reduced requirements (compared to Approach 1) for fracture toughness testing and qualification of individual heats of material. This may result in significant overall cost savings, particularly when the value of lower bound $K_{I(material)}$ does not result in excessively restrictive requirements concerning NDE or applied stress reduction during accidents.

Approach 3

The value of fracture toughness that is used in Approach 3 is the lower shelf value that represents full linear-elastic brittle behavior. Such a value is generally determined at a temperature below the lowest design temperature of -40°C. This is shown schematically in Figure 1. Using this lower shelf value for $K_{I(material)}$ incorporates the most restrictive assumptions concerning the resistance of the material to brittle fracture. Since the conservatism in selecting the $K_{I(material)}$ is greatest for this approach, the "actual margin of safety" is generally higher (as compared to Approaches 1 and 2). However the increase cannot be quantified and cannot be applied to the "design margin of safety" that must be satisfied to demonstrate the acceptability of a specific cask.

The primary incentive for using Approach 3 for the designer is that the test procedure for measuring a lower-shelf fracture toughness value is straightforward. The ease of establishing the value for $K_{I(material)}$ allows less cost to be directed towards material testing and qualification. This option can be very desirable for those cases where the applied stress intensity is small with respect to even the most conservative value for $K_{I(material)}$. Approach 3 is appropriate when the designer finds that an acceptable "design margin of safety" against brittle fracture can be demonstrated without creating undue difficulties in design (to lower applied stresses) or in inspection (for NDE requirements): credit for a higher level of fracture toughness inherent in Approaches 1 and 2 is not required to make the design viable.

Figure 1 shows the relative differences in the selection of $K_{I(materials)}$ using the three different approaches. The curves shown represent an example material response. Testing of specific materials will yield different curves.

Factor of Safety

As discussed above, the "design factor of safety" is the ratio of the $K_{I(material)}$ to the (maximum) applied stress intensity, ($K_{I(applied)}$). This overall factor of safety is achieved through an integrated process of material selection, design, and inspection. This allows the designer to manage three parameters that directly affect the "design factor of safety": $K_{I(material)}$, σ, and a. Selection of different materials (and/or whether Approach 1, 2, or 3 is chosen) gives the designer control over the value of $K_{I(material)}$. The overall design (e.g., section thicknesses, shape, impact limiters,...) allows the designer to control the level of applied stress. The inspection process permits the designer to determine the size of flaws which will be allowed in the cask. The overall "design factor of safety" can thus be met by applying "individual safety factors" to one or more of these parameters. In order to maintain generality of the criterion, Appendix IX guidance suggests that the factors of safety be justified by the cask designer and agreed to by the regulator.

Status

The TECDOC is nearly complete with the revised Appendix IX to Safety Series #37 included as a chapter. The TECDOC provides the justification for the technical positions adopted in the revised Appendix IX. The IAEA Safety Series will not be revised until 1995. It is therefore the intent of the CSM to publish the TECDOC so that guidance is available until Appendix IX can be formally incorporated into Safety Series #37. Publication of the TECDOC is anticipated in early 1993.

Conclusion

The revised Appendix IX of Safety Series #37 satisfies the list of five criteria that SAGSTRAM established for the CSM. The revised Appendix IX provides a general evaluation criterion that has been adopted through a technical consensus process and that is applicable to a wide range of materials. It is recommended that the approach outlined in the revised Appendix IX be incorporated into member nation design rules to further solidify the Type B(U) certification process with regard to brittle fracture evaluation.

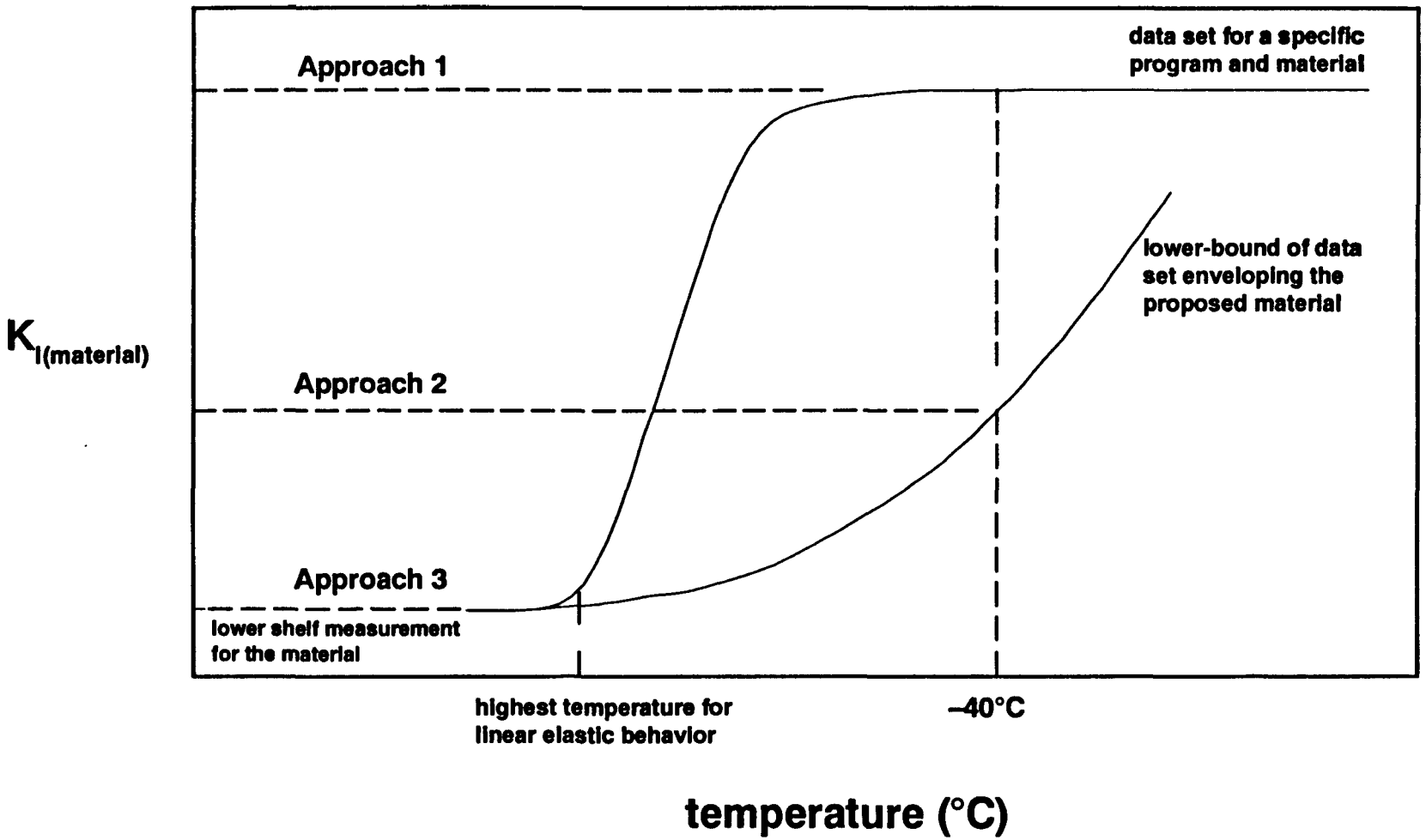

Figure 1. Schematic of the relative values allowed for $K_{I(material)}$ for Approaches 1, 2, or 3 for the IAEA revised Appendix IX of Safety Series #37.

References

1. U. S. NRC Regulatory Guide 7.12, "Fracture Toughness Criteria of Base Metal for Ferritic Steel Shipping Cask Containment Vessels With a Wall Thickness Greater Than 4 Inches (0.1 m) But Not Exceeding 12 Inches (0.3 m)," U. S. NRC Regulatory Guide, Office of Nuc. Reg. Research, June 1991.

2. Sorenson, K., Salzbrenner, R., Nickell, R., "A Proposal for an International Brittle Fracture Acceptance Criterion for Nuclear Material Transport Cask Applications," *Proceedings of The 9th International Symposium on the Packaging and Transportation of Radioactive Materials (PATRAM), Vol. 2,* Washington D.C., pp 753-760, June 1989.

3. Salzbrenner, R., Sorenson, K. B., Wellman, G. W., "Application of LEFM Design to Nuclear Material Transport Casks," *International Journal of Radioactive Materials Transport, vol. 1*, pp. 33-40, 1990.

Mechanical Properties Used for the Qualification of Transport Casks: Prototype Development and Extension to Serial Production*

R. Salzbrenner, T. B. Crenshaw, and K. B. Sorenson

Sandia National Laboratories,** Albuquerque, New Mexico, United States of America

Introduction

A thorough understanding of the mechanical behavior of material in a specific cask is required to properly analyze the structural response of the cask. An appropriate way to establish this understanding is through laboratory testing of cask material. The laboratory testing that was done to support the MOSAIK Drop Test Program is summarized as an example of how mechanical properties can be mapped for a prototype cask. The broad range of measured properties allows the critical aspects of mechanical behavior to be understood. This is necessary for the proper application of fracture mechanics, and focuses on fracture toughness as the inherent materials property which quantifies the fracture resistance of a material. The general fracture mechanics approach and its application to specific cask designs are described elsewhere (Salzbrenner et al. 1990, Sorenson et al. 1992a, Sorenson et al. 1992b). The understanding established by a thorough mapping of the mechanical properties is necessary to apply fracture mechanics to a particular prototype, but it is not sufficient for qualifying serially produced casks. The mechanical behavior of a prototype must be correctly associated with parameters which can be measured on production casks. Since the production casks cannot be destructively tested, measurements are commonly made on sub-size specimens. This may prevent direct measurement of valid design properties. An additional database may then be required to establish the correlation between sub-size specimen measurements and valid design properties. This is illustrated by outlining the additional testing which would be necessary to allow the successful verification of the MOSAIK Drop Test Program to be extended from the prototype to serially produced casks.

Mechanical Property Mapping of the MOSAIK KfK Cask

The MOSAIK KfK is a ferritic ductile iron (DI) cask used to transport and store transuranic waste. The cask was developed by the Gesellschaft für Nuklear-Service (GNS) Company of Germany, and is licensed for use throughout Europe. GNS donated a MOSAIK KfK cask to Sandia for testing purposes. The MOSAIK Drop Test Program was developed to demonstrate the fracture mechanics approach for quantifying the resistance to brittle fracture. The MOSAIK Drop Test Program is described in a companion paper in these proceedings. The MOSAIK KfK is an appropriate vehicle for demonstrating the fracture mechanics approach since it represents a class of alloys that can, under very severe conditions (high loading rate and low temperature), exhibit brittle fracture. A primary objective of the MOSAIK Drop Test Program was to quantify the fracture behavior of the MOSAIK KfK cask.

Figure 1 shows the dimensions of the MOSAIK KfK cask, along with the location of the coring which was removed from the bottom of the cask to provide material for the laboratory mechanical testing. The bottom coring was divided into five separate planes, each approximately 25mm thick. The labeling of these planes is shown in Figure 2 along with photomicrographs that depict the variation in microstructure through the coring. Both quantitative metallographic and chemistry measurements were made on samples taken from each plane. Results are presented in Table 1. The volume fraction of graphite and the average nodule spacing increased from the inner- (Plane 1) to the

* This work performed at Sandia National Laboratories supported by the U. S. Department of Energy under contract number DE-AC04-76DP00789.

** A U. S. Department of Energy Facility.

Figure 1. A cross-sectional sketch of the MOSAIK KfK cask, showing the location of the bottom and side corings.

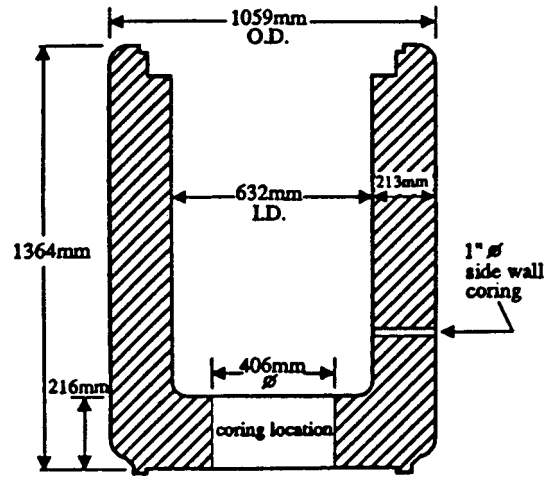

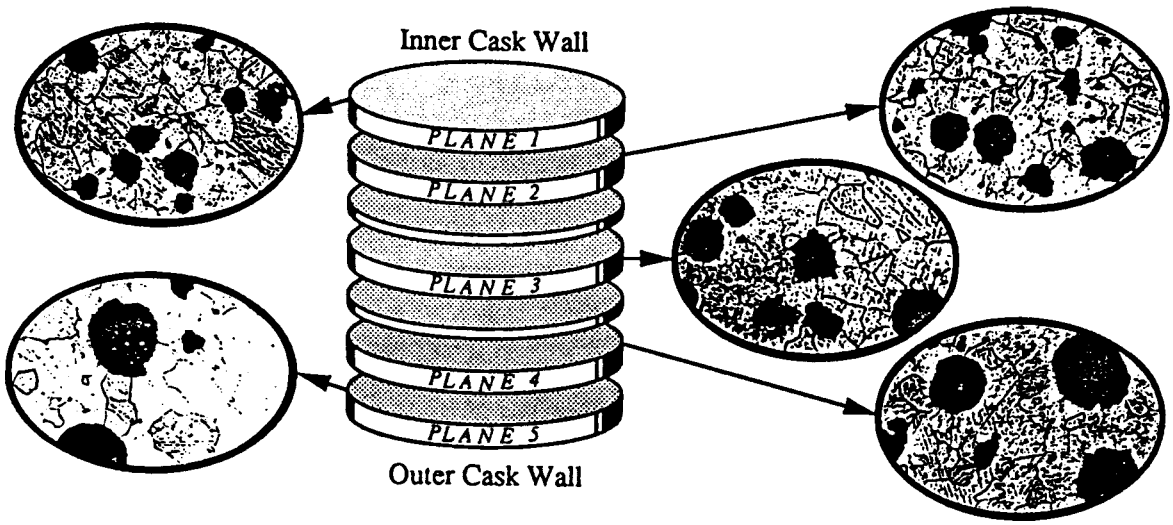

Figure 2. An exploded view sketch of the bottom coring from the MOSAIK KfK cask showing the plane locations and their mircostructure relative to the inner and outer cask surfaces.

Table 1. Microstructural and compositional measurements for Planes 1 through 5 of the bottom coring of the MOSAIK KfK Cask.

Sample Location	Graphite Vol. Frac. (%)	Pearlite Vol. Frac. (%)	Nodule Count (#/mm^2)	Nodule Spacing (mm)	Nodule Type	Ferrite Grain Size (mm)	C (wt. %)	Si (wt. %)	Ni (wt. %)	S (wt. %)
Plane 1	10.5	0	123	0.045	100% type I	0.030	3.56	1.72	0.06	0.006
Plane 2	13.8	0	122	0.045	100% type I	0.029				
Plane 3	10.8	3	74	0.058	100% type I	0.029	3.39	1.74	0.05	0.005
Plane 4	18.4	3	41	0.079	90% type I*	0.034				
Plane 5	18.0	5	48	0.073	75% type I*	0.037	3.32	1.70	0.06	0.005

* The balance is type II — see ASTM A 495 for description of nodule type.

outer-wall (Plane 5). The nodularity of the graphite was found to be somewhat degraded as the outer surface was approached. In orded to associate the behavior of the large bottom coring to the behavior of the material in the side wall of the cask, a small coring was taken through the wall (see Figure 1). The side wall coring displayed a similar chemistry, but the variation in microstructure was more limited. Planes 1 through 3 encompass the microstructural and chemistry variations which were displayed by the side wall coring. The chemistry and microstructure of the DI from the MOSAIK KfK (particularly Planes 1-3) are very similar the other DI alloys that have been tested at Sandia and elsewhere (Salzbrenner and Crenshaw 1991, Frenz 1992, CRIEPI Report 1988).

Mechanical Property Experimental Methods:

Elastic Constant Measurements – Elastic moduli were determined from ultrasonic velocity measurements. A pulse echo overlap technique was used to measure the velocity of 5 MHz shear and longitudinal waves (Papadakis 1967). Ultrasonic velocities and the material density were related to polycrystalline elastic moduli through standard formulas (Carnevale et al. 1964). Values determined by this method are not subject to the gross errors that can result from determining elastic constants from tensile tests. The absolute accuracy of this method is generally limited by the accuracy with which the material density can be determined. For this work, the density was measured with a maximum error of 1%, which can be considered the overall accuracy of the elastic moduli measurements.

Tensile Measurements – Tensile tests were conducted at strain rates of 10^{-3} and 1 sec^{-1} on a conventional servohydraulic test frame in accord with standardized testing procedures (ASTM E 8 1991). Standard round tensile specimens with a gage length of 2.5 cm were used. All testing was performed at –29°C to match the hypothetical accident conditions specified by U.S. regulations (10CFR71 1984). The test equipment was calibrated to within 0.1% accuracy for load, displacement, and time. The limited amount of sample material available allowed only single specimens from each plane to be tested. The yield strength (at 0.2 % offset), ultimate tensile strength, total elongation to failure, and total reduction in area were measured for each sample. Previous studies on similar DI alloys (Salzbrenner 1986, Yanagisawa and Lui 1985) indicate that the yield and ultimate tensile strengths will generally vary less than 1% for samples of the same high quality DI. However, the ductility may vary considerably more, often up to ±10% from sample to sample of nominally the same alloy of DI. Two specimens from Plane 3 were tested at a rate of 10^2 sec^{-1} (at –29°C) using a high rate hydraulic test frame. For these tests, the ultimate tensile strength, the total tensile elongation, and the total reduction in area are reported. Inertial ringing of the load cell prevented an accurate determination of the 0.2% yield strength for the high rate tests.

Static Rate Fracture Toughness Measurements – The fracture toughness was determined using a single specimen J_{Ic} technique which complies with the standard test method (ASTM E 813 1991). The testing was conducted on compact specimens (B_G=2.29 cm, B_{net}= 2.06 cm, W= 5 cm) in a temperature chamber held at –29°C. The load line displacement rate was fixed at 5 x 10^{-4} cm/sec. A detailed description of thie test technique and the method of analysis can be found in a previous report (Salzbrenner et al. 1985). The recognized accuracy of the J-integral method is ±15%. The square root relationship between the elastic-plastic fracture toughness, J_{Ic}, and the equivalent linear elastic fracture toughness, K_{JIc}, translates the ±15% accuracy in determining J_{Ic} to a ±4 % variation in K_{JIc}.

High Rate Fracture Toughness Measurements – The same type of compact specimens were used to conduct high rate fracture toughness measurements (at –29°C). The high rate elastic-plastic test method used a multiple specimen approach in which special testing fixtures allow precise control of the maximum displacement and loading duration. The test technique and the analysis of test results are based on the same principals used for static-rate testing. The fixturing was coupled with a high rate hydraulic frame in which the actuator rate was maintained at 125 cm/sec. This actuator rate delivers a stress intensity rate of approximately 10^5 MPa-$\sqrt{m}$ /sec (depending on the specific sample material and crack length). The laboratory testing rate exceeds the loading rate of the cask flaw caused by a 9 m drop. Further details on the high rate testing technique can be found elsewhere (Salzbrenner and Crenshaw 1990b). This high rate test method also allows the plain strain fracture toughness to be determined when samples behave in a suitably linear-elastic fashion. Since the same test set-up (fixturing, instrumentation,...) is used regardless of specimen behavior, no pretest assumptions need be made concerning whether the specimen will behave in a brittle fashion or in an elastic-plastic manner.

Other Measurements – The Charpy "V" notch impact (CVN) behavior (as a function of temperature from (–130 to +100°C) was also measured. These results are not included herein due to space limitations and because such values are useful only as qualitative indicators of material behavior. Charpy values are not inherent materials properties and cannot be used to quantify the mechanical performance. The Charpy test results are available elsewhere (Salzbrenner and Crenshaw 1990a).

Experimental Results:

Elastic Constants – There was a small, but distinct variation in the Young's and shear moduli in moving from Plane 1 toward Plane 5. This is shown graphically in Figure 3. This decrease is most probably caused by the increase in

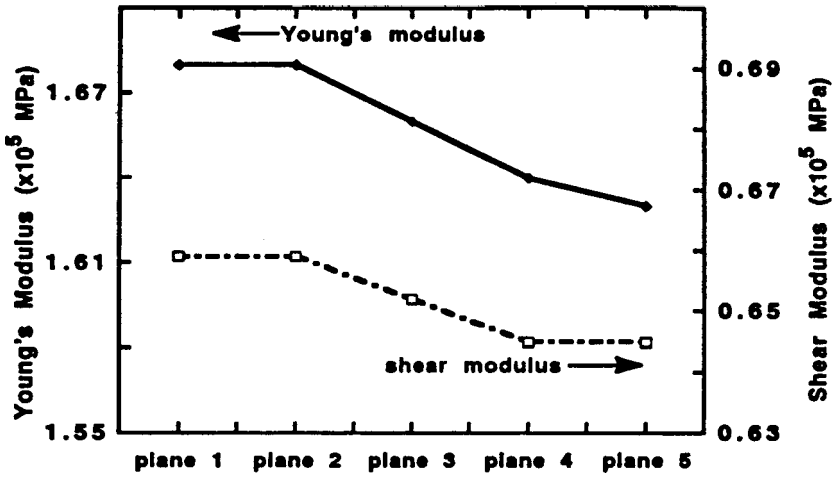

Figure 3. The variation of elastic moduli (derived from ultrasonic velocity measurements) with location for the bottom coring of the MOSAIK KfK cask.

the volume fraction of graphite in the bottom coring from the inner- to the outer-wall. There is, however, little practical engineering significance to the small variation, and the elastic constants are essentially constant through the bottom coring.

Tensile Properties – The results from the tensile measurements (at 10^{-3} sec^{-1}) exhibit little change in strength as a function of sample location (see Figure 4a). There is however a decrease in tensile ductility from the inner to the outer wall (Figure 4b). Similar results were found for the tests conducted at the higher strain rate of 1 sec^{-1}. Previous work (Salzbrenner 1986) demonstrated that the strength of ferritic DI is controlled primarily by material composition. Since the compositional measurements (Table 1) show little variation through the coring, the tensile results are in agreement with the previous study. The decrease in tensile ductility with increasing coarseness of the microstructure is consistent with results from another study (Frenz 1992). While this correlation may hold for a limited range of composition and variation in microstructure, it is not universally true for the broadest range of composition and microstructure available for DI (Salzbrenner 1986).

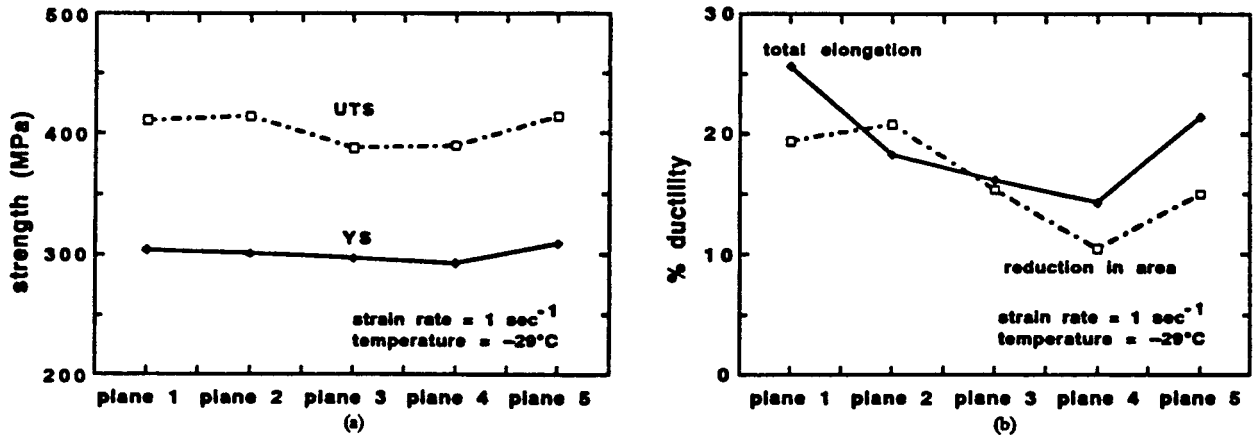

Figure 4. The variation in the tensile behavior (at –29°C) with location in the bottom coring of the MOSAIK KfK cask: (a) strength and (b) ductility).

The strength was found to exhibit a moderate increase with increased strain rate. This trend is shown in Figure 5 for Planes 1, and 3 (the other planes behave in a similar fashion). An increase in strength with increased strain rate is commonly observed for many alloys (Hertzberg 1976). The tensile ductility generally decreases with increased strain rate (see Figure 5). A decrease in ductility with increased strain rate has been observed in other ferrous alloys (Nakamura et al. 1968).

Static Rate Fracture Toughness Measurements – The static rate J_{Ic} measurement results are plotted in Figure 6 as a function of position. The static rate fracture toughness of all the DI in the MOSAIK KfK cask exceeds the minimum properties expected from material meeting the newly approved ASTM specification for a nuclear grade DI (ASTM

A 874 1991). The toughness of specimens from Planes 1 through 3 was almost constant. The toughness then showed an increase for specimens from Planes 4 and 5 which had larger nodule spacing. Nodule spacing, in a broad range of ferritic DI alloys, has been shown (Salzbrenner 1987, McConnell and Lombrozo 1987) to statistically correlate with changes in the static rate fracture toughness.

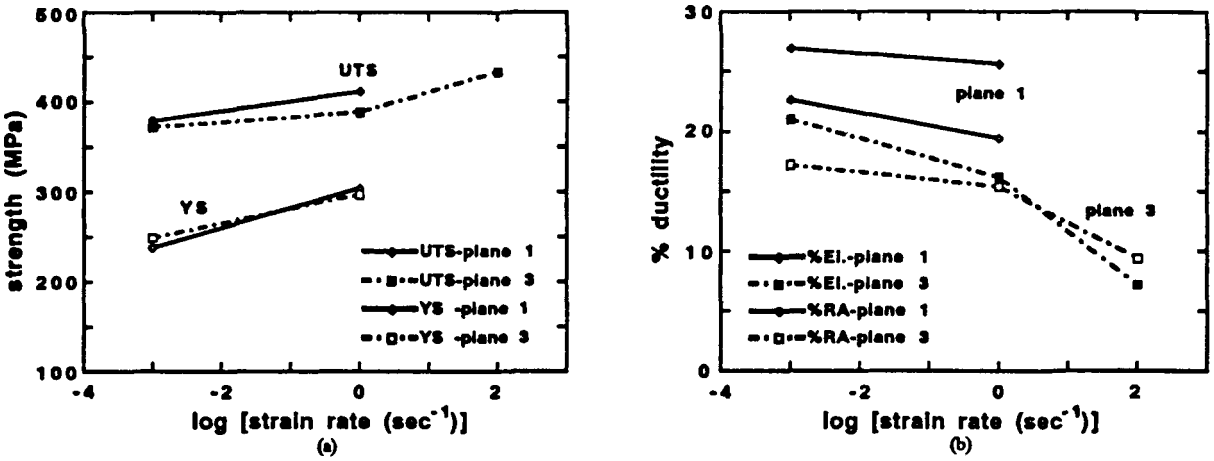

Figure 5. The variation in tensile behavior (at –29°C) with strain rate for material from the bottom coring of the MOSAIK KfK: (a) strength and (b) ductility.

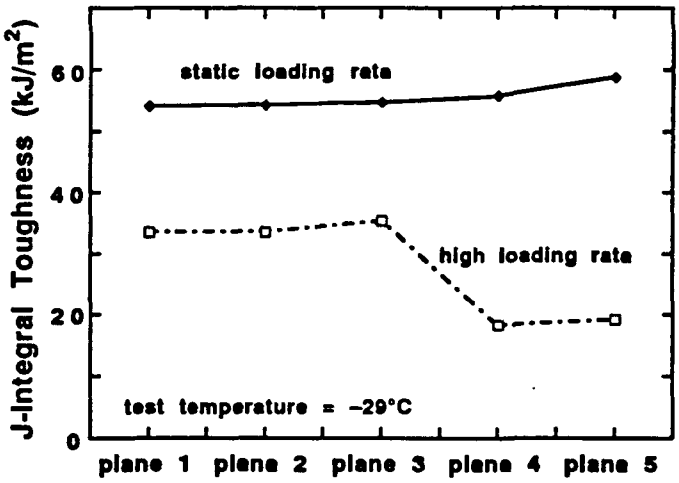

Figure 6. The fracture toughness as a function of location for the bottom coring of the MOSAIK KfK.

Elevated Rate Fracture Toughness Measurements – The elevated rate fracture toughness behavior (at –29°C) fell into two regimes. Planes 1, 2, and 3 behaved in an elastic-plastic manner, and a crack growth resistance curve was determined for each plane. The elevated loading rate initiation fracture toughness was determined in a manner consistent with ASTM Standard E 813 (i.e., for static loading rates). Plotting all the data from planes 1, 2, and 3 together produced a single crack growth resistance curve (shown in Salzbrenner and Crenshaw 1990b). The elevated rate initiation toughness for Planes 1 through 3 can thus be described as constant, as it was for the static rate testing. The value for the initiation toughness decreases from an average of 54.4 kJ/m^2 for static rate, to 33.1 for elevated rate. The reason for this decrease is not readily apparent, since scanning electron microscopic examinations of the fracture surfaces shows ductile tearing to dominate at both rates.

Fracture toughness specimens taken from Planes 4 and 5 behaved in a linear-elastic fashion when tested at high rate (at –29°C). The tests were analyzed as plane strain fracture toughness tests (governed by ASTM E 399 1991). Although requirements concerning linearity were met, the samples did not possess the minimum dimensions specified in the standard. The initiation values for the specimens from Planes 4 and 5 are used only as estimates of the true elevated loading rate fracture toughness for DI material from those planes. When compared to the results from Planes 1-3 the toughness of Planes 4 and 5 showed a substantial decrease (see Figure 6). Examination of fracture surfaces of samples from Planes 4 and 5 showed extensive cleavage (i.e., low energy) fracture.

Selection of Properties for Finite Element Model

Mechanical measurements encompassing all microstructures and compositions present in the cask provide the foundation for selecting the values for the material model for finite element analyses. The proper application of finite element analyses allow the mechanical response to be quantified. Systematic measurements determine if large variations, and/or unexpected discontinuities in the mechanical properties are present. When the variations are small, the selection of the representative mechanical properties is straightforward, and a simple (homogeneous) material model can be used. When the measurements indicate the presence of large variations, a more complicated material model may be needed to properly predict the mechanical response of the overall cask. The measurements on the prototype MOSAIK KfK are used to illustrate which mechanical properties are required for finite element analyses and provides an example of how values for each can be selected.

Elastic response is fully characterized by utilizing two elastic moduli of the material. The measured variation of the elastic constants (derived from ultrasonic velocity measurements through the bottom coring) is small and will have a negligible effect on the mechanical response of the cask. The average values for both the Young's modulus and Poisson's ratio were calculated and used in the material model.

The yield strength (as determined by tensile testing) is used as the engineering definition of the beginning of plastic deformation. Tensile testing as a function of strain rate, shows that the strain rate sensitivity is not large, and will not have a major effect on the analyses of 9m drops. The strain rate of 1 sec^{-1} provides the best overall match for the loading rate of the 9m drop test. Since the variation (through the coring) of the yield strength is small, the average of the five measured responses is a good estimation of the beginning of plastic deformation.

The plastic response of a material is characterized with a power law hardening material model (Stone et al. 1990). The stress-strain behavior of a tensile specimen furnishes the required information for this model. The stress-strain response of all specimens (particularly from planes 1 through 3) was similar and average values were used to determine the parameters for the power law hardening model. The largest variation in the tensile behavior through the coring was found in the tensile ductility (i.e., the engineering strain to failure). Such a variation could properly be accounted for in a FE material model through ductile failure criteria. For the transport casks under consideration here, such an inclusion is moot. This is due to the elastic design "rules" that are applied to transport casks in general, and to the MOSAIK KfK cask in particular. Specifically, only elastic deformations are allowed for all design loading conditions (including accident conditions). The through-section stresses which result from applied loads are below the yield strength of the structural material. The 9m drop of the MOSAIK KfK produced a maximum tensile stress at mid-span, of approximately 210 MPa (Sorenson 1988), and this is substantially below the yield strength of the cask. Plastic deformation occurs only in localized volumes in the vicinity of the artificially introduced flaws, or underneath the steel supports. (Details of the drop test conditions, including the steel end supports to enhance the tensile stresses in the vicinity of the artificial flaw are available in Sorenson et al. 1992b.) Since global plastic deformation does not occur for even the severe (hypothetical) accident condition of the 9m drop (onto an unyielding target), a failure criterion related to the ductility of the material is unnecessary, and the tensile ductility is not used in the finite element analyses.

The variation in the high rate fracture toughness (and the uncertainty in its measurement) is greater than that in the modulus or tensile measurements. Nonetheless, the measured values can be used to provide a reasonable estimation for finite element analyses. The appropriateness of the value chosen is ultimately validated by the full scale drop tests of the prototype cask. Measured values of the fracture toughness were effectively invariant for both static and elevated loading rate tests conducted on samples from Planes 1 through 3. The microstructure from Planes 1-3 closely matches the entire variation seen in the side wall, and it therefore is appropriate to estimate the toughness in the vicinity of the flaw in the sidewall as the average of the values from Planes 1-3. Since the rate of the laboratory fracture toughness tests was only slightly higher than that caused by the drop test, the best estimate of the fracture toughness is the average of the high rate measurements on specimens from Planes 1 through 3 (i.e., 33.1 kJ/m^2).

The finite element analysis of the response of the cask to a 9m drop is verified by the full scale testing. The elastic response of the cask is measured by appropriately placed accelerometers and strain gages, and is compared to the values calculated by the finite element analysis. Examination of the data and the cask after the drop confirm that through-wall (global) plastic deformation did not occur. Although the cask is designed to preclude failure occurring by tensile overload, the resistance to cracking (by ductile tearing and/or brittle cleavage) must also be demonstrated. An important purpose of the drop test of a prototype cask is to verify the accuracy of the fracture mechanics method used to predict the fracture behavior. The drop test confirms both the calculational methodology and the laboratory methods of determining the fracture toughness of the material. For the MOSAIK KfK example, the applied J-integral from the 9m drop was calculated by finite element analysis and compared to the (average) value determined by the laboratory measurements. The magnitude of the applied J-integral from the drop test was intentionally enhanced by the coincidence of the artificial flaw and the maximum tensile stress. The J-integral value of the

fracture toughness from the laboratory measurements was used as the global failure parameter. When the applied J-integral was less than the measured fracture toughness, the analysis predicted that crack extension from the artificial flaw would not occur. When the value of the applied J-integral exceeded the elevated rate fracture toughness, the analysis predicted that at least some crack extension would occur. The results from the MOSAIK Drop Test Program (Sorenson et al. 1992b) demonstrated i) the correctness of the finite element analysis, ii) the validity of using the J-integral as the failure parameter, and iii) the accuracy of the fracture toughness determined by the laboratory testing.

Extension to Serially Produced Casks

The work described above demonstrates the applicibality of the general qualification method. The detailed measurement of the mechanical properties as a function of location within a cask provides a foundation for understanding the mechanical response of the cask during normal and accident conditions. The drop testing of the prototype cask verifies the analysis and the mechanical property testing. A benchmark is thus established which allows other casks of the same material, specification, geometry, etc., to be qualified. Although the foregoing process of detailed mechanical property measurement and the prototype drop testing may be necessary (to establish the benchmark), it is not sufficient to qualify serially produced casks. Critical properties of each serial cask must be appropriately linked back to the prototype. Critical properties must meet or exceed minimum values for every cask which is to be qualified.

In the current example, the fracture toughness is the critical property that must be shown to be above a minimum value in each production cask. This might be done by measuring the fracture toughness directly on samples from representative material from each cask. The material for such measurements could be obtained from corings, prolongations, and/or test blocks that have been shown (by the mapping process) to incorporate the minimum toughness material found in the cask. When values from such specimens exceed the minimum acceptable value, the individual cask is acceptable. This procedure is very clear in concept, but may present difficulties in application. As an example, the determination of the fracture toughness on the relatively small specimens which might be available from corings may not produce a valid value. An additional database may need to be created which allows parameters which can be measured on small specimens to be statistically correlated to valid design properties. The results of mechanical measurements on subsize specimens such as a notched round bar (Arai 1992) may be shown to correlate to the fracture toughness of much larger specimens. As an alternative, the relationship between valid fracture toughness (on large specimens) and the microstructure/composition of the material may established, and allow straightforward chemistry and metallographic measurements to qualify the material. A relationship of this type has been shown for the static rate elastic-plastic fracture toughness of ferritic ductile irons (Salzbrenner 1987). This type of understanding must be extended to elevated loading rate fracture toughness (at low temperatures) in order to be applied to quality assurance of production casks.

Summary

The qualification process that should be sufficient for qualification of a specific cask (material/geometry combination) has been examined. The prototype cask should be tested to determine its overall variation in microstructure, chemistry, and mechanical properties. This prototype may also be subjected to "proof testing" to demonstrate the validity of the design analysis (including the mechanical properties used in the analysis). The complete mechanical property mapping does not necessarily have to precede the proof testing (i.e., portions of the cask which experience only low (elastic) loads during the drop test are suitable for mechanical test specimens). The behavior of the prototype cask and the production casks are linked by assuring that each cask possesses at least the minimum level of one or more critical mechanical properties. This may be done by measuring the properties of interest directly, or by relying on a secondary measurement (such as subsize mechanical test results or microstructure/compositional measurements) which has been statistically correlated to the critical properties. The database required to show the correlation between the secondary measurement and the valid design property may be established by tests on the material from the prototype cask. The production controls (e.g., on the casting process, feed materials, ...) must be demonstrated as being adequate to assure that a uniform product is produced. The testing of coring (or test block or prolongation) samples can only be viewed as providing a valid link to the benchmark results provided by the prototype cask if the process used to create follow-on casks remains essentially similar. The MOSAIK Test Program has demonstrated the qualification method through the benchmarking stage. The MOSAIK program did not establish a means for qualifying serial production casks through, for example, a correlation between small specimen parameters and valid design fracture toughness properties. Such a correlation would require additional experimental work.

References

10CFR71, *Title 10, Code of Federal Regulations, Part 71*, Office of the Federal Register, Washington, DC, (1984).

Arai, T., et al., "Determination of Lower Bound Fracture Toughness for Heavy-Section DCI and Estimation by Small Specimen Tests," *24th ASTM Fracture Mechanics Conference*, Gatlinburg, TN, June 30-July 3, (1992)

ASTM A 874-89, "Standard Specification for Ferritic Ductile Iron Castings Suitable for Low-Temperature Service," *1991 Annual Book of ASTM Standards, Section 1, Iron and Steel Products, Vol. 1.02*, American Society for Testing and Materials, Philadelphia, pp 493-95, (1991).

ASTM E 8-90a, "Standard Methods of Tension Testing of Metallic Materials," *1991 Annual Book of ASTM Standards, Section 3, Metals Test Methods and Analytical Procedures, Vol. 3.01*, American Society for Testing and Materials, Philadelphia, pp 131-45, (1991).

ASTM E 399-90, "Standard Test Method for Plane-Strain Fracture Toughness of Metallic Materials," *1991 Annual Book of ASTM Standards, Section 3, Metals Test Methods and Analytical Procedures, Vol. 3.01*, American Society for Testing and Materials, Philadelphia, pp. 485-515, (1991).

ASTM E 813-89, "Standard Test Method for J_{Ic}, A Measure of Fracture Toughness," *1989 Annual Book of ASTM Standards, Section 3, Metals Test Methods and Analytical Procedures, Vol. 3.01*, American Society for Testing and Materials, Philadelphia, pp 713-27, (1991).

Carnevale, E. H., et al., "Ultrasonic Measurement of Elastic Moduli at Elevated Temperatures, Using Momentary Contact," *J. Acoust. Soc. Am., Vol. 36*, pp 1678-84, (1964).

CREIPI Report, "Research on Quality Assurance of Ductile Cast Iron Casks," Central Research Institute of Electric Power Industry, *CREIPI Report EL87001*, (1988).

Frenz, H., "Mechanical Properties of Ferritic and Ferritic-Pearlitic Ductile Iron, *Sandia Report SAND92-0421*, Sandia National Laboratories, Albuquerque, NM, (1992).

Hertzberg, R. W., *Deformation and Fracture Mechanics of Engineering Materials*, John Wiley & Sons, New York, pp 35-37, (1976).

McConnell, P., and Lombrozo, P., "Ductile Iron Data Base - Correlations Between Microstructure and Fracture Toughness," *Sandia Report SAND86-7163*, Sandia National Laboratories, Albuquerque, NM, (1987).

Nakamura, T. , "The Strain Rate Dependence of Tensile Properties of Mild Steel at Low Temperatures," *Proceedings of the 11th Japan Congress on Materials Research*, Soc. of Materials Science, Japan, pp 82-5, (1968).

Papadakis, E. P., "Ultrasonic Phase Velocity by the Pulse-Echo-Overlap Method Incorporating Diffraction Phase Corrections," *J. Acoust. Soc. Am., Vol. 42*, pp 1045-51, (1967).

Salzbrenner, R., "Fracture Toughness Behavior of Ferritic Ductile Cast Iron," *Journal of Material Science, Vol. 22*, pp 2135-47, (1987).

Salzbrenner, R., "Tensile Behavior of Ferritic Ductile Cast Iron," *Sandia Report SAND86-0470*, Sandia National Laboratories, Albuquerque, NM, (1986).

Salzbrenner, R. and Crenshaw, T. B., "Multiple Specimen J-Integral Testing at Intermediate Rates," *Experimental Mechanics*, pp 217-23, (1990a).

Salzbrenner, R. and Crenshaw, T. B., "Mechanical Property Mapping of the Ductile Cast Iron MOSAIK Cask," *Sandia Report SAND90-0776*, Sandia National Laboratories, (1990b).

Salzbrenner, R. and Crenshaw, T. B., "Effects of Sample Size and Loading Rate on the Transition Behavior of a DI Alloy," *23rd National Symposium on Fracture Mechanics*, College Station, TX, June 18-20, (1991).

Salzbrenner, R., et al., "Fracture Toughness Testing of Ductile Cast Irons," *Proceedings of the Sixteenth Symposium on Fracture Mechanics, ASTM STP 868*, edited by M. F. Kanninen and A. T. Hopper, ASTM, Philadelphia, pp 328-44, (1985).

Salzbrenner, R. , et al., "Application of LEFM Design to Nuclear Material Transport Casks," *RAMTRANS, Vol. 1*, No. 1, pp 33-40, (1990).

Sorenson, K., et al., "MOSAIK Cask Test Program,"*Sandia Report SAND 88-0991*, Sandia National Laboratories, Albuquerque, NM, Dec. 1988.

Sorenson et al., "Development of a Brittle Fracture Acceptance Criterion for the International Atomic Energy Agency," *PATRAM '92*, Yokohama, Japan, Sept 13-18, (1992a).

Sorenson et al., "Results of the Sandia National Laboratories MOSAIK Cask Drop Test Program," *PATRAM '92*, Yokohama, Japan, Sept 13-18, (1992a).

Stone, C. M., et al., "A Vectorized Elastic / Plastic Power Law Hardening Material Model Including Lüders Strain," *Sandia Report SAND90-0153*, Sandia National Laboratories, Albuquerque, NM, (1990).

Yanagisawa, O. and Lui, T. S., "Effect of Carbon Content and Ferrite Grain Size on the Tensile Flow Stress of Ferritic Spheroidal Graphite Cast Iron," *Metallurgical Transactions A, Vol. 16A*, pp 667-73, (1985).

ELEVATED TEMPERATURE TENSILE PROPERTIES of BORATED 304 STAINLESS STEEL: EFFECT of BORIDE DISPERSION on STRENGTH and DUCTILITY*

J. J. Stephens, K. B. Sorenson and P. McConnell

Sandia National Laboratories, Albuquerque, New Mexico, United States of America

INTRODUCTION

Conventional cast and wrought ("Ingot Metallurgy") borated 304 stainless steel has been used for a number of years in spent fuel storage applications where a combination of structural integrity and neutron criticality control are required. Similar requirements apply for materials used in transport cask baskets, and borated stainless steel is, in fact, an attractive material for such applications. However, in the high boron contents (>1.0 wt.%) which are most useful for criticality control, the conventional cast and wrought material suffers from low ductility as well as low impact toughness. The microstructural reason for these poor properties is the relatively coarse size of the boride particles in these alloys, which act as sites for crack initiation.

Recently, a "premium" grade of borated 304 stainless steel has been introduced (Strobel and Smith, 1988) which is made by a Powder Metallurgy (PM) process. This material has greatly improved ductility and impact properties relative to the conventional cast and wrought product. In addition, an ASTM specification has been developed for borated stainless steel. This specification (ASTM A887) contains 8 different material Types with respect to boron content - with the highest level (Type B7) having permissible range from 1.75 to 2.25 wt. % boron - and each Type contains two different Grades of material based on tensile and impact properties. While the ASTM specification is properties-based and does not require a specific production process for a particular grade of material, the PM material qualifies as "Grade A" material while the conventional Ingot Metallurgy (IM) material generally qualifies as "Grade B" material.

This paper presents a comparison of the tensile properties of PM "Grade A" material with that of the conventional IM "Grade B" material for two selected Types (i.e., boron contents) as defined by the ASTM A887 specification: Types 304B5 and 304B7. Tensile properties have been generated for these materials at temperatures ranging from room temperature to 400°C (752°F). The data at higher temperatures are required for ASME Code Case purposes, since the use temperature of a basket under "worst case" cask conditions may be as high as 343°C (650°F), due to self-heating by the activated fuel elements. We will also discuss the current status of efforts aimed at obtaining an ASME Boiler and Pressure Vessel Code Case for selected grades of borated stainless steel covered by the ASTM A887 specification.

*This work conducted at Sandia National Laboratories, supported by the U. S. Department of Energy under contract number DE-AC04-76DP00789.

MATERIALS CHARACTERIZATION AND TESTING PROCEDURES

The SNL study (Stephens and Sorenson 1990) was designed to first examine the high boron content types (boron content >1 wt.%) in ASTM A887, i.e., the Types designated as 304B4, 304B5, 304B6 and 304B7 - since these types are the most useful for criticality control applications. For these high-boron Types, only the Grade A material appears to have adequate impact properties to permit inclusion in the ASME code case inquiry - based on the impact requirements shown in ASTM A887. In fact, the highest boron-bearing Grade B material with somewhat acceptable impact properties is Type 304B2 Grade B, which has a permissible boron content range of 0.50-0.75 wt.% and a required minimum Charpy V-Notch Energy of 22 Joules (16 ft-lbs). All four heats of material discussed in this paper - i.e., Type 304B5 Grades A and B, along with Type 304B7 Grades A and B - were produced and supplied by Carpenter Technology Corporation, the chemical analyses performed by Carpenter to certify conformance with ASTM A887 are shown in Table 1. All material was tested at SNL in the solution annealed condition.

Table 1. Chemical composition (in wt.%), heat number information and other required properties for the four different lots of borated stainless steel studied. Note the compact labels used for each lot of material in the remainder of this paper, and that the impact properties of both 304B5B and 304B7B are so low as to not have a required minimum value in ASTM A887.

Element	304B5, Grade A ("304B5A")	304B5, Grade B ("304B5B")	304B7, Grade A ("304B7A")	304B7, Grade B ("304B7B")
Carbon	0.032	0.034	0.027	0.034
Manganese	1.83	1.93	1.74	1.79
Phosphorus	0.014	0.014	0.024	0.022
Sulfur	0.002	0.001	0.004	0.004
Molybdenum	0.02	0.03	0.29	0.28
Copper	0.04	0.04	0.10	0.12
Cobalt	0.06	0.06	-----	0.22
Silicon	0.73	0.71	0.58	0.67
Chromium	18.39	18.22	18.40	18.00
Nickel	12.98	13.03	13.01	13.42
Boron	1.41	1.38	2.19	1.90
Iron	Balance	Balance	Balance	Balance
Heat #	C1835	11666	C1592	94480
Required Min. Elongation (%)	24.0	13.0	17.0	6.0
Required Min. Charpy V-Notch Energy - J(ft-lbs)	31(23)	-----	14(10)	-----

Previous X-ray diffraction results generated at our laboratory have indicated that virtually all of the boron is present in these materials as precipitates of either Cr_2B or as $(Cr,Fe)_2B$. This is because the solubility of boron in both 18Cr-15Ni and 20Cr-25Ni stainless steels is <0.001 wt.% at 600°C (Goldschmidt 1979) - boron would be expected to have a similar solubility in the alloys in the present study. Rolling plane cross sections were prepared from each lot of material and were examined using both scanning electron microscopy (backscattered electron images) and quantitative image analysis to characterize the boride dispersion. Figure 1 shows representative areas from each of the four lots of material. The boride phase is consistently finer in the PM-processed Grade A material compared to the IM-processed Grade B material. Close inspection of the Grade B material shown in Figures 1b and 1d also indicates the presence of cracks in some of the larger boride particles. The area of roughly 1000 particles from each material were obtained from BSE images, and the size distribution of these areas are plotted

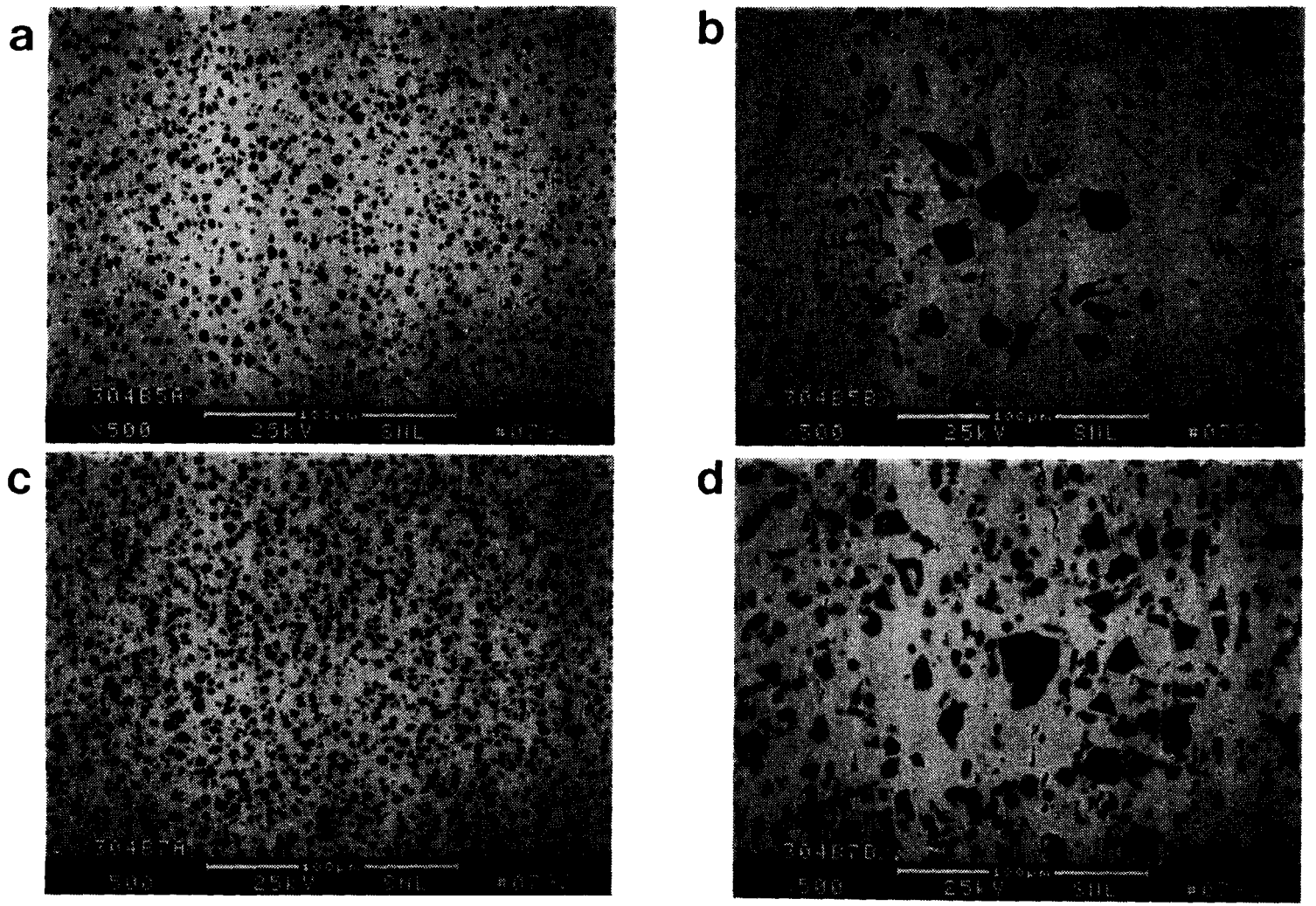

Figure 1. Backscattered electron micrographs (with atomic number contrast) obtained at an original magnification of 500x. The boride particles - either Cr_2B or as $(Cr,Fe)_2B$ - show up darker than the austenitic matrix due to their lower average atomic number. Roll direction is parallel to the short dimension of each photo. (a) 304B5A. (b) 304B5B. (c) 304B7A. (d) 304B7B.

using a log scale in Figure 2. The log scale is needed since the distribution of boride sizes in each lot of material is quite broad, spanning at least 2 orders of magnitude in area. For each lot of material, the area size distribution, $Y(x(\mu m^2))$, is well approximated by the log-normal distribution (Dixon and Massey 1957)

$$Y(x\ (\mu m^2)) = (1/(\ln \sigma\ (2\pi)^{1/2}))\ (\exp\ [-0.5((\ln x\ (\mu m^2) - \ln \mu\ (\mu m^2))/\ln \sigma)^2] \qquad (1)$$

where $\ln \mu\ (\mu m^2)$ and $\ln \sigma$ are known as the mean and variance of the distribution, respectively. The log-normal fit for each lot of material is plotted as a straight line in Figure 2. The log-normal parameters, as well as the average (first moment of eq.(1)), minimum and maximum boride areas for each lot of material are shown in Table 2. Whether one uses the average area or maximum area as the basis of statistical measure, the boride particles in the Grade A, PM-processed material are significantly finer than for the case of the Grade B, IM-processed material. There is no doubt that the largest particles present are most problematic with respect to limiting toughness and ductility in these materials. Thus, the fact that both Grade A materials have maximum boride particle areas roughly an order of magnitude smaller than their Grade B counterparts suggests that their toughness and ductility should be substantially improved relative to the properties of Grade B material.

Table 2. Log-normal distribution parameters and other area size information for each lot of material studied. Area size information obtained from rolling plane samples. The average area, denoted as <A>, for each lot is obtained from the *first* moment of the log-normal equation, and is equal to exp [$\ln \mu + 0.5*\ln^2\sigma$].

Item	304B5A	304B5B	304B7A	304B7B
$\mu\ (\mu m^2)$	2.07	12.46	4.47	14.83
$\sigma\ (\mu m^2)$	2.41	3.16	2.99	3.53
$<A>\ (\mu m^2)$	3.05	24.13	8.15	32.82
min. area (μm^2)	0.13	0.77	0.18	0.5
max. area (μm^2)	20.0	456.	69.7	597.

Round tensile specimens with a 3/8"-24 thread, 1/4" gage diameter and 1" long gage section were machined from both 304B5A and 304B5B material. Flat plate specimens were machined with a 1/2" wide gage, 2" long gage section and nominal thickness of 0.200" for the 304B7A and 304B7B materials. The majority of the samples were tested at all temperatures in the transverse direction; longitudinal samples were also tested both at room temperature and 400°C (752°F). In order to collect complete strength and ductility data, all tensile tests were run at a constant engineering strain rate to fracture. For 304B5A, 304B5B and 304B7A material, the majority of tests were performed at an engineering strain rate of 5%/min., while for 304B7B material, most testing was done at 0.5%/min. Additional tensile data for 304B5A and 304B7A samples were obtained at 0.5 and 50%/min. and temperatures of 23°C (73°F) and 400°C (752°F): these tests did *not* indicate any strain-rate sensitivity over this strain rate/temperature range. Similarly, 23°C (73°F) tests of 304B7B material run at 5%/min. showed no difference in properties compared with tests run at 0.5%/min.

TENSILE TEST RESULTS AND DISCUSSION

The strain to fracture as a function of temperature for both Grades of 304B5 and 304B7 material are shown in Figures 3a and 3b, respectively. For both material Types, the PM-processed Grade A material has substantially higher levels of strain to fracture than the IM-processed Grade B material. This observation is consistent with the generally finer boride particle size in the PM-processed material compared to IM-processed material. Within a particular Grade of material (A or B), increased boron content tends to reduce ductility. Regression analysis of the

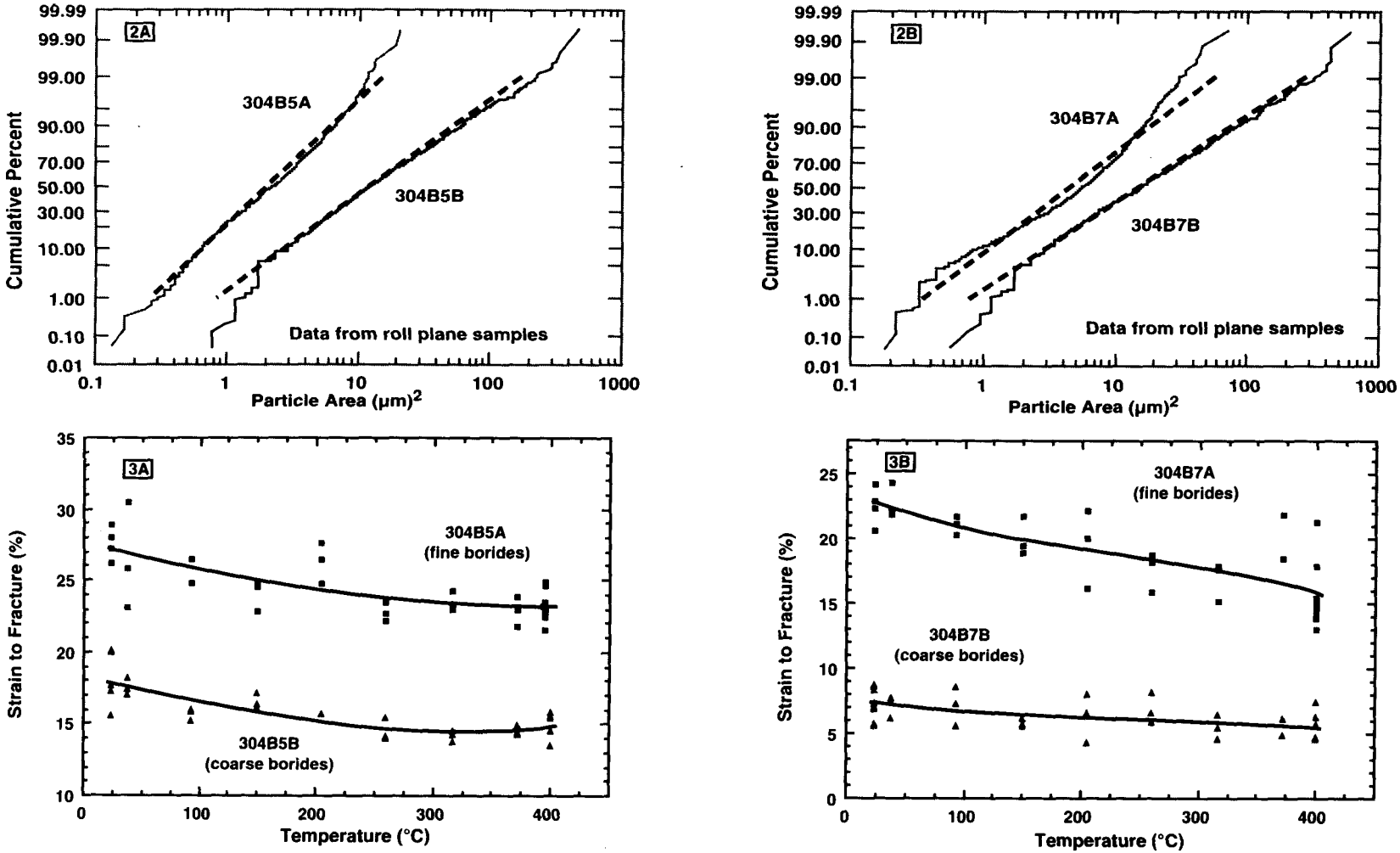

Figure 2. Area size distributions of boride particles plotted on logarithmic probability paper, where a straight line represents a log-normal size distribution. The lines from 1 to 99% represent the best fit log-normal distribution obtained by regression analysis. (a) 304B5A and 304B5B. (b) 304B7A and 304B7A.

Figure 3. Strain-to-fracture as a function of temperature for all four lots of material studied in this paper. The trend lines drawn were obtained from regression analysis using a cubic equation. (a) 304B5A and 304B5B material. (b) 304B7A and 304B7B material.

strain to fracture vs. temperature data was performed for each material lot using a cubic equation; these results were used to generate the trend lines shown in Figure 3. The trend lines indicate a general trend of decreasing ductility as temperature increases: the temperature effect is most pronounced for 304B7A. The trend lines are also useful for quantitative comparison of the effect of temperature on ductility for the two processing routes. The trend for Grade 304B5 is quite flat, as the average ductility of 304B5A is 1.51 times that of 304B5B at room temperature, and this ratio increases slightly to 1.53 at 400°C (752°F). For the 304B7 Type material, the average ducility of 304B7A is 3.19 times that of 304B7B at room temperature, and this ratio decreases to 2.93 at 400°C (752°F). No plastic strain was observed in the 304B7B samples past the point of uniform strain, while samples of 304B7A always exhibited deformation (i.e., necking) past this point. This helps to explain why there is such a dramatic increase in ductility for 304B7A compared to 304B7B. For the case of Type 304B5 material, both Grades exhibited deformation and evidence of necking past the point of uniform strain, but the typical 304B5A sample exhibited 5-6% additional plastic strain past the point of uniform strain, while the typical 304B5B spercimen deformed only 1-2% past the uniform strain before fracture.

The PM-processed Grade A material also has a higher 0.2% offset yield strength as a function of temperature relative to the IM-processed Grade B material. This effect is shown in Figure 4, where the trend lines again represent cubic fits to data obtained by regression analysis. Within a given Grade of material, the higher boron content Type 304B7 material leads to increase yield strength levels at all temperatures relative to Type 304B5 material: this is consistent with previous data for both Grades of borated 304 stainless steel at room temperature and 350°C (662°F) (Martin 1988). The higher yield strength for the Grade A material is undoubtedly due, to some degree, to the finer dispersion of borides, but a decreased grain size could also contribute to the increase in yield strength. The yield strength of all four lots of material at 371°C (700°F) are consistently higher than the yield strength of 103 MPa typically observed for 304L stainless steel (Japser 1989). It should be pointed out that the increase in strength observed in the borated grades are not reflected in the ASTM A887 specification, which requires minimum yield and tensile strength values of 205 and 515 MPa, respectively, for all Types and Grades.

The same trends are observed if tensile strength, rather than yield strength, were used as the basis of strength comparison between the boron-containing Grades A and B and boron-free 304L. The higher tensile strength levels suggest that high-cycle fatigue properties of the borated grades could be slightly higher for the boron-containing material. Recent results for strain-controlled fatigue experiments conducted at SNL (Stephens and Hatch 1992) have indicated that 304B5A has lower fatigue properties than boron-free 300 series stainless steel (ASME 1969) at the high strain amplitude/low cycle end of the test matrix, but this degradation disappears at lower strain amplitudes, where the elastic strain amplitude is greater than the plastic strain amplitude. This data is shown in Figure 5. Further work is needed to extend these results to lower strain amplitudes and different boron-containing Types as defined in ASTM A887.

ASME CODE CASE INQUIRY - STATUS AS OF JULY, 1992

The tensile data for selected Types of Grade A material have been used to initiate an ASME Boiler and Pressure Vessel (B&PV) Code Case Inquiry (#N90-27) for borated stainless steel. The requested applications in this inquiry are for use in "the construction of component supports for storage or transport of new or spent-fuel assemblies." The initial inquiry covers 304B4A, 304B5A and 304B6A material, and is currently awaiting approval by Section III. 304B7A material is not included in this code case because its required minimum impact energy (14 Joules = 10 ft-lbs.) was not deemed adequate: a value of 21 Joules (15 ft-lbs.) is considered necessary for consideration in a code case. At present, this code case is written so as to exclude welded material from receiving structural credit in the design. If approved, this inquiry will result in the establishment of design stress intensity values by which the approved material can be used in

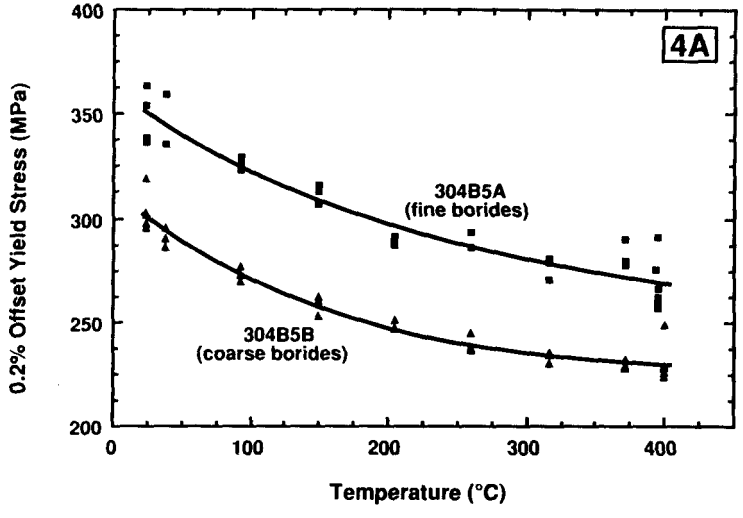

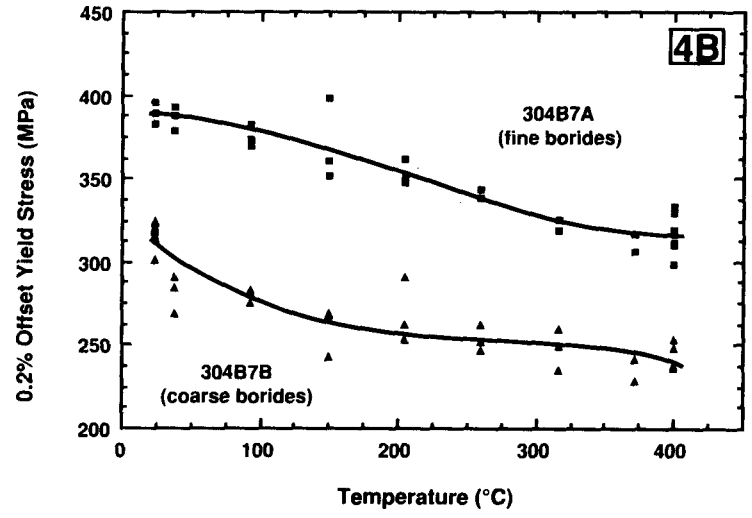

Figure 4. Yield strength (0.2% offset) as a function of temperature for all four lots of material studied in this paper. The trend lines drawn were obtained from regression analysis using a cubic equation. (a) 304B5A and 304B5B material. (b) 304B7A and 304B7B material.

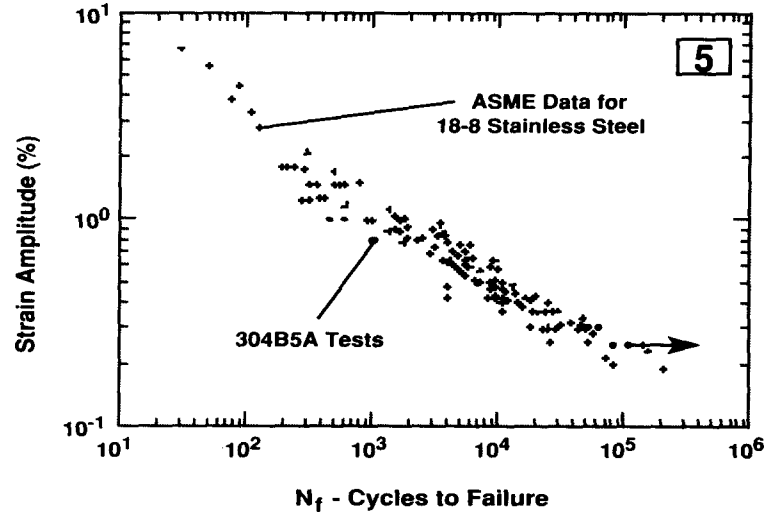

Figure 5. Room temperature, fully reversed low-cycle fatigue results for 304B5A are compared to the ASME data base for 300 series austentitic stainless steels. Strain-controlled tests run at a strain rate of 1x10-3 s-1 with a triangular waveform ramp using transverse samples.

designs according to Section III, Division 1 rules. This is an important step in qualifying borated stainless steel for structural applications in cask designs. At a future date, we anticipate inclusion of the lower boron Types of Grade A material (304BA, B1A, B2A and B3A) in an ASME code case for borated stainless steel.

SUMMARY

This paper has documented the increase in strain to fracture and yield strength obtained with Grade A versions of Types 304B5 and 304B7 relative to their respective Grade B, counterparts. The apparent microstructural reason for these property increases is the finer dispersion of boride in the Grade A material, obtained by means of a Powder Metallurgy process, relative to the conventional Grade B material which is produced using an Ingot Metallurgy process. The area size distribution of borides can be well approximated using a log-normal distribution, with the largest boride particles in the Grade B material having areas in the range of 450-600 μm^2. By comparison, the largest boride particles in the Grade A material have areas nearly an order of magnitude smaller than the largest particles in their Grade B counterparts. A Section III ASME B&PV Code Case inquiry has been initiated for non-welded versions of 304B4A, 3045A and 3046A material.

ACKNOWLEDGEMENTS

We would like to acknowledge the technical assistance of A. G. Greene, C. E. Heath and W. R. Sorenson. The help of R. S. Brown, Carpenter Technology Corporation, is also acknowledged for supplying the borated stainless steel plate discussed in this paper.

REFERENCES

American Society of Mechanical Engineers. "Criteria of the ASME Boiler and Pressure Vessel Code For Design by Analysis in Sections III and VIII, Divsion 2", New York: ASME, 1969. pp. 15-17.

W. J. Dixon and F. J. Massey, Jr. Introduction to Statistical Analysis, New York: McGraw-Hill Book Company, 1957, pp. 48-70.

H. J. Goldschmidt. "Effect of Boron Additions to Austenitic Stainless Steel", Journal of the Iron and Steel Institute, vol. 209, November, 1971, 900-912.

J. Jasper, Armco Steel, Inc., Middletown, Ohio. Private communication to J. J. Stephens, September, 1989.

J. W. Martin. "Effects of Boron Content and Processing on Mechanical Properties and Microstructure of Borated Stainless Steel," Research and Development Report #K86007 (September 23, 1988), Carpenter Technology Corporation, Reading, PA 19612-4662.

J. J. Stephens and K. B. Sorenson. "Tensile Behavior of Borated Stainless Steels: Phase 1", SAND 90-1247C (June, 1990). Sandia National Laboratories, Albuquerque, NM 87185-5800.

J. J. Stephens and P. W. Hatch. Unpublished research presented to ASME Subgroup on Fatigue Strength, May, 1992, San Antonio, Texas.

D. L. Strobel and B. A. Smith. "Premium Boron Stainless Steel Improves Ductility", Stainless Steel Industry, vol. 16, January, 1988, pp. 15-16.

Plutonium Air Transportable Package Development Using Metallic Filaments and Composite Materials*

J. D. Pierce and M. K. Neilsen

Sandia National Laboratories, Albuquerque, New Mexico, United States of America**

INTRODUCTION

A new design concept for plutonium air transport packagings has been developed by the Transportation Systems Department and modeled by the Engineering Mechanics and Material Modeling Department at Sandia National Laboratories (SNL). The new concept resulted from an in-depth review (Allen et al., 1989) of existing package design philosophies and limitations. This review indicated a need for a new package which could survive combinations of impact, fire, and puncture environments, and which could be scaled up or down to meet a wide range of requirements for various contents and regulations.

This new design concept uses a very robust primary containment vessel with elastomeric seals for protection and confinement of an inner containment vessel with contents. An overpack consisting of multiple layers of plastically-deformable metallic wire mesh and high-tensile strength materials is placed around the containment vessels to provide energy absorption for the primary containment vessel as well as thermal protection. The use of intermittent layers with high-tensile strength results in a limiter which remains in place during accidental impact events and can be relied upon to provide subsequent puncture and fire protection. In addition, an outer shell around the energy absorbing material is provided for handling and weather protection.

To validate the concept, numerous scoping tests were performed on material samples, wall sections, and partially modeled prototypes. To evaluate various design features, finite element analyses were performed on the package. The finite element analysis required the development of a new constitutive theory for layered composite materials. The effects of neglecting the anisotropic tensile behavior were investigated with a series of dynamic finite element analyses. The model was implemented in both static and dynamic finite element codes and a number of steps were completed to benchmark the model. Uniaxial compression and tension experiments were performed on various candidate materials to obtain appropriate material properties for the model. Scale model packages subjected to side and end impacts were analyzed. Prototype scale model packages were fabricated and subjected to 129 m/s side impact and 200 m/s end impact tests, respectively. Test results indicated that the overpack

*This work performed at Sandia National Laboratories, Albuquerque, New Mexico, and supported by the U.S. Department of Energy under Contract DE-AC04-76DP00789.
**A U.S. Department of Energy Facility.

would remain intact throughout a worst case accident, and that structural loads on the containment vessel could be limited to assure integrity of the containment vessel.

DESIGN REQUIREMENTS

A package design was needed that could not only meet but exceed the requirements for a large plutonium air transport package as prescribed in NUREG-0360. The sequential test environments in NUREG-0360 that a package weighing more than 227 kg must be subjected to and not release an A_2 quantity of material in one week are: (1) a 129-m/s perpendicular impact onto a flat unyielding target in the most severe location, (2) a 3-m drop onto a conical steel puncture probe in the most severe location, (3) two slash tests by a 45-kg section of structural steel dropped 46 m onto the package, (4) a fully-engulfing JP-4 fire test for a period of no less than one hour, and (5) a 1-m submersion test in water for a period of 8 hours. Recent U.S. legislation (U.S. Public Law 100-203) also requires that foreign shipments of plutonium through U.S. airspace be able to withstand a worst-case aircraft crash, therefore the requirements for packages used for these applications is expected to be even more severe. An examination of crash data indicated that an impact onto a rigid target at a higher velocity might be a required extrapolation of current impact requirements for future designs. An arbitrary impact velocity of 200 m/s was chosen as a design goal for this study.

The primary goals for the new package design were:

1. the overpack should remain in place after the impact to provide protection for subsequent environments such as crush, puncture, and fire;
2. the overpack should be well characterized and the performance well understood so that computer simulation of hypothetical accident events is possible;
3. the overpack material should perform the same when scaled for large or small applications;
4. the package parameters should be able to be easily changed to meet not only the requirements in NUREG-0360 but also any worst-case accident environment that might be part of future regulations or applications;
5. the overpack should be fabricated out of non-combustible materials to prevent the containment vessels from being subjected to unduly high heat loads in an accident environment; and
6. the package should be cost-effective for large quantities of material.

PACKAGE DESIGN

An in-depth review of existing package design philosophies and their limitations led to the development of a new package concept. This new design concept which met the above criteria consists of only a few basic elements.

1. An inner vessel is provided that is made of titanium, alloy steel, or any other material suitable for providing a containment boundary around the payload. The material and its configuration are chosen depending on the severity of the transportation accident environment to be encountered. The type and condition of the payload also determine the type of seal and method of securing the closure on the inner vessel.

2. Multiple layers of wire mesh are provided for energy absorption. This material may have various wire sizes, various mesh spacings, and may be aluminum, corrosion resistant steel, titanium, or other suitable material depending on the requirements.

3. Layers of high-tensile strength fabric are sandwiched in the wire mesh for confinement of the wire mesh in an impact environment and for puncture protection. This material may be aramid cloth, S-2 glass, graphite, or other suitable cloth depending on the environment.

4. Layers of insulation material are sandwiched in the wire mesh as needed for thermal protection and multiple layers at the external surface for primary thermal protection.

5. A thin shell encases the wire mesh, high-tensile strength cloth, and insulation materials for handling protection. This may be corrosion resistant steel, aluminum, resin impregnated cloth materials or other suitable material.

A baseline design capable of carrying 7.8 kg of plutonium was developed (Figure 1). The package utilizes a robust primary containment vessel fabricated from a titanium alloy with a 2.5-cm sidewall that can carry various configurations of inner containment vessels. A cylindrical overpack is provided as shown that has stepped end, caps. The composite wall is radially wrapped in the cylinder and stacked in layers in the end plugs to achieve a wall thickness of 60 cm and 120 cm on the sides and ends respectively. The end plugs are held in place by keyed pins and bolts. The layered wire mesh and cloth materials are encased in a 1.5-mm thick 304 stainless steel shell.

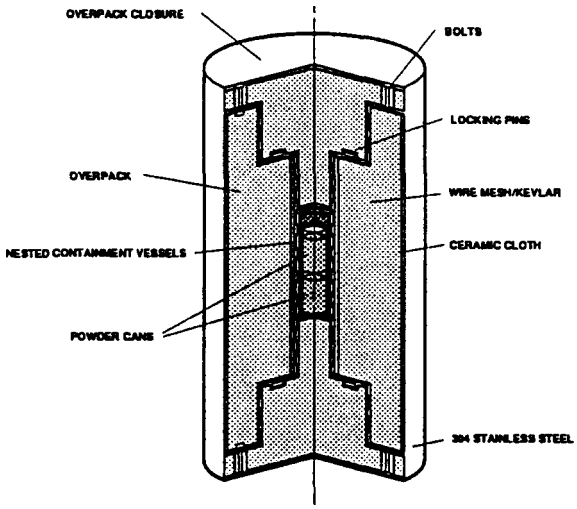

Figure 1. Plutonium Air Transport Package Design Concept

SCOPING TESTS

Many static tests were performed on small samples and wall sections of various wire mesh and high-tensile strength cloth materials. Dynamic tests were then performed on scale model prototypes. The best material for energy absorption for air transport applications was found to be aluminum wire mesh. The high-tensile strength cloth materials had less utility as energy absorbers, but were very necessary to provide confinement of the wire mesh, spread the load from a puncture environment over a much larger area, and provide thermal protection for the contents of the overpack.

Several radial sample wall sections with aramid cloth included at multiple locations in the wire mesh were tested to failure by crushing in the same configuration as a dynamic side impact test. A significant improvement in confinement was observed with the addition of the aramid cloth (approximately a factor of four improvement for the configuration tested).

The data from these tests were used to design and fabricate a simple quarter-scale wire mesh model capable of carrying 8 kg of PuO_2. This model was subjected to a side-impact reverse ballistic test at the 3 km rocket sled track at SNL. A 273-kg steel target mounted to a rocket sled with a catcher box was impacted onto the test model at 129 m/s. The overpack remained completely intact, and the containment vessel, which was fabricated of low carbon steel, sustained minimal (approximately 3% maximum at the center of the cylinder) deformation.

Next, a number of composite wall cross sections comprised of aluminum wire mesh and aramid cloth were assembled and tested statically to determine the performance of the overpack wall during an end impact test. The data from these tests were used to design and fabricate a simple quarter-scale wire mesh model of a package capable of carrying eight kilograms of PuO_2. This model was also subjected to a reverse ballistic test. The steel target impacted onto the test model in an end-on orientation at 129 m/s. The overpack remained completely intact, and the containment vessel, which was fabricated of low-carbon steel, sustained minimal deformation.

Another simple quarter-scale wire mesh model of a package carrying eight kilograms of PuO_2 was fabricated. This model was again subjected to a reverse ballistic test. A steel target mounted to a rocket sled with a catcher box was impacted onto the test model at 129 m/s. The package was impacted in a center-of-gravity over-the-corner orientation. The overpack remained completely intact, and the containment vessel, which was fabricated of low-carbon steel, had local permanent deformation, which was outboard of where the seals would be. A simple retaining ring technique was used to install the closure, and this appeared to work very well.

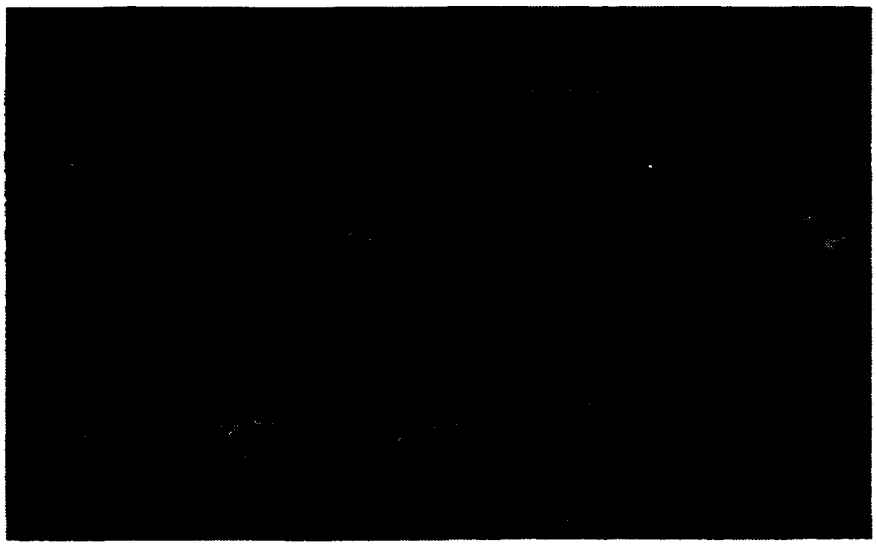

Figure 2. Section of Overpack Subjected to a Corner Impact

MATERIAL CHARACTERIZATION

The behavior of layers of aluminum wire mesh with and without aramid cloth fabric was characterized with a series of uniaxial compression and confined compression tests. Axial stress versus axial engineering strain curves generated during these tests are shown in Figures 3 and 4. In the first series of tests, samples with various layer orientations were subjected to confined compression (Figure 3). All of the samples used in these tests were manufactured by

alternatively stacking 20 layers of aluminum wire mesh and 2 layers of aramid cloth fabric. The undeformed samples all had a cubical shape with an edge dimension of 5.1 cm. The confined compression tests indicated that layer orientation had little effect on the crush strength of the material: thus, the crush strength is nearly isotropic. Also, the crush strength, σ^c, varies exponentially with axial engineering strain ε. The solid line in Figures 3 and 4 represents a best fit to the experimental confined compression test data which is given by the following equation.

$$\sigma^c = 17.0e^{-8.68\varepsilon} \qquad (1)$$

Since the lateral displacements are constrained, the axial engineering strain, ε is equal to the engineering volume strain, γ, in these tests.

In a second set of tests, layers of wire mesh and wire mesh with aramid cloth fabric were subjected to cyclic, unconfined uniaxial loads. In these tests, the load was always applied in a direction normal to the layers (0 degrees) but the number of aramid cloth layers and the sample size was allowed to change. In the first test, a sample with a length of 15.2 cm, a width of 17.8 cm and a height of 2.54 cm was used. In the remaining three tests, samples with lengths and widths of 5.1 cm inches and heights of 2.54 cm were used. In the first two uniaxial compression tests, the layering was identical to the layering used in the confined compression tests; but, in the last two tests, the aramid cloth layers were eliminated. Results from these tests indicated that inclusion of the aramid cloth fabric had little effect on the response of the material to uniaxial compression. Also, these tests indicated that the lateral strains generated by uniaxial compression are negligible. This means that the material has a Poisson's ratio that is nearly equal to zero. Furthermore, any plasticity theory that is developed to capture the behavior of this material should predict no lateral strains when the material is loaded in the plastic regime. The solid line in Figure 3 represents a best fit to the confined compression test data (Equation 1). Results from the limited number of uniaxial compression tests indicates that Equation 1 also represents the uniaxial compression data reasonably well.

In tension, the wire mesh material exhibits widely varying behavior. For example, when the material is loaded in tension in a direction parallel to the layers, the wire mesh has a tensile strength of approximately 158 newtons/cm of width per layer and the aramid cloth fabric has a tensile strength of 1922 newtons/cm of width per layer. However, when the material is loaded in a direction normal to the fabric layers the material exhibits essentially no strength as the layers are separated. The wire mesh has a wire diameter of 0.27 mm and the aramid cloth fabric has a thickness of 0.43 mm.

ANALYSIS

A review of existing constitutive theories indicated that no existing theory could adequately simulate the response of the layered composite materials. Thus, a new plasticity theory which captures the layered material behavior exhibited during the uniaxial and confined compression tests was developed (Neilsen and Pierce, 1992). This new plasticity theory is similar in many respects to a plasticity theory that was developed for polyurethane foam (Neilsen et al., 1987).

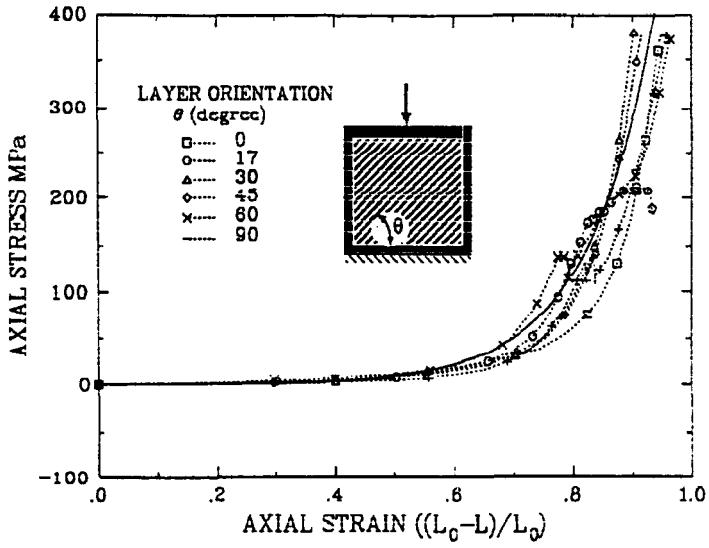

Figure 3. Confined Material Test Data

The new theory has yield functions which describe intersecting planes in principal stress space:

$$|\sigma^i| - Ae^{\beta\gamma} \qquad i= 1, 2, 3 \qquad (2)$$

$$|\sigma^i| - c \qquad i= 1, 2, 3 \qquad (3)$$

where σ^i is a principal stress and A, β, and c are material parameters. The first yield function (Equation. 2) is used when the principal stress is compressive and the second yield function (Equation. 3) is used when the principal stress is tensile. Material parameters A and β are selected based on the results from the uniaxial and confined compression tests. Material parameter c is a measure of the tensile strength of the material and is independent of the compressive response. This new plasticity theory uses associated flow rules.

This new constitutive theory was implemented into a static finite element code, SANTOS (Stone, 1992) and into dynamic finite element codes, PRONTO-2D (Taylor and Flanagan, 1987) and -3D (Taylor and Flanagan, 1987). The material characterization tests were numerically simulated to ensure that the new constitutive theory was properly implemented and that the new theory accurately captured the material behavior exhibited during these tests. Next, a number of impact tests were simulated to further benchmark the model. In some of these analyses, individual layers with alternating amounts of tensile strength were used to investigate the effect of layer separation. These analyses indicated that simulation of layer separation was not needed to generate accurate package response predictions. The response of the layered composite material during a hypothetical accidental impact event was adequately captured by the new isotropic plasticity theory.

Finally, the response of a baseline package subjected to side and end impact velocities of 129 m/s and 200 m/s was numerically simulated. Typical deformed shapes of the package predicted by these simulations are shown in Figure 4. Results from these simulations indicated that the primary container would be deformed only a small amount during a 200 m/s impact event and that the amount of predicted deformation would depend on the response of the contents.

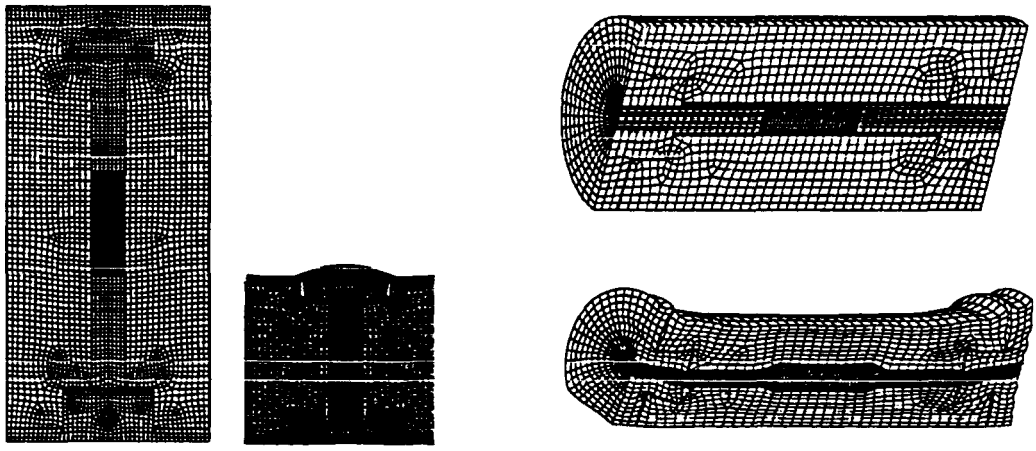

Figure 4. Deformed Shape of Baseline Package for End and Side Impacts Predicted by a Numerical Simulation of a 200 m/s Impact

THERMAL

A series of thermal tests was performed at the Radiant Heat Facility. A partial one-dimensional test article with the same composite makeup as an actual prototype was fabricated for each test. The test articles were subjected to a thermal environment for 30 minutes and 60 minutes to establish the preliminary thermal properties for the material. Samples are also being evaluated by use of a thermal compactor and a guarded hot plate to establish more accurate thermal data. The results of these tests will be used in a 3-D model currently under development. Initial results indicate that, depending on the heat load generated by the contents, the inner containment vessels will remain below the maximum allowable temperatures. Analyses performed on a package with approximate dimensions of only one fourth those for this package indicate temperatures would be below the allowable temperatures for elastomeric seals in a 30 minute fire. The results were conservative and do not account for heat flow through the shell, however they are an indication that temperature rise in a fire should not be a major design problem as long as the container remains surrounded by the composite material.

CONCLUSIONS

Experiments and analyses to date have verified and demonstrated several key points:

I. Although materials have not been optimized, aluminum wire mesh may be used as an overpack material with desirable and predictable results.

2. This concept allows a composite wall to be easily fabricated which can incorporate wire mesh for energy absorption, high-tensile strength cloths for puncture and intermediate thermal protection (i.e., aramid cloth, fiberglass, or graphite) and insulation material (i.e., ceramic cloth) for primary thermal protection. This allows the design to be easily tailored for a variety of applications.

3. Although the aluminum wire mesh has a higher density than redwood, other major components for confinement that previously designed packages required are not needed. Components such as full load spreaders and heavy outer shells inflict a severe weight penalty. This actually results in a better payload to total package weight ratio (efficiency) than with redwood designs for air transport applications.

4. The wire mesh exhibits global isotropic behavior when configured as a multilayer overpack for energy absorption. This allows for a simpler and less expensive computer simulation to predict the response of the package to a hypothetical accident event.

5. The *soft* overpack constructed of wire mesh allows the overpack to absorb a significant amount of its own kinetic energy even in areas above the payload. A *rigid* overpack constructed of a foam or redwood crushes primarily at the contact point. This is a key factor since the overpack for air transport may represent 80% to 95% of the total mass of the package.

6. Fabrication of a complex composite overpack is relatively simple and inexpensive.

REFERENCES

Allen, G. C., Design Aspects of Plutonium Air-Transportable Packages, PATRAM 89 Proceedings, Washington, DC., June 11-16, 1989.

Neilsen, M. K. and Pierce, J. D., "A Constitutive Model for Layered Wire Mesh and Aramid Cloth Fabric," SAND91-2850, Sandia National Laboratories, Albuquerque, NM (in preparation).

Neilsen, M. K., Morgan, H. S., and Krieg, R. D., "A Phenomenological Constitutive Model for Low Density Polyurethane Foams," SAND86-2927, Sandia National Laboratories, Albuquerque, NM, 1987.

NRC (U.S. Nuclear Regulatory Commission), Qualification Criteria to Certify a Package for Air Transport of Plutonium, NUREG-0360, U.S. Nuclear Regulatory Commission, January 1978.

Stone, C. M., "SANTOS A Two-Dimensional Finite Element Program for the Quasistatic, Large Deformation, Inelastic Response of Solids," SAND90-0543, Sandia National Laboratories, Albuquerque, NM (in preparation).

Taylor L. M. and Flanagan, D. P., "PRONTO-2D A Two-Dimensional Transient Solid Dynamics Program," SAND86-0594, Sandia National Laboratories, Albuquerque, NM, 1987.

Taylor L. M. and Flanagan, D. P., "PRONTO-3D A Three-Dimensional Transient Solid Dynamics Program," SAND87-1912, Sandia National Laboratories, Albuquerque, NM, 1987.

United States Public Law 100-203, Title V-Energy and Environment Programs, Subtitle A - Nuclear Waste Amendments, Part F-Miscellaneous, Section 5062, December 22, 1987.

Type B Plutonium Transport Package Development That Uses Metallic Filaments and Composite Materials*

J. D. Pierce, J. L. Moya, J. D. McClure, and G. F. Hohnstreiter
Sandia National Laboratories, Albuquerque, New Mexico, United States of America**

K. G. Golliher
U.S. Department of Energy, Albuquerque Operations Office, Albuquerque, New Mexico, United States of America

INTRODUCTION

A new design concept for a Type B transport packaging for transporting plutonium and uranium has been developed by the Transportation Systems Department at Sandia National Laboratories (SNL). The new design came about following a review of current packagings, projected future transportation needs, and current and future regulatory requirements.

United States packaging regulations specified in Title 49, Code of Federal Regulations Parts 173.416 and 173.417 (for fissile materials) offer parallel paths under the heading of authorized Type B packages for the transport of greater than A_1 or A_2 quantities of radioactive material. These pathways are for certified Type B packagings and specification packagings. Consequently, a review was made of both type B and specification packages.

A request for comment has been issued by the U.S. Nuclear Regulatory Commission (NRC) for proposed changes to Title 10, Code of Federal Regulations Part 71. These regulations may therefore change in the near future. The principle proposed regulation change that would affect this type of package is the addition of a dynamic crush requirement for certain packagings. The U.S. Department of Transportation (DOT) may also re-evaluate the specifications in 49 CFR that authorize the fabrication and use of specification packagings. Therefore, packaging options were considered that will meet expected new regulations and provide shipment capability for the U.S. Department of Energy well into the future.

The possible lack of available packagings caused SNL to undertake a preliminary development program for a new Type B packaging that could meet present and future regulatory requirements. As a result of this program SNL developed a new design for a package that could transport similar quantities of plutonium and uranium that are currently carried in the DOT-6M packagings. The new package design uses nested cylindrical containment vessels (double containment) with threaded closures and elastomeric seals. A composite overpack of metallic wire mesh and ceramic or quartz cloth insulation materials is provided for structural and thermal protection of the containment vessels in an accident environment.

---

*This work performed at Sandia National Laboratories, Albuquerque, New Mexico, and supported by the U.S. Department of Energy under Contract DE-AC04-76DP00789.

**A U.S. Department of Energy Facility.

Two prototype packages were fabricated and subjected to dynamic crush (500 kg steel plate dropped 9 meters onto the package) environments. Subsequent evaluation indicated no deformation in the seal areas of the containment vessels that would jeopardize containment of the material. Wall sections were fabricated to obtain empirical thermal physical data for the composite wall for pre- and post-accident conditions. Finally, a thermal computer model was developed and benchmarked by test results to predict package behavior during a fire environment. Numerous tests were performed on material samples to obtain structural data for the wire mesh and composite materials and a structural model developed to capture the performance of an air transport package subjected to a high speed impact (Neilsen and Pierce 1992). Data from that work demonstrated that the material performed isotropically in a global fashion.

PACKAGE DESIGN

The design that is presented in Figure 1 uses materials and assembly techniques different from those used in previous packaging designs. This new approach utilizes aluminum wire mesh and composite materials such as quartz cloth insulation, to provide impact, puncture, and thermal protection to a containment vessel during hypothetical accident environments prescribed in Title 10, Code of Federal Regulations Part 71. The overpack also enables the container to survive the severe dynamic crush environment proposed for inclusion to 10 CFR 71.

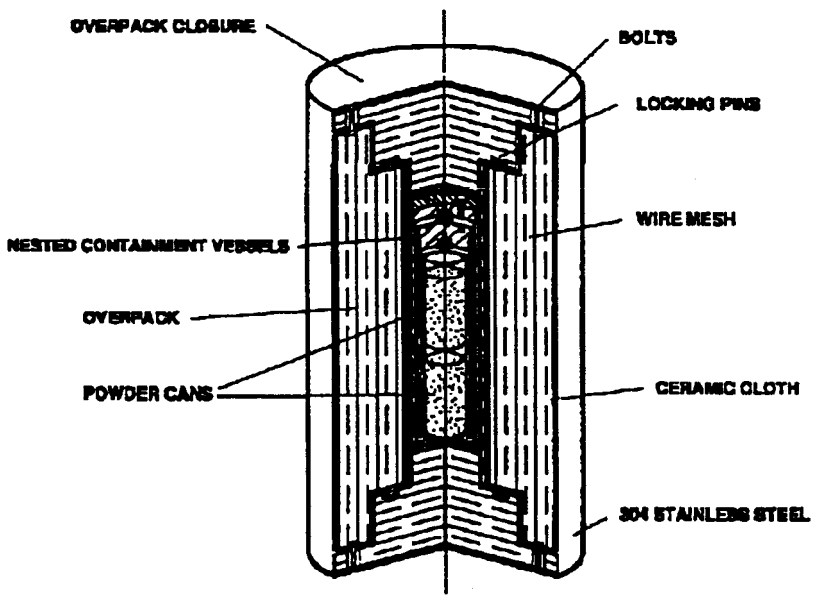

Figure 1. Type B Plutonium Transportation Package Concept

OVERPACK

The overpack was conservatively designed from empirical data to meet a dynamic crush environment and to provide thermal protection in a fire environment. The overpack was also sized to allow adequate dissipation of 20 watts of internally generated decay heat. Wire mesh made of aluminum alloy is used for crush protection and cloth insulation is sandwiched at intervals in the wire mesh to provide additional thermal protection. A thin shell of 304

stainless steel encases the wire mesh and insulating materials for handling purposes and weather protection. The overpack consists of a main cylindrical body with identical stepped-end plugs with redundant fasteners. The overpack is 45.7 cm in diameter and 98.9 cm in length with an overpack wall thickness of 15.2 cm. The overpack consists of a stackup of layers of 5154 aluminum wire mesh with wires that are .3 mm diameter on a mesh spacing of one wire every 1.5 mm. The ceramic insulation cloth is .4 mm thick. The composite wall in the cylinder was fabricated by radically wrapping 5 zones with 60 layers of wire mesh and two layers of insulation cloth in each zone. The overpack end caps were fabricated with the wire mesh and insulation configured the same as the sidewall.

Since the wire mesh composite material does not burn, it provides an alternative to organic materials typically used in transportation containers. A *typical* light-weight container designed to transport radioactive material consists of containment vessel(s) and overpack. A bolted o-ring closure typically is used to seal the containment vessel(s). Material placed in the overpack is designed to shield the radioactive contents, as well as to provide thermal and structural protection to the containment vessel during a postulated accident. Rigid polyurethane foam, or Celotex^{tm}, is commonly incorporated into the design to ensure the thermal and structural integrity of the container is not compromised during an accident condition. Thermal testing of a package must be performed sequentially as specified in 10 CFR 71. Structural damage to the outer skin of the container, resulting in sufficient oxygen access and heat exposure, can lead to extensive burning of organic materials. In addition, under certain conditions, the organic material could continue to burn slowly (self-sustained smoldering combustion) after the end of the fire test. If the organic material continues to burn long after the fire, it could provide a threat to the integrity of the containment vessel.

The composite overpack is designed so that during normal conditions of transport, the wire mesh does not adversely affect the container's ability to dissipate the decay heat generated by the radioactive material. The package relies on passive means (heat conduction through the wall) to dissipate the decay heat from the containment vessel to the environment by natural convection and thermal radiation. An inert gas may be used within the containment vessel as a cooling medium, however, this is not expected to be needed. The wire mesh, therefore, must be configured in such a way that it does not unduly impede the normal outward flow of heat from the radioactive material to the environment. For normal conditions of transport, if the wire mesh were to provide too much of a thermal barrier for the decay heat, undesirably high inner-container temperatures (i.e., high seal temperatures) could be reached.

The overpack costs for production were estimated to be approximately $3500, based on components purchased and fabrication costs for the prototype packages.

CONTAINMENT VESSELS

The containment vessels for the current design are nested one inside the other (Figure 2) and are fabricated from 304 stainless steel. These vessels provide a double containment boundary around the contents. The containment system is conservatively designed with the inner vessel having a 6.4 mm wall thickness and the outer vessel a 9.5 mm wall thickness. The inner vessel may be omitted if only single containment is required. The free space in the containment vessels is kept to a minimum.

Multiple concepts were established for an inner containment vessel that could carry two cans of material that are 10.8 cm outer diameter and 17.8 cm long. The vessels were similar, however, different closure techniques were evaluated. Three of the concepts were fabricated for evaluation. The vessels fabricated utilized threaded, breech-lock, and retaining ring closures. An overview of each design, including an evaluation of operational features such as operating

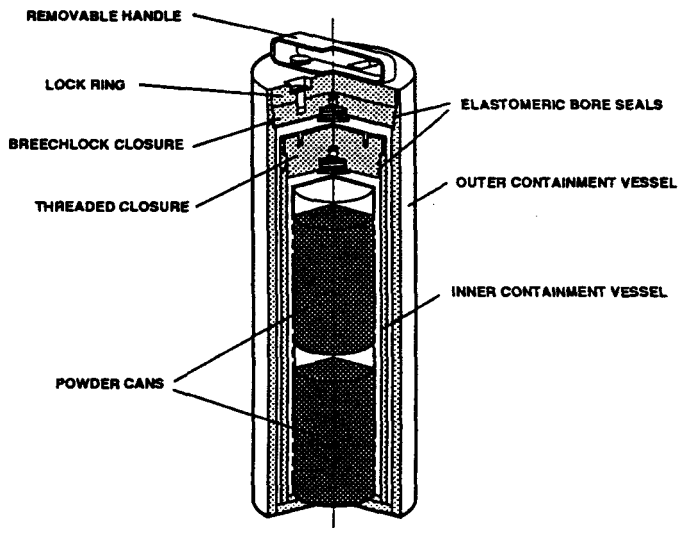

Figure 2. Nested Containment Vessels for Type B Package

the closure, performing leak tests, manufacturability was performed. A cost estimate for each was provided by means of a cost estimating computer program maintained and generated by the Mechanical Processing Department at SNL. The cost estimates were based on 1989 costs for a single vessel, and unit costs based on the production of 700 units. Two of the containment designs were felt to be the most promising.

Each design incorporates a bore seal for ease of assembly, seal testing, and seal protection. An elastomeric seal (o-ring) is used as the primary seal to establish the containment boundary, and a second o-ring used to establish a means of performing a helium leak test on the primary seal. Each design also incorporates a method of using the seal test port to introduce helium into the main cavity. This is done by seating the primary seal at the top of the sealing surface so that this seal is above the test port. Helium can then be introduced by (1) partially evacuating the cavity and backfilling with helium one or more times, (2) applying a slight over-pressure of helium and releasing one or more times, or (3) providing a second port on the same plane, establish a flow of helium gas for a fixed period of time and allowing the helium to mix with the inner atmosphere. Once helium gas has been introduced into the cavity, the closure is fully seated so that the seal test port is located between the primary seal and the secondary o-ring. A helium leak detector may then be used to determine the leak tightness of the vessel.

The first containment vessel evaluated was a threaded closure which was fabricated for evaluation and found to be easy to use. The leak testing method worked well, however, testing also demonstrated that dissimilar materials are required for the body and closure, in addition to the use of dry lubricant to prevent thread galling and seizing. The single prototype cost for the vessel was $1291 with unit cost for production being $306.

A breech-lock closure with a lock plate was also fabricated for evaluation. This design was found to work well but needed mechanical assistance for ease of operation. The leak test method worked well but testing demonstrated the friction of o-rings on the closure made the process somewhat difficult to perform by hand. A mechanically assisted external closure mechanism would be necessary for actual use. The single prototype cost was determined to be $2306 with a unit cost for production of $631.

An evaluation of the above options, as well as others, indicate that a simple containment vessel utilizing a threaded closure with two o-rings in a bore seal arrangement would be more cost

effective, and yet a very user-friendly design. A face seal with a threaded closure could also be easily incorporated into the design as an alternative to the bore seal.

For double containment, it is assumed a containment vessel identical to the inner containment vessel or one that utilized a separate type of closure would be used to enclose the inner vessel. Since the outer container is larger, it would require more materials and machining than the smaller design, however, for estimating purposes, the costs are assumed to be essentially the same for each vessel.

DYNAMIC CRUSH TESTS

Two prototype packages were fabricated to the above specifications for evaluation in dynamic crush environments. An axial dynamic crush test was performed on a prototype package at the Aerial Cable Test Facility at SNL. A 500 kg steel plate was dropped 9 m onto a prototype package that was positioned on end on the essentially unyielding target. The overpack was sectioned following the test for a post-test evaluation. The overpack skin buckled as desired without incurring any rips or tears. The overpack closure system also performed well with no loss of integrity. The wire mesh/composite impact mitigator also crushed as desired without any unexpected results. The containment vessel had no detectable deformation resulting from the test. Figure 3 shows a cutaway section of the overpack.

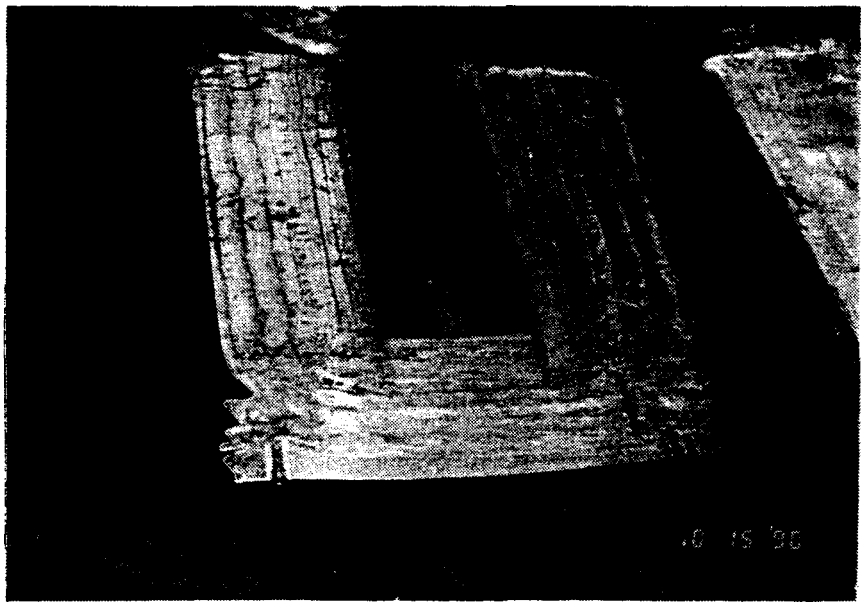

Figure 3. Cutaway Section of Package Following End-On Dynamic Crush Test

A second prototype transport packaging utilizing composite materials and wire mesh was subjected to a side-on dynamic crush test. A 500 kg steel plate was dropped 9 meters onto the prototype package that was positioned on its side on the unyielding target at the Aerial Cable Test Facility at SNL. The overpack materials absorbed the energy of the plate as desired without subjecting the containment vessel to high (yield level) stresses. The overpack shells

deformed without tearing or failing any bolts. The containment vessel suffered no permanent deformation and remained leak tight. Figure 4 shows a cutaway of the overpack that also has the undamaged containment vessel still in the unit.

Figure 4. Cutaway of Prototype Package Following Side-On Dynamic Crush Test

THERMAL EVALUATION

A series of thermal tests were performed at the Radiant Heat Facility at SNL. A one-dimensional test article with the same composite structure as the prototype was fabricated for each test. The test articles were subjected to an 800°C thermal environment for 30 minutes. The results of these tests were used to develop a two-dimensional, axisymmetric thermal model to investigate the thermal characteristics of the package when subjected to both normal and accident environments.

From the geometric description of the container, PATRAN (PDA Engineering 1990) was used to generate a two-dimensional computational mesh. The thermal analyzer, P/Thermal (Rockenbach 1990), was utilized to solve for the two-dimensional temperature distribution within the container. To simulate the decay heat load of a radioactive source, an energy generation rate of 20 watts was distributed evenly over the inner surface of the overpack. The boundary conditions for the hypothetical fire condition, exposed the whole package to a radiant heat source of 800°C, with an emissivity of 0.9 for 30 minutes and the package surface absorptivity was 0.8. The pre-fire steady-state temperature distribution assumed the container dissipates its 20 watts of decay energy to still ambient air at 38°C, but neglected any solar insulation to the container. To examine the possibility of further temperature increases within the container, the analysis continued beyond the 30-minute fire for a 3-1/2 hour cool-down

period. During both the fire and cool-down periods, the inner surface of the overpack was conservatively assumed to be adiabatic (perfectly insulated).

For normal conditions of transport, assuming the containment vessel is transporting radioactive material that dissipates 20 watts, the model predicts a temperature of 65.5°C at the wire mesh overpack/containment vessel interface. Figure 5 illustrates the temperature response, starting from the steady state profile of the wire mesh overpack during exposure to the radiant heat source and for 3-1/2 hours following the fire. Since the containment vessel is not explicitly modeled, the temperature of the inner wall of the overpack is assumed to be indicative of the containment vessel seal temperature. For an undamaged package, the predicted maximum seal temperature therefore is about 10°C below the continuous use temperature limit (232°C) for most elastomeric seals. Additional insulation material may be easily added to the package if testing indicates that the seal temperatures will exceed allowable limits when subjected to a regulatory accident environment.

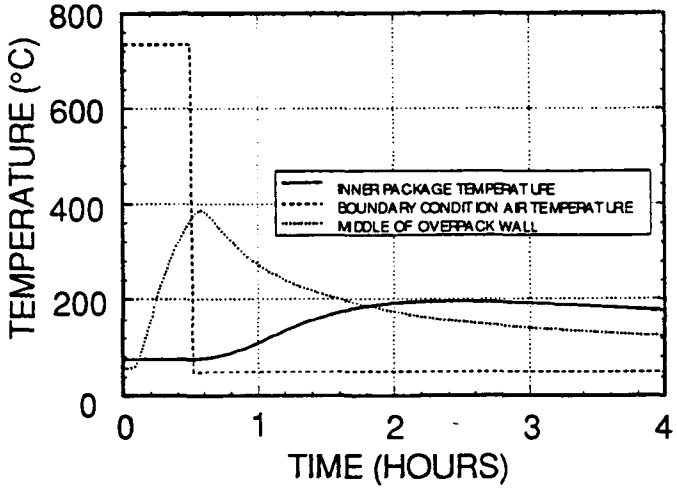

Figure 5. Predicted Temperature Profile of Package Subjected to 30 Minute Fire

CONCLUSIONS

The results of the experiments to date have verified and demonstrated several key points:

1. Although materials have not been optimized, aluminum wire mesh may be used as an overpack material with desirable and predictable results.

2. This concept allows a composite wall to be easily fabricated which can incorporate wire mesh for energy absorption, composites for puncture and intermediate thermal protection (i.e., Kevlar, fiberglass, or graphite) and insulation material such as ceramic cloth for primary thermal protection. This allows the design to be easily tailored to the application.

3. The wire mesh exhibits global isotropic behavior when configured as a multilayer overpack for energy absorption. This allows a simpler and less expensive computer model to be used to predict the crush performance of the package.

4. Fabrication of a complex composite overpack is relatively simple and inexpensive.

5. A Type B plutonium transport package could be developed and certified that could meet the requirements for DOE plutonium shipments for less than $5000 if manufactured in quantity.

REFERENCES

Neilsen, M. K. and Pierce, J. D., SAND91-2850, "A Constitutive Model for Layered Wire Mesh and Aramid Fabric," Sandia National Laboratories, Albuquerque, NM (in progress).

PDA Engineering, PATRAN Plus User Manual, Release 2.4, PATRAN Division, Costa Mesa, CA, January 1990.

Rockenbach, F. A., P/Thermal (O/TRAN) Technical Reference Manual, Version 2.4, PDA Engineering, PATRAN Division, Costa Mesa, CA, March 1989.

U.S. Code of Federal Regulations, Title 49 Part 173, U.S. Nuclear Regulatory Commission, Washington, DC, 1988.

U.S. Code of Federal Regulations, Title 10 Part 71, Proposed Rule Change, "Packaging and Transportation of Radioactive Material," Vol. 53, No. 110, U.S. NRC, Washington, DC, June 8, 1988.

U.S. Code of Federal Regulations, Title 10 Part 71, "Packaging and Transportation of Radioactive Material," U.S. NRC, Washington, DC, 1988.

Transportation Package Design Using Numerical Optimization*

D. C. Harding and W. R. Witkowski

Sandia National Laboratories, Albuquerque New Mexico, United States of America

Introduction

The design of structures and engineering systems has always been an iterative process whose complexity was dependent upon the boundary conditions, constraints and available analytical tools. Transportation packaging design is no exception with structural, thermal and radiation shielding constraints based on regulatory hypothetical accident conditions. Transportation packaging design is often accomplished by a group of specialists, each designing a single component based on one or more simple criteria, pooling results with the group, evaluating the "pooled" design, and then reiterating the entire process until a satisfactory design is reached. The manual iterative methods used by the designer/analyst can be summarized in the following steps: design the part, analyze the part, interpret the analysis results, modify the part, and re-analyze the part. The inefficiency of this design practice and the frequently conservative result suggests the need for a more structured design methodology, which can simultaneously consider all of the design constraints.

Numerical optimization is a structured design methodology whose maturity in development has allowed it to become a primary design tool in many industries. These include automotive, aircraft, and aerospace, where the number of performance and safety constraints dictates state-of-the-art technologies and design tools. Numerical optimization, used as a design tool, is only a logical extension of increased use of advanced analytical tools and increased safety awareness by designers and the general public.

The purpose of this overview is twofold: first, to outline the theory and basic elements of numerical optimization; and second, to show how numerical optimization can be applied to the transportation packaging industry and used to increase efficiency and safety of radioactive and hazardous material transportation packages. A more extensive review of numerical optimization and its applications to radioactive material transportation package design was performed previously by the authors (Witkowski and Harding 1992). A proof-of-concept Type B package design is also presented as a simplified example of potential improvements achievable using numerical optimization in the design process.

Optimization Theory

Optimization is defined as the process, or methodology, of making something (such as a design, system, or decision) as fully perfect, functional, or effective as possible. In numerical optimization analyses, the requirements of an engineering design problem are mathematically formulated through the use of an objective function, design variables, and constraints. The objective function, or cost or merit function, is

* This work conducted at Sandia National Laboratories, supported by the U. S. Department of Energy under contract number DE-AC04-76DP00789.

the function to be minimized/maximized, such as weight, volume, or cost, by variation of a set of design variables. Design variables are quantities that define a particular design, such as diameter, thickness, material strength, etc. Constraints are limitations on the performance or behavior of the system, such as stress or strain limitations, size restrictions, etc., and on the design objective specifically.

The general concept of gradient-based optimization techniques consists of

1) selecting initial values of the design variables
2) determining the active constraints
3) calculating a search direction based on the objective function and the active constraints
4) determining how far to go in the search direction (via one-dimensional search)
5) checking convergence and whether or not a local or global minimum has been found
6) iterating back to 2) if necessary

Gradient-based numerical optimization techniques differ from exhaustive search, random search, and other optimization techniques in that gradient-based techniques attempt to select the "best" search direction to minimize the objective function quickly. Inherently, gradient-based techniques require fewer function evaluations, which are frequently the most expensive and time-consuming aspect of structural design. Implicit in the use of gradient-based optimization techniques is having continuous design variables, objective and constraint functions, and continuous function derivatives.

The simplest minimization problems are those whose form is explicitly defined. The first derivative of the objective function with respect to the design variables can be set to zero and solved exactly. Unfortunately, most engineering problems of interest can not be expressed in this form. Typically, numerical approximation schemes, such as finite element and finite difference methods, must be used to provide function evaluations and derivative approximations. These values are used to select search directions and distances. One of the most common and simplest search schemes is based on the negative gradient of the objective function, often referred to as the steepest descent technique.

The method in which the search directions and distances are selected distinguishes different optimization schemes from one another. One pitfall of gradient-based optimization problems is that the analyst must insure that the achieved optimum is a global minimum and not just a local minimum. For most problems, nothing short of running the problem at several initial points in the design space and comparing optimal solutions can verify that the solution is a global minimum.

Structural Analysis and Optimization

Structural optimization involves coupling structural analysis (for function and constraint evaluations) and optimization routines. Often this is not a trivial chore with existing codes that have set interfaces and modes of operation. Use of in-house finite element analysis (FEA) codes is desirable since modifications can be easily made to access information that may be inaccessible in commercial codes at a particular point in a calculation. This may make interfacing between the FEA and optimization codes more efficient.

Initial research in the area of structural optimization was exclusively focused on determining the optimal set of sizing variables, such as plate thicknesses, bar cross-sectional areas, moments of inertia, and composite laminate angles. Sizing variable optimization does not change the shape of the structure, only its geometric properties. Therefore, the topology of finite element models do not require updating since only the internal stiffness properties change. Many problems cannot be properly analyzed only with sizing variable optimization. For example, if the stress concentration in a cask body due to a seal test port is analyzed, only shape optimization allows for modification of the hole's shape. Current research

primarily deals with finding the optimal shape, or shape optimization. In shape optimization, geometries and surface contours are free to "flow", therefore, the finite element model must be periodically updated to incorporate changes in the geometry and element connectivity.

Since one of the goals of optimization is to automate the design process, automatic mesh generation is a necessity. Even with slight changes in the geometry, distortion of the element mesh can severely corrupt the model predictions. Adaptive generation techniques are being investigated at Sandia National Labs (SNL) to produce 2 and 3-dimensional quadrilateral and brick element meshes for complicated geometries which are automatically refined in high stress gradient areas to retain accuracy (Blacker, et al. 1990). An example of an automatically generated mesh, formed by translating and rotating 2-dimensional meshes, is shown in Figure 1 (Blacker, et al. 1991). Automated, adaptive mesh generation is a requisite technology for automated numerical shape optimization, which requires model updates as the shape evolves during the optimization process.

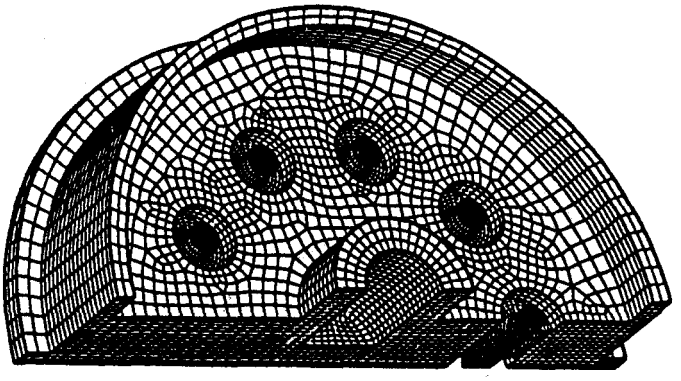

Figure 1. Three-dimensional mesh constructed by combining, translating and rotating two-dimensional meshes.

Current adaptive analysis research at SNL involves automatically re-meshing problems where the initial mesh becomes too distorted due to large deformations to complete a single analysis, such as occurs in the analysis of air transport packages. The algorithm takes the final deformed geometry before the analysis is halted, re-meshes the geometry, and restarts the analysis using the new meshed geometry. This capability allows large deformation calculations to run for much longer times.

After obtaining and/or developing the previously mentioned tools, i.e., an automatic mesher, structural and thermal analysis codes, and an optimization code, the actual numerical shape optimization process can be initiated. The initial and most important phase is to formulate the problem such that it is numerically tractable, yet still accurately represents the key characteristics that need to be modelled. If particular geometric regions are allowed to change, these areas must be represented using design variables. One approach to represent changing boundaries is to use polynomials to describe the boundaries and take the coefficients of the polynomials as the design variables. Only a small number of design variables are thus required to characterize the shape. Ideally, an accurate model using the smallest number of parameters and constraints should be posed to minimize the design space that the optimization routine must search.

The search algorithm involves individually perturbing each of the design variables by a small amount to see how the objective function value is affected. These data are referred to as sensitivity derivatives and are used to select new search directions. The calculation of these sensitivities requires many function evaluations and can be very costly, especially for detailed models with numerous design variables.

Therefore, approximate or reduced models are often used because they are less expensive to evaluate, assuming that a reliable approximate model can be developed.

The logic flow of the optimization process is shown in Figure 2. After the initial design has been defined,

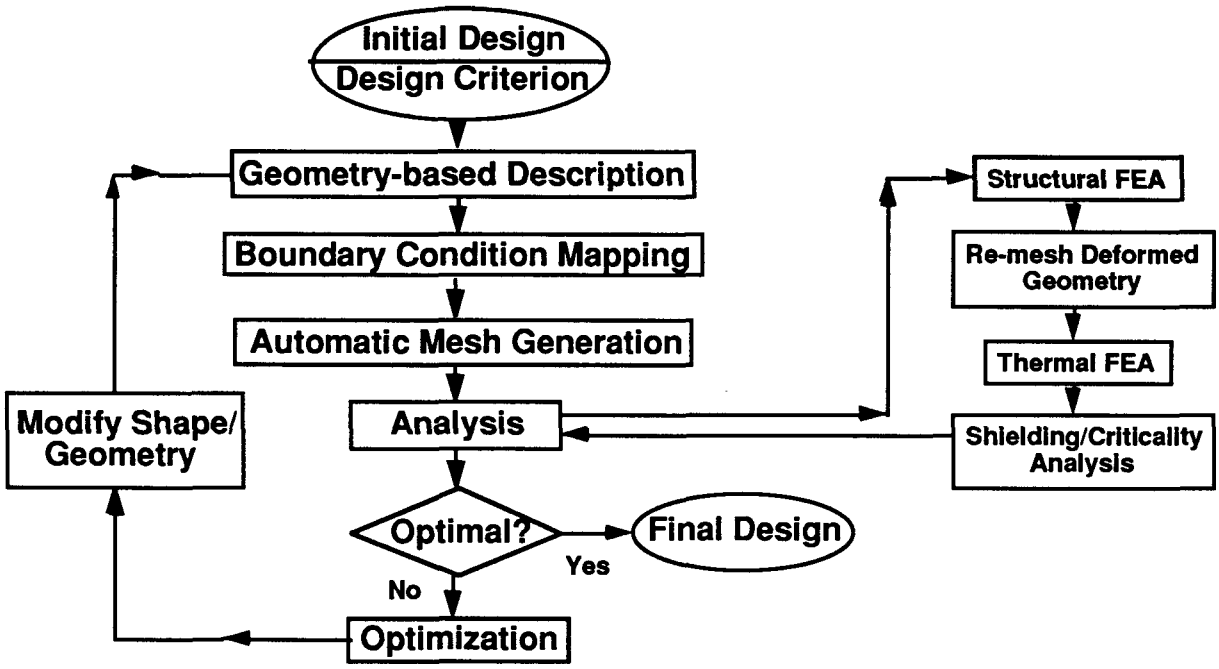

Figure 2. Flow chart for shape optimization analysis

constraints are evaluated to verify feasibility. Structural and thermal analyses, for example, would be required to determine whether containment constraints for radioactive material packagings were met after accident environments. If any of the constraints are violated or the objective function is not currently minimized, the optimization routine adjusts the design variables to find an improved solution. This involves calculating gradients and sensitivities of the objective function and constraints to the design variables. This information is used to select new search directions. Unfortunately, this step can be very costly since it involves several model, or constraint, evaluations and must be repeated whenever the design variables are changed. Note, that if a design variable is changed that affects the shape, a new finite element mesh must be generated to insure that an accurate model is available for further analysis. When a new set of "more-optimal" design variable values are determined the model must again be checked to see if the optimality tests are passed. This iterative loop is continued until the optimum is found, i.e., when the objective function value cannot be reduced any further and all of the constraints are satisfied.

Application of Numerical Optimization to the Transportation Cask Design Problem

A new generation of multipurpose radioactive material packagings will likely be needed in the United States in the near future and numerical optimization, as a design tool, could play a key role in developing more efficient and robust transportation packagings. Both sizing and shape optimization have the potential to make significant contributions in the design of new cask components, to be used in containers for on- and off- site transport and storage of radioactive, hazardous, and mixed hazardous wastes from civilian power generating reactors and the weapons complex.

Unfortunately, optimization analyses can be time consuming and expensive, thus, the use of this technology for a particular design problem must be warranted. It must also be highlighted that most shape optimization problems presented in the literature lack the complexity of the full cask design problem. A cask component design problem may be more cost effective than trying to optimize an entire packaging system design at once. Package components such as baskets, radiation shielding mechanisms, seal regions, closure mechanisms, cask bodies, access ports, lifting trunnions and rings, heat dissipating fins, skids, thermal shielding mechanisms, and impact limiters can be individually optimized with respect to active constraints. Parametric studies should elucidate component design sensitivities to the active constraints.

Once specific components are identified for optimization applicability, the proper objective function and constraints must be selected. Potential objective functions for cask design include: minimizing weight, cost, cask size, stress, or maximizing specific energy absorption, volume of contents, or a mixed weighted formulation of these functions. Constraints would include: resisting puncture and yielding during impact, remaining leak-tight after structural and thermal accident environments, shielding radioactivity and dissipating source-term heat, resisting internal/external pressure, and resisting water immersion and road vibration. Potential design variables which define the package geometry or shape and can be varied to meet the above constraints include, but are not limited to: linear dimensions (height, length, and width), wall thickness, surface shape (interior and exterior), and material properties, including composites. Material properties are usually considered discrete variables since only a limited number of material types are feasible for cask manufacturing. However, since optimization routines work much better with continuous variables, these parameters can be considered continuous and the best material is then selected after the analysis based on the "optimal" values.

A Type B package currently under development (Pierce, et al. 1992) serves to illustrate the different steps involved in sizing and shape optimization analysis and how this tool could be used to improve the transportation cask design process. The current package design consists of nested cylindrical containment vessels with elastomeric seals inside a composite overpack of metallic wire mesh and thermal insulation cloth for protection in an accident environment. The outer diameter and length of the containment vessel are 15.2 cm (6.0 in.) and 52.5 cm (20.7 in.), respectively. The outer diameter and length of the overpack are 45.7 cm (18.0 in.) and 98.9 cm (38.9 in.), respectively. The overpack consists of approximately 77 kg (170 lbm) of composite wire mesh material.

Package weight, defined as the sum of individual composite layer weights, is chosen as the objective function to be minimized. To minimize the number of design variables and keep the problem simple, thicknesses of three separate layers are chosen as the three design variables for the numerical optimization problem. X_1 is designated as the inner radial thermal blanket thickness, X_2 the middle wire mesh composite radial thickness, and X_3 the outer thermal blanket radial thickness, as shown in the cutaway in Figure 3. Thicknesses of these layers in the longitudinal directions are assumed to remain in the original ratios of the outer containment vessel and overpack diameters to lengths. Constraints include: 1) a minimum inner radius of 7.94 cm for the inner thermal blanket layer to accommodate the fixed-design containment vessels; 2) a minimum wire mesh composite layer thickness of 10 cm, an approximation of the minimum thickness to provide sufficient cushioning in a dynamic crush accident environment; 3) an internal radiative decay heat load of no greater than 20 Watts; and 4) a maximum inner surface temperature of 505 K (450 °F) to avoid heat degradation in the elastomeric seals. Shielding constraints are deemed negligible for the proposed contents.

A simplified one-dimensional axisymmetric (infinitely long cylinder) thermal model of the package is used to approximate the peak mid-plane inner surface temperature during the transient hypothetical fire accident condition. Previous two-dimensional P-Thermal (PDA Engineering 1991) transient conduction analyses indicated that peak inner temperatures occur at the mid-plane location. Emissivity/absorptivity

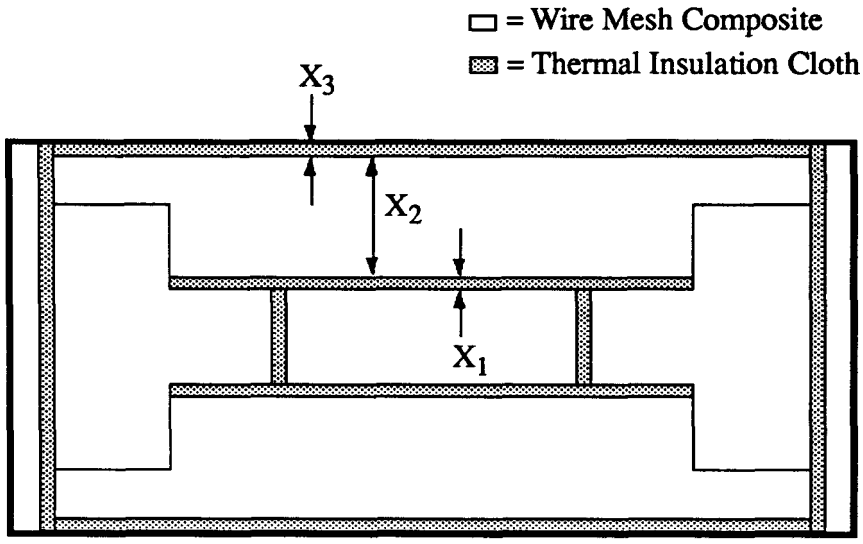

Figure 3 Cross section of wire mesh Type B example package with sizing design variables.

values of 0.9 and a convective heat transfer coefficient of 5 W/m^2K were assumed during the 30 minute 1075 K (1475 °F) fire and indefinite 311 K (100 °F) cool-down period. The model uses explicit finite difference methods to approximate the governing partial differential equation in cylindrical coordinates with 32 internal nodes. Temperature-variant material (thermal) properties are updated at each time step and peak internal surface temperatures are recorded over a three hour time period encompassing fire and cool-down periods. The time step was chosen as 0.03 seconds based upon numerical stability and accuracy criteria for the analysis technique.

Numerical optimization of the package design was accomplished in 27 iterations with ADS (Vanderplaats 1985), an optimization code using the Method of Feasible Directions for constrained minimization. The initial feasible design point was X_1=3 cm, X_2=20 cm, and X_3=5 cm. 106 function and constraint evaluations were performed automatically during the optimization process for gradient and search length calculations. The minimum package overpack weight (mass, actually) design, as determined by the numerical optimization code, was X_1=0.13 cm, X_2=12.7 cm, and X_3=0.13 cm, yielding an overpack mass of 49 kg, 36 percent less than the initial overpack mass of 77 kg. The three-dimensional plots of overpack mass and peak transient inner seal temperature as functions of X_2 and X_3 (with X_1 held constant at 0.13) shown in Figure 4 aid in visualizing the sensitivities of these parameters to the design variables and verify the optimal result. Although the overpack mass or weight can be reduced below the asterisked point in Figure 4, doing so increases the peak seal temperature thereby violating its maximum operating temperature constraint. Numerical verification that the optimal result is a global minimum was accomplished by starting at various feasible design points and arriving at the same minimum. Accuracy of the simplified model's inner surface or seal temperature at the optimum design point was verified using P-Thermal to solve a two-dimensional finite difference approximation of the same geometry and time dependent boundary conditions.

The optimal overpack design reduces overpack weight by over 35 percent from the original single composite layer design. Further reductions would be expected with a more accurate definition of the minimum wire mesh layer thickness for energy absorption. These results are meant only as an example of the potential weight savings to be gained since they were derived using relatively simple approximations of the actual design constraints. Also, if cost were the objective function to be

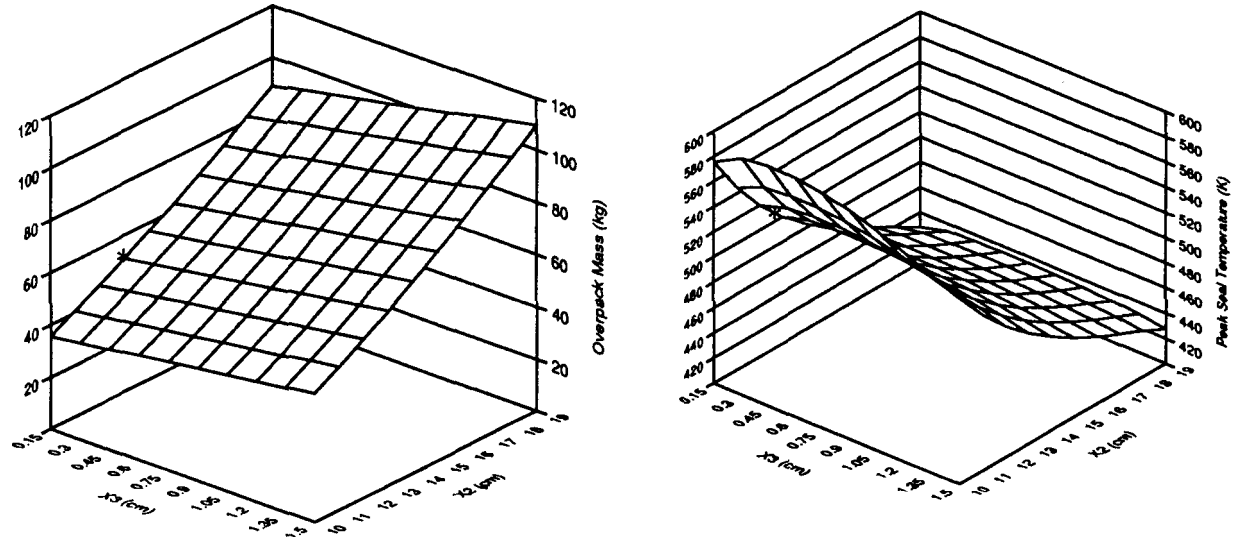

Figure 4 Package overpack mass and peak seal temperature as functions of design variables X_2 and X_3. The optimal design is X_1=0.13 cm, X_2=12.7 cm, X_3=0.13 cm, and is denoted by an asterisk (*).

minimized, the optimal result would likely be much closer to the original Type B package design without the thermal insulating cloth layers since these are relatively expensive on a per weight basis compared to the wire mesh composite material. However, the significant reduction in package weight without violation of the constraints suggests that improved transportation packaging designs are achievable through the use of numerical optimization.

Summary

Numerical optimization has proven to be successful in obtaining optimal designs in a more efficient and structured manner in many industries. Optimization of sizing variables is already a widely used design tool and even though shape optimization is still an active research topic, significant successes have been shown for many structural design problems. Coupled structural, thermal, and radiation design constraints make numerical optimization highly amenable to the efficient solution of the cask design problem. Current state-of-the-art technology at Sandia National Labs in the areas of structural mechanics, thermal mechanics, numerical analysis, adaptive finite element analysis, automatic mesh generation, and transportation cask design can enhance current industry-standard cask design and analysis techniques through numerical optimization. The complexity of transportation cask design problem with its numerous coupled constraints, however, cannot be over-emphasized. The automation of this design problem through numerical optimization requires integration of finite element analyses for thermal and structural evaluations, as well as codes for shielding and criticality. Numerous transportation-related constraints for system operations such as remote handling can be added as well. Development of this "black box" numerical design optimization tool has the potential to provide greater uniformity and cost effectiveness in package design through advanced, integrated analytical techniques.

References

Blacker, T. D., J. Jung and W. R. Witkowski, "An Adaptive Finite Element Technique Using Element Equilibrium and Paving," ASME Winter Meeting (1990).

Blacker, T. D., Stephenson, M. B., and Canann, S., "Analysis Automation With Paving: A New Quadrilateral Meshing Technique," Advances in Engineering Software and Workstations, Vol. 13, No. 5-6, pp. 332-337 (1991).

P/THERMAL User Manual, Release 2.5, PDA Engineering, PATRAN Division, Costa Mesa California (1991).

Pierce, J. D., McClure, J. D., Hohnstreiter, G. F., and Golliher, K. G., "Type B Plutonium Transport Package Development That Uses Metallic Filaments and Composite Materials," Paper for presentation in PATRAM '92 (1992).

Vanderplaats, G. N., "ADS--A FORTRAN Program for Automated Design Synthesis," Version 1.10 (1985).

Witkowski, W. R., and Harding, D. C., "Numerical Optimization Schemes for the Design of Transportation Packages," SAND91-2632 (1992).

Development and Evaluation of Measurement Devices Used to Support Testing of Radioactive Material Transportation Packages*

W. L. Uncapher, D. J. Ammerman, D. R. Stenberg, D. R. Bronowski, M. Arviso

Sandia National Laboratories,** Albuquerque, NM, United States of America

INTRODUCTION

Radioactive material package designers use structural testing to verify and demonstrate package performance. A major part of evaluating structural response is the collection of instrumentation measurement data. Sandia National Laboratories (SNL) has an ongoing program to develop and evaluate measurement devices to support testing of radioactive material packages. Measurement devices developed in support of this activity include evaluation channels, ruggedly constructed linear variable differential transformers, and piezoresistive accelerometers with enhanced measurement capabilities. In addition to developing measurement devices, a method has been derived to evaluate accelerometers and strain gages for measurement repeatability, ruggedness, and manufacturers' calibration data under both laboratory and field conditions. The developed measurement devices and evaluation technique will be discussed and the results of the evaluation will be presented.

EVALUATION CHANNELS

Foil-type resistance strain gages and piezoresistive accelerometers are common measurement devices used in radioactive material package testing. Strain gages are used to measure surface strain at the mounted location and accelerometers are used to measure deceleration of the package or specific components. In most cases, the measurement device and associated data acquisition equipment are characterized by either the manufacturer or the organization performing the testing. The measurement system includes the measurement device, data collection system, and any interconnecting cables. The effects of the interconnecting cables, as well as other external influences and their contribution to the measurement, are not generally well defined. Evaluation channels are measurement devices that can be mounted on the package and subjected to the same environments as active measurement devices. The purpose of the evaluation channels is to determine the magnitude of signal contributors caused by factors other than strain or acceleration. A fixed resistance simulating either an accelerometer or strain gage is desirable. This fixed resistance should indicate only nonstrain or acceleration-induced resistance changes from external effects. Since strain gages are usually used in conjunction with accelerometers, the evaluation channels were sized for mounting similar to a commonly used accelerometer. Evaluation channels representing both piezoresistive accelerometers and 350 ohm strain gages have been developed by SNL and are commercially available. The evaluation device (Figure 1) is located in a case (body) made from 17-4 PH stainless steel. The body is 15 mm (0.6 in.) by 7 mm (0.3 in.) by 2 mm (0.1 in.) thick. A cavity

*This work performed at Sandia National Laboratories, Albuquerque, New Mexico, supported by the United States Department of Energy under contract DE-AC04-76DP00089.

**A United States Department of Energy Facility.

is machined in the body to accept thick-film chip resistors matching the characteristics of an accelerometer or a strain gage. Cables are attached and routed through the case, and the body cavity is encapsulated to fix the position of the resistors. Two holes that accept 2.8 mm (0.11 in.) diameter screws are provided for mounting. Shock calibration performed on these devices indicated no apparent resistance change to shock levels as high as 15,000 g.

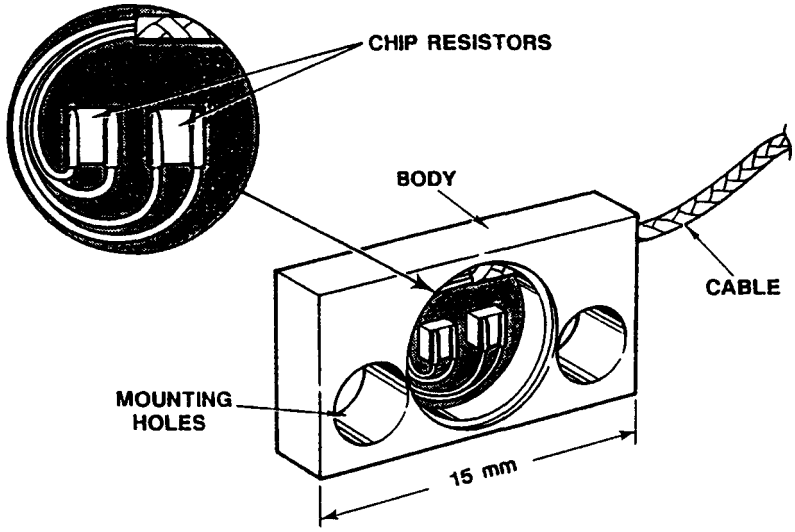

Figure 1. Diagram of an Evaluation Device

These accelerometer and strain gage evaluation channels provide a means of estimating the contribution of external factors in resistive-type measurement data. A comparison of these data to active measuring accelerometers or strain gages will determine the magnitude of possible unwanted contributors. Estimates of strain gage uncertainty based on test severity and gage installer expertise can range from 7% to 30% (Window and Holister 1982). By characterizing the contribution of nonstrain- or acceleration-induced effects, confidence in the data can be increased by demonstrating, using evaluation channels, that the external contribution levels are not a significant part of the measurement data. The evaluation channels provide a meaningful way of determining the magnitude of nonmeasurement-induced effects in dynamic data obtained during radioactive material package testing.

LINEAR VARIABLE DIFFERENTIAL TRANSFORMERS

A linear variable differential transformer (LVDT) is another measurement device used to collect data from radioactive material package testing. The device is used to measure small, single axis displacements, such as the distance change between a closure seal area and cask body, during dynamic testing. Conventional LVDTs are available from several manufacturers for low-shock and slow-displacement rate applications. In order to meet the need for a rugged measurement device suitable for high-shock dynamic displacement measurements, SNL, in conjunction with private industry, has developed a ruggedly constructed LVDT. The LVDT (Figure 2) consists of three major components. The 12.7 mm (0.5 in.) diameter threaded body-tube assembly contains electrical coils. A 2.5 mm (0.10 in.) diameter core is attached to a 1.5 mm (0.06 in.) diameter threaded rod that is allowed to move axially inside the body. As the core assembly is moved within the body, the voltage output changes in proportion to the position of the core. Displacements as small as 0.02 mm (0.001 in.) can be easily resolved. The nominal sensitivity of the LVDT is approximately 0.1 V/0.02 mm (0.001 in.). The device is designed to have a measurement range of ±1.27 mm (0.05 in.) and produces ±5 V at maximum range with linearity of approximately 0.5%. The input and output circuits are electrically isolated from each other and from the body, allowing either electrical floating or grounding of the device. The operating temperature for the LVDT ranges from -45°C (-50°F)

to 122°C (250°F). The 25 mm (1.0 in.) long threaded housing was designed for easy installation and positive contact with the mounting surface. Conventional machining techniques are employed to mount these devices using American standard threads. This type of LVDT has been shock tested at amplitudes exceeding 1000 g (Madsen et al. 1987). The ruggedly constructed LVDTs can be used to characterize displacement changes at sealing surface to cask body interfaces during dynamic testing. These LVDTs provide a useful measurement tool in a small, rugged, and inexpensive package.

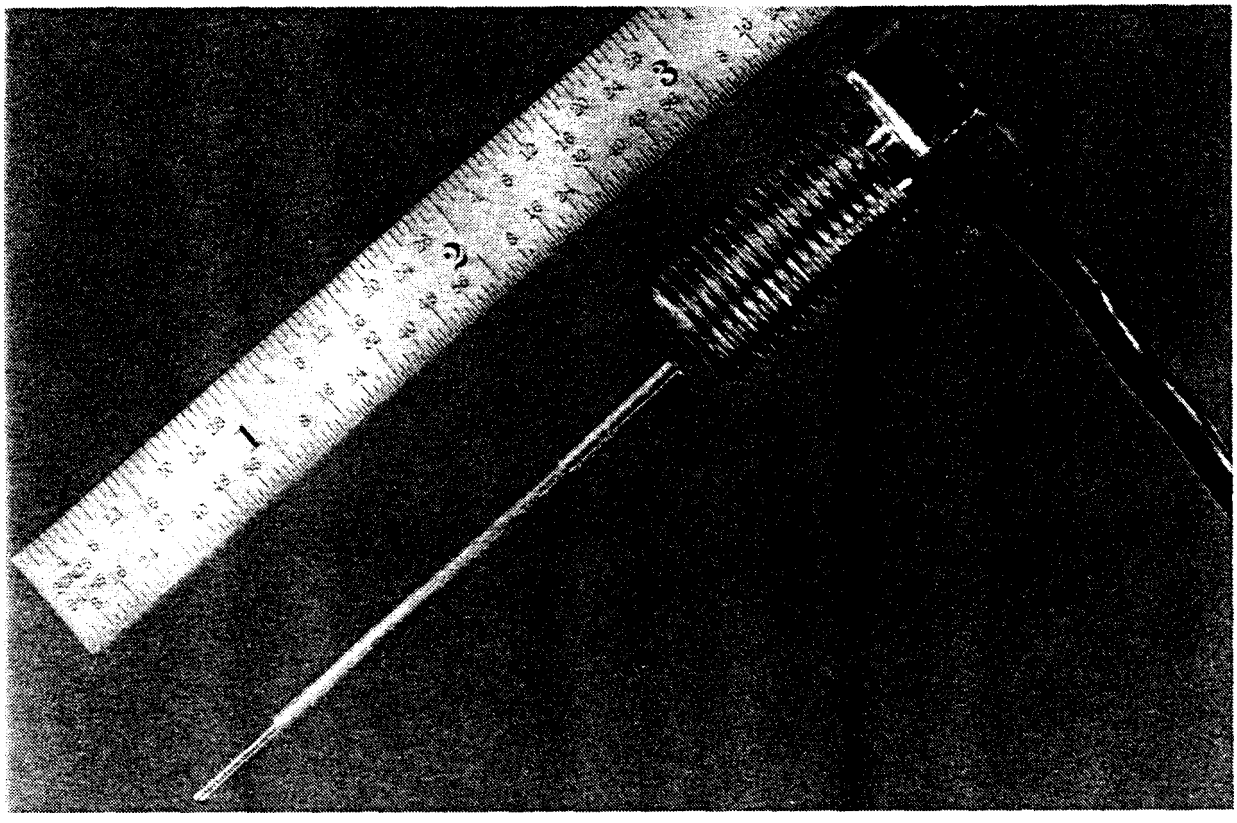

Figure 2. Ruggedly Constructed LVDT

PIEZORESISTIVE ACCELEROMETER

Piezoresistive accelerometers are commonly used in determining the structural response of radioactive material packages. In a piezoresistive accelerometer, the interrogating input is voltage. The output is a voltage which is proportional to acceleration. Piezoresistive accelerometers are essentially single-degree-of-freedom devices and are usually developed based on a cantilever beam principal. Impact testing of radioactive material packages may produce rapid acceleration rise-time response. This response can excite resonant frequencies in the accelerometer and possibly cause loss of data or permanent damage. To overcome the possibility of damage to the accelerometer, viscous damping may be used to reduce the frequency response of the accelerometer. The usable temperature range of viscous-damped accelerometers may not meet the requirements of the experiment. In most cases, the accelerometer selected should optimize the measurement output for the specific application. A compromise has been made in the past of selecting a measurement device with the proper range, frequency response, and output. In response to the need for an optimal piezoresistive accelerometer, SNL, in conjunction with private industry, has developed a pair of rugged, undamped piezoresistive accelerometers with integral hybrid microelectronics applicable for high-shock measurements. The accelerometers are available in either 2000 g or 20,000 g

acceleration ranges. A monolithic sensing element is sculpted from a single chip of silicon which provides high-resonant frequency response. The nominal resonant frequency is 120 kHz for the 2000 g units and 400 kHz for the 20,000 g units. The accelerometers require a standard 10-volt excitation and produce ±2 volts output at full scale. The package (Figure 3) is also epoxy sealed for moisture protection. The accelerometers have an operating temperature range from -34°C (-30°F) to 66°C (150°F). The accelerometer linear frequency response extends to 30 kHz with an internally mounted 2-pole butterworth low pass filter. The accelerometer housing is 12.7 mm (0.5 in.) by 6.4 mm (0.25 in.) and mounts using an integral mounting stud. The nominal sensitivity (output voltage per unit acceleration) ranges from 1 mv/g for the 2000 g units to 0.1 mv/g for the 20,000 g units. Development testing on these accelerometers shows advantages in using the increased output voltage to provide better signal to noise ratios in acquired data, as well as to reduce the possibility of resonating, which may damage the accelerometers due to a rapidly rising acceleration pulse.

Figure 3. Rugged, Undamped Piezoresistive Accelerometer

ACCELEROMETER AND STRAIN GAGE EVALUATION METHOD

In conjunction with instrumentation measurement device development, a method has been derived to compare results from selected accelerometers and strain gages in both laboratory and field environments (Ammerman et al. 1991). Two types of accelerometers and strain gages were selected and evaluated. The evaluation is based on the results of tests conducted to measure ruggedness, failure frequency, repeatability, and manufacturer's calibration data. The accelerometers selected for this evaluation were Endevco 7270 series piezoresistive and Bruel and Kjaer (B&K) 8309 piezoelectric devices. The strain gages selected were manufactured by Micro-Measurement and BLH. The accelerometers were evaluated using calibration, shock, and end-impact testing. The strain gages were evaluated using static loading and impact testing. The range of evaluations provided well-characterized laboratory tests for both the accelerometers and the strain gages. The end-impact tests were used since they closely model

the environment measurement devices encounter during testing of radioactive material packages. Multiple tests of each type were performed to determine the repeatability of the results.

The sensitivity, amplitude linearity, and frequency response of the accelerometers were determined using factory and SNL calibration. Three types of calibration were performed on the Endevco 7270 accelerometers at SNL: shock, centrifuge, and frequency response. The B&K accelerometers were calibrated using shock and frequency response methods. The nature of piezoelectric accelerometers precludes the use of centrifuge calibration techniques. The frequency response calibration was performed at room temperature and -29°C (-20°F). Three separate sets of accelerometers of each type were calibrated and compared to manufacturers' supplied data. The results of the calibration tests showed good agreement between the calibration techniques. The standard deviation of the sensitivities determined from all calibrations performed on any specific accelerometer was less than 3% of the average sensitivity.

Shock testing was performed on the accelerometers at levels representing package impact conditions. The evaluation consisted of a series of shocks applied to each of the three sets of accelerometers. Accelerometers were mounted to a fixture (Figure 4) which was attached to a vertical shock frame. The fixture was shocked at each of three levels: 1000, 5000, and 10,000 g. These acceleration levels were chosen to characterize the accelerometers in a range that envelops the response experienced in typical package tests. Each level was repeated three times for a total of nine shocks per accelerometer set. The data from the three sets of accelerometers were normalized with respect to a reference accelerometer mounted on the fixture. Figure 5 shows the distribution of the normalized peak accelerations for all shock tests. The standard deviation of the peak accelerations for the normalized shock testing was 3.4% of the average value.

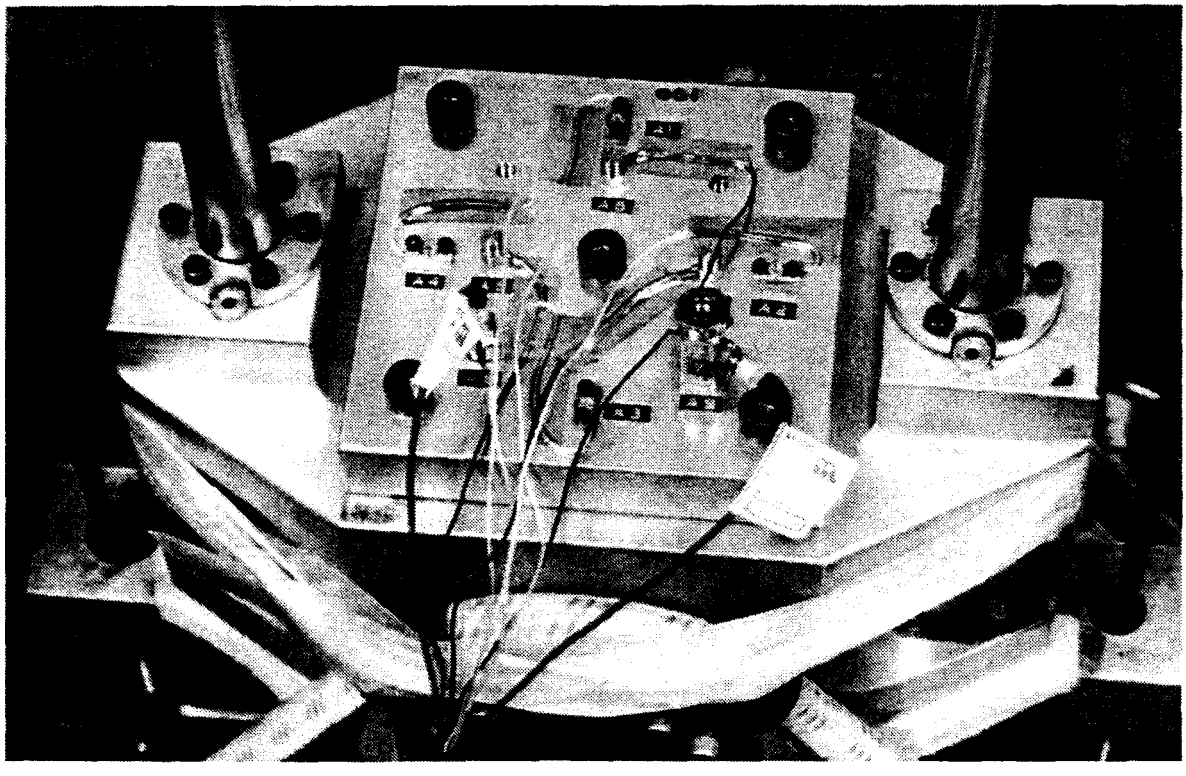

Figure 4. Mounting Fixture and Accelerometers for Shock Tests

Strain gages were initially evaluated by a series of static crush tests. Ten tests were performed on individual aluminum cylinder test units. Twelve biaxial strain gages from the two manufacturers were installed to measure strains in the axial and hoop directions. The instrumented test units were placed in a compression test machine and loaded. The load was cycled four times to 188 kN (40,000 lb), which is at approximately 70% of the elastic limit of the material. Data were collected on the response of the strain gages. For these tests, the strain gages exhibited similar behavior. Figures 6 and 7 show the distributions of maximum axial strain and maximum hoop strain from the first and fourth cycles of the elastic test. The average peak strain for the axial gages in the first cycle was 310 x 10^{-6} m/m (microstrain), with a standard deviation of 33 microstrain, and the average peak strain on the fourth cycle was 302 microstrain with a standard deviation of 29 microstrain. These values compare well with the theoretically calculated strain value of 308 microstrain. In the hoop direction, the average peak strain for the first cycle was 102 microstrain, with a standard deviation of 13 microstrain, and the average for the fourth cycle was 99 microstrain, with a standard deviation of 8 microstrain. The test results show that even in a well-characterized test, there was some scatter in the data. The standard deviation of the strain gage measurements was approximately 10% of the average value. The strain gages exhibited little hysteresis during the four load cycles.

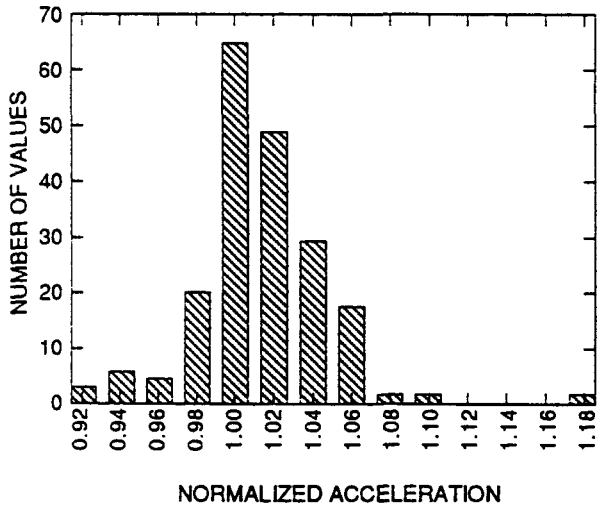

Figure 5. Distribution of Normalized Accelerations from Shock Tests

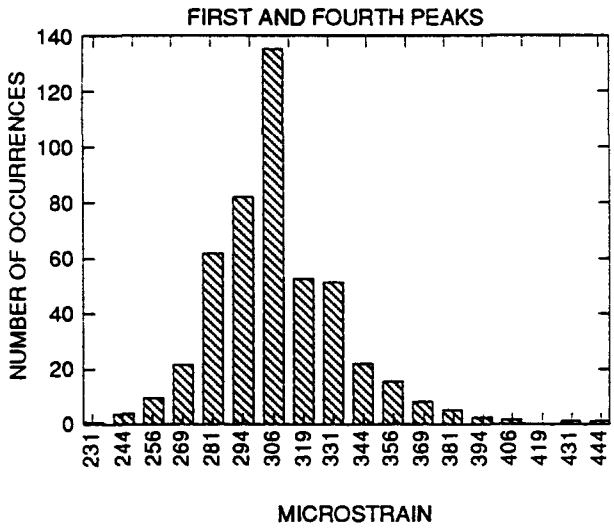

Figure 6. Elastic Axial Strain Distribution from Static Crush Tests

After the load cycle test, each test unit was loaded through the elastic range to a strain approaching 2%. Strain, load, and displacement data were recorded. Loading was applied up to 623 kN (140,000 lb) with a corresponding deflection of approximately 12.7 mm (0.5 in.). The average axial strain from the Micro-Measurement gages was 17,103 microstrain with a standard deviation of 1198 microstrain and the average permanent strain calculated from the change in gage resistance was 17,186 microstrain with a deviation of 1147 microstrain. The average axial strain from the BLH gages was 17,613 microstrain, with a standard deviation of 1500 microstrain and the average calculated permanent strain was 17,494 microstrain with a standard deviation of 1537 microstrain. The distribution of measured plastic strains from all of the gages is shown in Figure 8. Measured permanent strain from the two types of gages was within one standard deviation (7%) of the calculated results determined from post-test dimensional inspection.

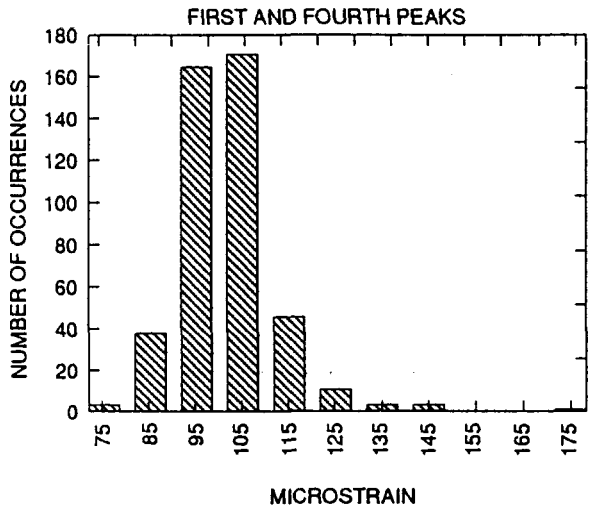

Figure 7. Elastic Hoop Strain Distribution from Static Crush Tests

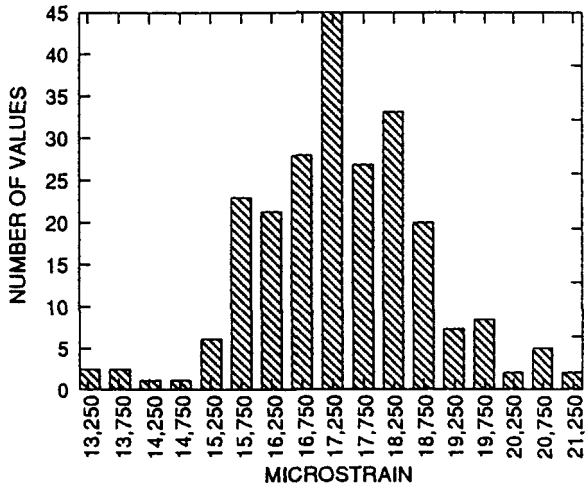

Figure 8. Plastic Axial Strain Distribution from Static Crush Tests

To evaluate the accelerometers and strain gages in an environment similar to package testing, a series of ten impact tests was performed. The structural code benchmark test unit (Glass 1989), shown in Figure 9, was selected to provide an economical vehicle that produces varying strain levels and accelerations with rapid amplitude changes. The test units were instrumented with four Micro-Measurements biaxial strain gages and two uniaxial strain gages. Four BLH biaxial strain gages and two uniaxial strain gages were also installed. The test cylinder was also instrumented with four Endevco accelerometers and three B&K accelerometers. The instrumented test units (Figure 9) were impacted at velocities of 13.4 m/s (44 ft/s) onto an unyielding steel target. The accelerometer data were filtered at 1000 Hz to best represent the rigid body response of the test unit. The filtered peak acceleration data had a standard deviation of 15% from their average value.

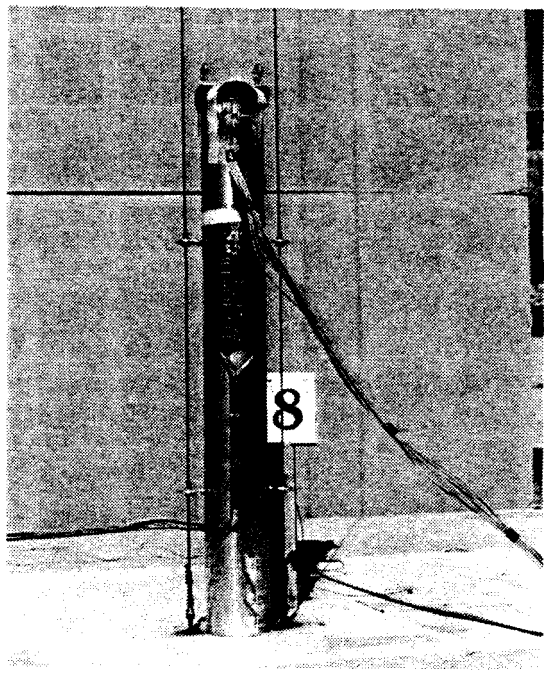

Figure 9. Structural Code Benchmark Test Unit Used for Impact Tests

CONCLUSION

Measurement devices have been developed to support specific testing applications associated with radioactive material packages. These measurement devices include evaluation channels, ruggedly constructed LVDTs, and piezoresistive accelerometers. In addition, a method was developed to evaluate accelerometers and strain gages in both laboratory and field environments. The results of this evaluation showed no major difference in the measurements obtained by transducers manufactured by different companies. Table 1 gives a summary of the results from the accelerometer and strain gage evaluations. These results showed that test data were not, in general, more accurate than ±10% of the measured result. It is very likely that the majority of these deviations are due to changes in the quantities being measured, rather than transducer response. This is because the transducer only measures the response at the mounting location, which may not be the same as the response at a nearby location.

Table 1. Results of the Accelerometer and Strain Gage Evaluations

Test Sequence	Measure	Mean	σ	%
Shock	Normalized Acceleration	1.01	0.034	3.40
Static Crush	Permanent Axial Strain	17,354 με	1,379 με	7.95
End Impact	Peak 1,000 Hz Filtered Acceleration	2,454 g	360 g	14.7

REFERENCES

Ammerman, D. J., Madsen, M. M., Uncapher, W. L., Stenberg, D. R., and Bronowski, D. R., *Acceleratometer and Strain Gage Evaluation*, SAND91-0077, Sandia National Laboratories, Albuquerque, NM, 1991.

Glass, R. E., *Structural Code Benchmarking Data Report*, SAND88-3362, Sandia National Laboratories, Albuquerque, NM, 1989.

Madsen, M. M., Uncapher, W. L., Stenberg, D. R., and Baynes, E. E., *Testing the Half-Scale Model of the Defense High Level Waste Transportation Cask*, SAND86-1130, Sandia National Laboratories, Albuquerque, NM, 1987.

Window, A. L. and Holister, G. S., Strain Gage Technology, Chapter 5, *Errors and Uncertainties in Strain Measurements*, Elsevier Science Publishing Co., Inc., New York, NY, 1982.

Transportation Accidents/Incidents Involving Radioactive Materials (1971-1991)*

C. E. Cashwell[1] *and J. D. McClure*[2]

[1]Applied Physics, Inc., Albuquerque, New Mexico, United States of America

[2]Sandia National Laboratories,** Albuquerque, New Mexico, United States of America

INTRODUCTION

The Radioactive Materials Incident Report (RMIR) database contains information on transportation-related accidents and incidents involving radioactive materials that have occurred in the United States. The RMIR was developed at Sandia National Laboratories (SNL) to support its research and development program efforts for the U.S. Department of Energy (DOE).

This paper will address the following topics: background information on the regulations and process for reporting a hazardous materials transportation incident, overview data of radioactive materials transportation accidents and incidents, and additional information and summary data on how packagings have performed in accident conditions.

REPORTING REQUIREMENTS FOR TRANSPORTATION INCIDENTS INVOLVING RADIOACTIVE MATERIALS

The two federal agencies with primary responsibility for developing and promulgating regulations for the transport of radioactive materials in the United States are the U.S. Department of Transportation (DOT) and the U.S. Nuclear Regulatory Commission (NRC). The reporting requirements for these two agencies differ. The DOT regulations for reporting a hazardous materials incident (of which radioactive material is a subset) are specified in the Code of Federal Regulations (49 CFR 171.15). The DOT requires that a report be filed after each incident that occurs during the course of radioactive materials transportation (including loading, unloading, handling, and temporary storage) in which one of the following directly results: (1) a person dies; (2) a person is injured and requires hospitalization; (3) estimated carrier or other property damage exceeds $50,000; (4) fire, breakage, spillage, or suspected contamination involving radioactive materials; or (5) a situation that the carrier believes should be reported. The NRC regulations are also outlined in the Code of Federal Regulations (10 CFR 20.402 and 20.403) and require that the theft or loss of radioactive materials, exposure to radiation, or release of radioactive materials be reported.

*This work performed at Sandia National Laboratories, Albuquerque, New Mexico, supported by the United States Department of Energy under Contract No. DE-AC04-76DP00789.

**A United States Department of Energy facility.

In addition to the reports received from the DOT and NRC, the RMIR contains data obtained from state radiation control offices, the DOE Unusual Occurrence Report database, and media coverage of radioactive materials transportation incidents.

ANALYSIS OF U.S. RADIOACTIVE MATERIALS TRANSPORTATION ACCIDENT/INCIDENT DATA

To evaluate the history of transporting radioactive materials, it is helpful to obtain a perspective by viewing the hazardous materials shipment record. According to the Final Environmental Statement on the Transportation of Radioactive Material by Air and Other Modes (1977), it is estimated that during a given year, approximately 500 billion packages of all commodities are transported by all modes throughout the United States. Of those 500 billion packages, approximately 100 million packages are classified as hazardous materials (flammables, explosives, poisons, and radioactive materials). The most recent study of the transport of radioactive materials (Javitz, et al., 1985) indicates that approximately 2 million shipments of radioactive materials are made each year which constitutes about 2.79 million packages. Thus, radioactive materials are only 2% of the total number of hazardous materials transported each year.

When the RMIR database was established in 1981, it was designed primarily to accommodate the information on the DOT Form 5800 (Hazardous Materials Incident Report) for the recording of transportation accidents and incidents. The RMIR makes a definite distinction between an accident and a reported incident. The three kinds of reported events classified in the RMIR are defined as follows:

> **Transportation Accident:** A transportation accident is any accident that involves the vehicle which is transporting radioactive material.
>
> **Handling Accident:** Damage to a shipping container during loading, handling, or unloading operations; e.g., a forklift puncturing a package at an air terminal.
>
> **Reported Incident:** This is a very broad term which includes transportation occurrences where there is an actual or suspected release or surface contamination of radioactive materials exceeding the regulatory requirements from either the package or transport vehicle.

Table 1 tabulates the transportation accidents, handling, accidents and incidents that have occurred for the 21-year time frame of 1971 through 1991. Accidents comprise 22% of the events compiled for the United States; a slight increase over the 19% tabulated for the period 1971-1988. This percentage increase is the result of two factors: (1) the inclusion in the database of accidents that occurred in 1991 and (2) the accident information for prior years from contact with state radiation control offices. Further, 61% of all transportation occurrences tabulated in Table 1 are classified as reported transportation incidents.

TABLE 1

U.S. RADIOACTIVE MATERIALS TRANSPORTATION EVENTS (1971-1991)

Transportation Accidents	329
Handling Accidents	253
Transportation Incidents	924
TOTAL	1506

Most radioactive materials are transported on the highway; these shipments generally include industrial gauges, radioactive material used in or as a result of the nuclear fuel cycle, low-level radioactive materials or waste, and teletherapy sources. Radioactive materials that are shipped by air are generally isotopes with short half-lives that are being shipped over 500 miles from the shipper's location. Upon arrival at an airport, these radioisotopes are generally delivered to their consignees by a courier service. Radioactive materials transported by modes other than aircraft are usually those that do not require immediate delivery. Most radioactive materials traveling by highway are those involving industrial gauges, radioactive material used in or as a result of the nuclear fuel cycle, low-level radioactive materials or waste, and teletherapy sources.

Table 2 shows the RMIR breakdown for accidents, incidents, and handling accidents by transportation mode. As Table 2 illustrates, radioactive material packages transported on highways account for about 79% of all the incidents that have occurred and 88% of all accidents. Over one-half (54%) of all handling accidents recorded in the RMIR database have occurred with low-level materials at air terminals. Most of these handling accidents occurred during loading and unloading operations.

TABLE 2

TRANSPORTATION ACCIDENTS/INCIDENTS BY MODE (1971-1991)

Mode	Accidents	Incidents	Handling Accidents	Total
Air	18	150	137	305
Courier	2	4	2	8
Freight Forwarder	0	12	5	17
Highway	288	731	100	1119
Rail	20	14	2	36
Warehouse	0	3	1	4
Water	1	5	4	10
Other, unidentified	0	5	2	7
TOTALS	329	924	253	1506

PACKAGING PERFORMANCE IN TRANSPORTATION ACCIDENTS

Generally, an accident condition will be the most severe occurrence that a package will be subjected to during the course of transportation. Between the years 1971 and 1991, 3506 radioactive material packages, as documented in Table 3, were involved in transportation accidents. Of that total, only 223 (6%) were classified as having been damaged with no loss of contents or failed (package damaged with loss of radioactive contents). Industrial packages, or those that are classified as strong and tight, have been involved in 44 accidents. Of the 1342 strong and tight packages involved in those accidents, only 18 were damaged without loss of contents and 65 were damaged to the extent that they sustained loss of contents. These industrial packages are designed to withstand normal transport conditions; they are not designed nor tested to withstand accident conditions. Type A packages accounted for the majority (62%) of the package damages/failures in accident conditions. However, like industrial packages, Type A packagings are designed and tested for the rigors of normal transport conditions, not accidents.

TABLE 3

PACKAGE BEHAVIOR DURING TRANSPORTATION ACCIDENTS
(1971-1991)

Package Category	No. of Accidents	No. of Packages in Accidents	No. of Packages Damaged	No. of Packages Failed
Industrial (Strong & Tight)	44	1342	18	65
Type A	175	2079	83	55
Type B	53	85	2	0
Accidents with package category unknown[1]	62			
	334			
Accidents with 2 package types	- 5			
	329	3506	103	120

[1]These are mainly accidents that occurred in 1970's and early 1980's. Every attempt is being made to determine the package category type.

Most of the industrial and Type A packages included in the columns labeled "Damaged" and "Failed" in Table 3 were packages that were damaged without a loss of contents. For packages classified as being strong and tight, only 4.8% of those packages that were involved in accidents sustained a release. Only 2% of the Type A packages involved in accidents were damaged to the extent that there was a release, and in most of those accidents, the release was minor.

The most notable transportation accident that has occurred in the United States over the last 3 years involved the shipment of 12 containers, each of which contained 2 unirradiated nuclear fuel assemblies destined for the Vermont Yankee Nuclear Power Plant. The accident occurred on December 16, 1991, at 3:15 a.m. on Interstate 91 in downtown Springfield, Massachusetts. A car was traveling on the wrong side of the interstate, and although the truck driver swerved to avoid a collision, the car struck the tractor-trailer on the right side near the right fuel tank. The truck continued northbound and hit the center guardrail then rebounded and continued northbound striking the curb and guardrail on the opposite side of the road. After striking the outside guardrail, the truck skidded across the highway and came to rest against the center guardrail.

A fire started in the engine compartment of the tractor and spread to the entire tractor and then the trailer. The NRC's report on the accident (Carlson and Fischer, 1992) indicated that the fire burned for at least three-quarters of an hour before the cargo was affected. At that time, the entire payload was entirely intact. However, since the fire was not extinguished, the flatbed trailer and the payload also burned. The entire fire lasted approximately 3 hours.

The tractor-trailer was completely destroyed by the fire and there was significant damage to several of the Type A containers and their contents. Eight containers fell off the trailer and sustained minor damage from the impact. The wooden outer containers were burned and the inner metal containers sustained damage ranging from minor to severe.

Table 4 provides a tabulation of the 53 accidents involving Type B packages. Of these accidents, seven involved spent nuclear fuel (three of them occurred during rail transport and four occurred on the highway). There has been only one spent nuclear fuel accident which resulted in more than trivial damage to the cask. This accident, which is probably the most well known nuclear transportation accident, occurred on December 8, 1971, on U.S. 25 in Tennessee. The cask was thrown from the trailer and was embedded in the ground. The radiation surveys taken at the accident scene indicated that the structural integrity of the cask was intact and there was no release of contents. Almost one-half of the other accidents involving Type B packages have involved Iridium-192 sources.

TABLE 4

SUMMARY OF ACCIDENTS INVOLVING TYPE B PACKAGES (1971-1991)

Date of Accident	Mode	Package Description	RAM Involved	Packages Shipped/ Damaged	Accident Conditions
07/10/71	Highway	Lead container	Co-60	1/0	Collision
12/05/71	Highway	Radiography camera	Ir-192	1/0	Truck left road and overturned
12/08/71	Highway	Cask, spent fuel	Spent fuel	1/1	Truck left road; cask thrown off
03/10/74	Highway	Container	Ir-192	1/0	Trailer involved
03/29/74	Rail	Cask, spent fuel	Spent fuel	1/0	Derailment
08/09/75	Highway	Cask	U-235, U-238, Pu-239	1/0	Trailer ran off road & overturned
05/06/77	Highway	Radiography camera	Ir-192	1/0	Collision
08/11/77	Highway	Radiography camera	Ir-192	1/0	Collision with gas truck
08/25/77	Rail	Cylinders	UF6	4/0	Derailment
10/03/77	Highway	Radiography source	Ir-192	1/0	1 vehicle accident
02/09/78	Highway	Cask, spent fuel	Spent fuel	1/0	Trailer buckled from truck weight
04/10/78	Highway	Radiography camera	Ir-192	1/0	1 vehicle accident
07/07/78	Highway	Cask	Mixed fission	1/0	Collision
07/26/78	Highway	Steel cask, lead lined	Cs-137	2/0	Jeep overturned
08/13/78	Highway	Cask, spent fuel	Spent fuel, empty	1/0	Empty cask broke through trailer bed
08/27/78	Highway	Radiography camera	Ir-192	1/0	Collision
09/11/78	Highway	Radiography camera	Ir-192	1/0	Truck overturned
09/15/78	Highway	Radiography camera	Ir-192	1/0	Truck overturned
11/28/78	Highway	Radiography camera	Ir-192	1/0	Truck overturned
01/10/79	Highway	Cylinder	Ir-192	5/0	Vehicle rear-ended truck
08/12/79	Highway	Cask	Empty	2/0	Truck sideswiped
12/11/79	Highway	Cylinder	UF6	5/0	Truck jackknifed; icy roads
01/14/80	Highway	Cask, teletherapy	Co-60	1/0	Semi struck truck
01/31/80	Highway	Cask	Low level waste	2/0	Semi jackknifed
07/21/80	Highway	Source	Ir-192	1/0	Collision

TABLE 4 (Concluded)

Date of Accident	Mode	Package Description	RAM Involved	Packages Shipped/ Damaged	Accident Conditions
08/22/80	Highway	Cylinder, 30B	UF6	5/0	Truck forced-off road
09/06/80	Rail	Cylinder, 30B	UF6	8/0	Train wreck
09/29/80	Rail	Radiography source	Sr-90, Y-90	3/0	Rail accident
06/09/81	Highway	Source, shielded	Am-241/Be	1/0	Pickup accident
09/02/81	Highway	Source	Ir-192	1/0	Collision
10/26/81	Highway	Radiography camera	Ir-192	1/0	Collision & fire
11/03/82	Highway	Cask	Empty LLW	2/0	Truck overturned; cask thrown off
03/11/83	Highway	Cask	LLW	1/0	Truck sideswiped
05/10/83	Highway	Radiography source	Ir-192	1/0	Head-on collision
07/14/83	Air	Cask	Y-90, Ir-192	2/0	Plane crashed
12/09/83	Highway	Cask, spent fuel	Spent fuel	1/0	Tractor separated from trailer
07/16/84	Air	Container	Ir-192	1/0	Plane ran off runway
08/08/84	Highway	Container	Reactor waste	1/0	Trailer overturned
02/11/85	Highway	Steel drum	Ir-192	1/0	Trailer jackknifed
02/13/85	Highway	Steel drum	Ir-192	1/1	Vehicle overturned
12/04/85	Highway	Radiography camera	Ir-192	1/0	Collision
01/10/86	Highway	Source	Cs-137	1/0	Truck ran off road
08/15/86	Highway	Cylinder, 30B	UF6	3/0	Collision
03/24/87	Rail	Cask, spent fuel	Spent fuel	2/0	Train/auto wreck
10/26/87	Highway	Radiography source	Ir-192	1/0	Truck overturned
01/09/88	Rail	Cask, spent fuel	Spent fuel	1/0	Train derailed
01/23/88	Highway	Radiography camera	Ir-192	1/0	Truck ran off road
09/23/88	Highway	Radiography camera	Ir-192	1/0	Truck ran off road
03/27/89	Highway	Radiography camera	Ir-192	1/0	Collision
05/19/89	Highway	Cask	Low Level Waste	1/0	Auto struck tractor trailer
06/08/91	Highway	Radiography camera	Ir-192	1/0	Truck overturned
09/15/91	Highway	Radiography camera	Ir-192	1/0	Truck caught fire
11/03/91	Highway	Radiography camera	Ir-192	1/0	Collision

SUMMARY AND CONCLUSIONS

The data provided by the Radioactive Materials Incident Report database for this paper in part reflects the adequacy of the transportation regulations that are in effect. That is, the packages that have experienced releases are those that contain limited quantities of radioactive materials. The regulations require that Type B packagings be used for the transport of larger quantities of nuclear materials, thus posing a potentially greater consequence if the contents are released. However, the DOT regulations also specify that Type B packagings be designed and tested to withstand "hypothetical" accident conditions which are outlined in the NRC regulations (10 CFR 71). The data from RMIR indicate that Type B packages have performed extremely well in accidents. There have been two minor damages to Type B packages, but no release of radioactive materials.

Since its development in 1981, the RMIR database has evolved to become one of the most comprehensive compilations of information on transportation accidents and incidents

involving radioactive materials. Every attempt is made to report a transportation incident as accurately as possible and to augment the available resources by establishing a network of contacts in addition to the two primary federal reporting agencies. Efforts are currently under way to contact each state radiation control office to obtain any additional data they may have for their respective state and to also obtain concurrence on the data already entered for their state. Additionally, each record is being reviewed for completeness and accuracy.

It is important to provide a credible and complete history of radioactive transportation incidents since the data are used in the following ways: transportation environmental analyses, safety analyses, regulatory actions, public information materials, responses to public inquiries, and in mitigating institutional concerns. In order to maintain and enhance the database, any additional information on transport events is welcomed.

REFERENCES

Carlson, R. W. and L. E. Fischer, "A Highway Accident Involving Unirradiated Nuclear Fuel in Springfield, Massachusetts, on December 16, 1991," NUREG/CR-5892, U.S. Nuclear Regulatory Commission (1992).

Javitz, H. S., et al. "Transport of Radioactive Material in the United States: Results of a Survey to Determine the Magnitude and Characteristics of Domestic Unclassified Shipments of Radioactive Materials," SAND84-7174, Sandia National Laboratories (1985).

TRANSNET–Access to Radioactive and Hazardous Materials Transportation Codes and Databases*

J. W. Cashwell

Sandia National Laboratories**, Albuquerque, New Mexico, United States of America

ABSTRACT

TRANSNET has been developed and maintained by Sandia National Laboratories under the sponsorship of the United States Department of Energy (DOE) Office of Environmental Restoration and Waste Management to permit outside access to computerized routing, risk and systems analysis models, and associated databases. The goal of the TRANSNET system is to enable transfer of transportation analytical methods and data to qualified users by permitting direct, timely access to the up-to-date versions of the codes and data.

The TRANSNET facility comprises a dedicated computer with telephone ports on which these codes and databases are adapted, modified, and maintained. To permit the widest spectrum of outside users, TRANSNET is designed to minimize hardware and documentation requirements. The user is thus required to have an IBM-compatible personal computer, Hayes-compatible modem with communications software, and a telephone. Maintenance and operation of the TRANSNET facility are underwritten by the program sponsor(s) as are updates to the respective models and data, thus the only charges to the user of the system are telephone hookup charges.

TRANSNET provides access to the most recent versions of the models and data developed by or for Sandia National Laboratories. Code modifications that have been made since the last published documentation are noted to the user on the introductory screens. User friendly interfaces have been developed for each of the codes and databases on TRANSNET. In addition, users are provided with default input data sets for typical problems which can either be used directly or edited. Direct transfers of analytical or data files between codes are provided to permit the user to perform complex analyses with a minimum of input.

Recent developments to the TRANSNET system will also be discussed in the final paper. Some of these include use of the TRANSNET system to directly pass data files between both national and international users as well as development and integration of graphical depiction techniques.

*This work performed at Sandia National Laboratories, Albuquerque, New Mexico, supported by the United States Department of Energy under Contract DE-AC04-76DP00789.

**A United States Department of Energy facility.

TERM--A Transportation Emergency Response Management, Resource Identification and Planning Technique*

J. W. Cashwell[1] and G. F. List[2]

[1]Sandia National Laboratories**, Albuquerque, New Mexico, United States of America
[2]Rensselaer Polytechnic Institute, Troy, New York, United States of America

ABSTRACT

Under the sponsorship of the United States Department of Energy (DOE) Office of Environmental Restoration and Waste Management Emergency Preparedness Program, Sandia National Laboratories and Rensselaer Polytechnic Institute developed an emergency planning code to identify existing emergency response resources, estimate response times, and determine deficiencies in the emergency response system. This code, entitled TERM, has been linked to network databases and routing models available on the DOE's TRANSNET system, a centralized dial-up computer system containing routing, risk, and systems analysis codes and associated data.

Assessment of emergency response resources and their capabilities and planning for improved capabilities along transportation routes have been identified as areas of concern by states and Indian tribes as well as the Federal Government. The purpose of this project is to develop a computerized technique to assess and plan optimal siting strategies for emergency response resources that can be used by the DOE and state/local governments.

Following development, the code will be applied on the transportation routes used for the test phase of the Waste Isolation Pilot Plant (WIPP), a geologic storage site for DOE Defense Programs transuranic wastes located in southern New Mexico. Testing of the technique by a state or local emergency response planning agency will precede general release of the code. Potential long-term applications of this technology could include expansion of the scope of commodities handled to include other hazardous materials. Future integration of this technique with routing and systems analysis codes will permit users to address the requirements of the United States Hazardous Materials Transportation Uniform Safety Act in assessing routing alternatives for radioactive and hazardous materials.

This paper will provide an overview of the technique, illustrate its application to the WIPP Program, and discuss integration of the technique into the comprehensive transportation network analysis capabilities available on the TRANSNET system.

*This work performed at Sandia National Laboratories, Albuquerque, New Mexico, supported by the United States Department of Energy under Contract DE-AC04-76DP00789.
**A United States Department of Energy facility.

A Radioactive Waste Transportation Package Monitoring System for Normal Transport and Accident Emergency Response Conditions*

G. S. Brown, J. W. Cashwell, M. L. Apple

Sandia National Laboratories**, Albuquerque, New Mexico, United States of America

INTRODUCTION

Shipments of radioactive material (RAM) constitute but a small fraction of the total hazardous materials shipped in the United States each year. Public perception, however, of the potential consequences of a release from a transportation package containing RAM has resulted in significant regulation of transport operations, both to ensure the integrity of a package in accident conditions and to place operational constraints on the shipper. Much of this attention has focused on shipments of spent nuclear fuel and high level wastes which, although comprising a very small number of total shipments, constitute a majority of the total curies transported on an annual basis.

Shipment of these highly radioactive materials is made in what is described in the regulations as a Type B packaging. Type B transportation packages are designed to withstand a sequence of accident scenarios, including drop, puncture, fire, and immersion with virtually no release of contents. A bulk of the Type B packages currently in use are utilized in the transport of survey and well logging sources. These packagings, while extremely robust, are not large and move daily in general commerce. Large Type B packagings, or casks, are used to transport spent nuclear fuels and high level wastes.

Due to the quantities of spent fuel and high level wastes carried in Type B casks and the public perception and apprehension regarding the potential consequences of a release, involvement of a packaging containing spent fuel or high level wastes in any accident will result in a very cautious emergency response until it can be determined that the integrity of the cask is maintained. Typically this involves closure of the transport link or pathway, evacuation of all unnecessary personnel, diversion of traffic from the area, and subsequent investigative and mitigative procedures from trained specialists.

Cask integrity is not addressed without inspection, both visual and with radiation detection instruments. These actions are typically time consuming, due to the lack of first responders with specialized training in the mitigation of radioactive materials incidents and availability of specialized equipment. Detection instrument operational condition and calibration are also concerns, which,

*This work performed at Sandia National Laboratories, Albuquerque, New Mexico, supported by the United States Department of Energy under Contract DE-AC04-76DP00789.
**A United States Department of Energy facility.

when combined with the lack of adequate training, have resulted in some states actually placing the equipment in a centralized storage area and relying on specialty responders for accident assessment. This results in long delays before normal transportation operations can be restored.

An "onboard" instrumentation/communications package has been developed that, when affixed to a spent fuel or high level waste cask, can monitor key indicators of the integrity of the cask and communicate these parameters to emergency responders. Entitled the Transportation Intelligent Monitoring System (TRANSIMS), this package links a monitoring system located inside the transportation cask with instrumentation and communications modules on the vehicle. The first responder can then monitor the status and integrity of the cask remotely, thus lessening the need to approach the container. Use of this unit also relieves the first responder of the necessity of mobilizing specially trained response units unless a release is indicated or some doubt about the integrity of the cask remains. This will effectively minimize transportation system downtime for all but the most severe accidents.

This paper addresses spent fuel and high level waste transportation history and prospects, discusses accident histories of RAM transport, discusses emergency responder needs and provides a general description of the TRANSIMS design.

BACKGROUND

It is estimated that 100 million packages classified as containing hazardous materials are shipped in the United States each year (U.S. Congress 1986). Approximately 2 million shipments of radioactive materials are shipped annually (Javitz et al. 1991), thus making radioactive materials about 2% of the total number of hazardous materials shipped each year. These radioactive materials are shipped in one of the following basic package types:

(1) Exempted packagings,
(2) Strong, tight containers,
(3) Type A packagings,
(4) Type B packagings, and
(5) Fissile material packagings.

Of the packaging types, the Type B packages must be demonstrated to be able to withstand test conditions designed to simulate severe hypothetical accident conditions. Specified by the United States Nuclear Regulatory Commission in 10 CFR 71, these test standards are:

(1) 30 foot drop onto a flat, unyielding surface so that the package's weakest point is struck,
(2) 40 inch drop onto a vertical steel rod at least 8 inches long, striking the package at its most vulnerable point,
(3) exposure of the entire package to an all-engulfing fire of at least 1475°F for 30 minutes, and
(4) total submersion of the package under at least 50 feet of water for at least 8 hours.

These Type B packages are typically used to transport radioisotopes, spent nuclear fuel, nuclear wastes, or similar highly radioactive materials. The majority of these shipments are made to transport radioisotopes, commonly used for surveying or well logging. Large Type B transportation packages typically range from 20 to 25 tons for legal weight transport and 70 to 100 tons for rail transport. These containers are typically used for transport of spent nuclear fuel and high level wastes. Between 1964 and 1989, a total of 2660 cask shipments of commercial spent nuclear fuel

were made (Cashwell and McClure 1992). A small number of shipments of research reactor spent nuclear fuel and high level wastes were also made during this period. Averaging approximately 100 shipments per year, shipment activity fluctuates with the start-up and decommissioning of commercial storage and processing facilities. Requirements for shipments of commercially generated spent nuclear fuel to a Monitored Retrievable Storage (MRS) facility in 1998, as specified in the contractual agreements between the Department of Energy and the utilities, in conformance with the Nuclear Waste Policy Act, could result in 1000 to 6000 shipments per year (U.S. Department of Energy 1985).

Historical accident rates for rail and truck transport are approximately 1.5 and 2.5 accidents per million vehicle miles (McClure 1981), respectively. Thus, while historically there have been no releases from a Type B cask carrying spent nuclear fuel, these shipments will be involved in accidents in which emergency response actions are taken. Although analysis of historical data indicates that the probability of a release is extremely low, emergency response actions and measures must be taken until the integrity of the cask and protection of the public is assured. The TRANSIMS concept will permit all interruptions to the transportation network to be minimized and will reduce the current necessity for undue delays for trained responders to answer all, even minor, accidents.

EMERGENCY RESPONSE

Most Type B shipments are routed whenever possible through rural areas, and the first responder to an accident will most likely be a local law enforcement officer or other public service volunteer. In the event of such an accident, the local first responder, having no package status information, must assume the worst case condition, i.e., a radioactive material release, and initiate an appropriate emergency response.

One of the primary functions of the emergency responder in the event of a hazardous material shipment accident is the protection of the general public. Using a conservative approach, dictated by the assumption of a RAM release, to protect the public, the responder would typically close the transport route, divert traffic, evacuate all unnecessary personnel, and wait for a response team trained in radiation assessment.

The TRANSIMS provides responders with immediate vital information on package integrity, external and internal temperature and radiation levels, and internal pressure. The pressure, temperature, and radiation level rates of change are also provided to allow the response team adequate warning of significant changes in the container condition. With this information, emergency responders can accurately assess the situation and implement an appropriate plan of action to protect the public and mitigate the emergency situation.

SYSTEM DESCRIPTION

The TRANSIMS consists of several independent modules. The first is the internal sensor and data processing module. This module measures the internal temperature, pressure and radiation level; logs the measurements; and transmits the data to the acoustic data transmitter/receiver module. The acoustic data transmitter encodes and transmits the digital data as acoustic energy through the package wall to the acoustic receiver, which decodes the signal for input into the microcontroller module. The microcontroller and external sensor module measures the cask external temperature and radiation level, receives internal sensor data, stores and mathematically manipulates all data, determines the appropriate response to emergency responder queries, maintains timing on all

routines, and outputs the appropriate voice message. The last element of the system is the communications module. This module consists of a Citizen Band radio frequency transmitter and receiver, with associated decoding and encoding circuitry, and is the emergency responder/TRANSIMS interface. A diagrammatic representation of the TRANSIMS is shown in Figure 1.

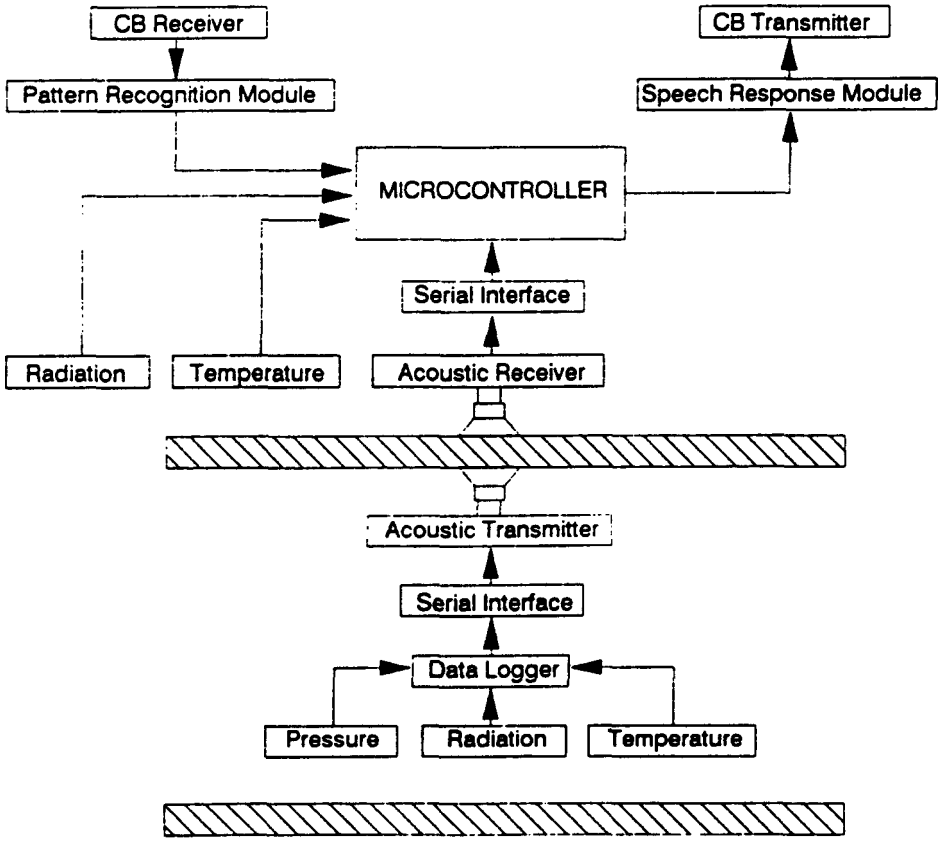

Figure 1. The Transportation Intelligent Monitoring System

As presently configured, the internal sensor module consists of a series of temperature probes, a pressure sensor, radiation sensors and accelerometers. The temperature and pressure sensor measurements are logged by a low power data logger at one second intervals. The accelerometer outputs are processed by a threshold detector which sets a flag high if a predetermined acceleration has been exceeded. These threshold flags are sampled at one second intervals and are used to determine normal or accident transport conditions. The radiation sensor outputs are continuously logged by two pulse count channels. All data are transmitted to the external microcontroller at 15 second intervals.

Data transmission from the internal package cavity to the external environment poses some unique problems. Primarily, the Type B certification is invalidated if any modifications affecting package integrity are made. Such a modification would be a new package penetration for data signal conductors. A novel approach is taken to transmit data and avoid the certification issue, i.e., ultrasonic acoustic transmission of digitized data through the existing package wall. The acoustic transmitter is attached at any point inside the package that has metal to metal contact with the main cask body, and the acoustic receiver is attached at a convenient point on the external wall of the transportation cask. The attachment points are welded to the existing surfaces and do not affect the package certification.

The digitized data are used to pulse width modulate the 220 Khz carrier frequency of the ultrasonic transmitter. The modulating pulse width varies between approximately 0.8 and 6.4 milliseconds, depending on the data bit pattern being transmitted. The original digitized data stream is restored after demodulation by the acoustic receiver.

Two potential problems in data transmission have been identified as: (1) acoustic noise and (2) data synchronization. The frequency range of acoustic noise, introduced by rail or truck transport vehicle vibration, is reported to be less than 2 Khz (Magnuson and Wilson 1977). The ultrasonic receiver transducer responds poorly to these frequencies, and very little vibrational energy at these frequencies is converted into electronic noise. Additionally, active electronic filters in the receiver circuit eliminate any low frequency electronic signal that may be present. The data synchronization problem is solved by placing a unique bit pattern at the beginning of each data frame to ensure proper timing in the decoding of the transmitted data stream.

The microcontroller module accepts input from the following sources: (1) the external sensors, (2) the internal data logger, and (3) the pattern recognition module. All incoming sensor data from both the external and internal sensors is stored and manipulated by the primary control algorithm. Rates of change are calculated using the most current data set.

The primary control algorithm responds at two levels. The first level simply notifies the requestor that package integrity has been maintained and that the external radiation levels are not above the established background. The second level is for more highly trained responders and provides details on internal temperatures and pressures, including rates of change. This enhanced response level provides emergency responders with the necessary information to properly assess the effectiveness of a specific course of action.

A TRANSIMS response is initiated by the transmission of a predetermined click pattern over a Citizen Band radio link. A pattern recognition module decodes the emergency responder request and activates the proper response algorithm in the microcontroller. Originally a speaker independent speech recognition scheme was proposed. However, the current technology for speaker independent recognition is expensive and gives less than 90% recognition, so to provide reliable operation, a

pattern recognition scheme is used. The TRANSIMS responds using synthesized speech which is transmitted to the emergency responder via the Citizen Band radio link.

CONCLUSION

Based on the historical RAM transport accident rate, at least one surface transportation accident involving spent fuel or high level waste can be expected each year. Initial response to the accident will most likely be by personnel untrained in the mitigation of a RAM incident. Due to the lack of immediate cask integrity information, the worst case situation, a radioactive material release, will be assumed by the emergency responder. A conservative and possibly costly emergency response will be initiated and followed until specialized radiation assessment teams arrive.

A new approach to RAM transport accident assessment is the Transportation Intelligent Monitoring System (TRANSIMS), an "onboard" cask status monitor. This system provides the emergency responder with the ability to remotely monitor package status information, accurately assess the situation, and initiate the appropriate response in a timely and cost-effective manner.

REFERENCES

Cashwell C., and J. D. McClure, "Data Bases Concerning the Transportation of Radioactive Materials," SAND92-0090C, Sandia National Laboratories, 1992. U.S. Congress, Office of Technology Assessment, Transportation of Hazardous Materials, OTA-SET-304, 1986.

Javitz, H. S., et al., "Transport of Radioactive Material in the United States: Results of a Survey to Determine the Magnitude and Characteristics of Domestic, Unclassified Shipments of Radioactive Materials," SAND84-7174, Sandia National Laboratories, 1991.

Magnuson, C. F., and L. T. Wilson, "Shock and Vibration Environments for Large Containers on Rail Cars and Trucks," SAND76-0427, NUREG-766510, Sandia National Laboratories, 1977. U.S. Department of Energy, "Environmental Assessment for a Monitored Retrievable Storage Facility," Monitored Retrievable Storage Submission to Congress, vol. 2, RW0035, 1985.

McClure, J. D., "The Probability of Spent Fuel Transportation Accidents," SAND80-1721, Sandia National Laboratories, 1981.

U.S. Congress, Office of Technology Assessment, Transportation of Hazardous Materials, OTA-SET-304, 1986.

U.S. Department of Energy, "Environmental Assessment for a Monitored Retrievable Storage Facility," Monitored Retrievable Storage Submission to Congress, vol. 2, RW0035, 1985.

Surveying the Transportation of Radioactive Material (STORM) in the U.S.A.*

J. D. McClure[1] and D. Hopkins[2]

[1]Sandia National Laboratories**, Albuquerque, New Mexico, United States of America
[2]U.S. Nuclear Regulatory Commission, Washington, D.C., United States of America

ABSTRACT

In 1988, a Technical Committee (TC-556.2) was convened by the International Atomic Energy Agency (IAEA) to advise the Agency on the collection of transport data as a means of assessing the radiological effects of radioactive material (RAM) transport. There is value in gathering such data because, from this information, Member States and the IAEA can develop environmental impact studies which demonstrate the efficacy of the packaging and transport regulations. In addition, guidance for emergency response operations can be obtained from an examination of RAM shipment patterns. Finally, there is considerable public information value to developing a compilation of the magnitude of RAM shipments on a national and international basis. This paper will describe a new program, STORM, in the U.S. to acquire RAM transport shipment data.

There is presently no U.S. national system that periodically evaluates the numbers and characteristics of RAM shipments in the United States. There have been two occasions where estimates of these numbers and characteristics have been made. The first, in 1975, was completed under a contract by Battelle Pacific Northwest Laboratory for use in developing an environmental impact statement on the transportation of RAM in the United States. Based on this survey, there were approximately 2.5 million packages of RAM shipped each year in the United States. The second time that radioactive material shipment data were surveyed was in the 1981- 1983 time period. SRI International, acting as subcontractor to Sandia National Laboratories, estimated that there were 2.8 million packages shipped on an annual basis.

The present data collection effort under the STORM project involves two phases. The product of Phase 1 of the STORM project is a developed survey plan to systematically update parts of the shipment data base on a periodic basis so that:

(a) as much data as possible will be obtained from sources which have already collected the data for other purposes (e.g., waste burial grounds) rather than from a tedious surveying system;
(b) licensees and the Federal Government can anticipate the periodic collection of data and can adjust their systems (of records, budgets, and contracts) to best accommodate that collection;
(c) the shipment data base will always be reasonably up-to-date for those tasks required for continuation of the relatively free transport of radioactive material.

*This work performed at Sandia National Laboratories, Albuquerque, New Mexico, supported by the United States Department of Energy under Contract DE-AC04-76DP00789.
**A United States Department of Energy facility.

Phase 2 of the project will exercise the plan developed in Phase 1 to refine the collection of data to make certain the government receives the data it needs and that any adverse impacts of the transport process are minimized for all participants. This paper will describe the survey plan generated in Phase 1 and any results available by July 1992.

RADTRAN 5 - A Computer Code for Transportation Risk Analysis*

K. S. Neuhauser[1] and F. L. Kanipe[2]

[1]Sandia National Laboratories**, Albuquerque, New Mexico, United States of America
[2]GRAM, Inc., Albuquerque, New Mexico, United States of America

Introduction

RADTRAN 5 is a computer code developed at Sandia National Laboratories (SNL) in Albuquerque, NM, to estimate radiological and nonradiological risks of radioactive materials transportation. RADTRAN 5 is written in ANSI Standard FORTRAN 77 and contains significant advances in the methodology for route-specific analysis first developed by SNL for RADTRAN 4 (Neuhauser and Kanipe, 1992). In RADTRAN I through III, a route had to be divided into three population-density zones per run (usually labelled rural, suburban, and urban), and multiple runs of the code were required to examine any breakdown of a route into more than three such zones (Taylor and Daniel, 1977; Madsen et al., 1983; Madsen et al., 1986). This methodology was retained as a user option in RADTRAN 4 for the sake of continuity; it has been removed from RADTRAN 5. The new methodology is discussed in this paper. The code also includes several improved and/or updated numerical models. RADTRAN 5 will be released after benchmarking and other quality assurance tests are complete.

Like the previous RADTRAN codes, RADTRAN 5 contains two major modules for incident-free and accident risk analysis, respectively. All commercially important transportation modes may be analyzed with RADTRAN 5: highway by combination truck; highway by light-duty vehicle; rail; barge; ocean-going ship; cargo air; and passenger air.

Incident-Free Module

The incident-free module contains a series of numerical models that describe relevant infrastructure features of each transportation mode and roadway type (the latter for highway modes only) such as minimum distance to "offlink" population (i.e., population adjacent to transportation link). The models are simplified as much as possible, partly by neglecting features that, if considered, would reduce the consequence and risk estimates. For example, the buffer zone that generally is present between lanes in each direction on interstate highways in the United States is omitted because including it would reduce the estimated incident-free risk.

*This work performed at Sandia National Laboratories, Albuquerque, New Mexico, supported by the United States Department of Energy under Contract DE-AC04-76DP00789.
**A United States Department of Energy facility.

The numerical models for the various types of stops (e.g., truck stop, inspection stop) have been modified. Stop parameters are now included in the array of user-defined route-specific parameters in the LINK subroutine, which is described below.

Accident Module

RADTRAN 5 permits the user great flexibility in accident risk analysis. Parameter values that were formerly fixed within the code may now be user-defined (Table 1). For example, the time of groundshine exposure prior to emergency response action was formerly fixed at the very conservative value of 24 hours. In recognition of the fact that public evacuations can often be accomplished in far shorter time periods, this parameter is now user-definable. All parameters in the optional economic model are initialized at zero, and most default values have been removed. RADTRAN 5 users are provided, instead, with a number of sample input data sets for various types of shipments. These data sets may be edited by the user to tailor them to the user's problem, and, of course, the user may still construct entirely new data sets.

Table 1
RADTRAN 5 Parameters with Formerly Fixed Values

Parameters	Value(s)
Number of handlers	2 (intermediate packages) 5 (large packages)
Handling time	15 min (intermediate packages) 30 min (large packages)
Handler distance	1 m (all packages)
Minimum groundshine exposure time	24 hr
Interdiction level	40X clean-up action level
All economic parameters	various; now initialized at zero

The health-effect and dispersion models, which are used in the accident risk calculations, have been modified. The changes in these models are discussed under their separate headings below. In addition, a new numerical model that calculates dispersion-related doses to individuals located at specified downwind distances has been added to RADTRAN 5.

Health-Effects Model

Several health-effects models have been published since the 1986 Hiroshima-Nagasaki dosimetry reassessment (e.g., ICRP 60, 1990; BEIR V, 1990; UNSCEAR 1988; and NRC 1989). While similar, they are not identical, and various governmental entities in the United States and around the world have expressed preferences for one or the other. This has resulted in a need for new flexibility in the health-effects calculations in RADTRAN 5. Therefore, conversion factors in RADTRAN now can be modified by the user to conform with any of the cited health-effects models.

Dispersion Model

RADTRAN 5, like its predecessors, contains no internal dispersion model. Dispersion is highly dependent on physical-chemical properties of the material being shipped and can vary from flow scenarios (liquids and heavier-than-air gases) to explosive dispersal. Therefore, RADTRAN 5 allows the user to enter input data obtained from any of a large number of suitable dispersion codes. The data must be entered in the form of tables of downwind isodose areas (isopleths) and associated time-integrated concentrations. For the user's convenience, default data from a Gaussian puff dispersion model (for a ground-level, small diameter, instantaneous release) calculated either with average U.S. meteorological factors or with Pasquill atmospheric stability categories A through F are provided. To use the latter, one must enter a frequency value for each category. Puff models are usually used in transportation accident applications, and dispersion codes that model continuous releases are almost always unsuitable.

A second, closely related code modification concerns aerosol deposition velocities. In RADTRAN 4, deposition velocity was a variable on the isotope level, but since aerosol particulates are generally made up of mixtures of isotopes reflective of the makeup of the original material, the location of this parameter in the logic flow was inappropriate. In RADTRAN 5, deposition velocity has been placed among parameters defined at the physical-chemical group level.

The tables of meteorological input data also have been modified to permit optional entry of a third column of values for maximum downwind distance in each isopleth. If these optional values are entered, they are included in the output in the tables of downwind dose data, which permits the user to correlate dispersion-related doses with distance from release point. The expected dose to an individual in each isodose area also is calculated and printed. If no values for this parameter are entered, then a "no entry" message appears in the output. In the past, these individual doses could only be estimated by performing a calculation external to the code, and the calculation simply has been incorporated into RADTRAN for the convenience of the user. These values are of interest to persons who must demonstrate compliance with International Commission on Radiation Protection recommendations and/or U.S. Environmental Protection Agency regulations that address individual as well as population doses.

Route-Specific Analysis and the LINK Subroutine

Route-related parameters are entered separately for each user-defined route segment in the LINK subroutine. In LINK, a route segment can be created that represents either (a) an actual segment of a route or (b) an aggregate of route segments that have the same characteristics. The latter application renders the three-zone method used in RADTRAN I through III redundant. Coding for the three-zone method has been removed from RADTRAN 5. However, the user must still indicate segment type (i.e., whether a segment is rural, suburban, or urban in character). This designation controls selection of building shielding factor and calculation of ingestion pathway dose (rural areas).

The segment-specific variables have been expanded over those in RADTRAN 4 to include designators for land under cultivation (rural segments) and for selection of dispersion conditions (can select from several user-defined dispersion data tables). The user-defined parameters for each route segment are given in Table 2.

Because conveyance stops may vary considerably in character, RADTRAN 5 allows the user to define stops along a route by use of what are termed "stop links" in the LINK subroutine. To

accomplish this, the LINK subroutine was modified to allow the user to enter stop-specific variables formerly entered in the NORMAL array in RADTRAN 4. When the user enters a "zero" for segment-length parameter, that segment is then modelled by RADTRAN 5 as a stop. Parameters for that segment that do not relate to stops are either set to fixed values or replaced by distinct parameters. The parameters for a stop in the LINK subroutine are shown in Table 2.

Table 2
Comparison of LINK Parameters for Route Segments and Stops

Route Segment	Stop Link
mode	mode
distance (km)	[set to zero]
vehicle speed (km/hr)	stop time [hr]
offlink population density (person/km^2)	surrounding population density (person/km^2)
vehicle density on-link (vehicles/hr)	population at stop
accident rate (acc/km)	[set to zero]
segment type	stop type
road type	near-field (number of persons)
fraction of land in agricultural use	near-field (time; hr)
dispersion conditions	near-field (distance; m)

In RADTRAN 5, persons at stops are modelled as three separate populations occupying annular areas around the shipment (Figure 1). This approach was used to model rail stops and loss-of-shielding accidents in RADTRAN 4 and now models stops in all modes in RADTRAN 5. The population density of the area surrounding the stop is analogous to the offlink population for a travelling shipment and replaces the latter parameter in a stop link.

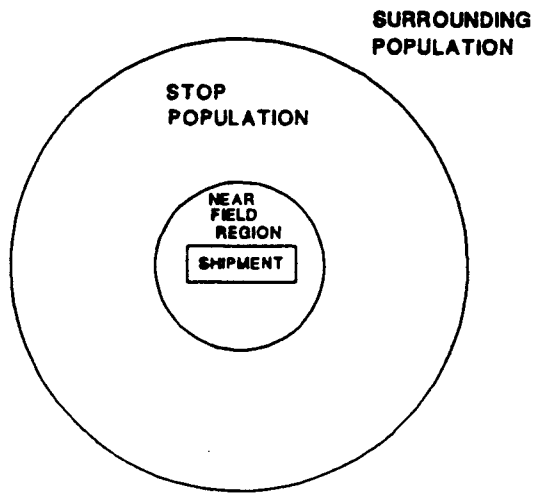

Figure 1. Populations modelled at stops.

The population in the immediate vicinity of a stop is often different from the surrounding population density and may be separately specified by the next parameter, for which the user enters an expected number (not density) of persons within an annular area surrounding the stopped shipment. The annular area extends from a minimum radial distance equal to twice the characteristic package (or shipment) dimension out to a maximum distance of at least 50 m, depending on mode. Persons who are closer are modelled as being in the "near-field," where a line-source model is used to estimate doses. The last three stop parameters are concerned with near-field exposures.

Separate accident rates for stops are not used in RADTRAN 5. Most sources of accident statistics already include accidents that involve stopped conveyances or anchored ships, accidents that occur at roadside locations, etc., and do not identify such accidents separately. These accident subsets may not be easily extracted from the overall statistics.

The stop-type designator allows the user to indicate the nature of the stop—fuel or rest stop, intermodal transfer, inspection stop, etc. In each of these types of stops, persons may come into the near-field range. As noted above, that range is defined as all radial distances equal to or less than twice the effective package dimension. These persons may be facility attendants, handlers, inspectors, etc. For each such stop, the user must enter a set of three variables describing the number of persons, the time they are in the near-field (which may be distinct from the total stop time), and their average distance from the package. In earlier versions of RADTRAN, these values were fixed for a number of scenarios, and the user could not change them.

Output Format

As a result of valuable comments from RADTRAN 4 users, the RADTRAN 5 output has been modified to inform the user when certain calculations have been performed. For example, if the predicted level of ground contamination in a dispersion isopleth exceeds the level at which the area would be interdicted rather than cleaned up (a user-defined parameter), then a message will appear in the output telling the user what downwind isopleths would be interdicted. Another type of message informs the user when an output value is zero because one or more input parameters were initialized at zero. This allows users to distinguish between actual zero-value results and those that appear to be zero-value only because real values were not entered in one or more input fields which contain initial values of zero.

Results are now reported in SI units (person-sieverts and becquerels) as well as in person-rems and curies.

Nonradiological Risks

Nonradiological risk factors have been incorporated to allow users to estimate nonradiological fatalities and injuries that might occur during the transportation event(s) being analyzed. These fatalities include prompt accidental fatalities from mechanical causes. Values of these risk factors for the United States (Neuhauser et al., 1984) have been made available in the code as optional defaults.

Uncertainty Analysis

Work is underway at SNL to develop a special auxiliary code that allows uncertainty analyses to be readily performed with RADTRAN. A functional prototype that uses Latin Hypercube Sampling (LHS) methods (Wheeler et al., unpublished results) has been developed for use with RADTRAN 4, and it is anticipated that this code will be adapted for general use with RADTRAN 5 in the next two years.

Summary

The RADTRAN 5 computer code combines great flexibility with improvements in route-specific analysis capabilities and user friendly output formats. The code and the LHS auxiliary code will be publicly available in 1993.

References

Health Effects of Exposure to Low Levels of Ionizing Radiation - BEIR V., BEIR V. Committee on the Biological Effects of Ionizing Radiations, National Academy of Sciences, Nation Academy Press, Washington, D.C. (1990).

Health Effects Models for Nuclear Power Plant Accident Consequence Analysis, U.S. Nuclear Regulatory Commission, Washington, D.C., NUREG/CR-4214, Rev. 1, Part II, Scientific Bases for Health Effects Models (1989).

Madsen, M. M., et al., *RADTRAN II User Guide*, Sandia National Laboratories, Albuquerque, NM, SAND83-2681 (1983).

Madsen, M. M., et al., *RADTRAN III*, Sandia National Laboratories, Albuquerque, NM, SAND84-0036 (1986).

Neuhauser, K. S., and F. L. Kanipe, *RADTRAN 4: Volume 3 User Guide*, Sandia National Laboratories, Albuquerque, NM, SAND89-2370 (1992).

Neuhauser, K. S., et al., *A Preliminary Cost and Risk Analysis for Transporting Spent Fuel and High-Level Wastes to Candidate Repository Sites*, Sandia National Laboratories, Albuquerque, NM, SAND84-1795 (1984).

Recommendations of the International Commission on Radiological Protection, ICRP Publication 60, Annals of the ICRP 21(1-3) (1990).

Sources, Effects, and Risks of Ionizing Radiation, Annex F. Radiation Carcinogenesis in Man, United Nations Scientific Committee on the Effects of Atomic Radiation, E.88.IX.7, United Nations, NY (1988).

Taylor, J. M., and S. L. Daniel, *RADTRAN: A Computer Code to Analyze Transportation of Radioactive Material*, Sandia National Laboratories, Albuquerque, NM, SAND76-0243 (1977).

Intermodal Transfer of Spent Fuel*

K. S. Neuhauser[1], *R. F. Weiner*[2]

[1]Sandia National Laboratories**, Albuquerque, New Mexico, United States of America
[2]Western Washington University, Bellingham, Washington, United States of America

INTRODUCTION

As a result of the international standardization of containerized cargo handling in ports around the world, maritime shipment handling is particularly uniform. Thus, handler exposure parameters will be relatively constant for ship-truck and ship-rail transfers at ports throughout the world. Inspectors' doses are expected to vary because of jurisdictional considerations. The results of this study should be applicable to truck-to-rail transfers.

A study of the movement of spent fuel casks through ports, including the loading and unloading of containers from cargo vessels, afforded an opportunity to estimate the radiation doses to those individuals handling the spent fuels with doses to the public along subsequent transportation routes of the fuel. A number of states require redundant inspections and for escorts over long distances on highways; thus handlers, inspectors, escort personnel, and others who are not normally classified as radiation workers may sustain doses high enough to warrant concern about occupational safety. This paper addresses the question of radiation safety for these workers.

Data were obtained during observation of the offloading of reactor spent fuel (research reactor spent fuel, in this instance) which included estimates of exposure times and distances for handlers, inspectors and other workers during offloading and overnight storage. Exposure times and distance were also measured for other workers, including crane operators, scale operators, security personnel and truck drivers. RADTRAN calculational models and parameter values then facilitated estimation of the dose to workers during incident-free ship-to-truck transfer of spent fuel.

CASE STUDY

This paper considers a case study of the intermodal transfer of 12 casks (in containers) of research reactor spent fuel in the Port of Hampton Roads, Virginia. The ship under study had berthed during the night at the southern end of the terminal at Newport News, Virginia. No ships were berthed nearby, the adjacent pier was not in use, and there was little activity near the ship while it was being unloaded. The casks had been loaded under supervision of the International Atomic Energy Agency (IAEA) at their point of origin, and three separate radiological inspections of each cask were performed at the entry to the port (Hampton Roads) by the U.S. Coast Guard, the state of Virginia, and the shipping firm. Additional inspections for non-radiological purposes also are performed.

*This work performed at Sandia National Laboratories, Albuquerque, New Mexico, supported by the United States Department of Energy under Contract DE-AC04-76DP00789
**A United States Department of Energy Facility

The casks were subsequently transported by truck to the USDOE Savannah River site in South Carolina. Use of the port properties and facilities are regulated by a state agency, the Virginia Port Authority (VPA). Container cranes are load-tested at least every four years, and the VPA requires that all cables be inspected immediately before use with highway-route-controlled quantities within port facilities. The VPA Risk Manager has the authority to select an appropriate terminal and berth for a ship carrying radioactive and other hazardous cargo. VPA Police escort all movements of highway-route-controlled quantities within port facilities. Historically, the probability of a drop resulting from a container failure is lower for shipments of this type than for ordinary containerized cargo; for the latter, the drop probability is estimated to be 2.7×10^{-6} per single operation (or "move").

A spent fuel cask that is to be shipped to the United States by vessel is secured in an approved intermodal container of the type defined as a specially modified closed transport unit. All approved intermodal containers must meet minimal structural requirements, and intermodal containers used with massive spent fuel casks have additional structural reinforcement. The application of standards established by the International Convention for Safe Containers (ICSC) and the International Standards Organization to all intermodal containers has led to worldwide standardization of cargo handling procedures at ports. All major commercial ports in the world have container cranes specifically constructed to move this type of approved container. The procedures and manpower requirements for securing and moving a container with a crane from a ship to a truck chassis and vice versa are comparable in all ports.

Handler and Inspector Dose

Two groups, each consisting of four handlers and a spotter, transferred the container from the ship to the truck trailer. One handler was positioned at each corner of the container and the spotter checked that the tiedowns were secure. These ten people were at an average distance of one meter from each cask, for about 2 minutes per cask. A radiological inspection was performed on each container by the U.S. Coast Guard and the state of Virginia. The shipper also performed a radiological inspection, and replaced Chinese-language placards with English-language placards (Neuhauser and Weiner 1992). In addition, the inland carrier performed a mechanical inspection of the tiedowns. The configuration and location of inspectors and handlers during and after offloading are shown in Figure 1. The distances from the source and exposure times for individuals close to the cask are given in Table 1.

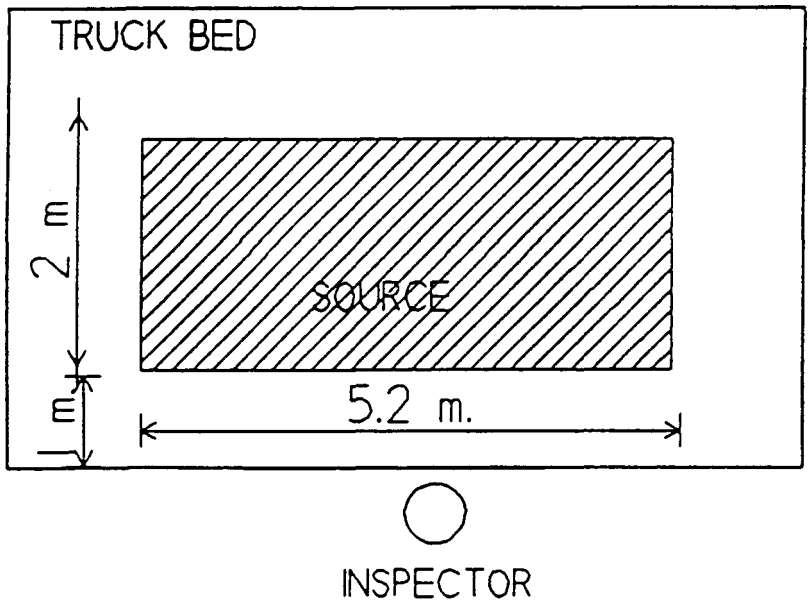

Figure 1. Configuration and location of inspectors and handlers during intermodal cask transfer.

The dose for incident-free handling was calculated using the RADTRAN 4 formulation of the dose to handlers of large packages (Neuhauser and Kanipe 1992)

$$D=\frac{K\cdot DR\cdot PPS}{r}\cdot T_H\cdot PPH\cdot N_H\cdot SPY \qquad (1)$$

where D = population dose in person-mrem
K = line source coefficient = $(1+d_{eff}/2)$; d_{eff}, the effective package dimension = 4.68 m.
DR = dose rate in mrem/hr at 1 m. from the package surface
PPS = packages per shipment = 1
T_H = exposure time in hours
PPH = number of handlers
N_H = number of handlings per shipment = 2 for this calculation
SPY = number of shipments = 1 for this calculation
r = distance of handler from the source, in meters

Total dose for the 12 casks was calculated by multiplying the dose per cask by 12. This calculation overestimates the total exposure time, but was retained in the interest of conservatism. Table 1 shows the incident-free doses to handlers, spotters and inspectors for this particular case. For comparison, the allowed annual occupational whole body dose in restricted areas, as cited in 10 CFR 20.101(b)(2), is 50 mSv (5000 mrem), and the permissible occupational level of radiation in unrestricted areas, as cited in 10 CFR 20.105(a), is 5 mSv (500 mrem). The annual permissible level of general public exposure used by the U.S. Environmental Protection Agency (EPA), as cited in 40 CFR 191.12, is 0.25 mSv (25 mrem) per source.

Table 1. Doses to Handlers and Inspectors.

Personnel	PPH	r in meters	Exposure time; hours	Dose per container; 10^{-3} person-Sv (person-rem)	Total dose; 10^{-3} person-Sv (person-mrem)
Handlers	4	1	0.258	9.66 (966)	116 (11,600)
Spotters	1	2	0.258	1.21 (121)	14.5 (1,450)
Inspectors	5	1	0.083	3.90 (390)	46.8 (4,680)
Weighmaster	1	8	0.083	9.75×10^{-3} (0.975)	0.117 (11.7)

Dose to Escort Personnel

The U.S. Nuclear Regulatory Commission (NRC) requires an escort for a spent fuel shipment only in urban areas (10 CFR 73.37 and 49 CFR 173.22). The State of Virginia, however, requires an escort to the state border. Dose to escort personnel during incident-free transportation were calculated using the on-link incident-free dose calculation in RADTRAN 4. In this model the shipment is treated as a point source, since r is much larger than the package dimension, and that the dose is proportional to $1/r^2$ rather than $1/r$. The equation used is

$$D=\frac{N}{V}\cdot PPV\cdot\frac{DIST}{V}\cdot K\cdot\int_{min}^{\infty}\frac{1}{r^2}dr \qquad (2)$$

where D = population dose in person-mrem
K = package shape factor for a point source
PPV = number of people per vehicle = 2
N = number of vehicles per hour
V = velocity in km/hr; N/V = 1 for this calculation
DIST = segment length in km
r = distance of escort personnel from the source, in meters

Table 2 shows the dose to the escort personnel and compares it to the off-link dose (the dose to people along the route who are not moving with the shipment).

Table 2. Doses to Escort Personnel.

Route segment	Segment length; km	Escort dose; 10^{-9} person-mSv (10^{-9} person-mrem)	Off-link population	Off-link dose; 10^{-9} person-mSv (10^{-9} person-mrem)
NNMT to highway	3.3	2.64 (264)	2905	0.69 (69)
Norfolk	70	5.90 (590)	129049	11.8 (1180)
Norfolk/Portsmouth	45	3.80 (380)	71176	284 (28400)
Isle of Wight Co.	13	3.01 (301)	349	1.62 (162)
Suffolk	3.3	0.765 (76.5)	147	0.59 (58.9)
Emporia	3.3	0.765 (76.5)	345	13.8 (1380)
Greenville Co.[a]	117	27.6 (2760)	1431	6.43 (643)
TOTALS	255	44.5 (4448)	202497	318 (31820)

[a] The data for Southampton County are not given in the reference used, so data for Greenville County were used.

Table 4 compares the average individual doses of personnel involved with the shipment to the average urban, suburban and rural off-link doses. In making these calculations, a population of two individuals per escort vehicle was assumed, although in practice it may be as low as one person. In addition, the urban, suburban and rural averages were calculated according to the criteria shown in Table 3.

Table 3. Criteria for Identifying Urban, Suburban, Rural Segments.

	Population density range (per km^2)	Links used in averaging (from Table 2)
Urban	≥ 1285	NNMT to highway, Norfolk, Portsmouth
Suburban	55-1284	Suffolk and Emporia
Rural	0-54	Isle of Wight and Greenville Counties

CONCLUSIONS

Inspectors and handlers of shipments of radioactive materials are exposed to higher dose rates than any other transportation workers or members of the public. No cask or container is handled more than is necessary, and modern equipment and standardization have minimized handling time. However, the number of inspections is not restricted, each container is inspected several times even before leaving the dock, and the activities of inspectors are not so closely standardized as those of the handlers. Inspectors not only inspect for radiological contamination and for mechanical security, but change placards, fill out forms, watch other activities, and so on. Even the crew members participate in the inspections to the extent of tagging the tiedowns (a 15-minute operation, including walking around the container to tag each tiedown).

As may be seen in Table 4, the average radiation dose for an inspection of this particular shipment was almost 10% of the EPA limit to the general public of 25 mrem per source, about 0.5% of the permissible level of radiation in unrestricted areas, and about 240 times the average dose to the general urban population along the route (urban off-link dose) on this particular route. The average dose to escort personnel, on the other hand, is comparable to the off-link dose.

Table 4. Comparison of Average Individual Doses.

Receptor	Average individual dose; mSv (mrem)
Handler	0.0290 (2.90)
Spotter	0.0145 (1.45)
Inspector	0.00936 (0.936)
Weighmaster	0.00117 (0.117)
Escort	2.23×10^{-5} (0.00223)
Urban Off-link	9.88×10^{-5} (0.00988)
Suburban Off-link	0.720×10^{-5} (0.00072)
Rural Off-link	0.403×10^{-5} (0.000403)

Doses to Inspectors

Hoskins, et al. (Hoskins, et al., 1992) evaluated near-field personnel dose using a dose rate map. The dose rate at one meter from the surface of the cask studied by Hoskins was about ten times the dose rate at one meter from the surface of the Newport News container (1.29 mrem/hr as compared to 0.14 mrem/hr). Figure 2 compares Hoskins' measured dose rates perpendicular to the center of the cask to those calculated using RADTRAN for the same conditions and distances from the source, and shows the essential conservatism of the RADTRAN approximation. Hoskins calculates a total dose to an inspector of 0.0181 mSv (1.81 mrem) for a 45-minute (0.75 hour) inspection, which is consistent with the doses calculated by RADTRAN in Figure 2. RADTRAN calculations for the Newport News fuel yield a 45-minute inspection dose of 0.0842 mSv (8.42 mrem).

Figure 2 compares the dose rate calculated by RADTRAN using the dose one meter from the surface as measured by Hoskins with the dose rate map given by Hoskins, and shows the overestimate of the dose rate given by RADTRAN. The overestimate probably occurs because the package shape factor (K) in Equation (1) is probably not a constant, as in the equation used, but a function of distance from the package. The package shape factor will be addressed in a future edition of RADTRAN. It may be noted that the package shape factor appropriate for the TN-8L cask in the Hoskins study is slightly larger than that for the Newport News container.

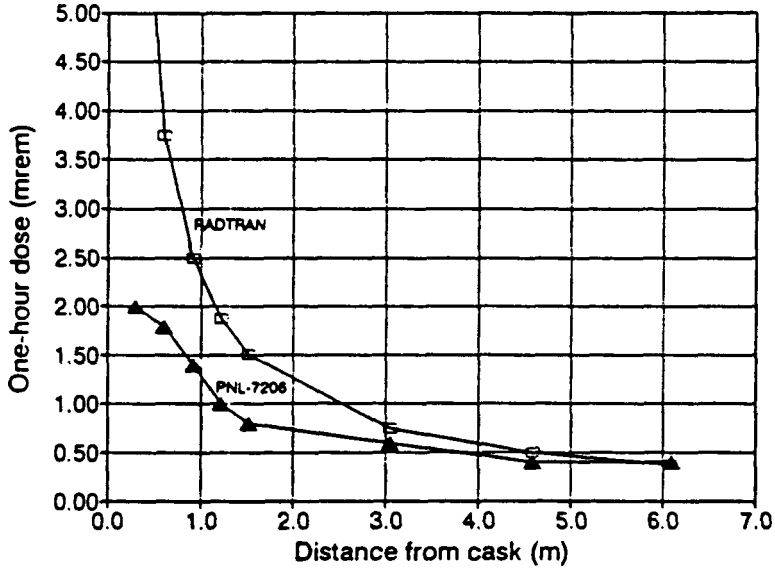

Figure 2. Comparison of the near-field dose rate calculated by RADTRAN with that from the dose rate map given by Hoskins, et al (PNL-7206).

What is the function of inspections? Even the first inspection of a cask or container entering the United States by sea will be at least the second radiological inspection that the container will have undergone since it was prepared for shipment. The results of the initial inspection (when the container was loaded) are entered on the shipping papers. The purpose of the USCG inspection at the port of entry is to verify the initial radiological inspection. Subsequent inspections are presumably intended to confirm the USCG inspection. However, they would be made only if the USCG inspection confirms the initial inspection, which in turn must have been a maximum dose rate within regulatory limits; that is, if a dose rate deviated significantly from that recorded on shipping papers during offloading at the port, a different set of protocols will apply, and the container would not be transported, as is, further in the continental U.S. nor undergo further inspections by non-federal personnel. If the results of initial inspection are confirmed by the USCG inspection, further inspections in the absence of any transportation incident or accident can only reconfirm the initial dose rate, but could compound any calibration errors and unnecessarily expose the inspectors themselves.

"Cask weeping" can result in external contamination and can thus cause a discrepancy between the surface dose rate recorded at the shipment origin and that recorded at a port of entry. Detection of contamination due to "cask weeping" on inspections after the first destination inspection (second inspection) when it had not been observed during the first destination inspection is highly unlikely. Recently, a cask shipment from India arrived at Dounreay, Scotland, with a low level of external contamination due to "weeping." The contamination was detected immediately on arrival at Dounreay, i.e., on the first destination inspection and the second inspection overall (Wilkinson, 1991).
Multiple inspections result in sufficient exposure to inspectors to invoke ALARA considerations. There does not appear to be any offsetting benefit in radiological protection of the general public.

Doses to Escort Personnel

Doses to escort personnel appear to be comparable to the average off-link dose. Thus, ALARA considerations would not play a part in regulating escort services. However, the purpose and benefit of an escort through rural areas is not clear. The same escort provisions ought to apply to transportation of radioactive material as apply to any oversize vehicle on the road.

REFERENCES

Hoskins, C. J., et al., *Time/Motion Observations and Dose Analysis of Reactor Loading, Transportation, and Dry Unloading of an Overweight Truck Spent Fuel Shipment PNL-7206*, Pacific Northwest Laboratories, Richland, WA (1992)

Neuhauser, K. S., and F. L. Kanipe, *RADTRAN 4: Technical Manual, SAND89-2370 (TTC-0943)*, Sandia National Laboratories, Albuquerque, NM, in preparation (1992).

Neuhauser, K. S., and R. F. Weiner, *Intermodal Transfer of Spent Nuclear Fuel at United States Ports, SAND91-1903 (TTC-1087)*, Sandia National Laboratories, Albuquerque, NM, in preparation (1992).

Title 10 Code of Federal Regulations, Part 20, Office of the Federal Register, Washington, DC (1991).

Title 10 Code of Federal Regulations, Part 71, Office of the Federal Register, Washington, DC (1991).

Title 10 Code of Federal Regulations, Part 73, Office of the Federal Register, Washington, DC (1991).

Title 40 Code of Federal Regulations, Part 191, Office of the Federal Register, Washington, DC (1991).

Title 49 Code of Federal Regulations, Part 173, Office of the Federal Register, Washington, DC (1991).

Wilkinson, Helen, SRD, UK, personal communication, September 1991.

Application of RADTRAN to Estimation of Doses to Persons in Enclosed Spaces*

K. S. Neuhauser

Sandia National Laboratories**, Albuquerque, New Mexico, United States of America

Introduction

The RADTRAN computer code for transportation risk analysis (Neuhauser and Kanipe, 1992) can be used to estimate doses to persons in enclosed volumes. This application was developed in response to a need to examine consequences of a hypothetical container leak during accident-free transportation by cargo air. The original problem addressed tritium containers, but the method can be applied to any gaseous or suspended particulate material potentially released in an airplane or other enclosed area (e.g., warehouse) under accident-free conditions. Such leakage can occur during shipment of any radioactive gas or material with a gaseous phase. Atmospheric dispersion is normally modeled in RADTRAN as a series of downwind isopleths each of which is assigned a dilution factor (also known as time-integrated concentration or X/Q value). These values are located in look-up tables in RADTRAN and are normally taken from externally performed Gaussian dispersion calculations. The dilution factors are used to estimate inhalation dose to persons in the specified downwind areas. The basic equation for inhalation dose in RADTRAN is:

$$Dinh = Ci \bullet PPS \bullet RF \bullet AER \bullet RESP \bullet RPC \bullet DF \bullet BR \bullet PD \bullet A \quad (1)$$

Where

Dinh	=	inhalation dose (person-rem)
Ci	=	curies in package (Ci)
PPS	=	number of packages in shipment
RF	=	fraction of material released from a package
AER	=	fraction of released material in aerosol form
RESP	=	fraction of aerosol material that is respirable
RPC	=	dose conversion factor (rem/Ci)
DF	=	dilution factor (Ci-sec/m^3/Ci released)
BR	=	breathing rate (m^3/sec)
PD	=	population density (persons/m^2)
A	=	isopleth area (m^2).

*This work performed at Sandia National Laboratories, Albuquerque, New Mexico, supported by the United States Department of Energy under Contract DE-AC04-76DP00789

**A United States Department of Energy facility

Equation 1 is located in the accident module of RADTRAN; it is usually applied iteratively. That is, a separate calculation is performed for each potentially released isotope in each downwind area for each accident severity specified by the user, and the results of these intermediate calculations are then summed. The following sections outline the procedure by which terms in Equation 1 can be replaced to yield a single calculation for an enclosed-volume dose for a fixed time of exposure.

Define Population within Enclosed Volume

The user models the enclosed volume as a single isopleth. This single isopleth must be assigned a nonzero area (m^2); the areas of all other isopleths should be set to zero. Note in Equation 1 that the product of the terms (PD • A) gives the number of persons in the isopleth. The user selects values of these two terms such that their product gives the number of persons in the crew, which is the potentially exposed population.

Substitute Concentration for Dilution Factor and Total Volume Inhaled for Breathing Rate

An isopleth would normally be assigned a dilution factor as described above, but dilution factors include a time term that accounts for wind speed. Exposure of persons within an enclosed volume does not depend on wind speed. Thus, in the application described here, the user substitutes a concentration for the dilution factor in the single isopleth being used to simulate the enclosed volume. Note that in Equation 1 the product of dilution factor (Ci-sec/m^3/Ci) and breathing rate (m^3/sec) gives curies inhaled per curie released. Note also that the product of concentration (Ci/m^3) and total volume inhaled (m^3) gives the same result. Thus, in order to preserve the equality in Equation 1, the user must also substitute total volume inhaled for the breathing rate term.

Calculation of Maximum Concentration and Total Volume Inhaled

The concentration value parameter depends on the interior volume of the aircraft and the amount of material released. Calculation may not be straightforward, however. In the tritium example, the material was shipped as tritium gas (T_2), which has a lower dose conversion factor than tritiated water (H3WTR). Tritium oxidizes rapidly in air, however, and it is conservative to model all released tritium as oxidizing instantaneously. Therefore, in this application the material was modelled as THO in vapor form. Additional complexity is introduced when what is being modeled is a potentially leaking container rather than one that releases a fraction of its contents all at once, because the enclosed-volume concentration will vary with time. A simple and conservative treatment of this problem consists of calculating the total amount of material that would be released if the container began leaking (at a constant rate) at the beginning of the flight and using this amount to calculate concentration. Using a concentration calculated in this manner to characterize the entire flight is conservative because that concentration in fact would only be achieved at the end of a flight (in-flight air exchange is neglected). Knowledge of container behavior is required, specifically expected leak rate. If there is more than one leak mechanism, then each must be analyzed separately.

Calculation of total volume inhaled (V_t) is more straightforward. One must know the number of persons in the crew, and the flight time. Using the standard ICRP breathing rate parameter for an adult male at work, one calculates V_t as follows:

$$V_t = BR \bullet T \bullet N$$

Where

BR	=	breathing rate (3.30E-04 m^3/sec)
T	=	flight time (sec)
N	=	number of crew members = PD • A

Other Parameters

In order for the calculation to proceed correctly, one must consider the other terms in Equation 1 and make certain that they are properly evaluated. The product Ci • RF normally gives the total number of curies released, but since that is already accounted for with the concentration value substituted for DF, these parameters should be set equal to 1.0. The number of packages per shipment (PPS) should represent the number of potentially leaking packages in the shipment; this may be varied in a series of runs if a probabilistic treatment is desired. The aerosol and respirable fractions (AER and RESP) should be set to 1.0. The dose conversion factor (RPC) and deposition velocity for H3WTR in vapor form are called from the internal radioisotope library in RADTRAN. The deposition velocity is not used in Equation 1, but it must be set to zero; otherwise all isopleths are automatically depleted to account for deposition, which skews the results. The default value for deposition velocity for H3WTR in the internal radioisotope library is zero. Had this not been the case, the user would have had to use the RADTRAN DEFINE function to redefine H3WTR.

Summary of Substitutions

When fully substituted as described above, the Equation 1 can be rewritten as follows

$$Dinh = Ci \bullet PPS \bullet RF \bullet AER \bullet RESP \bullet RPC \bullet C \bullet V_t \qquad (2)$$

Where

Dinh	=	inhalation dose (person-rem)
Ci	=	1.0
PPS	=	number of leaking packages in shipment
RF	=	1.0
AER	=	1.0
RESP	=	1.0
RPC	=	dose conversion factor (rem/Ci)
C	=	concentration (Ci/m^3)
V_t	=	total volume inhaled (m^3)
	=	BR (m^3/sec) • T (sec) • PD (persons/m^2) • A area (m^2).

The parameter values that must be entered in RADTRAN to realize the relationship in Equation 2 are summarized below.

- Substitute the value of C for the usual dilution factor (DF) in a single isopleth and enter zeros for all other isopleths.
- Substitute volume inhaled per person (BR • T) for the usual breathing rate value.
- Enter values of PD and A such that the product equals the number of persons in the enclosed volume.

The user must also set the accident rate equal to the probability (per flight) that a leak is expected to occur. If the failure rate is known or can be estimated (failure events/hr), then the probability is equal to the product of the failure rate and the total time per trip.

Output Formats

The risk results are listed under the output table entitled Expected Values of Population Risk in Person-Rem. In RADTRAN, consequences are calculated prior to multiplication by the probability term, and this consequence result is also given in the output in the Accident Summary in the table entitled Radiological Consequences—Mode [Cargo Air], 50-Year Population Dose in Person-Rem.

The user is encouraged to use the Comment capability of RADTRAN to enter as many comment lines (i.e., text lines) as necessary to describe the parameter substitutions being used.

Since these comments are automatically printed in the output, the user retains a record of what was done along with the results. A sample of a fully commented RADTRAN output for a tritium example is attached.

References

Neuhauser, K. S., and F. L. Kanipe, *RADTRAN 4: Volume 3, User Guide*, SAND89-2370, Sandia National Laboratories, Albuquerque, NM, 1992.

RUN DATE: [2-SEP-92 AT 10:04:48]

```
RRRR     AAA    DDDD    TTTTT  RRRR     AAA    N    N
R   R   A   A   D   D     T    R   R   A   A   NN   N
R   R   A   A   D   D     T    R   R   A   A   N N  N
RRRR    A   A   D   D     T    RRRR    A   A   N  N N
R R     AAAAA   D   D     T    R R     AAAAA   N   NN
R  R    A   A   D   D     T    R  R    A   A   N    N
R   R   A   A   DDDD      T    R   R   A   A   N    N
```

```
    4
4   4
4   4
44444
    4
    4
    4
```

RADTRAN 4.0.12 VERSION DATE: NOVEMBER 19,1991

MODE DESCRIPTIONS

NUMBER	NAME	CHARACTERIZATION
1	TRUCK	LONG HAUL VEHICLE
2	RAIL	COMMERCIAL TRAIN
3	BARGE	INLAND VESSEL
4	SHIP	OPEN SEA VESSEL
5	CARGO AIR	CARGO AIRCRAFT
6	PASS AIR	PASSENGER AIRCRAFT
7	P-VAN	PASSENGER VAN
8	CVAN-T	COMMERCIAL VAN
9	CVAN-R	COMMERCIAL VAN
10	CVAN-CA	COMMERCIAL VAN

RUN DATE: [2-SEP-92 AT 10:04:48]

ECHO CHECK

```
TITLE ROUTE A, AIR SHIPMENT, S18, NON-ACCIDENT
&& 8 PERSONS DC-9 FLIGHT WITH NO VENTILATION (AREA OF 60 M**2)
&& LEAK RATE = 1E-7 CI/SEC,  FAILURE RATE = 3E-8/HR
&& TRIP_TIME = 2.25 HR = 8100 SEC
FORM UNIT
DIMEN 1 1 1 10 2
PARM 0 2 2 1 0
POPDEN      133333      1.0       1.0
&&          133333 PERSONS/KM**2 -> 8 PERSONS/60 METERS**2
PACKAGE
   LABGRP   GROUP1
SHIPMENT
   LABISO   H3WTR
NORMAL
   NMODE=5
       1.000E+00  0.000E+00  0.000E+00  6.440E+02  6.440E+02  6.440E+02
       2.000E+00  6.100E+00  0.000E+00  0.000E+00  0.000E+00  0.000E+00
       0.000E+00  0.000E+00  1.000E+00  0.000E+00  0.000E+00  1.000E+00
       0.000E+00  0.000E+00  0.000E+00  0.000E+00  0.000E+00  0.000E+00
       0.000E+00
ACCIDENT
   ARATMZ
       NMODE=5  6.75E-8      0.0 0.0
&&          RATE OF FAILURE IS 3E-8/HR, PROBABILITY = 3E-8*TRIP_TIME
   SEVFRC
     NPOP=1
       NMODE=5
       1.0
     NPOP=2
       NMODE=5
       1.0
     NPOP=3
       NMODE=5
       1.0
RELEASE
   RFRAC
     GROUP=1
       1.0
   AERSOL
     DISP=8
       1.0
   RESP
     DISP=8
       1.0
   AREADA
       0.0  60.0
&& ISOPLETH REPRESENTS AREA OF DC-9  (60 SQ METERS)
   DFLEV
       1.35E-5 1.35E-5
&&     CONCENTRATION IN CURIES/M**3 DURING FLIGHT, LEAK RATE OF 1E-7,
&&     CONSERVATIVE ESTIMATION USING TOTAL CONCENTRATION AT TIME = 0,
```

RUN DATE: [2-SEP-92 AT 10:04:48]

ROUTE A, AIR SHIPMENT, S18, NON-ACCIDENT

```
&&      MAXIMUM CONCENTRATION = 1E-7*TRIP_TIME/60 CUBIC METERS

OTHER    BRATE  2.67
&& AMOUNT INHALED BY ONE PERSON OVER TRIP_TIME AT A RATE
&& OF 3.3E-4 M**3/SEC IS 2.67 M**3
EOF
ISOTOPES  -5      1.00      1.00      0.00      1.00      0.00  TRITIUM
           H3WTR  1.0     GROUP1    8
&&         CURIES ENTERED AS PERCENTAGE OF CONCENTRATION DUE TO EACH ISOTOPE
   DISTKM NMODE=5  1
&&                 DISTANCE = 1 FOR ONE TRIP
EOF
```

RUN DATE: [2-SEP-92 AT 10:04:48]

ROUTE A, AIR SHIPMENT, S18, NON-ACCIDENT

ZONE	POPULATION DENSITY (PERSONS PER SQ KM)
RURAL	133333.
SUBURBAN	1.
URBAN	1.

PACKAGE CHARACTERISTICS

FOR MATERIAL	DIMENSION (METERS)	EFFECTIVE DIMENSION	K(0) METERS SQ.
TRITIUM	0.000E+00	0.000E+00	1.000E+00

K(0) IS TI TO DOSE RATE CONVERSION FACTOR

PACKAGE HANDLING THRESHOLDS (METERS)
PKGSZ1= 5.000E-01
PKGSZ2= 1.000E+00
PACKAGES .LE. PKGSZ1 ARE HAND CARRIED
PACKAGES .GT. PKGSZ1 AND .LE. PKGSZ2 ARE HANDLED BY SMALL EQUIPMENT
PACKAGES .GT. PKGSZ2 ARE HANDLED BY HEAVY EQUIPMENT

MATERIAL CHARACTERISTICS

MATERIAL	FRACTION OF GAMMA	FRACTION OF NEUTRON
TRITIUM	1.000E+00	0.000E+00

RUN DATE: [2-SEP-92 AT 10:04:48]

ROUTE A, AIR SHIPMENT, S18, NON-ACCIDENT

MODE CHARACTERISTICS

MODE	DISTANCE TRAVELED	EXCLUSIVE USE	NUMBER OF SHIPMENTS	MATERIALS	TRANSPORT INDEX (TI)	PACKAGES/ SHIPMENT
CARGO-AIR	1.00E+00	YES	1.00E+00			
				TRITIUM	0.00E+00	1.00E+00

BUILDING SHIELDING OPTION= 2
(1=TOTAL SHIELDING, 2=PARTIAL SHIELDING, 3=NO SHIELDING)

RPD= 6.000E+00
(RATIO OF PEDESTRIAN DENSITY (PEDESTRIAN/KM SQ OF SIDEWALK)
TO POPULATION DENSITY (PEOPLE/KM SQ IN URBAN AREAS)

RR = 1.000E+00
(TRANSMISSION FACTOR FOR RURAL AREAS)

RS = 8.700E-01
(TRANSMISSION FACTOR FOR SUBURBAN AREAS)

RU = 1.800E-02
(TRANSMISSION FACTOR FOR URBAN AREAS)

RUN DATE: [2-SEP-92 AT 10:04:48]

ROUTE A, AIR SHIPMENT, S18, NON-ACCIDENT

NO		DNORML INPUT CARGO-AIR
1	FRACTION OF TRAVEL IN RURAL POPULATION ZONE	1.000E+00
2	FRACTION OF TRAVEL IN SUBURBAN POPULATION ZONE	0.000E+00
3	FRACTION OF TRAVEL IN URBAN POPULATION ZONE	0.000E+00
4	VELOCITY IN RURAL POPULATION ZONE (KILOMETERS/HOUR)	6.440E+02
5	VELOCITY IN SUBURBAN POP. ZONE (KILOMETERS/HOUR)	6.440E+02
6	VELOCITY IN URBAN POPULATION ZONE (KILOMETERS/HOUR)	6.440E+02
7	NUMBER OF CREWMEN	2.000E+00
8	DISTANCE FROM SOURCE TO CREW (METERS)	6.100E+00
9	NUMBER OF HANDLINGS	0.000E+00
10	STOP TIME PER KM (HR/KM)	0.000E+00
11	MINIMUM STOP TIME PER TRIP (HR)	0.000E+00
12	ZERO STOP TIME PER TRIP (HR)	0.000E+00
13	MINIMUM NUMBER OF RAIL CLASSIFICATIONS/INSPECTIONS	0.000E+00
14	PERSONS EXPOSED WHILE STOPPED	0.000E+00
15	AVERAGE EXPOSURE DISTANCE WHILE STOPPED (METERS)	1.000E+00
16	STORAGE TIME PER SHIPMENT (HR)	0.000E+00
17	NUMBER OF EXPOSED PERSONS DURING STORAGE	0.000E+00
18	AVERAGE EXPOSURE DISTANCE WHILE IN STORAGE (METERS)	1.000E+00
19	NUMBER OF PEOPLE PER VEHICLE ON LINK	0.000E+00
20	FRACTION OF URBAN TRAVEL DURING RUSH HOUR TRAFFIC	0.000E+00
21	FRACTION OF URBAN TRAVEL ON CITY STREETS	0.000E+00
22	FRACTION OF RURAL-SUBURBAN TRAVEL ON FREEWAYS	0.000E+00
23	*TRAFFIC COUNT PASSING A SPECIFIC POINT-RURAL ZONE	0.000E+00
24	*TRAFFIC COUNT PASSING A SPECIFIC POINT-SUBURBAN ZONE	0.000E+00
25	*TRAFFIC COUNT PASSING A SPECIFIC POINT-URBAN ZONE	0.000E+00

*(ONE WAY VEHICLES/HR)

RUN DATE: [2-SEP-92 AT 10:04:48]

ROUTE A, AIR SHIPMENT, S18, NON-ACCIDENT

ISOTOPE RELATED DATA

NUCLIDE	CURIES PER PKG	RELEASE GROUP	RESUSP FACTOR	LUNG TYPE	DISPERS. CATEGORY	1YR INHAL LUNG	REM/CI MARROW
TRITIUM							
H3WTR	1.00E+00	GROUP1	1.00E+00	2	8	6.00E+01	6.00E+01

NUCLIDE	HALF LIFE	GAMMA ENERGY	CLOUD FACTOR	TRANSFER CROPS	TRANSFER SOIL	DEPOS SPEED
TRITIUM						
H3WTR	4.51E+03	0.00E+00	0.00E+00	0.00E+00	0.00E+00	0.00E+00

NUCLIDE	50-YR EFFECTIVE REM/CI INHALE	INGEST
TRITIUM		
H3WTR	6.30E+01	6.30E+01

RUN DATE: [2-SEP-92 AT 10:04:48]

ROUTE A, AIR SHIPMENT, S18, NON-ACCIDENT

RELEASE RELATED DATA

ACCIDENT RATES (PER KM)

MODE	RURAL	SUBURBAN	URBAN
CARGO-AIR	1.402E-07	2.681E-06	1.599E-05

RELEASE FRACTIONS

GROUP	SEVER: 1
1	1.00E+00

ACCIDENT SEVERITY FRACTIONS
FOR CARGO-AIR

ZONE	SEVER: 1
1	1.00E+00
2	1.00E+00
3	1.00E+00

RUN DATE: [2-SEP-92 AT 10:04:48]

ROUTE A, AIR SHIPMENT, S18, NON-ACCIDENT

AEROSOLIZED FRACTION OF RELEASED MATERIAL

DISP CAT	SEVER: 1
1	0.00E+00
2	1.00E+00
3	1.00E-02
4	5.00E-02
5	1.00E-01
6	1.00E+00
7	1.00E+00
8	1.00E+00
9	1.00E+00
10	1.00E+00
11	1.00E+00

FRACTION OF AEROSOLS BELOW 10 MICRONS AED

DISP CAT	SEVER: 1
1	0.00E+00
2	5.00E-02
3	5.00E-02
4	5.00E-02
5	5.00E-02
6	5.00E-02
7	1.00E+00
8	1.00E+00
9	1.00E+00
10	1.00E+00
11	1.00E+00

RUN DATE: [2-SEP-92 AT 10:04:48]

ROUTE A, AIR SHIPMENT, S18, NON-ACCIDENT

COST RELATED DATA

EMERGENCY RESPONSE COST

SEVER: 1
1 0.00E+00

ON-SCENE COSTS
(RF=RELEASE FRACTION)

RF=0.	0.<RF<=.01	.01<RF<=0.1	.1<RF<=1.
0.	0.	0.	0.

RUN DATE: [2-SEP-92 AT 10:04:48]

ROUTE A, AIR SHIPMENT, S18, NON-ACCIDENT

HEALTH RELATED DATA

EARLY FATALITY PROBABILITIES

DOSE(REM)	LUNG-1	LUNG-2	LUNG-3	MARROW
100000.000	1.000E+00	1.000E+00	1.000E+00	1.000E+00
80000.000	1.000E+00	8.500E-01	8.000E-01	1.000E+00
70000.000	1.000E+00	8.000E-01	5.000E-01	1.000E+00
40000.000	1.000E+00	7.000E-01	0.000E+00	1.000E+00
30000.000	1.000E+00	5.000E-01	0.000E+00	1.000E+00
25000.000	1.000E+00	2.000E-01	0.000E+00	1.000E+00
20000.000	1.000E+00	8.000E-02	0.000E+00	1.000E+00
10000.000	6.000E-01	0.000E+00	0.000E+00	1.000E+00
8000.000	1.000E-01	0.000E+00	0.000E+00	1.000E+00
6000.000	6.000E-02	0.000E+00	0.000E+00	1.000E+00
4000.000	3.000E-02	0.000E+00	0.000E+00	1.000E+00
3000.000	0.000E+00	0.000E+00	0.000E+00	1.000E+00
2000.000	0.000E+00	0.000E+00	0.000E+00	1.000E+00
1000.000	0.000E+00	0.000E+00	0.000E+00	1.000E+00
800.000	0.000E+00	0.000E+00	0.000E+00	9.960E-01
700.000	0.000E+00	0.000E+00	0.000E+00	9.000E-01
600.000	0.000E+00	0.000E+00	0.000E+00	4.000E-01
500.000	0.000E+00	0.000E+00	0.000E+00	5.000E-02
400.000	0.000E+00	0.000E+00	0.000E+00	0.000E+00
300.000	0.000E+00	0.000E+00	0.000E+00	0.000E+00
100.000	0.000E+00	0.000E+00	0.000E+00	0.000E+00
75.000	0.000E+00	0.000E+00	0.000E+00	0.000E+00
50.000	0.000E+00	0.000E+00	0.000E+00	0.000E+00
30.000	0.000E+00	0.000E+00	0.000E+00	0.000E+00
15.000	0.000E+00	0.000E+00	0.000E+00	0.000E+00
5.000	0.000E+00	0.000E+00	0.000E+00	0.000E+00
1.000	0.000E+00	0.000E+00	0.000E+00	0.000E+00
0.100	0.000E+00	0.000E+00	0.000E+00	0.000E+00
0.010	0.000E+00	0.000E+00	0.000E+00	0.000E+00
0.010	0.000E+00	0.000E+00	0.000E+00	0.000E+00

RUN DATE: [2-SEP-92 AT 10:04:48]

ROUTE A, AIR SHIPMENT, S18, NON-ACCIDENT

DISPERSAL ACCIDENT INPUT

AREADA (M SQ)	DILUTION FACTOR*
0.000E+00	1.350E-05
6.000E+01	1.350E-05

* DILUTION FACTOR UNITS ARE (CI-SEC/M**3/CI-RELEASED)

NON-DISPERSAL ACCIDENT INPUT

RADIST(M)		
RURAL	SUBURBAN	URBAN
3.050E+00	3.050E+00	3.050E+00
6.100E+00	6.100E+00	6.100E+00
9.100E+00	9.100E+00	9.100E+00
1.220E+01	1.220E+01	1.220E+01
1.520E+01	1.520E+01	1.520E+01
3.050E+01	3.050E+01	3.050E+01
6.100E+01	6.100E+01	6.100E+01
9.140E+01	9.140E+01	9.140E+01
1.524E+02	1.524E+02	1.524E+02
3.050E+02	3.050E+02	3.050E+02

BUILDING DOSE FACTOR	= 8.600E-03
FRACTION OF LAND UNDER CULTIVATION	= 5.000E-01
CONTAMINATION CLEAN UP LEVEL (UCI/M**2)	= 2.000E-01
BREATHING RATE (M**3/SEC)	= 2.670E+00

RUN DATE: [2-SEP-92 AT 10:04:48]

ROUTE A, AIR SHIPMENT, S18, NON-ACCIDENT

RUN DATE: [2-SEP-92 AT 10:04:48]

ROUTE A, AIR SHIPMENT, S18, NON-ACCIDENT

MODE CARGO-AIR

1-YEAR LUNG DOSE - INHALATION PATHWAY
BDF = 1 (REM)

AREA #	SEVER: 1
1	2.16E-03
2	2.16E-03

1-YEAR MARROW DOSE - INHALATION PATHWAY
BDF = 1 (REM)

AREA #	SEVER: 1
1	2.16E-03
2	2.16E-03

RUN DATE: [2-SEP-92 AT 10:04:48]

ROUTE A, AIR SHIPMENT, S18, NON-ACCIDENT

MODE CARGO-AIR

GROUND SURFACE CONTAMINATION TABLE (MICRO CI/M**2)
BEFORE CLEANUP

AREA #	SEVER: 1
1	0.00E+00
2	0.00E+00

RUN DATE: [2-SEP-92 AT 10:04:48]

ROUTE A, AIR SHIPMENT, S18, NON-ACCIDENT

ACCIDENT SUMMARY
******** *******

NUMBER OF EXPECTED ACCIDENTS -- MODE CARGO-AIR

CATEGORY	RURAL	SUBURB	URBAN
1	6.75E-08	0.00E+00	0.00E+00

EARLY FATALITY CONSEQUENCES -- MODE CARGO-AIR

CATEGORY	RURAL	SUBURB	URBAN
1	0.00E+00	0.00E+00	0.00E+00

ECONOMIC CONSEQUENCES -- MODE CARGO-AIR

CATEGORY	RURAL	SUBURB	URBAN
1	0.00E+00	0.00E+00	0.00E+00

RADIOLOGICAL CONSEQUENCES -- MODE CARGO-AIR
50 YEAR POPULATION DOSE IN PERSON REM

CATEGORY	RURAL	SUBURB	URBAN
1	1.82E-02	1.36E-07	8.24E-08

RUN DATE: [2-SEP-92 AT 10:04:48]

ROUTE A, AIR SHIPMENT, S18, NON-ACCIDENT

EXPECTED VALUES OF POPULATION RISK IN PERSON REM

	GROUND	INHALED	RESUSPD	CLOUDSH	*INGESTION	TOTAL
TRITIUM						
H3WTR	0.00E+00	1.23E-09	0.00E+00	0.00E+00	0.00E+00	1.23E-09
TOTALS:	0.00E+00	1.23E-09	0.00E+00	0.00E+00	0.00E+00	1.23E-09

* NOTE THAT INGESTION RISK IS A SOCIETAL RISK;
THE USER MAY WISH TO TREAT THIS VALUE SEPARATELY.

RUN DATE: [2-SEP-92 AT 10:04:48]

ROUTE A, AIR SHIPMENT, S18, NON-ACCIDENT

EXPECTED RISK VALUES - OTHER

LINK	ECON $$	EARLY FATALITY
1	0.00E+00	0.00E+00
TOTAL	0.00E+00	0.00E+00

EOI
END OF RUN

Conservatism of RADTRAN Line-Source Model for Estimating Worker Exposures*

R. F. Weiner[1] and K. S. Neuhauser[2]

[1]Western Washington University, Bellingham, Washington, United States of America
[2]Sandia National Laboratories**, Albuquerque, New Mexico, United States of America

Introduction

Concern about the risks posed to people who live along spent nuclear fuel transportation routes has led to demands for redundant inspections of the transported spent fuel. Several states appear to be considering mandatory state inspections. In actual practice, for example, research reactor spent fuel returned to the United States by sea may receive five redundant inspections (Neuhauser and Weiner, 1991) before leaving the dock area where it has been offloaded. It would be prudent to examine the radiological risk to the inspectors themselves before state or federal regulations are promulgated which require redundant inspections.

Federal regulations (10 CFR 71 and 49 CFR 173-178) require that the radiation dose rate at 1 meter from any accessible external surface of a radioactive materials package not exceed 0.1 mSv/hr (10 mrem/hr) except for packages shipped by exclusive-use vehicles (e.g., spent fuel casks). In the latter case, the maximum dose rate at any point 2 m from the vertical planes projected by the outer lateral surfaces of a closed vehicle or by the outer edges of an open vehicle may not exceed 0.1 mSv/hr. Important steps in the preparation of any radioactive materials shipment are measurement of the package dose rate at the point of origin and recording this dose rate on the shipping papers. To obtain these measurements, an individual must be 2 or 3 meters from the package surface for at least several minutes. Some state inspections take much longer: 30 to 45 minutes (Hostick, et al., 1992).

Other workers may also come close to a spent fuel cask during normal operations, even though the casks are actually lifted and moved with heavy cranes. For example, five handlers (one at each corner fitting, plus a spotter) are needed to load a containerized cask of spent fuel onto a truck with a crane (Neuhauser and Weiner, 1992). They align the corner fittings while the cask is suspended from the crane, and then secure the fittings after the cask has been lowered into place. These individuals spend several minutes within a few meters of the cask. Still another individual may inspect and tag the fittings after the cask is secured to the truck. The drivers of the truck also inspect the fittings, handle shipping papers, and so on, and have been observed to spend up to ten minutes a few meters from the cask.

*This work performed at Sandia National Laboratories, Albuquerque, New Mexico, supported by the United States Department of Energy under Contract DE-AC04-76DP00789
**A United States Department of Energy facility

The dose rate to which these inspectors and handlers are exposed is higher than the dose rate to which any other group is exposed during incident-free truck transportation (other groups include occupants of other vehicles on the route, persons residing near the route, others who might share the rights-of-way with trucks carrying the spent fuel, and persons at stops), and higher than the dose rate to the drivers when they are in the truck cab. For most radioactive materials shipped in the United States there are only two handlings: one at the origin and one at the destination. The number of handlers does not vary greatly from one shipment to another of the same type. However, the number of inspections a given shipment might experience en route cannot be predicted with confidence because it can vary with changing state regulations, since there is no regulatory limit on the number of inspections that might occur. The potential population dose and risk associated with redundant inspections of spent fuel shipments should be evaluated carefully in the context of ALARA. That is the focus of this study.

Two different methods were used to estimate gamma doses to inspectors for a representative fuel shipment. These methods were compared, and the results of the dose calculations were compared to other components of incident-free dose. Comparison is also made to a measured dose rate mapped in another investigation (Hostick, et al., 1992).

Basic Parameters

In this study inspection time was estimated at 10 minutes. A typical inspection takes about 7.5 minutes (Neuhauser and Weiner, 1992), so that 10 minutes per inspection was considered a conservative estimate for these calculations. Doses to the public from incident-free transportation (D_{IF}) were calculated for three routes of increasing length (817 km, 1732 km, and 4363 km, respectively). For this analysis all three routes were assigned the same fractions of travel in each of the population density zones as those representative of interstate truck routes in the populous eastern United States. These fractions and the population densities used for each are given in Table 1.

Table 1. Population Densities and Fractions of Travel .

Population Density Zone	Population Density:persons/km^2	Percent of Route
Rural	6	88
Suburban	719	10
Urban	3861	2

The source considered was spent fuel in a current-design cask similar to those used with the Taiwan research reactor fuel offloaded at the port of Hampton Roads, VA, in 1991 and earlier (Neuhauser and Weiner, 1991).

Albedo Dose

The albedo dose is the contribution to total dose from scattering from nearby surfaces. Albedo dose rates for scattering from the ground surface and from the back of a semi-tractor cab were calculated from the equations given by Selph (Selph, 1968). The ground surface was assumed to scatter like concrete; the cab was assumed to scatter like a metal building. In calculating albedo dose, only scattering of 0.4 MeV to 0.9 MeV gammas was considered. Almost 98% of the cask surface gamma are within this range for spent fuel shipments (Sandquist, et al., 1985). The calculation was

performed in order to determine whether scattering from the back of the cab was a potentially significant contributor to inspector dose rate at any distance from the cask. Table 2 summarizes the results of these calculations. The perpendicular distance of the receptor from the cask was 2 meters, in order to remain consistent with the PATHRAE analysis (Sandquist, et al., 1985); perpendicular distances from the scattering surfaces are given in Table 2. As may be seen from Table 2, scattering from surfaces other than the truck and the ground beneath accounted for 8% of the 0.4MeV gamma dose and 6% of the 0.9 MeV gamma dose.

Scattering from the ground surface at all distances is explicitly considered in the equations from the PATHRAE computer code, which also models the radiation field around a spent fuel cask explicitly (Sandquist, et al., 1985). In contrast, the RADTRAN computer code uses a line-source approximation (i.e., a model in which the dose rate is a function of 1/r where r is the minimum perpendicular distance to the source) to estimate the dose to persons close to a radioactive materials shipment (the near-field dose) (Neuhauser and Kanipe, 1991). Any distance within about 10 meters of a spent fuel cask is considered "close." Albedo dose is not explicitly evaluated in RADTRAN. In this report the two methods are compared to determine whether the tendency to overestimate dose in the RADTRAN model is sufficient to account for the albedo dose.

As may be seen from the table, scattering from the ground constitutes the only significant contribution of albedo dose to the radiation dose, and only to the dose received by persons within a few meters of the cask (e.g., inspectors and handlers). Contribution to the albedo dose from scattering from the back of the truck cab was negligible compared to ground scatter. The total incremental albedo dose was about 28% of the direct gamma dose for 0.4MeV gamma radiation and about 15% of the direct gamma dose for 0.9 MeV gamma radiation.

Table 2. Results of Albedo Calculations.

Scattering Surface	Perpendicular Distance from Scattering Surface	Fraction of Dose from Albedo	
		0.4MeV Gamma	0.9MeV Gamma
Ground	1.6 m.	0.1983	0.0883
Truck cab	9.3 m.	0.05	0.05
Backscatter of ground albedo from truck cab	9.3 m.	0.0297	0.0132
Total albedo		0.2780	0.1515

Inspection Doses

Doses to inspectors were compared to the doses to the public from incident-free transportation of radioactive material. The inspector dose (D_{insp}) was calculated for inspectors located 2 meters from a cask for 10 minutes per inspection. Doses to the public from incident-free transportation (D_{IF}) were calculated for the three routes described above. Since the total population dose to the public in incident-free transportation is a function of the total distance traveled by the shipment when population densities are held constant, the comparison may be expressed in terms of incremental dose per inspection per kilometer of travel, or as the ratio of total inspection dose to total dose to the public during incident-free transportation.

The ratio of these two doses was examined, rather than the absolute doses themselves, to remove dependence on actual cask dose rates. The dose rate used for the RADTRAN and PATHRAE calculations was 13.68 mrem/hr (the dose rate at 1 m from the surface in the RADTRAN spent fuel example). The inspection dose was calculated using the RADTRAN equations for handler/inspector dose; and dose to the public was calculated using the RADTRAN equations for the incident-free transportation dose to the public for typical routes (Neuhauser and Kanipe, 1991). This, in turn, allows the ratio D_{insp}/D_{IF} to be expressed in terms of population dose (person-sievert) per hour of inspection per kilometer of travel, or as person-sievert of inspection dose per person-sievert of public dose.

RADTRAN is based on a conception of the field around the source which has a simpler geometry than the actual field. Differences between the modeled and measured fields tend to be greater close to the field source than further away. The near-field dose calculated by RADTRAN was therefore compared both to that obtained by another more detailed model and to a dose map obtained by measurements made around a spent fuel cask (Hoskins, et al., 1992). For these comparisons, near-field doses were calculated using the equations of the PATHRAE model (Sandquist, et al., 1985). The dose per unit source strength was examined in order to eliminate any factor due to a difference in sources. The PATHRAE expression is

$$H_P = \left(\frac{1}{2\pi r}\right)\left(1.21+\mu\sqrt{r^2+(L/2+z)^2}\right)\left(\arctan\frac{L}{2r}\right) \qquad (1)$$

where H_P = dose per unit source strength in PATHRAE
r = radial position from the center of the line source (Figure 1)
z = axial position from the center of the line source
μ = effective photon attenuation coefficient for air
L = one-half of the effective source length = 2.56 m.

The expression derived from the RADTRAN equation (Neuhauser and Kanipe, 1991, Section 4.8), taking into account the package shape factor in RADTRAN, is

$$H_R = e^{-\mu r}\left(1.21+\mu\sqrt{r^2+(L/2+z)^2}\right)\left(.725+(1+L/2)^{.75}\right) \qquad (2)$$

where H_R = dose per unit source strength in RADTRAN

Figures 1 and 2 compare the calculated RADTRAN dose rate and PATHRAE dose rate at various distances from the surface of the cask. In the calculations, "z" is the distance from the center of the cask along the cask's long axis; "r" is the distance perpendicular to the long axis of the cask. Recall that PATHRAE includes ground-surface albedo explicitly, while RADTRAN uses a line source approximation which is independent of "z." The normalized dose rate as modeled by PATHRAE is less than the dose rate modeled by RADTRAN at all distances from the cask for which the 1/r approximation for RADTRAN is appropriate. Hostick, et al., (Hostick, et al., 1992) mapped the near-field dose around a TN-8L cask having the same dimensions as the cask in the RADTRAN and PATHRAE calculations, and qualified their measured values with the statement that 72% of the measured dose rate around the cask is from background radiation. The figures show the measured values taken from Hostick, et al., normalized for source strength (dose rate at 1 m from the surface), both with and without correction for background.

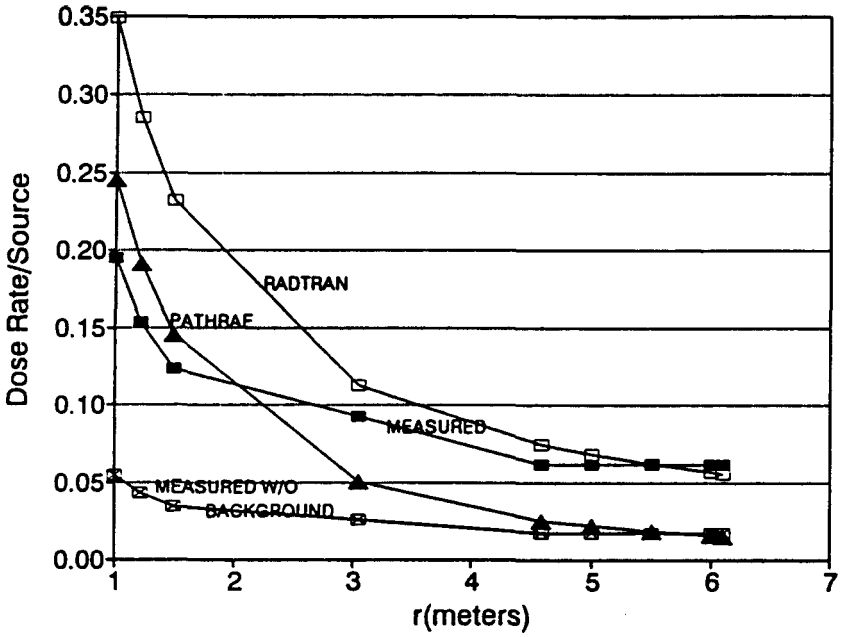

Figure 1. **Dose Rate Per Unit Source Strength at z=0.**

The average dose to an inspector per inspection of a spent fuel shipment, as calculated by RADTRAN, in 2.17 mSv (217 mrem). An individual who inspects 23 shipments a year (fewer than one every other week) will have received his or her annual allowed occupational dose of .05 Sv (5 rem) (10 CFR 20.1201). By comparison, the average annual external gamma dose to workers in all aspects of the nuclear industry during the period 1943-1985 was 0.0506 mSv (5.06 mrem) (Upton, 1991), or about 2.3% of the calculated dose per inspection. It should be noted that the inspection (handler) dose calculated by RADTRAN for the present study is based on the maximum package dose rate (DR_p) allowed by regulation (49 CFR 173.941). DR_p is the dose rate in mrem/hour at 1 meter from the surface of the package. If the measured DR_p is less than the maximum allowed by regulation, as it usually is, the inspection dose will also be less.

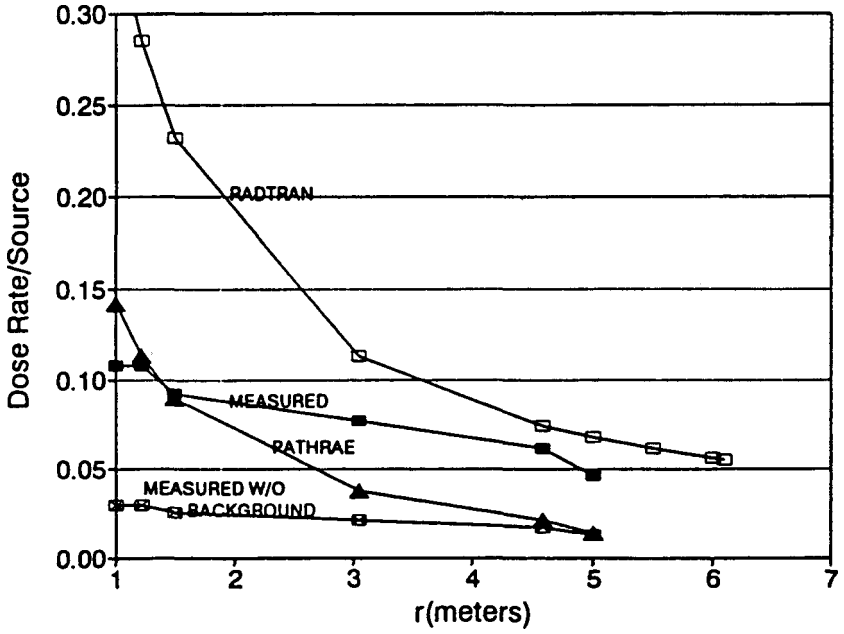

Figure 2. **Dose Rate Per Unit Source Strength at z=3 m.**

In another paper (Weiner and Neuhauser, 1992) the authors discussed the ratio of the inspection dose (D_{insp}) to the dose to the general public (D_{IF}). The D_{insp}/D_{IF} ratio for a typical cross-country route was found to be 1.72E+4/km/hour, where the "hour" in the denominator refers to hours of inspection and the "km" is the kilometers of incident-free transportation. This ratio is independent of cask dose rate. Table 2 illustrates the influence of trip length on D_{insp}/D_{IF} for a single 10-minute inspection. The contribution to total dose of each inspection is inversely proportional to trip length.

Table 3. Influence of Trip Length on D_{insp}/D_{IF}.

Trip Length (km)[a]	D_{insp}/D_{IF} Per Inspection
817	3.56
1732	1.68
4363	0.67

[a] Fractions of travel were held constant at 88% rural, 10% suburban, 2% urban.

Conclusions

Both RADTRAN and PATHRAE overestimate the dose to the population subgroup of handlers and inspectors, and anyone else very close to the container, to an extent that is may be overly conservative. It is not surprising that a model which is a simplified representation of a source field (a straight line in the case of RADTRAN and a rectangular area in the case of PATHRAE) represents that field less accurately the closer the receptor is to the source. Both RADTRAN and PATHRAE accommodate the inaccuracy by (1) accepting the conservatism and (2) introducing a factor for package shape and dimensions to improve the accuracy of the representation. Clearly, however, in RADTRAN the overestimate within a few meters of the package is large, in part because a field depending on 1/r goes to infinity as r becomes very small and in part because the RADTRAN model, by neglecting the cask diameter, places the receptor much closer to the source than he or she actually is. Alternative representations of the package shape factor and a refinement of the near-field model in RADTRAN are presently under study.

The total dose to inspectors per shipment is a function of total inspection time, i.e., the sum of all times during which the inspectors are within a few meters of the cask surface during a single trip from origin to destination. Since the RADTRAN calculation of inspector dose has been demonstrated to be conservative, the results presented here represent upper-bound estimates rather than actual expected values of inspector dose for ten-minute inspections. The estimated dose would, of course, increase for longer inspection times. The results suggest that superfluous inspections of radioactive materials shipments and long inspection times are not compatible with ALARA principles.

No need has been demonstrated for additional inspections beyond the radiological inspection at the point of origin (and possibly at a modal transfer point). There already are nonradiological operations performed at the point of origin and at modal transfer points (e.g., inspection of tie-downs, placarding of vehicle, etc.) that cannot be dispensed with and that require individuals to come into proximity with the shipment. Actual experience with the Taiwan shipments shows that the dose rates measured during Coast Guard inspections agreed with the values given on the shipping papers prepared at the point of origin in Taiwan. Since the shipments were inspected by International Atomic Energy Agency personnel before they left Taiwan, this is not surprising. Additional radiological inspections, which were performed by the state police and the shipping firm on the same day as the Coast Guard inspection, but with separate, independently calibrated instruments,

were also in close agreement with the original values. A reasonable conclusion is that some of these inspections were unnecessary.

RADTRAN files used in these calculations are available to the public through the TRANSNET system (Neuhauser and Kanipe, 1992).

References

Hostick, C. J. et al., *Time/Motion Observations and Dose Analysis of Reactor Loading, Transportation, and Dry Unloading of an Overweight Truck Spent Fuel Shipment PNL-7206*, Pacific Northwest Laboratories, Richland, WA (1992).

Neuhauser, K. S. and F. L. Kanipe, *RADTRAN 4: Technical Manual*, Sandia National Laboratories, in preparation (1991).

Neuhauser, K. S. and F. L. Kanipe, *RADTRAN 4: User Guide, SAND 89-2370*, Sandia National Laboratories (1992).

Neuhauser, K. S. and R. F. Weiner, *Intermodal Transfer of Spent Nuclear Fuel at United States Ports, SAND91-1903 (TTC-1087)*, Sandia National Laboratories, in preparation (1991).

Sandquist, G. M., et al., *Exposures and Health Effects from Spent Fuel Transportation*, Rogers and Associates, Salt Lake City, UT (1985).

Selph, W. E., *Neutron and Gamma Ray Albedos Weapons* in Radiation Shielding Handbook (1968).

Title 10 Code of Federal Regulations, Part 20, Section 20.1201(a)(1)(i), (1991).

Title 49 Code of Federal Regulations, Sections 173.941(b) and 177.842(a), (1991).

Upton, A. C., *Health Effects of Exposure to Low Levels of Ionizing Radiation (BEIR V)*, National Academy Press, Washington, DC (1990).

Weiner, R. F. and K. S. Neuhauser, *Near-Field Radiation Doses from Transported Spent Nuclear Fuel*, International High-Level Waste Management Conference, Las Vegas, NV, April 12-15, (1992).

A Methodology for the Transfer of Probabilities between Accident Severity Categories*

J. D. Whitlow and K. S. Neuhauser

Sandia National Laboratories**, Albuquerque, New Mexico, United States of America

INTRODUCTION

Evaluation of the radiological risks of accidents involving vehicles transporting radioactive materials requires consideration of both accident probability and consequences. The probability that an accident will occur may be estimated from historical accident data for the given mode of transport. In addition to an overall accident rate, information regarding accident severity and the resulting package environments across the range of all credible accidents is needed to determine the potential for a release of radioactive material from the package or for an increase in direct radiation from the package caused by damage to packaging shielding. This information is usually obtained from a variety of sources such as historical data, experimental data, analyses of accident and package environments, and expert opinion. The consequences of an accident depend on a number of factors including the type, quantity, and physical form of radioactive material being transported; the response of the package to accident environments; the fraction of material released from the package; and the dispersion of any released material.

One approach for the classification and treatment of transportation accidents in risk analysis divides the complete range of critical accident environments resulting from all credible accidents into some number of accident-severity categories. The types of accident environments that a package may be subjected to in transportation are often classified into the following five groups: impact, fire, crush, puncture, and immersion. A "critical" accident environment is one of a type that could present a plausible threat to a package. Each severity category represents a portion of all credible accidents, and the total of all severity categories covers the complete range of critical accident environments. This approach is used in the risk assessment codes RADTRAN (Neuhauser and Kanipe 1992) and INTERTRAN (Ericsson and Elert 1983).

Accident-severity categories are ordinarily illustrated on a set of axes forming a grid, as shown in Figure 1 and Figure 2. The axes indicate critical accident environment types and describe the ranges of the parameters used to define the severity categories from zero (no accident) to some value which includes the most severe credible accident. Not all possible types of accident environments present a plausible threat to a package, and these environment types are usually not included in the set of axes on which the severity categories for that package are defined. For example, crush is not considered a critical type of accident environment for massive spent nuclear fuel highway transportation casks because a crush environment severe enough to present a threat to one of these casks is implausible. Although Figures 1 and 2 show two critical types of accident environments (impact and fire), any number of critical environment types may be considered in a severity category scheme. The magnitudes of the most severe credible accident environments depend on a number of

*This work was performed at Sandia National Laboratories, Albuquerque, New Mexico, supported by the United States Department of Energy under Contract DE-AC04-76DP00789.

**A United States Department of Energy facility.

factors including the mode of transport, route characteristics, etc., and usually requires consideration of accidents that are plausible but have never actually occurred. An infinite number of accident environments can be imagined, and a risk analysis need not include those environments that either are physically implausible or have probabilities less than some predetermined cutoff value (e.g. probability less than 10^{-6} per annum).

No constraints are placed on the number or definition of severity categories by the accident-severity category approach, although the previously mentioned codes do provide a maximum on the number of categories. As such, past studies have used different numbers and definitions of severity categories to represent the range of all credible accidents. The authors are not suggesting that restrictions should be placed on the number or definition of severity categories. Each investigator should have the freedom to use any number of categories, defined in any manner as is appropriate for the situation being analyzed. At times the division between two categories is made at an environmental condition where a change in the integrity of the package is anticipated and, thus, is dependent on a specific package.

Some of the differences that can exist between severity category schemes are indicated by the differences between Figure 1 and Figure 2. The category scheme depicted in Figure 1 is similar to schemes published in a 1977 U. S. Nuclear Regulatory Commission report (U.S. Nuclear Regulatory Commission 1977). The scheme shown in Figure 2 consisting of twenty response regions, comparable to severity categories, is similar to a scheme published in a 1987 U. S. Nuclear Regulatory Commission study performed by the Lawrence Livermore National Laboratory (Fischer et al. 1987). Not only are the number of categories different between Figures 1 and 2, but the parameters used to define the categories are also different and no correspondence exists between the definitions of any two categories in the different schemes. The differences in number and definition of severity categories used in different studies make direct comparisons between schemes, with the exception of total risk values, extremely difficult. These differences may also lead to confusion and misinterpretation. An example of such misinterpretation is discussed in Luna, et al. (Luna et al. 1986).

To address these problems, a methodology has been developed which will allow accident probabilities associated with one severity category scheme to be transferred to another severity category scheme. The methodology will permit meaningful comparisons of different studies at the category level in cases where the accident probability information used to determine the category probabilities initially is not available or is not adequate to determine category probabilities across the range of the critical accident environments. If the initial accident probability information is available and adequate, probabilities may be calculated directly for a different category scheme.

METHODOLOGY

A methodology for transferring probabilities between accident-severity category schemes was previously considered in a study performed at Sandia National Laboratories (Spanks 1990). This earlier study developed a matrix to transfer accident probabilities from an eight-category scheme similar to the one shown in Figure 1 to a twenty-category scheme similar to the one shown in Figure 2. Spanks proposed mapping the two severity category schemes onto a common set of axes to form two overlying grids. In this case, correlations between the mechanical parameters of impact speed and cask structural response and the thermal parameters of fire duration and cask thermal response were needed to map the two schemes onto a common set of axes. The probabilities associated with the eight-category scheme were then transferred to the twenty-category scheme using an "equal area weighting" technique which assumes that the accident probability is constant for all accident environments within each severity category.

The assumption that accident probability is constant across the range of accidents represented by each severity category is not representative of actual accident experience. The methodology described in this paper maps the severity category schemes onto a common set of axes to form overlying grids, as was done by Spanks, but transfers probabilities between accident-severity category schemes based on the probability of occurrence of each parameter used to define the severity categories (the parameters along the axes of the overlying grids).

The first step in applying the methodology to transfer probabilities between accident-severity category schemes is to map the schemes onto an appropriate common set of axes. This step, depending on the parameters used with the original axes of the schemes and available accident probability data, may require information or assumptions about package characteristics, accident scenarios and environments, possible impact targets, or other factors in order to relate the original category-defining parameters to the parameters along the common set of axes. In order to be appropriate for the transfer methodology, the parameters for the common set of axes must be chosen such that relationships between probability of occurrence and each of these category-defining parameters can be obtained. The parameters used for the common set of axes may or may not be among the parameters used for any of the original axes. The most commonly reported relationships of probability of occurrence to accident environments use simple accident parameters such as some form of impact velocity, fire duration, etc. Care should be taken not to misinterpret these or any other accident parameters. For example pre-accident speed, velocity change in an impact, and equivalent speed onto an unyielding target are different parameters but might all be loosely referred to as "impact velocity." The methodology described here cannot be used with a scheme in which the parameters defining the severity categories are not explicitly defined.

After the severity category schemes are mapped onto an appropriate common set of axes, the two schemes that are to have probabilities transferred between them are overlaid. To illustrate this, consider the three-category scheme shown in Figure 3 and the four-category scheme shown in Figure 4. Both of these schemes are depicted on a common set of axes. For the purpose of illustration, consider that these simple accident-severity category schemes are for studies of spent nuclear fuel truck transport, have impact and fire as the critical types of accident environments, consider pre-accident speeds of zero to 160 km/hr to be credible, are only for accidents that involve fires, and consider fire durations for an 800 °C, hypothetical, fully engulfing fire of up to two hours. Figure 5 shows the overlay of these two category schemes. The severity categories are not required to be graphically depicted and overlaid to apply the transfer methodology. The boundaries of every category in both schemes need only be accounted for mathematically; however, graphical depiction can provide a good physical awareness of the problem.

Since pre-accident speed and fire duration are the parameters used to define the severity categories depicted in Figure 5, relationships between probability of occurrence and both pre-accident speed and fire duration are needed to apply the methodology to the transfer of probabilities between these category schemes. Information on the severities of transportation accidents provided in a study published by Sandia National Laboratories (Clarke et al. 1976) is used in this study to obtain the needed relationships. The cumulative probability distribution of pre-accident speed shown in Figure 6 and the cumulative probability distribution of fire duration shown in Figure 7 are both adapted from Clarke et al. The cumulative probability distribution shown in Figure 7 was generated, because of a lack of historical accident data, by a Monte Carlo prediction scheme for a model of the expected duration of truck fires for trucks carrying only nonflammable cargo. The relationship shown in Figure 7 is assumed, for the purpose of illustrating the transfer methodology, to be equivalent to the 800 °C, hypothetical, fully engulfing fire used to define the severity categories in Figure 5.

Transportation accidents are random events and as such are not well suited for recording, in exact engineering terms, the environments created during an accident. This lack of historical data describing accident environments in exact terms and the measures necessary to convert data or model results to the parameters used to define severity categories may result in a loss of resolution with the transfer methodology.

The relationships between probability of occurrence and each parameter used to define the severity categories should be as representative as possible of the information used to originally determine the accident probability associated with each category in the scheme that one is transferring from. The purpose of these relationships is to indicate how an accident probability associated with any severity category is distributed within that category so that it may be appropriately transferred to categories in another scheme. The relationships are not used to calculate probabilities directly, but since they are used to determine how accident probabilities are distributed to categories in a different category scheme, they should be consistent with actual accident experience.

To illustrate the transfer of probabilities between severity category schemes, consider that the three-category scheme shown in Figure 3 has a probability associated with each category and these probabilities are desired to be transferred to the four-category scheme shown in Figure 4. The overlay of these two schemes depicted in Figure 5 shows that the range of accident environments represented by category A of the three-category scheme encompasses all accident environments represented by category 1 and part of the environments represented by categories 2, 3, and 4 of the four-category scheme. The probability associated with category A, therefore, should be distributed to categories 1, 2, 3, and 4 of the four-category scheme.

The fraction of accident probability associated with category A to be distributed to each of the four categories in the four-category scheme is determined by use of the cumulative distributions shown in Figures 6 and 7. The joint probability of occurrence for category 1 and for the portions of categories 2, 3, and 4 encompassed by category A is calculated from these cumulative distributions. The value calculated by dividing each of these joint probabilities by the sum of the four joint probabilities gives the fraction of accident probability associated with category A to be distributed to each of the four categories (1, 2, 3, and 4) in the four-category scheme. The parameters of pre-accident speed and fire duration are modeled as independent of each other, which appears reasonable based on accident data (Clarke et al. 1976). For a severity category scheme in which dependence between the parameters defining the scheme is modeled, additional steps or other methods must be used to determine the distribution of the category probabilities within the categories and subsequently transfer the probabilities to another category scheme.

To illustrate the procedure described above, note from Figure 6 that 86% of the truck accidents occur at pre-accident speeds less than 70 km/hr and 72% occur at pre-accident speeds less than 50 km/hr. Figure 7 shows, for truck accidents involving fires, that 97% have fire durations less than 0.5 hours and 79% have fire durations less than 0.25 hours. The joint probability of occurrence for category 1, which includes pre-accident speeds up to 50 km/hr and fire durations up to 0.25 hours, is calculated as

$(0.72) \times (0.79) = 0.57.$

Likewise, the joint probability for the portions of categories 2, 3, and 4 encompassed within category A is calculated;

for the portion of category 2 as $(0.72) \times (0.97 - 0.79) = 0.13$,

for the portion of category 3 as $(0.86 - 0.72) \times (0.79) = 0.11$,

and for the portion of category 4 as $(0.86 - 0.72) \times (0.97 - 0.79) = 0.03$.

The sum of these four probabilities equals 0.84.

The fraction of the accident probability associated with category A to be distributed to category 1 can now be calculated as

$0.57 / 0.84 = 0.68.$

Similarly, the fraction of the accident probability associated with category A to be distributed to categories 2, 3, and 4 is calculated;

for category 2 as $0.13 / 0.84 = 0.16$,

for category 3 as $0.11 / 0.84 = 0.13$,

and for category 4 as $0.025 / 0.84 = 0.03$.

A convenient check on this step is that the fractions should add to one for each category that probabilities are being transferred from. The fractions calculated above for category A do add to one,

$0.68 + 0.16 + 0.13 + 0.03 = 1.00.$

Following a similar procedure shows that the range of accident environments represented by category B of the three-category scheme encompasses a portion of the accident environments represented by categories 2 and 4 of the four-category scheme. The accident probability associated with category B is distributed to categories 2 and 4 in the following fractions: 0.84 to category 2, and 0.16 to category 4.

Likewise, the range of accident environments represented by category C of the three-category scheme encompasses a portion of the accident environments represented by categories 3 and 4 of the four-category scheme. The fraction of the accident probability associated with category C to be distributed to category 3 was calculated to be 0.79 and the fraction to be distributed to category 4 was calculated to be 0.21.

The fractions calculated above that indicate how the accident probabilities associated with each of the three categories (A, B, and C) in the three-category scheme are distributed to each of the four categories (1, 2, 3, and 4) in the four-category scheme are displayed in matrix form in Table 1. The total accident probability associated with each of categories 1, 2, 3, and 4 is calculated by summing the probabilities distributed to each of these categories from categories A, B, and C. As Table 1 shows, the accident probability of category 1 is calculated by multiplying 0.68 by the accident probability of category A. Likewise, the accident probability of category 2 is the sum of the products of 0.16 multiplied by the accident probability of category A and 0.84 times the accident probability of category B. The accident probabilities of categories 3 and 4 are calculated in a similar manner.

SUMMARY AND CONCLUSIONS

A methodology has been developed which allows the accident probabilities associated with one accident-severity category scheme to be transferred to another severity category scheme. The methodology requires that the schemes use a common set of parameters to define the categories. The transfer of accident probabilities is based on the relationships between probability of occurrence and each of the parameters used to define the categories. Because of the lack of historical data describing accident environments in engineering terms, these relationships may be difficult to obtain directly for some parameters. Numerical models or experienced judgement are often needed to obtain the relationships. These relationships, even if they are not exact, allow the accident probability associated with any severity category to be distributed within that category in a manner consistent with accident experience, which in turn will allow the accident probability to be appropriately transferred to a different category scheme.

The ability to transfer accident probabilities between severity category schemes will allow some comparisons at the category level of studies which used different category schemes. This may be useful when comparing, for a similar transport situation, older studies with more recent studies or studies done at different institutions or by different countries. The methodology will allow category probabilities from past studies to be used in current severity category schemes for comparison purposes. By promoting a better understanding of how severity categories in different category schemes relate to one another, the methodology presented in this paper will reduce some of the confusion and misinterpretation associated with comparing different studies.

The ability to transfer accident probabilities between severity category schemes will not directly allow all quantities commonly associated with severity categories to be transferred between the schemes. Risk, for example, is a function of both accident probability and consequence. If this methodology were to be used for the transfer of risk between category schemes, one could transfer the accident probabilities as outlined above and then perform a consequence analysis on the new category scheme to obtain risk values in the new scheme. The basic methodology described in this paper can, however, be used for any quantity, not just accident probability, if the relationships between that quantity and the parameters used to define the categories

are obtainable. Risk, therefore, could be transferred directly between category schemes by following the steps of the methodology and substituting the relationships between risk and each of the category-defining parameters for the relationships between probability of occurrence and each of the category-defining parameters. These risk relationships, however, could be difficult to obtain because of the many factors upon which risk depends and would apply only to the particular case for which it was developed.

REFERENCES

Clarke, R. K., et al., *Severities of Transportation Accidents*, Sandia National Laboratories, Albuquerque, NM, SLA-74-0001 (1976).

Ericsson, A., and Elert, M., *INTERTRAN: A System for Assessing the Impact from Transporting Radioactive Material*, International Atomic Energy Agency, Vienna, Austria, IAEA-TECDOC-287 (1983).

Final Environmental Statement on the Transportation of Radioactive Material by Air and Other Modes, U.S. Nuclear Regulatory Commission, Vol. 1, NUREG-0170 (1977).

Fischer, L. E., et al., *Shipping Container Response to Severe Highway and Railway Accident Conditions*, U.S. Nuclear Regulatory Commission, Washington, D.C., Vol. 1-2, NUREG/CR-4829 (1987).

Luna, R. E., et al., *Response to the Report Entitled "Transportation Risks: Appendix A, DOE Environmental Assessment-Analysis of RADTRAN II Model and Assumptions"*, Sandia National Laboratories, Albuquerque, NM, SAND86-1312 (1986).

Neuhauser, K. S., and Kanipe, F. L., *RADTRAN 4: Volume 3 Users Guide*, Sandia National Laboratories, Albuquerque, NM, SAND89-2370 (1992).

Spanks, L., *A Method To Expand Existing Severity Category Matrices for RADTRAN to 20 Categories*, Sandia National Laboratories, Albuquerque, NM, TTC-0845 (1990).

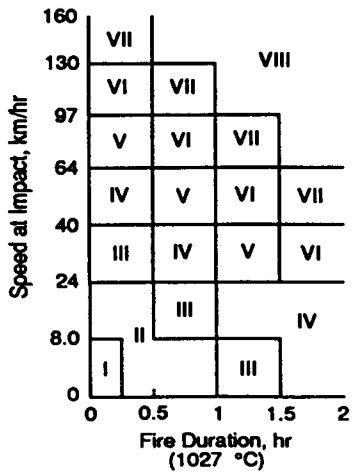

Figure 1: Eight-category accident-severity classification scheme (adapted from U.S. Nuclear Regulatory Commission 1977).

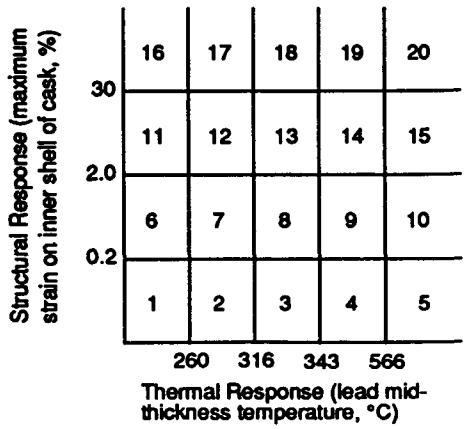

Figure 2: Twenty-category accident-severity classification scheme (adapted from Fischer et al. 1987).

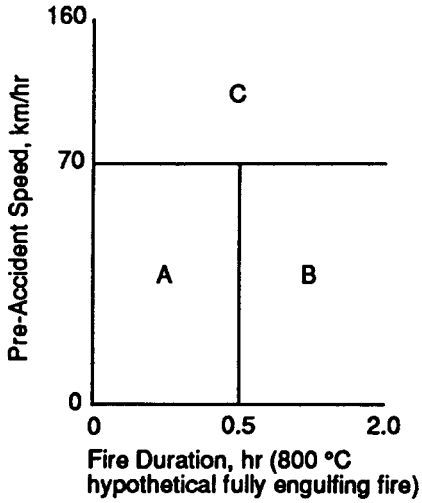

Figure 3: Three-category accident-severity classification scheme.

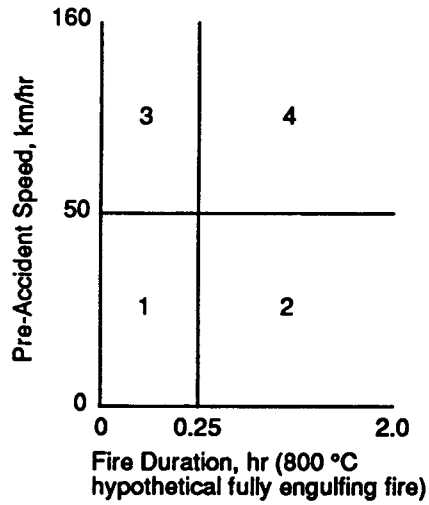

Figure 4: Four-category accident-severity classification scheme.

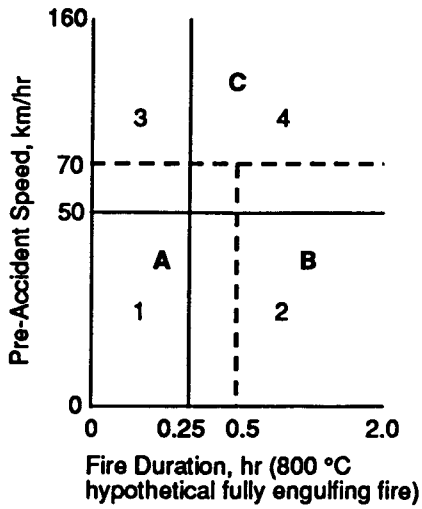

Figure 5: Overlay of three-category and four-category schemes.

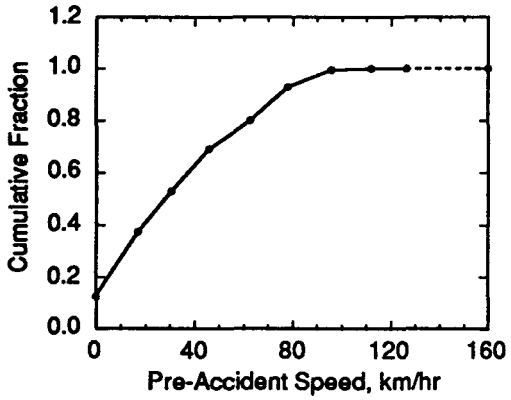

Figure 6: Cumulative probability distribution of pre-accident truck speeds (adapted from Clarke et al. 1976).

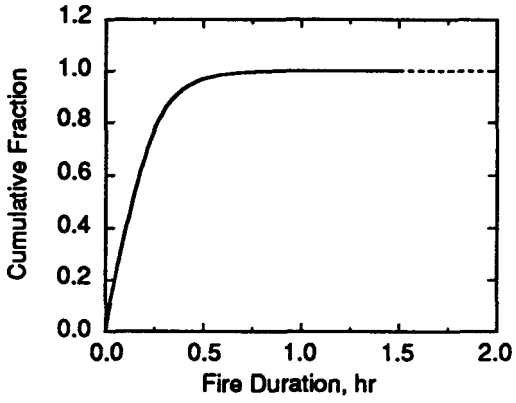

Figure 7: Cumulative probability distribution of fire duration in truck accidents involving fire (adapted from Clarke et al. 1976)

Table 1: Transfer fractions from example in text.

Categories that accident probabilities are being transferred to.	Categories that accident probabilities are being transferred from. A	B	C	
1	.68	---	---	$P_1 = 0.68P_A$
2	.16	.84	---	$P_2 = 0.16P_A + 0.84P_B$
3	.13	---	.79	$P_3 = 0.13P_A + 0.79P_C$
4	.03	.16	.21	$P_4 = 0.03P_A + 0.16P_B + 0.21P_C$

Design of an Actively Cooled Plate Calorimeter for the Investigation of Pool Fire Heat Fluxes*

J. A. Koski, N. R. Keltner, and V. F. Nicolette

Sandia National Laboratories, Albuquerque New Mexico, United States of America

S. D. Wix

Gram, Inc. Albuquerque, New Mexico, United States of America

INTRODUCTION

For final qualification of shipping containers for transport of hazardous materials, thermal testing in accordance with regulations such as 10CFR71 must be completed. Such tests typically consist of 30 minute exposures with the container fully engulfed in flames from a large, open pool of JP4 jet engine fuel. Despite careful engineering analyses of the container, testing often reveals design problems that must be solved by modification and expensive retesting of the container. One source of this problem is the wide variation in surface heat flux to the container that occurs in pool fires. Average heat fluxes of 50 to 60 kW/m^2 are typical and close the values implied by the radiation model in 10CFR71, but peak fluxes up to 150 kW/m^2 are routinely observed in fires (Keltner, et al,

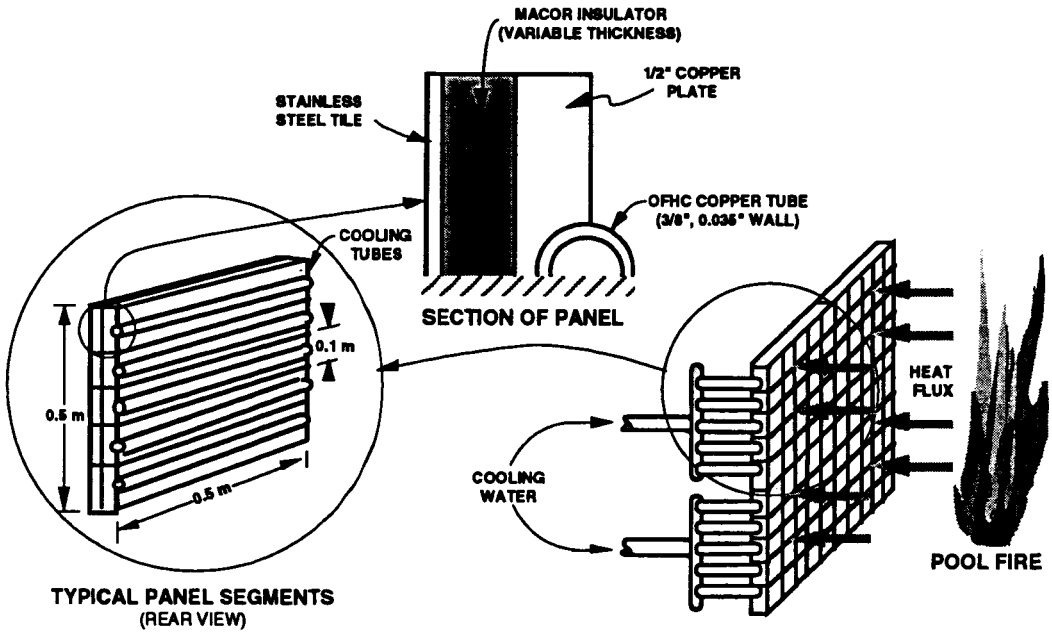

Figure 1. Sketch of actively cooled calorimeter experiment.

* This work supported by the U.S. Department of Energy under Contract No. DE-AC04-76DP00789.

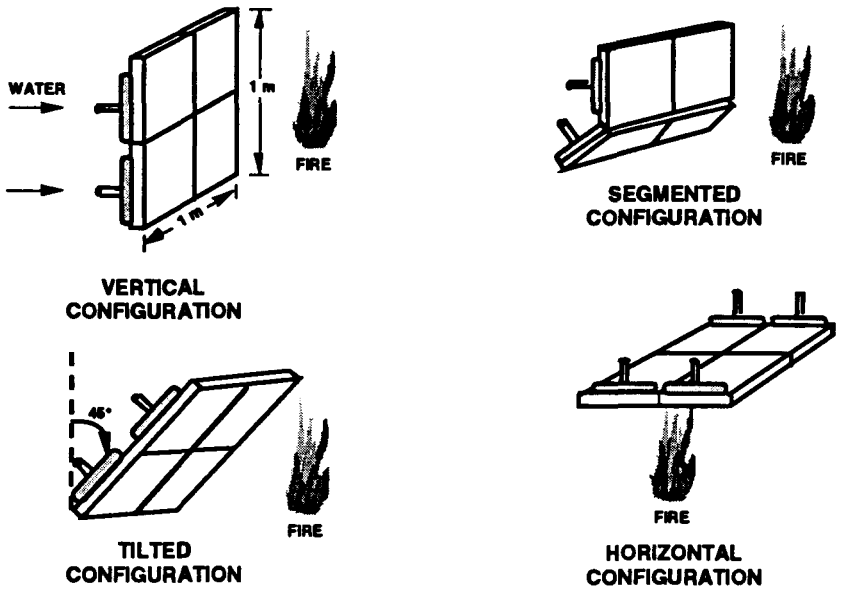

Figure 2. Future test configurations for actively cooled panels.

1990). Heat fluxes in pool fires have been shown to be a function of surface temperature of the container, height above the pool, surface orientation, wind, and other variables (Nicolette and Larson, 1990). If local variations in the surface heat flux to the container can be better predicted, design analyses will become more accurate, and fewer problems will be uncovered during testing. The objective of the calorimeter design described in this paper is to measure accurately pool fire heat fluxes under controlled conditions, and to provide data for calibration of improved analytical models of local flame-surface interactions.

The calorimeter design consists of an actively cooled plate as shown in Figure 1. The initial configuration consists of a water cooled flat plate that is 1 m square. Later configurations may be tried to simulate different surface geometries as shown in Figure 2. The purpose of the water cooling is twofold: first, it permits approaching steady state surface temperatures during the fire, and, second, by measuring water temperature rise and flow rate, it allows determination of the heat flux to the cooled surface. Segmentation of the surface into zones permits some local resolution of surface heat fluxes. The vertical flat plate geometry was chosen for the initial experiments because it matches a geometry already analyzed by one of the authors (Nicolette and Larson, 1990). Water cooled calorimetry also has some advantages over methods used for previous similar experiments.

In the past (Gregory, et al. 1989, Gregory, et al. 1987, Nelsen 1986, Longenbaugh, et al. 1990) transient inverse heat conduction methods have been used to estimate surface temperatures and heat fluxes. The inverse technique consists of monitoring temperature rises at internal calorimeter or shipping container locations, and then solving the heat conduction problem "backwards" to estimate surface heat fluxes and temperatures that are consistent with the internal temperatures. Such tests have shown (Keltner, et al. 1990) that "massively thermal" objects behave differently in fires than smaller objects. Indications are that the object size or surface temperature of the container can play a role in determining local heat fluxes that are beyond the effects predicted from the simple radiative heat transfer laws. The analytical model described briefly here and in Nicolette and Larson, 1990 can be used to understand many of these characteristics. Unlike the previous experiments that provide only a brief time at each surface temperature as the calorimeter heats up, the current approach will allow a more careful near steady-state investigation of the effect of surface temperature and other variables. The technique also lends itself to the easy inclusion of other diagnostic methods such as radiometers, intrinsic thermocouples, heat flux gauges, and fiber optic probes. By performing the initial tests in the Smoke Emissions Reduction Facility (SMERF), a wind shielded facility, a major source of test-to-test experimental variation will be removed. Later tests in open pools will be used to assess wind effects.

DESIGN ANALYSES

To balance the various design choices for the calorimeter, finite element analyses were conducted with the Topaz2D computer code (Shapiro, 1986). Typical issues addressed were temperature uniformity of the actively cooled surface, time to reach steady state conditions, selection of appropriate materials, temperature rise of the coolant, and methods for controlling surface temperature. Where necessary, hand calculations of the hydraulics and convective film coefficient augmented the finite element analyses.

Initial calculations indicated that simply varying the flow velocity of the cooling water could not provide the desired plate surface temperature range of 200°C to 1000°C. This led to a design where water velocities are held constant, but installations of insulating tiles of various thicknesses permit temperature control as shown in Figure 1. Tile thicknesses of 3.2 mm, 6.4 mm and 11.7 mm permit the controlling surface temperatures as shown in Figure 3 where constant heat fluxes have been applied to the actively cooled surface. As indicated in the figure, the calorimeter surface temperature is a function of the surface heat flux, so that in practice, insulating tile thickness will be chosen based on previous experimental results. Transient calculations indicate that all configurations reach steady state surface temperatures in less than 10 minutes. To prevent heat flux to the rear surface of the calorimeter, the piping manifold and other components behind the actively cooled surface will be enclosed in a heavily insulated support frame and box. All instrumentation leads will be routed along cooling pipes and wrapped with commercial high temperature insulating material.

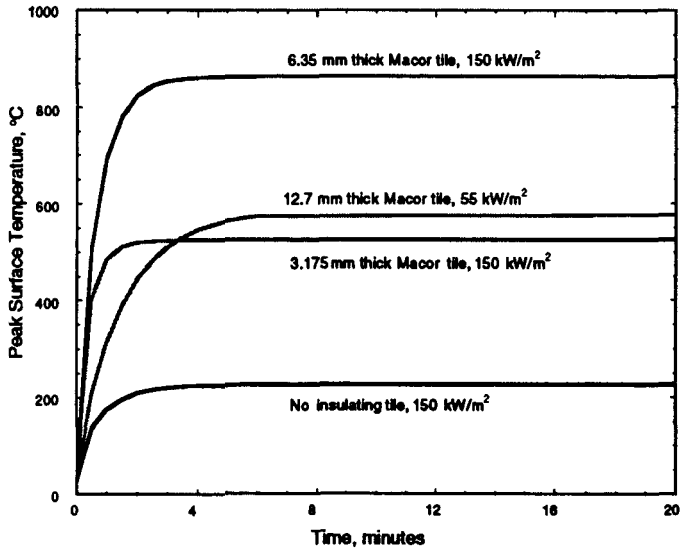

Figure 3. Time to reach steady state for constant heat flux to calorimeter surface

Early calculations showed that, because of relatively low thermal conductivity, the use of stainless steel tubes and base plates would lead to variations in surface temperature of hundreds of degrees unless very close tube spacing and a thick plate was used. Since copper is widely available, easy to join to tubing by brazing, and has a high thermal conductivity, it solved this problem. With copper, even with a 10 cm tube spacing, surface temperatures could be held within 40 to 50°C across the entire plate as shown in Figure 4. This includes the effect of temperature rise in the cooling tubes as water flows across the plates. The calculations demonstrate that more uniform surface temperatures occur for the thicker insulating tiles and the low surface heat fluxes.

In early designs, the actively cooled 1 m x 1 m surface was broken into four equal quadrants, each with its own insulating tile and a 6 mm thick stainless steel cover plate as shown in Figure 2. Analysis of thermal stresses during heating of the stainless steel plates led to concerns about bowing of the center of these plates toward the fire when heated. This would create a significant gap between the stainless steel and the underlying ceramic. The solution to this problem was to break the stainless steel surface and underlying ceramic tiles into smaller 10 cm x 10 cm tiles, use thinner 1.8 mm thick stainless steel tiles, and to provide the attachment bolts near the center of the tiles to resist the bowing tendency. Infrared thermography of the tiles during radiant heat testing will be used to assure that no surface tile temperature variations occur due to thermal bowing. The underlying copper cooling plates were broken into 20 segments that are 0.5 m x 0.1 m as shown in Figure 1.

For the maximum anticipated heat flux of 150 kW/m^2, the water temperature rise through the tubes for a 2 m/s flow velocity is about 30°C. This difference can be accurately measured by thermocouples. If experimental heat fluxes prove to be lower, the water flow velocity can be reduced to achieve the desirable temperature rise necessary for good measurements.

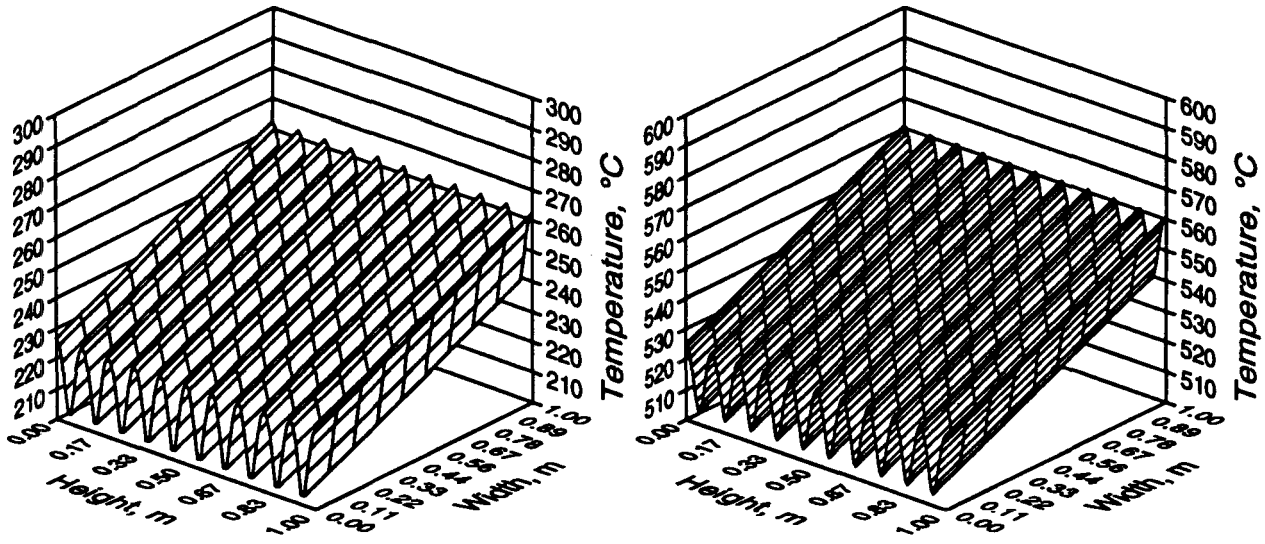

(a) no insulating tiles

(b) 3.2 mm insulating tiles

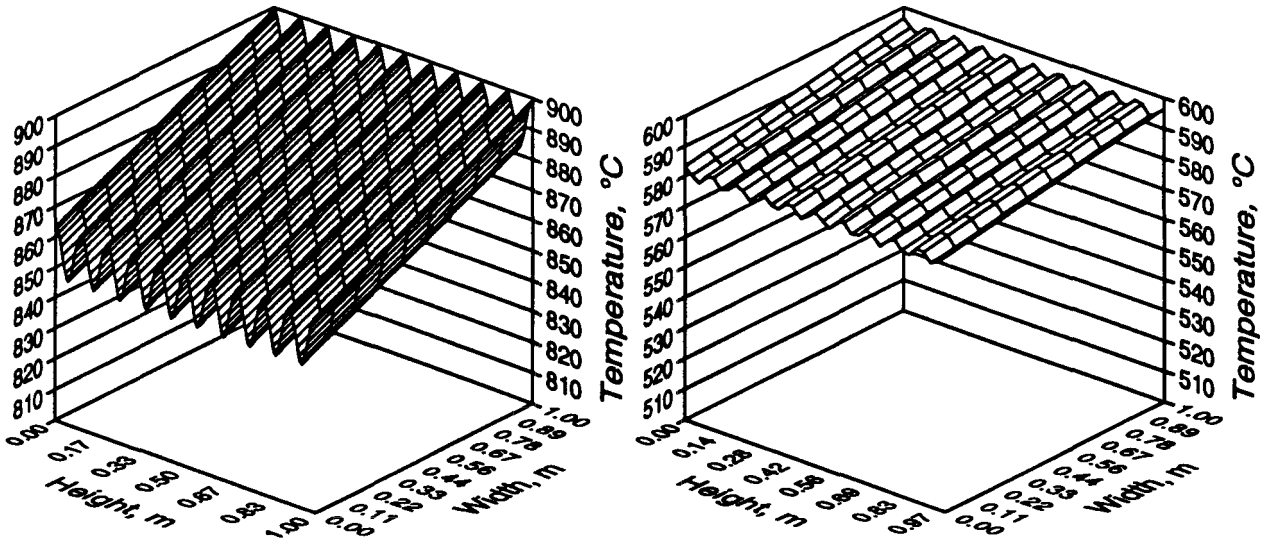

(c) 6.4 mm insulating tiles

(d) 12.7 mm insulating tiles

Figure 4. Calorimeter surface temperature distribution for constant heat flux to surface. Upward slope across width is due to heating of water. For (a), (b), and (c) a surface heat flux of 150 kW/m^2 is assumed. For (d) the surface heat flux is 55 kW/m^2.

INSTRUMENTATION AND DIAGNOSTICS

The calorimeter diagnostic instrumentation includes intrinsic thermocouples, radiometers, turbine flow meters, thermocouple probes and washer thermocouples. Since the primary function of the calorimeter is water calorimetry, selection of the instrumentation used to measure the flow rate and temperatures of the water through the calorimeter is very important. The turbine flow meters have a linearity of +/- 0.5 per cent and a repeatability of +/- 0.1 per cent over the calibrated flow rate range. A filter is used with the flow meter to prevent damage. The flow meter is located on the inlet of the calorimeter and straight lengths of pipe have been included both upstream and downstream of the flow meter to ensure accurate flow measurement. For water temperature measurement, Type K thermocouple probes were selected. There is a single temperature probe in the inlet pipe to the calorimeter

and a probe in the outlet pipe of each section of the calorimeter. Type K thermocouples were selected because of the accuracy, (+/- 1°C), operating temperature range, and output voltage. A small diameter probe is used to ensure adequate transient response.

Radiometers are used to measure the radiative heat flux of the pool fire. Since the calorimeter measures total heat flux (radiation and convection), data from the radiometers will allow determination of the convective heat flux contribution. Previous experiments (Nakos and Keltner, 1989) indicate that the convective contribution is on the order of 10 to 20 per cent of the total surface heat flux for the fires of interest. The radiometers are also calibrated as optical pyrometers. This will permit data to be acquired on the black-body flame temperature during the open pool fire tests. The radiometers are the Schmidt-Boelter type. The Schmidt-Boelter type was chosen to minimize error due to convective effects are seen with a Gardon type gauge. The body of the radiometer is water-cooled to prevent damage to the instrument. The gauge range is 200 kW/m^2, which is well above the expected maximum heat flux of 150 kW/m^2 from the pool fire. The radiometers will be located behind the calorimeter copper plate and can see the fire through small holes (approximately 12 mm) in the calorimeter. The radiometer field of view is 11 degrees, which allows the radiometer to see the pool fire without seeing the calorimeter. A nitrogen gas purge nozzle is located next to the radiometer to prevent soot from accumulating on the radiometer window.

Intrinsic thermocouples are used to measure the back surface temperature of the stainless steel plates. An intrinsic thermocouple consists of two thermocouple wires welded near each other to the stainless steel plate. Properly used, this technique produces a good estimate of the rear surface temperature of the plate. By knowing the back surface temperature of the stainless steel plate, the heat flux on the front surface of the plate, and the thermal conductivity of the plate, the front surface temperature can be estimated. This will provide data on localized cooling zones near the surface of the calorimeter. The surface temperature and heat flux measurements will also provide indirect data on the effect of soot particles on surface heat flux.

Type K washer thermocouples are used to monitor the back side of the copper plate temperature. This temperature measurement is used as a safety feature and a data check to determine that the copper plates remain cool at all times during the test.

GRAY GAS MODEL

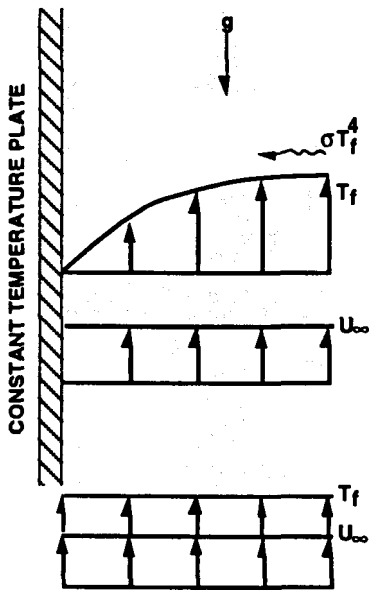

Figure 5. Model for study of effects of gray gas on radiation heat transfer.

Measurements made with the calorimeter can be used to calibrate analytical models of the geat flux to an object in a fire. There are many instances where it would be advantageous to have a simple analytical model to calculate heat fluxes to large objects in pool fires. For small objects in a fire, heat fluxes are reasonably approximated by assuming a simple σT^4 radiative boundary condition. However, as discussed above, large objects can significantly influence the local fire environment, resulting in reduced heat fluxes to the large object. An analytical model that could model the interaction between a large object and a fire, and calculate an appropriate heat flux for such an object in a fire would be of great benefit to shipping container designers. The calculated thermal boundary conditions could then be used with a finite element model of a shipping container to predict its thermal response in a fire.

In order to capture this influence of a large object on the local fire environment, a model should have the following features: 1) It should focus on the radiative interaction between the large object and the fire (since 80-90 per cent of the heat transfer is radiative for the pool fires of interest to shipping cask designers); and, 2) It should account for the influence of object size and orientation on the fire.

Such a model has been developed previously (Nicolette and Larson, 1990), and will only be summarized here. The model consists of a vertical flat plate at constant uniform temperature completely engulfed by flames of large thickness (Figure 5). Combustion gases flow upward along the plate at a specified uniform velocity. Thermal radiation exchange between the surface of the plate and the combustion products is modeled assuming 1-D gray gas radiative heat transfer normal to the plate surface. The gray gas is assumed to have a constant, uniform absorption coefficient. For fires of this type,

scattering can be neglected, and the extinction coefficient is well approximated by the absorption coefficient. The combustion source term can be modeled in a variety of ways, including: 1) a uniform heat generation rate, 2) an Arrhenius-based heat generation rate, or 3) zero heat generation (representative of large quenched regions near the object).

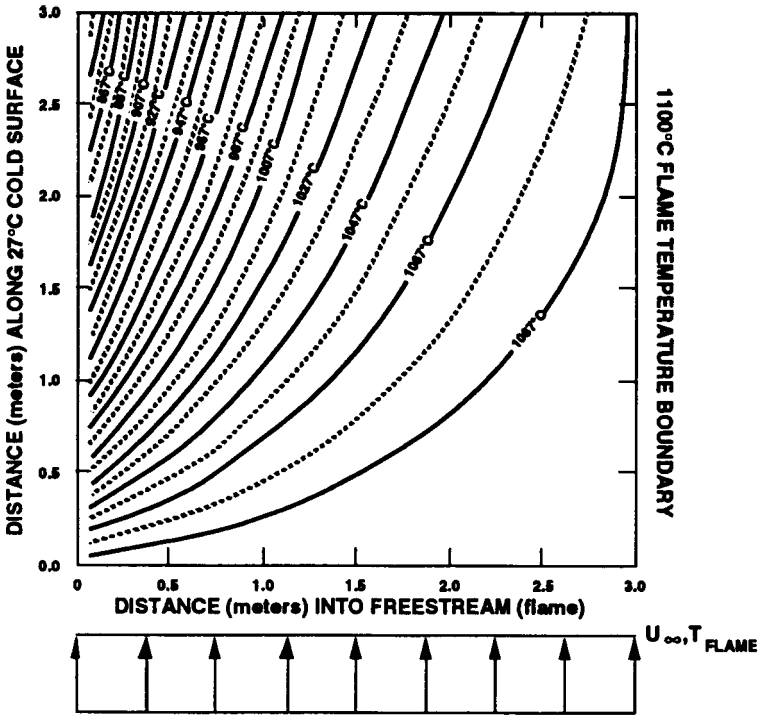

Figure 6. Typical isotherms calculated with gray gas model.

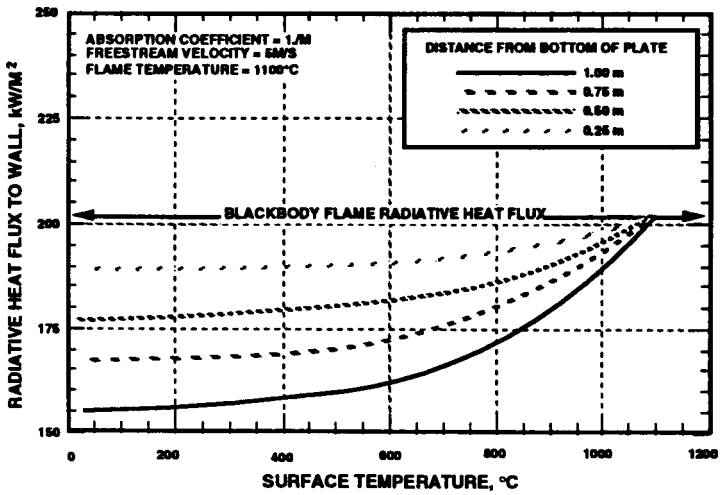

Figure 7. Incident heat fluxes to surface calculated with use of gray gas model.

This simple model predicts the development of a radiation boundary layer (Figure 6) as a result of the radiation/convection interaction between a large, cold plate and a fire. This boundary layer lowers the combustion gas temperatures near the plate, which results in a reduction in the incident radiative heat flux to the plate. Larger plates show a greater reduction in the incident radiative heat flux. For a 1 meter long plate, the reduction in incident radiative heat flux is calculated to be almost 25 per cent near the end of the plate for typical pool fire conditions (Figure 7).

With an actively cooled plate calorimeter, we can assess whether or not we are capturing the essential physics with our simple gray gas model. Since the gray gas model presently uses a constant and uniform plate temperature, the actively cooled plate calorimeter (with its relatively constant and uniform surface temperature) can provide an appropriate test for the analytical model. In particular, do the incident heat fluxes measured by the calorimeter show the same trends along its length as predicted by the simple model? If so, then we can have further confidence that our simple gray gas model does indeed capture the essential physics of the problem.

The other important benefit of the actively cooled plate calorimeter experiments is that they will allow us to better quantify two of the important parameters in the simple model. To date, the gray gas model has been used in an interpretive rather than predictive manner because of large sensitivities in the model to the values of extinction coefficient and heat generation rate. It would be necessary to incorporate complicated soot production, combustion, and turbulence models into the gray gas model in order to accurately predict these parameters from first principles. This is not desirable for such a simple model. Instead, data from the actively cooled calorimeter experiments will allow us to estimate the magnitude of these sensitive parameters that best enable the gray gas model to match the experimental heat fluxes. Our intent is that we will then be able to use the gray gas model to predict with confidence the heat fluxes to a large object in a pool fire.

SMERF FACILITY

Initial tests with the calorimeter will be performed in the Smoke Emissions Reduction Facility (SMERF) at Sandia. This facility will permit elimination of wind as a variable during early tests. Wind produces the biggest, uncontrollable effect on open pool fires used to simulate postulated transportation accident environments. In developing wind shielded facilities, demonstration was necessary to prove that they closely simulate the environment in a large open pool fire. Demonstration tests in the Small Wind Shielded Facility (SWISH) have shown that it can reproduce the thermal environment of an open pool fire and comply with local air quality regulations (Keltner and Kent, 1989). The larger unit, SMERF, is based on a scale-up of SWISH. Certification tests of SMERF are underway.

SMERF has a 3 m x 3 m pool centered in the floor of a "cubical" test chamber that is approximately 6 m on a side. A sketch of the facility is shown in Figure 8. The walls of the chamber are water cooled to provide an appropriate boundary condition for radiative heat loss from the flames; this provides part of the control of the temperature in the flames. Air flow into the chamber is controlled by four variable speed fans.

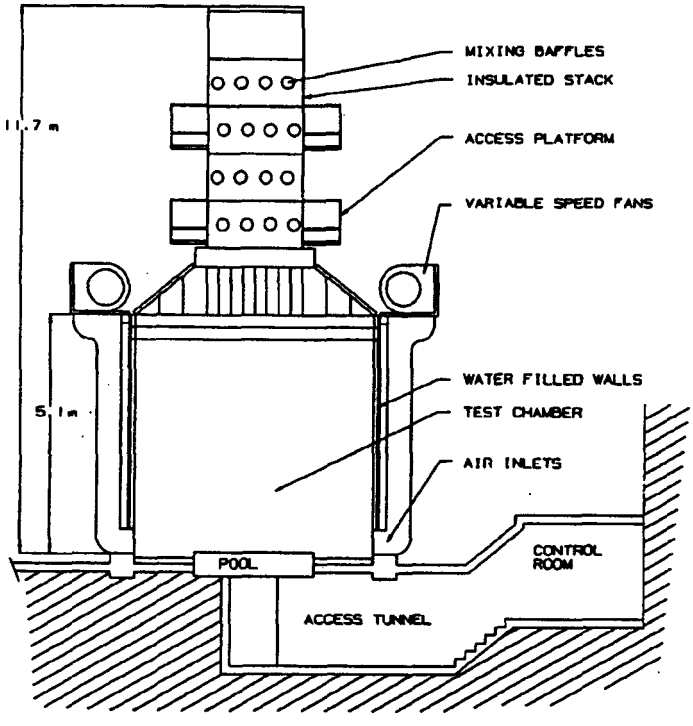

Figure 8. Smoke Emissions Reduction Facility (SMERF)

Control of the facility and data acquisition will be handled by a minicomputer based system with a total capacity of 140 channels of thermocouples and high level signals. Instrumentation or visual access to the test unit can be provided from a tunnel under the pool floor. There are observation ports in the walls of the facility to provide for viewing of the test unit, for real time or flash radiography, or for optical instrumentation.

A number of tests have been run using a 1.8 m circular pool in SWISH to define the thermal environment for comparison with extensive data from tests conducted at Sandia in a 9 m x 18 m open pool. The wind-shielded facility was shown to provide a stable environment for making detailed fire measurements. These tests were summarized for the 1989 PATRAM (Keltner and Kent, 1989).

The use of a wind-shielded facility, such as SMERF, offers significant advantages for studies of heat transfer in pool fires. The fuel recession rate is measured continuously. The current system uses hydrostatic pressure; an ultrasonic system is under development. The air flow rate is measured continuously and controlled. Measurements of these two parameters provide accurate inputs for fire models. By eliminating the wind effects, SMERF offers a fairly stable flame volume in which temperature, heat flux, velocity, and other parameters can be measured. This provides good data to compare with model predictions.

SUMMARY

In order to better measure local heat fluxes in open pool fires, an actively cooled calorimeter has been designed and analyzed. As this paper is being prepared, the calorimeter is in fabrication. Following fabrication, testing in a radiant heat facility is planned to assure proper performance before introduction into the pool fire environment. Initially, testing in the SMERF facility will assure reproducibility of tests by removing wind effects. As the program progresses, tests in open facilities, and with different geometries are anticipated. Experimental data from the initial tests will be compared continuously to the gray gas model, and as experiments proceed, the gray gas analytical model will be refined with the goal of improving finite element code analysis of shipping containers.

REFERENCES

Gregory, J. J., R. Mata, Jr., and N. R. Keltner, *Thermal Measurements in a Series of Large Pool Fires*, SAND 85-0196, Sandia National Laboratories, Albuquerque, NM, 1987.

Gregory, J. J., N. R. Keltner, and R. Mata, Jr., *Thermal Measurements in Large Pool Fires*, Journal of Heat Transfer, No. 111 (1989), pp. 446-454.

Keltner, N. R. and L. A. Kent, *A Wind Shielded Fire Test Facility*, in Proc. of The 9th Symposium on the Packaging and Transportation of Radioactive Materials, July 11-16, 1989, Washington, D.C., CONF-890631, prepared by Oak Ridge National Laboratory, 1989.

Keltner, N. R., V. F. Nicolette, N. N. Brown, and B. L. Bainbridge, *Test Unit Effects in Large Fires*, Journal of Hazardous Materials, No. 25, (1990), pp. 33-47.

Longenbaugh, R. S., L. C. Sanchez, and A. R. Mahoney, *Thermal Response of a Small Scale Cask-Like Test Article to Three Different High Temperature Environments*, DOT/FRA/ORD-90/01, U. S. Department of Transportation, Federal Railroad Administration, Washington, D.C., 1990.

Nakos, J. T., and N. R. Keltner, *The Radiative-Convective Partitioning of Heat Transfer to Structures in Large Pool Fires*, in HTD - Vol. 106, Heat Transfer Phenomena in Radiation, Combustion, and Fires, R. K. Shah, Ed., American Society of Mechanical Engineers, 1989.

Nelsen, J. M., *Determination of Net Heat Fluxes and Assessment of Test-to-Test Thermal Input Variation for Three Large Engulfing Open Pool Fire/Calorimeter Tests*, SAND 85-1821, Sandia National Laboratories, Albuquerque, NM, 1986.

Nicolette, V. F., and D. W. Larson, *The Influence of Large, Cold Objects on Engulfing Fire Environments*, Proceedings of AIAA/ASME Thermophysics and Heat Transfer Conference, Seattle, WA, June 18-20, 1990.

Shapiro, A. B., *Topaz2D -- A Two-Dimensional Finite Element Code for Heat Transfer Analysis, Electrostatic, and Magnetostatic Problems*, UCID-20824, Lawrence Livermore National Laboratory, Livermore, CA, 1986.

Hazardous Materials Package Performance Regulations*

N.A. Russell, R.E. Glass, J.D. McClure, and N.C. Finley

Sandia National Laboratories**, Albuquerque, New Mexico U.S.A. 87185

INTRODUCTION

The hazardous materials (hazmat) packaging development and certification process is currently defined by two different regulatory philosophies, one based on "specification" packagings and the other based on "performance" standards. With specification packagings, a packaging is accepted for hazmat transport if it is constructed according to an agreed set of design specifications. In contrast, performance standards do not specify the packaging design; they specify performance standards that a packaging design must be able to pass before it can be certified for transport. In this case, the packaging can be designed according to individual needs as long as it meets these performance standards. Performance standards have been used nationally and internationally for about 40 years to certify radioactive materials (RAM) packagings. In the United States, two major packaging categories for RAM, Type A and Type B, must satisfy distinct performance standards listed in Title 10, Code of Federal Regulations part 71 (10CFR71) (USNRC 1991). Type A packagings are for transporting relatively small quantities of RAM as defined by curie level and hazard level, and Type B packagings are for transporting larger quantities. Thousands of these packages are shipped annually, yet, since the performance standards were instituted, there have been no documented releases above the regulatory limit from a Type B package during transportation and only limited releases from Type A packages (Cashwell and McClure, 1992). Thus, it is reasonable to state that for RAM transport, performance specifications have maintained transport safety.

A committee of United Nations' experts recommended the performance standard philosophy as the preferred regulation method for hazmat packaging (United Nations 1986). Performance standards for hazmat packagings smaller than 118 gallons have been adopted in 49CFR178 (USDOT 1991). Packagings for materials that are classified as toxic-by-inhalation must comply with the performance standards by October 1, 1993, and packagings for all other classes of hazardous materials covered in 49CFR178 must

*This work performed at Sandia National Laboratories, Albuquerque, New Mexico, U.S.A., supported by the U.S. Department of Energy under Contract No. DE-AC04-76DP00789.

**A United States Department of Energy Facility

comply by October 1, 1996. Compressed gas cylinders are excluded from 49CFR178.

A main concern when setting performance standards is determining the appropriate standards necessary to assure adequate public protection without making the packagings prohibitively expensive for the shipping industry. For packages containing bulk (in excess of 118 gallons) quantities of materials that are extremely toxic by inhalation, there currently are no performance requirements. This paper discusses a Hazmat Packaging Performance Evaluation (HPPE) project being conducted at Sandia National Laboratories for the U.S. Department of Transportation Research & Special Programs Administration (DOT-RSPA) to look at the subset of bulk packagings that are larger than 2000 gallons. The objectives of this project are to evaluate current hazmat specification packagings and develop supporting documentation for determining performance requirements for packagings in excess of 2000 gallons that transport hazardous materials that have been classified as extremely toxic by inhalation (METBI).

HAZARDOUS MATERIALS PACKAGING PERFORMANCE EVALUATION METHODOLOGY

One major component of the HPPE project involves using atmospheric dispersion codes to estimate the effects of packaging leak rate of METBI on the distance from the release within which the airborne concentration of METBI is considered dangerous. This involves studying the toxicity data for the METBI materials to determine which toxicity parameters to use to determine what concentration limits to consider dangerous and how to apply these data to exposure durations that differ from the duration reported for the particular toxicity parameter. Another major component of the HPPE project involves estimating the performance of current bulk hazmat specification packagings. These estimates of packaging performance can be combined with the calculations of the effects to provide guidance for selecting packaging performance specifications.

The project has been divided into the following tasks: review existing regulations, review current specification packagings, describe accident environments, characterize the METBI materials, select appropriate toxicity parameters, develop computer modeling capabilities, and develop guidance for selecting packaging performance requirements.

The review of existing regulations showed that, although hazmat is required to be transported in its corresponding specification packaging or packagings, these specification packagings were developed primarily on a case by case basis and do not provide a consistent level of protection between specification packaging designs.

The review of specification packagings is currently under way. Bulk packaging provisions for METBI materials shipped in quantities in excess of 2000 gallons are specified in 49CFR178. The following representative specification packagings have been chosen for review: DOT51, MC331, MC105, MC112, MC113, MC114, IM101, and MC312. These particular specification packagings span both the truck and rail transportation modes and include cargo tanks, portable tanks, and pressurized and non-pressurized rail tank cars. The salient parameters for these specification packagings will

be obtained from the appropriate sections in 49CFR and the ASME Boiler & Pressure Vessel Code (ASME 1992). These salient parameters will subsequently be used to estimate the predicted response of these specification packagings to thermal, impact, and crush loads such as those specified in the 49CFR and 10CFR performance specifications.

The task of describing transportation accident environments involved reviewing hazmat accident literature. Hazmat accident data indicate that 98% of light truck/van accidents have velocity changes during impact of less than 30 mph (UMTRI 1980). However, other than this study, there is little data specific to hazmat transportation. For hazmat that is transported by routine road and rail, it has been decided for this project that the accident severity studies for radioactive materials can be applied to hazmat transport.

To characterize the METBI materials, a literature review was performed to compile data on material properties and measures of toxicity for the METBI materials. Thermodynamic properties of the METBI materials are necessary because some of the dispersion modeling requires thermodynamic properties. Data on toxicity is necessary to help determine the level of dangerous of a release. In addition, the METBI materials have been studied to determine their relevant release characteristics. The relevant release characteristics include: determining if a particular METBI material disperses as a dense gas, buoyant gas, or remains liquid; determining if it contains aerosol which will be removed by gravitational settling from the airborne concentration as it disperses; and determining if it reacts with compounds prevalent in surrounding air (such as water vapor) to disperse as a reaction product rather than as the original METBI. This information is necessary to accurately model the dispersion of METBI in the event of an accidental release.

Selecting appropriate toxicity parameters involved studying the various measures of toxicity to determine which are most appropriate to this application. There are several different types of toxicity parameters reported in the literature for toxic materials, but there is a large degree of uncertainty associated with using the readily available toxicity parameters for calculating comparative risks for this project. Common toxicity parameters include: the ERPG-2, which is the maximum airborne concentration below which it is believed that nearly all individuals could be exposed for up to one hour without experiencing irreversible or other serious health effects or symptoms that could impair an individual's ability to take protective action; the LC_{50}, which is defined as an inhalation exposure level that is lethal to half of an exposed population; the LD_{50}, which is defined as an ingestion exposure level that is lethal to half of an exposed population; the LClo, which is defined as the lowest observed lethal inhalation exposure level; the LDlo, which is defined as the lowest observed lethal ingestion exposure level; the TLV, which is defined as a safe level of occupational exposure (customarily a time-weighted average value for 40 hours of exposure); and the STEL, which is defined as the level of exposure permitted for brief periods of time, such as to permit life saving activities, etc.) (Landis and van der Schalie, 1990).

One of the main uncertainties in using these parameters stems from the fact that most toxicity data are measured on animals in a laboratory setting. Therefore, applying the toxicity data to humans introduces uncertainty. Additional uncertainty is introduced by

the difference between the exposure time expected during an accidental release (i.e., either the time a population is exposed while the toxic cloud drifts by, or the time the population is exposed before they are either evacuated or isolated by the emergency responders) and the exposure time reported for the toxicity parameter. For example, if a material has a reported exposure limit that was measured for an 8-hour exposure and the toxic cloud is calculated to be gone within an hour, how does that one hour exposure compare to the limit reported for an 8-hour exposure? Depending on how the human body reacts to this particular toxic material, a one hour exposure to a concentration of 8 times the 8-hour limit is not necessarily the same as an 8 hour exposure to the 8-hour concentration limit (i.e., the integrated dose is not necessarily the controlling factor). A third but related uncertainty is caused by the inconsistency of exposure times reported for the various toxicity data. The exposure times are frequently inconsistent even for the same parameter. For example, for the METBI materials, the LClo is reported for exposure times ranging from 1 minute to 8 hours.

The method chosen for applying existing toxicity parameters to this project provides a general rule of thumb for using toxic parameters for exposure times that are different than that reported for the parameter. This method was chosen because it has been used in other DOT-RSPA supported research. For an exposure time that is on the order of the time period of the particular toxic parameter, the method recommends using the value of that parameter as an "average concentration" during the exposure, rather than a peak concentration never to be exceeded during the exposure time. When the predicted exposure time is less than ¼ the time period of the reported guideline, the method recommends scaling factors based on exposure time. However, it must be emphasized that these guidelines are general and do not necessarily accurately represent each individual chemical.

The atmospheric dispersion of METBI in the event of a release is being modeled to determine the effect of packaging leak rate on the distance at which the half-hour integrated airborne concentration exceeds the chosen exposure limits. The dispersion model selected depends on whether the METBI released is a buoyant or dense gas. Instantaneous releases of buoyant ideal gases have been modeled with Gaussian dispersion, which is a theoretical solution to the partial differential equations governing diffusion. This Gaussian dispersion model relies on characterizing the meteorological conditions according to atmospheric stability and wind speed. The continuous releases of buoyant gases and both the instantaneous and continuous releases of denser-than-air gases are being modeled with the SLAB code (Ermak 1988). The SLAB code solves modified forms of the mass/energy conservation equations.

A generic atmospheric dispersion graph for hypothetical METBI Material X is shown in Figure 1. In Figure 1, the packaging leak rate which produces a maximum 30-minute average downwind airborne concentration equal to a selected exposure limit is graphed as a function of downwind distance from the release. The critical leak rate for each METBI is analogous to the A2/week leak rate used in RAM transport.

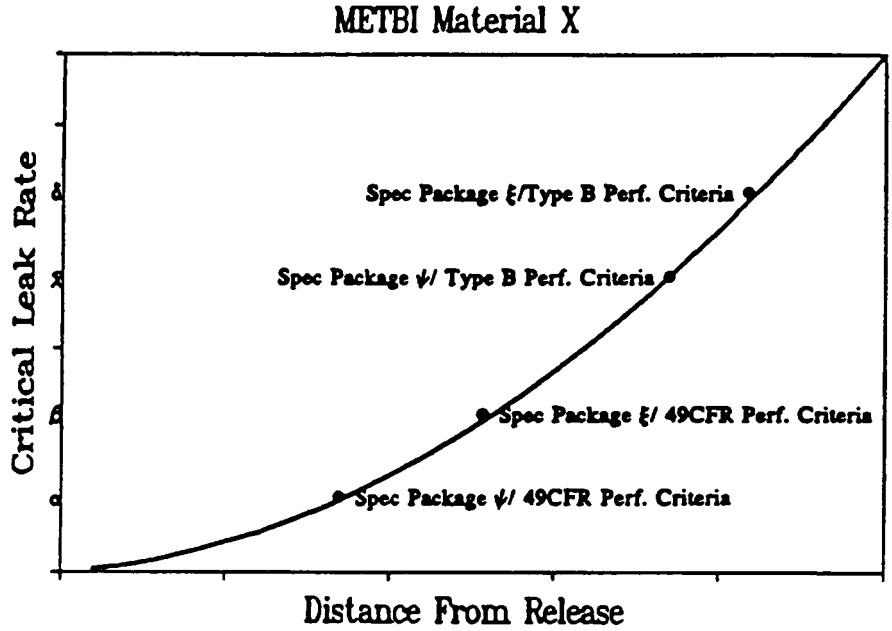

Figure 1. Critical Packaging Release Rate versus Distance At Which 30-minute Exposure Limit Occurs for METBI Material X

For this project, the exposure limits have been chosen such that harmful effects are not expected to occur from a 30-minute exposure. This is based on the assumption that the emergency responders can intervene within this time. Figure 1 provides quantitative evaluation of the effect of leak rate on the distance away from the release (which, if population density is known, relates to number of people) exposed to levels in excess of the exposure limit.

The estimated leak rates for the existing specification packagings can also be plotted as shown in Figure 1. For example, Specification Packaging Design ψ may be expected to experience a particular leak rate when exposed to 49CFR performance tests. The same specification packaging may be expected to experience a different leak rate if exposed to Type B performance tests. In addition, Specification Packaging Design ξ may be expected to experience different leak rates than Specification Packaging Design ψ when exposed to the same loading conditions. When plotted as shown in Figure 1, this provides a relative comparison of the level of safety provided by the different specification packagings.

A performance-based packaging standard can be defined for the hypothetical METBI material X such that the packaging must be able to sustain the 49CFR without leaking more than α and Type B loading conditions without leaking more than β, as shown in Figure 1. Since α and β represent the leak rates expected from the current specification packaging ψ, this type of performance standard would provide approximately the current level of safety associated with specification packaging ψ while changing the regulations from specification-based to performance-based. Furthermore, accident probability data can be used to estimate the probability of occurrence of the performance test conditions used to estimate the leak rates shown in Figure 1. This, in turn, can be used to estimate

the probability of people being exposed to these levels. If it is desired to decrease the risks associated with hazardous material transportation, the methodology presented in this paper can be used to quantify the risk reduction provided by a given increase in the performance standards. The performance standards can be increased either by specifying a lower allowed leak rate or by specifying more strenuous (and, therefore, less probable) loading conditions for packaging certification.

CONCLUSION

In conclusion, two of the results of this hazardous material packaging performance evaluation project are the evaluation of the current specification packagings and the development of a methodology for selecting performance based packaging standards. The methodology being used gives a quantifiable measure for assessing the gains associated with increased performance standards. This methodology is especially useful for balancing the need to provide safe transport of hazardous materials without setting regulations so strict that the shipping industries can not afford to comply.

REFERENCES

"1992 ASME Boiler & Pressure Vessel Code", The American Society of Mechanical Engineers, July 1, 1992.

Cashwell, C. and McClure, J.D. "Data Bases About the Transportation of Radioactive Materials," Proceedings of the International High Level Radioactive Waste Management Conference, Las Vegas, NV, 1992.

Ermak, D.L. "SLAB: A Denser-Than-Air Atmospheric Dispersion Model", Proceedings of EPA Workshop on Toxic Air Contamination Modeling, San Francisco, California, October 17-21, 1988.

Landis, W. G. and van der Schalie, W. H. "Aquatic Toxicology and Risk Assessment," ASTM STP 1096, 1990

"NCSS (National Crash Severity Study) Statistics: Light Trucks and Vans", L. L. Ricci, University of Michigan Transportation Research Institute, National Highway Safety Administration, Washington, DC, June 1980.

"Recommendations on the Transport of Dangerous Goods", Fourth Revised Edition, ST/SG/AC.10/1/Rev 4, United Nations, 1986.

Title 49, Code of Federal Regulations, part 178, United States Department of Transportation, 31 December 1991.

Title 10, Code of Federal Regulations, part 71, United States Nuclear Regulatory Commission, 31 December 1991.

APPLICATION OF ADVANCED HANDLING TECHNIQUES TO TRANSPORTATION CASK DESIGN[1]

P. C. Bennett

Sandia National Laboratories
Albuquerque, New Mexico 87185-5800 USA

Sandia National Laboratories supports the U.S. Department of Energy (DOE) Office of Civilian Radioactive Waste Management (OCRWM) applying technology to the safe transport of nuclear waste. Part of that development effort includes investigation of advanced handling technologies for automation of cask operations at nuclear waste receiving facilities. Although low radiation levels are expected near transport cask surfaces, cumulative occupational exposure at a receiving facility can be significant. Remote automated cask handling has the potential to reduce both the occupational exposure and the time necessary to process a cask. Thus, automated handling is consistent with DOE efforts to reduce the lifecycle costs of the waste disposal system and to maintain public and occupational radiological risks as low as reasonably achievable.

This paper describes the development of advanced handling laboratory mock-ups and demonstrations for spent fuel casks. Utilizing the control enhancements described below, demonstrations have been carried out including cask location and identification, contact and non-contact surveys, impact limiter removal, tiedown release, uprighting, swing-free movement, gas sampling, and lid removal operations. Manually controlled movement around a cask under off-normal conditions has also been demonstrated.

Advanced techniques are described that have been developed for the control of robotic equipment which enhance commercial robots' capabilities, improve suitability for nuclear facility application, and reduce constraints on cask designers due to automated equipment limitations. Computer models of casks and facilities are accessed by the supervisory control system to automatically program robotic motion, eliminating manual point-to-point teaching. Multiple sensors have been integrated into the control system to constantly verify the expected real-world conditions, preventing collision and damage. Animated graphical programming has also been integrated into the control system, offering options to pre-program and preview anticipated movement, move the robots telerobotically using the collision prevention features of the graphics, or view automatic motion from any desired perspective. The pre-programming feature has been used to help determine compatibility of new cask designs with automated equipment.

[1] This work performed at Sandia National Laboratories, Albuquerque, New Mexico, supported by the United States Department of Energy under Contract DE-AC04-76DP000789.

[2] A United States Department of Energy Facility

BURNUP CREDIT ISSUES IN TRANSPORTATION AND STORAGE*

M. C. Brady, T. L. Sanders, K. D. Seager, and W. H. Lake[1]

Sandia National Laboratories**, Albuquerque, New Mexico 87185 USA
[1]U.S. Department of Energy, Washington, District of Columbia 20585-0002 USA

ABSTRACT

Reliance on the reduced reactivity of spent fuel for criticality control during transportation and storage is referred to as burnup credit. This concept has attracted international interest and is being actively pursued in the United States in the development of a new generation of transport casks. An overview of the U.S. experience in developing a methodology to implement burnup credit in an integrated approach to transport cask design is presented in this paper. Specifically, technical issues related to the analysis, validation and implementation of burnup credit are identified and discussed.

INTRODUCTION AND BACKGROUND

Current practice for criticality analysis in spent fuel cask design is based on the assumption that the fuel is fresh. Spent fuel transportation and storage casks designed under this assumption have a limiting k_{eff} of 0.95 which represents a safety margin of 0.05 Δk. Using the fresh fuel assumption, it is necessary to control only one parameter, the initial enrichment, to prevent criticality. Criticality analyses using the burnup credit approach (accounting for the reduced reactivity of the spent fuel) will also have a limiting k_{eff} of 0.95 and, therefore, a safety margin of 0.05 Δk. Burnup credit reduces the conservatism in the cask design as a direct result of explicitly considering the actual fuel characteristics (i.e., initial enrichment, burnup and cooling time). The effects of these primary fuel characteristics on system reactivity are well known; reactivity increases with initial enrichment, and decreases with burnup and cooling time (Sanders et al. 1987, Cerne et al. 1987). In the U.S. approach, a minimum cooling time of 5 years is being considered with no additional reactivity credit for cooling times in excess of this value. The initial enrichment and burnup of the fuel are parameters that are used to qualify a fuel assembly for loading into a specific cask design. Use of these multiple-parameter limits for cask loading provide a substantial increase in cask capacity which translates to fewer shipments and directly reduces both occupational and public risk of exposure and transportation costs. However, the multiple-parameter limits also result in requirements for additional administrative controls to verify that the loading restrictions are met.

The U.S. has integrated analysis, validation and operations issues into a comprehensive strategy for the specification of design and operating criteria for the development of burnup credit casks. Factors that can affect design and safety have been identified and prioritized. Methods to validate the calculational methods and reduce data uncertainties are crucial to the successful implementation of burnup credit and are actively being pursued. Lessons learned are translated into design and operational guidance for the implementation of burnup credit.

---

* This work performed at Sandia National Laboratories, Albuquerque, New Mexico, supported by the United States Department of Energy under Contract No. DE-AC04-76DP00789.

** A United States Department of Energy Facility

This paper identifies the current status in the resolution of physics and validation issues using the reference analysis methodology described below. Operational issues associated with the implementation of burnup credit are also discussed.

REFERENCE ANALYSIS METHODOLOGY

Evaluating a spent fuel system using the burnup credit approach has two fundamental requirements; predicting the isotopic composition of the spent fuel and analyzing the system reactivity based on these isotopics. The US-DOE Burnup Credit Program utilizes an analysis methodology developed at Oak Ridge National Laboratory (ORNL) based on the SCALE computer code system (NUREG/CR-0200 1992) which is primarily an away-from-reactor analysis tool. The reference analysis methodology is described in detail in Brady and Sanders (1992). In this methodology, the Monte Carlo code KENO V.a is used to perform criticality calculations. The ORIGEN-S code uses point depletion models (i.e., no spatial dependence) to predict the isotopic composition of the spent fuel. These codes are utilized via the automated sequences CSAS25 and SAS2H, respectively. The SCALE 27 group cross-section library, 27BURNUPLIB, is used in the calculations. Fission-product cross sections in this library are based on ENDF/B-V data; the actinide and light element (low Z materials such as those used in structural and moderator materials) cross-section data are primarily ENDF/B-IV data. Results using this reference methodology have been compared with independent calculations using in-core analysis tools such as PDQ7 (Brady and Sanders 1992) and CASMO-3/SIMULATE-3 (Napolitano 1990) and with alternative analyses performed by cask designers and national laboratories using codes such as MCNP, KENO-IV, and ORIGEN-2. The validation and sensitivity results presented in this paper are based on the SCALE reference methodology.

ANALYSIS ISSUES

Regardless of the computational tools utilized to evaluate burnup credit, there are specific analysis or physics issues which must be addressed. Factors which influence safety and design such as initial enrichment, fuel cycle history, etc. have been investigated and prioritized. The primary fuel characteristics affecting reactivity are initial enrichment, burnup and cooling time. Each of these is considered independently to provide the limiting criteria for loading spent fuel into a burnup cask.

Primary Fuel Characteristics

Infinite multiplication factors were calculated in Cerne, et al. (1987) for a pressurized water reactor (PWR) lattice were calculated for six initial enrichments, seven burnups, and five cooling times. The results were used to develop an equation for estimating k_∞ as a function of initial enrichment, E (weight percent ^{235}U); burnup, B [gigawatt days per metric ton uranium (GWd/MTU)]; and cooling time, C (years). This result, as given in Eq. 1, has been used to evaluate the sensitivity of the multiplication factor to the three primary fuel characteristics.

$$\begin{aligned} k_\infty = {} & 1.060 - 0.010B - 0.002C + 0.114E + 7.081e\text{-}05B^2 \\ & + 7.565e\text{-}05C^2 - 0.007E^2 - 2.671e\text{-}04BE \\ & - 1.145e\text{-}04BC + 2.312e\text{-}04CE + 9.366e\text{-}06BCE \end{aligned} \quad (1)$$

Based on partial derivatives, k_∞ is most sensitive to initial enrichment, then burnup and lastly, the cooling time. Since the multiplication factor increases with enrichment and is more sensitive to this parameter than any other, the initial enrichment should be used explicitly in any criticality calculation. Increasing the burnup has a negative effect on the multiplication factor and it is this fact that is the impetus for pursuing burnup credit. In an infinite array of PWR fuel, the reactivity difference between fresh fuel and fuel burned to 40 GWd/MTU is between 30 and 40% (assuming an initial enrichment of 4.2 wt % ^{235}U). In the U.S. approach, a minimum burnup is to be established as a function of initial enrichment for each cask design. Fuel assemblies with a burnup less than the minimum are unacceptable for transport in that cask design. All fuel assemblies whose burnup exceeds the minimum are permitted to be shipped, however no additional reactivity credit is allowed.

Obviously this is a conservative approach and there are many other options for integrating the burnup requirements into an implementation scheme. It is clear from Eq. 1 that k_∞ decreases with cooling time, there is also a significant influence from the burnup-cooling cross term. This means that for higher burnups the negative change in k_∞ with cooling occurs at faster rate. Since k_∞ is least sensitive to the cooling time, a minimum cooling time of 5 years was chosen as the design basis. The minimum cooling time requirement is independent of initial enrichment and burnup and is consistent with shielding requirements. As with the burnup restriction, fuel cooled less than 5 years is not acceptable and fuel with longer cooling times is acceptable with no allowance for the additional reactivity loss.

Fuel Uncertainties

Although initial enrichment, burnup and cooling time represent the major factors in determining the reactivity of spent fuel, there are several secondary parameters affecting spent fuel reactivity which should be addressed. These include variations in assembly design, differences in reactor operating histories (exposure histories of the assemblies), possible effects of low density moderation, and axial effects (reactivity effects due to the non-uniform axial burnup distribution for an assembly). Each of these factors is taken to represent an uncertainty in the spent fuel, i.e. they are not explicitly considered in the criticality analysis but are compensated for in terms of a penalty as a percentage Δk derived from sensitivity studies.

The largest of these uncertainties comes from the axial effect. Using conservative assumptions, studies (Brady et al. 1990, Turner 1989) have shown that the axial effect is on the order of 2-4 % Δk and varies with burnup, cooling time and assumed profile. The axial effect generally refers to the difference in reactivity due to the axial distribution in burnup (profile) relative to the integral or assembly average burnup. This reactivity effect increases with both burnup and cooling time. The variation with cooling time can be neglected since no reactivity credit is sought for cooling times in excess of 5 years and the decrease in the overall multiplication factor with cooling exceeds any increase in the secondary axial effect. Variations with burnup and profile are interrelated as the profile varies with burnup. The most severe profiles are associated with the lower burnups as the distribution tends to flatten with increased burnup. Efforts are underway to compile a profile database in order to more clearly define a methodology which predicts the uncertainty due to the axial effect. The axial effect is also dependent on the specific cask design (relative leakage rates at the ends of the cask) and should be evaluated for each design.

The most reactive assembly design [e.g., Westinghouse (WE) 17x17, Babcock and Wilcox (BW) 15x15, Combustion Engineering (CE) 14x14, etc.] has been shown to vary with burnup (Napolitano 1990) based on three-dimensional calculations using the CASMO-3/SIMULATE-3 code system assuming an initial enrichment of 4.5 wt % ^{235}U. The most reactive fuel assembly in the burnup range of 0-20 GWd/MTU was determined to be the CE 14x14; from 20-35 GWd/MTU, BW 15x15; 35-50 GWd/MTU, WE 17x17. The least reactive assembly for all burnups was the WE 14x14 design. However, in the range of burnups used for the fuel loading criteria in the U.S. approach (approximately 25 GWd/MTU for 5 wt % enriched fuel), the differences observed between 7 U.S. PWR fuel assembly designs was less than 0.5 %. The cask designer may choose any assembly type for the design basis (the WE 14x14 would not be recommended) and apply the biases given in Table 1 as a function of burnup. In burnup regions where the design basis assembly type is the same as the most reactive for the burnup region, no bias is necessary. The biases in Table 1 represent a 95 percent confidence level (2σ) derived from the CASMO-3/SIMULATE-3 calculations.

Table 1. Fuel assembly type Δk bias as a function of burnup

Burnup (GWd/MTU)	0	5	10	15	20	25
Most Reactive Assembly Type	CE 14x14	CE 14x14	CE 14x14	CE 14x14	BW 15x15	BW 15x15
Δk bias	0.006	0.006	0.006	0.005	0.004	0.003

Exposure history has been shown to have a minor second-order effect on assembly reactivity. Nine exposure scenarios, including several variations in the percentage uptime and specific power during the exposure cycles as well as power increases at the end of the last and next-to-last fuel cycles were evaluated using SAS2H for an integral burnup of 33 GWd/MTU (NUREG/0200 1992). Additional calculations were performed at a burnup of 50 GWd/MTU with four exposure scenarios. The maximum Δk (0.0034) was observed at discharge and decreased with cooling time and increasing burnup. The maximum value of k_∞ resulted from the fuel exposure history in which 100% uptime when a specific power based on the total fuel residence time and reactor power rating was assumed. Using this conservative exposure history would alleviate any need to add an uncertainty for exposure history, otherwise an exposure uncertainty value of 0.0015 (based on a 95 percent confidence level derived from the 33 GWd/MTU data at a 5 year cooling time) should be used. Effects due the presence of burnable poison rods (BPRs) during the fuel exposure were also investigated. Both CASMO-3/SIMULATE-3 and SAS2H(ORIGEN-S) calculations were utilized in this study. No dependence on cooling time was observed in either set of calculations for this effect. Both studies indicated that for burnups less than 15 GWd/MTU the presence of BPRs resulted in a lower k_∞ than similar cases without BPRs. For burnups greater than 15 GWd/MTU the inclusion of BPRs during the exposure resulted in an increase of approximately 0.01 in the infinite multiplication factor which decreased slightly with increasing burnup. Including the effect of two standard deviations in the results from both codes, the recommended bias for the presence of BPRs would be: no bias for burnups less than 15 GWd/MTU; 0.0128, 15-25 GWd/MTU; 0.0114, 25-35 GWd/MTU; and 0.0092, greater than 35 GWd/MTU.

Low-density moderation effects have also been investigated and have been found not to be a concern for closely packed arrays. Cask designs that have flux traps would require analyses to evaluate low-density moderation effects.

Another area of concern is determining which nuclides should be included in the analyses. The answer is dependent on the analysis method used. Isotopic depletion codes such as ORIGEN-S utilize data for about 800 fission products. However, more general purpose cross-section libraries such as the 27BURNUPLIB used in the reference analysis library have data for only a fraction of these (e.g., 191 fission-products and actinides are included in 27BURNUPLIB). Analyses (Sanders et al. 1987, Parks 1989) have been performed to identify and rank 37 nuclides that are considered important in the characterization of spent fuel reactivity. The US-DOE burnup credit program uses a subset of 25 of these (Brady and Sanders 1992). Volatile nuclides and those that are known to migrate in fuel are not considered since their presence in spent fuel can not be systematically assured. An additional criteria for including specific nuclides was the availability of experimental data verifying the ability of the depletion codes to accurately predict the quantity of a particular nuclide in spent fuel. An experimental chemical assay program is underway at Pacific Northwest Laboratory in Richland, Washington, USA, to produce isotopic measurements for each of the nuclides included in the analysis (Bierman 1990). The major fissile nuclides (^{235}U, ^{238}U, and ^{239}Pu) and the major actinide absorbers (e.g. ^{240}Pu and ^{241}Am) are among the 10 actinides included in the set of 25. Approximately two-thirds of the reactivity loss in spent fuel is due to the depletion and buildup of these actinides. There are 14 fission products included in the set of 25 nuclides. The buildup of these fission products account for approximately 80% of the remaining reactivity loss in spent fuel.

VALIDATION ISSUES

Three sources of experimental data have been identified for utilization in the validation of burnup credit analysis methodologies: (1) commercial reactor restart criticals; (2) fresh fuel critical experiments, including experiments with mixed-oxide fuels and neutron absorber materials; and (3) spent fuel chemical assay data. The validation of the reference analysis methodology against experimental data is discussed in detail in Brady and Sanders (1992). An additional goal is to develop and qualify a set of reference benchmark data to be utilized in the validation of independent analysis methods.

Results for five commercial reactor restart critical configurations were presented in Brady and Sanders (1992). Three additional calculations have been performed based on data for the Tennessee Valley Authority's Sequoyah Unit 2 reactor. This reactor was subject to an extended (31 month) downtime in the middle of cycle 3, after

which it was restarted with no refueling. This situation is one uniquely suited to the validation of burnup credit: the system reactivity is completely due to spent fuel since no fresh fuel is present, the fuel is cooled sufficiently to approximate the isotopic composition of the fuel to be shipped, and the soluble boron in the water is relatively low. The result for this middle-of-cycle (MOC) configuration at hot full power (HFP) is given in Table 2 along with results for HFP and hot zero power (HZP) conditions at the beginning-of-cycle(BOC) 3 which is before the extended shutdown. These calculations were performed using the SAS2H and KENO V.a methodologies as described in Brady and Sanders (1992). In total, eight reactor restart criticals have been analyzed using the reference analysis methodology. Two additional reactor restart configurations are being evaluated. These are for the Three Mile Island Unit 1 reactor which also experienced an extended outage and will have an isotopic content (particularly fission products) that is consistent with the spent fuel to be shipped. However the reactor was refueled before restart and approximately one-third of the core is fresh fuel which is typical of most reactor restart configurations. In this situation it has been shown that the spent fuel will contribute about two-thirds of the core reactivity and is still a reasonable benchmark for burnup credit.

Table 2. KENO V.a calculated results for Sequoyah Unit 2 Cycle 3

Burnup Conditions	Power Conditions	Boron (ppm)	k_{eff}	Neutron Histories
BOC	HZP	1685	1.00063+/-0.00093	286,000
BOC	HFP	1150	1.00259+/-0.00089	336,000
MOC	HZP	475	1.00014+/-0.00095	298,000

In addition to the reactor restart criticals which fulfill the role of spent fuel criticals, fresh fuel criticals are used to validate the performance of the analysis methodology for geometries representative of a spent fuel cask environment, i.e. assembly interaction, presence of neutron absorbers and shielding materials, etc. At present, 31 fresh fuel critical experiments have been evaluated using the reference analysis methodology. The calculated results for the 18 UO_2 and 13 mixed-oxide (MOX) criticals are summarized in Table 3. Twelve mixed-oxide critical configurations from Smith and Konzek (1976, 1978) and Taylor et al. (1965) have been added to the original data which was reported in Bowman (1991). Poor results obtained for the single MOX configuration that had been analyzed previously prompted the evaluation of additional MOX criticals to either refute or confirm these results. The more recent evaluation of MOX criticals give very good results as indicated in Table 3. Data used for the MOX configuration reported in ref. 12 is currently being reviewed in order to resolve the discrepancy in the performance of the analysis method for that problem relative to the current calculations.

Table 3. Summary of k_{eff} results for fresh fuel critical configurations.

Reference	Fuel Type	No. Configurations	Mean k_{eff}
EPRI NP-196 (Smith and Kinzek 1976, 1978)	UO_2	2	0.9925+/-0.0035
	MOX	6	1.0015+/-0.0061
WCAP-3385-54 (Taylor et al. 1965)	UO_2	2	0.9921+/-0.0027
	MOX	6	1.0042+/-0.0038
ORNL/M-1332 (Bowman 1991)	UO_2	14	0.9936+/-0.0036
	MOX	1	0.9801+/-0.0018*
Summary	UO_2	18	0.9933+/-0.0034
	MOX	13	1.0011+/-0.0079

* Calculation is currently being reviewed.

The final source of validation data is directly aimed at validating the depletion methodology against experimental assay data. Six principle sources of chemical assay data for light-water reactor (LWR) spent fuel have been identified (Brady and Sanders 1992). These are primarily data for fuel elements taken from the U.S. spent fuel inventory which have been identified for characterization as approved testing materials (ATMs) at the Materials Characterization Center at the Pacific Northwest Laboratory (Brady and Sanders 1992, Bierman 1990). Data for the German Obrigheim PWR have also been utilized in the validation analyses. Results for four cases were given in Brady and Sanders (1992), three additional cases will be evaluated in 1993. The U.S. program is also sponsoring measurements of the fission product content of the ATM samples, the first results are expected in late 1992.

In order to aid the validation of alternative methodologies, a "reference problem set" has been established (Brady and Sanders 1992). Also included are descriptions and references for a set of fresh fuel critical experiments validating geometries typical of a spent fuel cask environment and the cross-sections for the major fissile uranium and plutonium isotopes. A set of calculated reference isotopics, complete with a description of the physical and operating history information, etc. needed to generate such data, are given for various burnups and initial enrichments. In the final version of the reference problem set, these data will include at least one set of isotopics directly traceable to the reactor restart critical calculations used in the validation process. Calculational benchmarks have been established using these reference isotopics to represent spent fuel in the geometries described for the fresh fuel critical experiments. The burnup credit analysis methods established in the US-DOE program have been used to compute a reference k_{eff} for these spent fuel subcriticals. The final reference problem set will also include experimental data used in the isotopic validation studies and their references. Recommendations and guidelines for evaluating a calculation bias for the users' analysis methodology will also be included.

OPERATIONS ISSUES

Because burnup credit places restrictions on the spent fuel characteristics, it requires an integrated approach to assure efficiency in both the cask design and operations. Operational issues can directly influence cask design. For example, the likelihood and advantages of using automated systems for cask-handling operations at the receiving facility has prompted recommendations about cask closures, trunnions, tie downs, etc. Additional operational issues have been identified as a result of the development of verification and fuel acceptance procedures. Probabilistic risk assessment (PRA) tools are utilized to evaluate the impact of utilizing burnup credit on the overall package reliability and safety.

Operator error has been identified as one of the primary uncertainties associated with the implementation of burnup credit in cask design. Therefore, the technical feasibility of using automatic intelligent systems to validate crucial cask operations has been examined. These systems would monitor activities, verify that proper tools are used, verify that proper and acceptable measurements are taken in the course of cask operations, and automate the quality assurance procedures. The reliability of the monitoring system and its impact on criticality safety will be examined by : (1) identifying key operations during cask loading which could contribute to a criticality event, (2) identifying sensory devices that could monitor key operations and verify operational correctness, and (3) characterizing and collecting reliability data on sensory devices and supervisory computer operation.

Strategies (procedures and guidelines) for implementing burnup credit in the design and operation of spent fuel transport and storage casks are being analyzed using a relative risk methodology. Fault tree analyses of nuclear criticality safety issues indicate that the fresh fuel and burnup credit approaches to calculating criticality safety follow similar pathways, and both involve risks. In the case of burnup credit, the criticality control system consists of both an "external" control component that includes poisons in the cask or basket and an "internal" control component which is the compensation of the loaded spent fuel. Fault tree analyses have determined that exceeding the fuel reactivity limits could result from an error in the analysis used to develop fuel-loading procedures, or an error in the burnup characterization of the spent fuel (from erroneous in-core measurements or subsequent analyses). In theory, the number of opportunities for error increases with burnup credit because

the characteristics of spent fuel must be included in the cask design basis. However, an analysis of the actual inventory of spent fuel in the U.S. indicates that only a small fraction (on the order of 2 percent) of the existing spent fuel inventory is likely to be nonspecification for typical cask designs using burnup credit.

A nuclear criticality event during transport is highly unlikely because (1) it requires a failure in the control system, and also that (2) this failure occurs in conjunction with an accident severe enough to breach the cask which (3) must then be flooded with essentially pure water. The only credible source of error is a misloading event which would result from an error in the fuel-loading procedure or failure to correctly identify a fuel assembly during cask-loading operations. Errors of this type are mitigated by use of the automated intelligent systems described earlier. These dominant failure modes arise because of the significant time lapse between fuel discharge and transport. The initial enrichment and burnup of the fuel are parameters that are part of the required utility records for each fuel assembly and can be verified by measurement prior to cask loading. A measurement system to fulfil these requirements is being developed in a joint program by Sandia National Laboratories, Los Alamos National Laboratory, and the Electric Power Research Institute. It appears likely that standard gamma-ray and neutron yield measurements could be used to verify that a spent fuel assembly meets the minimum cooling time and burnup requirements. An appropriate on-site measurement and calibration system will be designed to minimize interference with loading operations and accurately verify the spent fuel characteristics against utility records for each fuel assembly. The FORK radiation detector, used by the International Atomic Energy Agency in safeguards inspections, is being tested to determine its applicability for this task. A detailed discussion is given in Ewing (to be published).

CONCLUSIONS

The current U.S. approach to the analysis and implementation of burnup credit is conservative and results in a two-parameter (burnup and initial enrichment) loading curve for fuel acceptance. Utility records for these parameters will be verified by a physical measurement as a part of the cask loading procedure. By designing casks that are optimized to the specifications of the older spent fuel that will be shipped, the new generation of spent fuel casks will be more efficient (with an increased capacity factor of four for a legal-weight truck cask design and an increase of nearly a factor of three for rail/barge casks) and at least as safe as current cask designs (Lake 1992).

The U.S. is also a participant in an international working group operating under the auspices of the Organization for Economic Cooperation and Development (OECD) to benchmark burnup credit for criticality safety analyses. A direct benefit from participation in this group is the independent verification of the U.S. analysis methodology. As work progresses in the development of the U.S. burnup credit program and via international cooperation, additional data will become available and many of the analysis and fuel uncertainties may be reduced. Future work includes moving towards optimizing cask design by balancing the burnup credit requirements and the relative reactivity worth of the cask basket (by reducing the neutron poisons in the basket). This could result in a reduction in the unit cost of the casks with no degradation in reliability and safety.

ACKNOWLEDGEMENTS

The US-DOE burnup credit program is dependent on a range of expertise, and the authors would like acknowledge S. M. Bowman, O. W. Hermann, C. V. Parks, J.-P. Renier and R. M. Westfall of ORNL for their substantial contributions to the different phases of the project. We would also like to express our appreciation for the technical expertise, assistance and advice from S. R. Bierman (Pacific Northwest Laboratory), R. I. Ewing (Sandia National Laboratories), C. R. Marotta (Marotta Consulting), D. Napolitano (Nuclear Assurance Corporation), O. Ozer and R. Williams (Electric Power Research Institute), and M. Smith (Virginia Power Company). This work is supported by the Office of Civilian Radioactive Waste Management of the US-DOE.

REFERENCES

Bierman, S. R., "Benchmark Data for Validating Irradiated Fuel Compositions Used in Criticality Calculations", *Trans. Am. Nucl. Soc.*, **62**, 311-312 (November 1990).

Brady, M. C., C. V. Parks, and C. R. Marotta, "End Effects in the Criticality Analysis of Burnup Credit Casks", *Trans. Am. Nucl. Soc.*, **62**, 317-318 (November 1990).

Brady, M. C. and T. L. Sanders, "A Validated Methodology for Evaluating Burnup Credit in Spent Fuel Casks," *Nucl. Energy*, **31**, No. 2, 135-142 (April 1992).

Bowman, S. M., *Validation of SCALE-4 for a Reference Problem Set*, Oak Ridge National Laboratories report ORNL/CSD/TM-1332 (July 1991).

Cerne, S. P., O. W. Hermann, and R. M. Westfall, *Reactivity and Isotopic Composition of Spent PWR Fuel as a Function of Initial Enrichment, Burnup, and Cooling Time*, Oak Ridge National Laboratory report ORNL/CSD/TM-244 (October 1987).

Ewing, R. I., "Burnup Verification Measurements for Spent Nuclear Fuel," *Proceedings of the 10th International Symposium on the Packaging and Transportation of Radioactive Materials, PATRAM'92*, September 13-18, 1992, Yokohama City, Japan (to be published).

Lake, W. H., "A Comparison of a New Generation of Spent Fuel Cask Designs with Current Cask Design Characteristics," *Proceedings of the Third International Conference on High Level Radioactive Waste Management*, April 12-16, 1992, Las Vegas, Nevada (April 1992).

Napolitano, D. G., Personal Communication, 1990. [See also, D. G. Adli and D. G. Napolitano, *Burnup Credit Analysis Using Advanced Nodal Techniques*, Sandia National Laboratories report SAND91-7026, TTC-1045, (to be published 1992).]

Parks, C. V., "Parametric Neutron Analyses Related to Burnup Credit Cask Design," *Proc. Workshop on the Use of Burnup Credit in Spent Fuel Transport Casks*, Sandia National Laboratories report SAND89-0018, TTC-0884 (October 1989).

Sanders, T. L., R. M. Westfall, and R. H. Jones, *Feasibility and Incentives for the Consideration of Spent Fuel Operating Histories in the Criticality Analysis of Spent Fuel Shipping Casks*, Sandia National Laboratories report, SAND87-0157, TTC-0713 (August 1987).

SCALE: A Modular Code System for Performing Standardized Computer Analyses for Licensing Evaluation, available from the Radiation Shielding Information Center, Oak Ridge national Laboratory, NUREG/CR-0200, Rev. 4.1, 1-3 (1992).

Smith, R. I., and G. J. Konzek, *Clean Critical Experiment Benchmarks for Plutonium Recycle in LWR's*, EPRI NP-196, Volumes I and II (April 1976 and September 1978).

Taylor, E. G., et al., *Saxton Plutonium Program Critical Experiments for the Saxton Partial Plutonium Core*, WCAP-3385-54, (December 1965).

Turner, S. E., "An Uncertainty Analysis - Axial Burnup Distribution Effects," *Proc. Workshop on the Use of Burnup Credit in Spent Fuel Transport Casks*, Sandia National Laboratories report SAND89-0018, TTC-0884 (October 1989).

STACE: Source Term Analyses for Containment Evaluations of Transport Casks*

K.D. Seager[1], S.E. Gianoulakis[1], P.R. Barrett[2], Y.R. Rashid[2] and P.C. Reardon[3]

[1]Sandia National Laboratories**, Albuquerque, New Mexico, United States of America
[2]ANATECH Research Corporation, La Jolla, California, United States of America
[3]GRAM, Inc., Albuquerque, New Mexico, United States of America

INTRODUCTION

The containment requirements for the transportation of radioactive material are defined by both International Atomic Energy Agency (IAEA) and U.S. Nuclear Regulatory Commission (NRC) regulations (IAEA 1990; 10 CFR 71). Procedures generally acceptable to the NRC for assessing compliance with these provisions have been identified in Regulatory Guide 7.4 (US NRC 1975). This guide endorses the containment and leak test procedures that are specified in American National Standards Institute (ANSI) Standard N14.5 (ANSI 1987). ANSI N14.5 states that "compliance with package containment requirements shall be demonstrated either by determination of the radioactive contents release rate or by measurement of a tracer material leakage rate." The maximum permissible leakage rates from the transport cask L_i (cm^3/s), where i represents either normal (N) or accident (A) conditions of transport, can be determined from the maximum permissible release rates R_i (Ci/s) and the time-averaged volumetric concentrations of suspended radioactivity within the cask C_i (Ci/cm^3) by:

$$L_i = R_i / C_i . \quad (1)$$

The maximum permissible release rates are specified in ANSI N14.5 to be $A_2 \times 10^{-6}$ per hour for i = N, and A_2 per week for i = A (the exception is ^{85}Kr in which 10,000 Curies are permitted to be released in one week). The quantity A_2 is an activity limit which, under specific release scenarios, would prevent radiological effects from exceeding a specified level consistent with radiological protection standards of the International Commission on Radiological Protection (ICRP). Values of A_2 (e.g., A_2 = 7 Ci for ^{60}Co; A_2 = 10 Ci for ^{137}Cs) are tabulated in Appendix A of 10 CFR 71.

ANSI N14.5 further states that "C_N and C_A shall be determined by the performance of tests on prototypes or models, reference to previous demonstrations, calculations, or reasoned argument," with "consideration given to the chemical and physical forms of the materials within the containment system, the possible release modes, and the maximum temperature, pressure, vibration, and the like, to which the contained material would be subjected for normal and accident conditions of transport." The development of the Source Term Analyses for Containment Evaluations (STACE) methodology provides a unique means for estimating the probability of cladding breach within transport casks, quantifying the amount of radioactive material released into the cask interior, and calculating the releasable radionuclide concentrations and corresponding maximum permissible leakage rates. STACE, which is being developed at Sandia National Laboratories (SNL), is a task of the Cask Systems Development Program (CSDP) sponsored by the United States Department of Energy's Office of Civilian Radioactive Waste Management (OCRWM). The STACE methodology follows the procedures of ANSI N14.5 by estimating the releasable radionuclide concentrations for specific cask designs, fuel assemblies, and initial conditions. These calculations are based on defensible analysis techniques that credit multiple release barriers, including the internal fuel structure, the cladding, and the internal cask walls.

* This work performed at Sandia National Laboratories, Albuquerque, New Mexico, supported by the United States Department of Energy under Contract No. DE-AC04-76DP00789.
** A United States Department of Energy Facility.

An alternative to computing C_N and C_A is to limit the maximum permissible leakage rate to 10^{-7} std cm^3/s, which is the practical limit of "leak tightness" as defined by ANSI N14.5. This approach generally leads to increased cask maintenance costs, personnel exposure, and limited lifetime usage of the casks in the certification and recertification process. By directly computing C_N and C_A the source term methodology is expected to significantly improve cask economics and safety by relaxing the maximum permissible leakage rates.

SOURCE TERM METHODOLOGY

The development of a source term methodology considers the individual contributions of the three distinct media from which the radionuclides in a spent fuel transport cask originate:

- radionuclides that can be released through breaches in the spent fuel cladding;
- activated corrosion and free fission products, referred to as CRUD, adhering to the surface of spent-fuel rods; and
- residual contamination that may build up in the cavity of a cask over time.

Containment of cask contents by a transport cask is a function of the cask body, one or more closure lids, and various bolting, hardware, and seals associated with the cavity closure and other containment penetrations. In addition, characteristics of cask contents that impede the ability of radionuclides to move from an origin to the external environment also provide containment. In essence, multiple release barriers exist in series in transport casks, and the magnitude of the releasable activity available in the cask is considerably lower than the total activity of its contents. A source term approach accounts for the magnitude of the releasable activity available in the cask by assessing the degree of barrier resistance to release provided by material characteristics and inherent barriers that impede the release of radioactive contents.

Example leakage rate calculations in ANSI N14.5 conservatively assume that 3% of the fuel rods fail during normal conditions of transport and 100% fail under hypothetical accident conditions of transport. This paper presents a defensible methodology to be used in conjunction with ANSI N14.5 to estimate fuel rod failure rates and the corresponding releasable fission products. The critical normal and hypothetical accident conditions are, respectively, a 0.3-meter drop and 9-meter drop of the cask containing the fuel rods onto an unyielding target. STACE models the response of the fuel rods to these impacts and evaluates the release of radioactive materials in the event of fuel cladding failure. The fuel assemblies and cask internal hardware are modeled in detail, allowing for interactions between assemblies and the cask basket, and between spacer grids and fuel rods.

Three reports have been prepared which together present a methodology for determining the concentration of freely suspended radioactive materials within a spent-fuel transport cask. Each report treats one of the three sources of radioactivity: (1) the loaded spent fuel (Sanders et al. 1992), (2) the radioactive material, CRUD, attached to the external surface of the cladding (Sandoval et al. 1991), and (3) the residual contamination adhering to the interior surfaces of the cask cavity (Sanders et al. 1991). Since the concentrations of the individual sources are additive, the maximum permissible leakage rate for the combined source is written:

$$L_{total} = \frac{R}{C_{SF} + C_{CRUD} + C_{RC}} . \qquad (2)$$

The individual concentrations C_{SF}, C_{CRUD}, and C_{RC} determine individual leakage rates L_{SF}, L_{CRUD}, and L_{RC}, respectively, when considered as sole sources of radioactivity. Expressing the individual concentrations in terms of the individual leakage rates through Equation (1), Equation (2) can be rewritten in terms of the individually determined maximum permissible leakage rates:

$$L_{total} = \frac{L_{SF} \times L_{CRUD} \times L_{RC}}{L_{CRUD} L_{RC} + L_{SF} L_{RC} + L_{SF} L_{CRUD}} . \qquad (3)$$

This method of combining individually determined containment requirements should only be done after all terms are converted to the same temperature and pressure conditions.

Spent Fuel Contribution

Spent fuel contains the largest potential source of releasable radioactivity (Sanders et al. 1992). The contribution of spent fuel to the overall maximum permissible leakage rate largely depends upon its initial pre-transport condition and on subsequent fuel rod response to transportation conditions. The type and amount of radioactive materials that may be released from the fuel rod to the cask cavity are governed by fuel cladding failure which is a function of cask and assembly designs, transport loading conditions, fuel irradiation histories, and other initial conditions. Since cladding failures are highly statistical events, criteria for evaluating the spent fuel source term is probabilistic, although it may depend upon deterministically derived response characteristics. Therefore, the source term methodology combines a detailed deterministic mechanical response of fuel rods and assemblies with probabilistic failure evaluations and release estimates.

Four steps are used to apply the source term methodology to spent fuel for normal and hypothetical accident conditions:

1. Characterization of the dynamic environment experienced by the cask and its contents.

2. Deterministic modeling of the stresses induced in spent fuel cladding by the dynamic environment.

3. Evaluation of these stresses against probabilistic failure criteria for ductile tearing and material fracture at generated or pre-existing cracks partially extending through the cladding wall's thickness.

4. Prediction of the activity concentration in a cask cavity using knowledge of the cask void volume, the inventory of radionuclides residing in fuel-cladding gaps, and estimates of the fraction of gases, volatile species, and fuel fines released.

The dynamic environments in the first step are defined in 10 CFR 71 and are divided into normal and hypothetical accident conditions. The most severe normal and hypothetical accident conditions are the 0.3-m and 9-m free drop impacts onto unyielding targets, respectively (Sanders et al. 1992). Other regulatory events such as shock and vibration, a fully engulfing fire, and puncture events, have been evaluated and shown to have minimal impact on the assemblies' response (Sanders et al. 1992). A rigid-body kinematics model is used to analyze the impact event by characterizing the crushing behavior of the impact limiters for all possible drop orientations. This analysis defines the center of gravity deceleration load history applied to the fuel assemblies. This is then input to the assembly computational models.

The second step develops detailed geometric and computational models which are analyzed using discrete finite element methods to obtain the deterministic mechanical response of the fuel rods and assemblies. A deterministic response analysis of a loaded transport cask and its contents is performed by isolating smaller substructures from the total system and analyzing them separately. This isolation takes place at naturally identifiable interfaces so that force or displacement boundary conditions can be properly defined. The smallest structural element that is isolated is a single fuel rod. The force transfer interfaces for the rod are tie plates, spacer grids, and to a lesser extent, adjacent rods. Under certain conditions (e.g., end impact) the single rod model response adequately represents the response of the whole assembly, assuming that all rods in the assembly have similar deformation patterns. This assumption is conservative because the predominant end-drop failure mode is caused by high tensile bending strains produced by lateral displacement. However, a single rod model is inapplicable to other impact orientations (e.g., side drop and slapdown), and the more complex structure of a single assembly is required.

The single assembly models individual rods, spacer grids, and end-tie plates. The force transfer interface for the single assembly is the basket structure. Depending on the structural design of the basket, force transfer between assemblies may be replaced by displacement boundary conditions that isolate the object assembly from surrounding assemblies. The basket/assembly interface is replaced by a line support for a typical continuous-plate basket design. The basket structure itself is not part of the structural model. The detailed geometric model of the single assembly consists of several hundred beam-column elements that represent individual rods, and special nonlinear hysteretic truss elements that represent spacer grids at each interface (Barrett et al. 1992). To capture the detailed deformation characteristics of the fuel rods, each rod is represented by no fewer than thirty beam-column elements with elastic-plastic and large displacement and strain capabilities. Rod-to-rod interaction is simulated by nonlinear contact spring elements with contract/release capabilities. Deterministic

response parameters, cladding stresses and strains, and rod interaction forces are obtained at critical points along each length of the rod. These quantities are then used in the third step.

The third step involves the application of probabilistic methods to determine the likelihood of cladding breach in the spent fuel (Foadian et al. 1992). Two properties specifically used in this evaluation are the material ductility, which is related to ductile tearing from excessive strain, and fracture toughness, which is used to determine the extension of generated or pre-existing partial (partially through the wall) cracks. Three cladding failure modes which can occur are transverse tearing, rod breakage, and longitudinal tearing. Experimental data are used to define the various failure modes, and these data have been translated into specific failure criteria (Bauer et al. 1977, Miyamoto et al. 1976, Barsell 1987). Transverse tearing requires that the strain exceed the material ductility limits. It is assumed that once a crack is initiated, it will immediately extend through the wall, thus forming a pinhole or narrow transverse crack. Rod breakage is the extension of an existing transverse crack, and it requires a bending stress intensity that exceeds the fracture toughness of the intact material. Depending on the amount of available energy, a narrow transverse tear could extend through a large portion of the cladding cross section, or even result in a guillotine break. Longitudinal tearing, the opening of a part-wall longitudinal crack on the inside of the cladding, requires a hoop stress intensity that exceeds the fracture toughness. The driving force for the hoop stress intensity is a pinch load arising from rod-to-rod interaction. The source term methodology determines probabilities for the three different types of cladding breach. This is an essential prerequisite for defining release mechanisms, because the physical composition of fuel rod contents that could be released through a cladding breach is strongly dependent on the geometry of the cladding breach. A pinhole failure, for example, could result in the release of fission gases, volatile species, and finely dispersed fuel, whereas a guillotine break could further permit the release of fuel fragments.

The fourth step concerns the prediction of the activity concentration in the cask cavity. Many radionuclides are produced within fuel rods during reactor operation. The specific nuclide composition depends on the initial enrichment, irradiation history, and length of time since reactor discharge. Estimates of the radionuclide composition are obtained from the Oak Ridge LWR Spent Fuel Database (OCRWM 1987). ORIGEN2 calculations (Croff 1983) were carried out for several burnup levels to represent current and projected (extended) burnup limits for BWR and PWR fuel assemblies. These results are compiled in a radionuclide inventory database within STACE and input data for specific analyses are obtained by interpolation for the specified fuel type, burnup level, and time of transport after reactor discharge.

Having quantified the radionuclide inventory of fuel assemblies prepared for transport, the amount of this source released to the cask cavity during a cladding breach is determined. The spent fuel source term includes radionuclides released from the fuel matrix to the fuel-cladding gap in gaseous and vapor form, as well as gas-borne particulate fines. A model for the gap inventory has been developed to account for the buildup of xenon and krypton isotopes in the fuel-cladding gap. To determine the buildup of moderately volatile species (iodine, cesium, and tellurium) in the gap, it is assumed that they have the same mobility and diffusion characteristics as the noble gases, thereby establishing relationships for magnitude and distribution between the long-lived isotopes of volatile species and fission gases. The entire gap inventory is conservatively assumed to be readily available for release in the event of cladding breach, irrespective of breach location or size. The mass of fuel fines released through the cladding breach is taken to be 0.003 percent of the fuel mass in the rod, based on observation of the quantity of material released from rod segments in burst rupture experiments at Oak Ridge National Laboratory and Battelle Columbus Laboratory (Burian et al. 1985, Lorenz et al. 1980, Lorenz et al. 1981). This does not account for new fines, if any, produced due to crushing of the fuel pellets. Ninety percent of the fuel fines that reach the cask cavity are assumed to settle or plate-out, and thus be unavailable for release (Sanders et al. 1992).

CRUD Contribution

The methodology for modeling the CRUD source term differs from that for spent fuel due to the wider range and better quality of available data (Sandoval et al. 1991). There are two types of CRUD: a fluffy, easily removed CRUD composed mostly of hematite that is usually found on BWR rods; and a tenacious type composed of nickel-substituted spinel occurring on PWR rods. In a few BWR reactors, copper is also an important constituent. Along individual rod cladding, the average to peak observed density of CRUD radioactivity is approximately two, independent of the radionuclide. The nuclides which are important in the CRUD total activity depend on the time since discharge from the reactor; for shipments of five-year or older fuel, ^{60}Co accounts for over 92% of the activity in PWR fuel and 98% of the activity in BWR fuel.

The concentration of CRUD suspended in the cavity of a loaded spent fuel transport cask depends on the amount of CRUD initially adhering to the transported assemblies, on the fraction spalled in normal and hypothetical accident transport conditions, and on depletion and resuspension mechanisms acting on the suspended particles. The amount of CRUD present on spent fuel rods has been characterized in prior work (Sandoval et al. 1991). Most recently discharged fuel has no discernible or only slight CRUD deposits. CRUD aerosols have a time-dependent concentration after a spallation-inducing event. An expected particle size distribution for CRUD has been developed based on one sample of fuel that is believed to be representative of BWR fuel. The distribution has a precise log-normal shape with a mean number diameter equal to 3 μm and a standard deviation of 1.87 μm. Since a detailed distribution is available, it is possible to account for the behavior of aerosols inside the cask cavity. In the absence of resuspension, the rate of decrease in aerosol concentration is proportional to the concentration itself. The average CRUD concentrations in a cask cavity can be expressed as the concentration immediately after spallation and initial mixing, multiplied by a Release Reduction Factor that incorporates all geometrical information on the cask volume, settling and collection areas, and the aerosols' time-varying size distribution. C_{CRUD} can then be calculated directly, based on the specified cask cavity.

Residual Contamination Contribution

After casks have been used to transport spent fuel, their interior surfaces (especially the bottom) accumulate a residual contamination from CRUD spalled off the transported assemblies, or from immersion in storage pool water during loading and unloading of the assemblies. The residual contamination report (Sanders et al. 1991) discusses the mechanisms leading to spallation but does not quantify the adhesion forces themselves, and it presents previously unpublished data that clarify the amount of residual contamination present.

The largest amount of residual contamination reported is approximately 1 Ci. This amount is conservatively assumed to be present in the transport cask, and all of it is assumed to spall in both normal and hypothetical accident conditions of transport. An extensive set of example calculations for normal and hypothetical accident conditions is presented in the residual contamination report.

STACE

The methodology developed in the previous sections is implemented through the integrated STACE software package (Seager et al. 1992). STACE is a system of software modules operating under a graphics controller that performs source term analyses of spent fuel transport casks. STACE extracts relevant data from its built-in database module to perform thermal, mechanical, cladding breach, and release analyses. Figure 1 summarizes the STACE design elements. The output of STACE includes steady-state thermal contours for normal transport, temperature versus time in hypothetical accidents, and the structural response of the fuel rods and spacer grids. The probabilities of cladding breach are given for three different failure modes, and an isotopic breakdown is given of the initial and time-averaged activity released to the cask cavity for normal and hypothetical accident conditions. Finally, the maximum permissible leakage rates are given for normal and hypothetical accident conditions.

EXAMPLE SOURCE TERM ANALYSES

Table 1 presents the time-averaged volumetric concentrations of suspended radioactivity, C_i, and the maximum permissible leakage rates, L_i, for the spent fuel, CRUD, and residual contamination contributions to the releasable source term for the example case in which one Westinghouse 17x17 PWR assembly is transported in a representative lead-shielded truck cask. The assembly is assumed to have an average burnup of 30 GWd/MTU, and to be transported 10 years following reactor discharge. Calculations are performed for the normal condition of a 0.3-m end drop and the hypothetical accident condition of a 9-m side drop of the truck cask with impact limiters onto an unyielding target. The cladding temperature during the normal and hypothetical accident conditions is assumed to be 27°C.

The mechanical and cladding breach analyses predict a single rod failure probability of 5×10^{-5} for the 0.3-m normal transport event. Since the assembly contains 264 fuel-bearing rods, 0.013 fuel rods are expected to fail. However, these analyses conservatively assume that one rod fails due to normal conditions of transport. The peak cask accelerations are conservatively assumed to be 100 g during the 9-m side drop, and the analyses

predict a single rod failure probability of 3.7×10^{-3}. Therefore, slightly less than one fuel rod is expected to fail in the 17x17 assembly due to the hypothetical accident condition. The CRUD and residual contamination are assumed to be composed entirely of ^{60}Co and to completely spall during both normal and hypothetical accident conditions. The maximum permissible leakage rates due to the spent fuel, CRUD, and residual contamination contributions to the source term are combined using Equation (3) to give total maximum permissible leakage rates for both normal and hypothetical accident conditions of transport. These results are also given in Table 1.

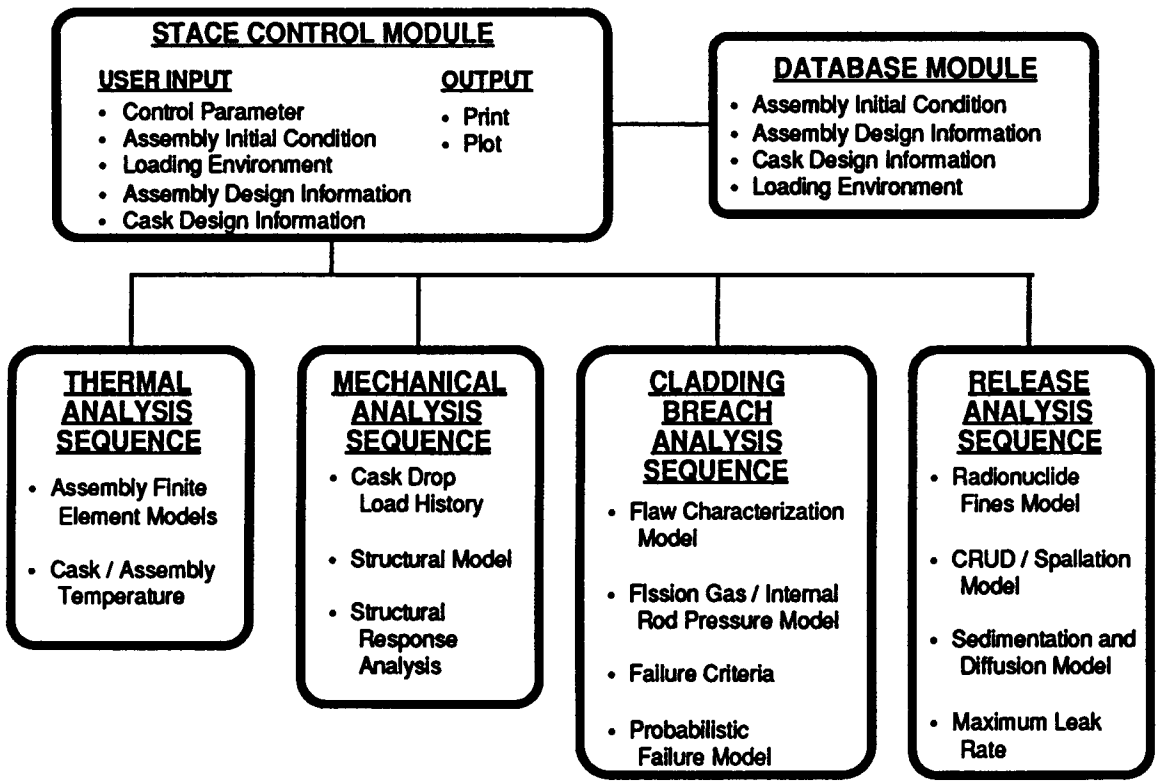

Figure 1. Design elements of STACE software system.

Table 1. Example Source Term Analyses for a Westinghouse 17x17 PWR Assembly.

Transport Condition	Spent Fuel		CRUD		Residual Contamination		Total
	C_{SF} (Ci/cm^3)	L_{SF} (cm^3/s)	C_{CRUD} (Ci/cm^3)	L_{CRUD} (cm^3/s)	C_{RC} (Ci/cm^3)	L_{RC} (cm^3/s)	L_T (cm^3/s)
Normal (0.3-m drop)	2.1×10^{-6}	5.6×10^{-3}	3.4×10^{-7}	5.6×10^{-3}	4.7×10^{-9}	4.1×10^{-1}	2.8×10^{-3}
Accident (9-m drop)	2.1×10^{-6}	33	2.1×10^{-9}	5.6×10^{3}	2.8×10^{-11}	4.1×10^{5}	33

CONCLUSIONS

Following the guidance of ANSI N14.5, the STACE methodology provides a technically defensible means for estimating maximum permissible leakage rates. These containment criteria attempt to reflect the true radiological hazard by performing a detailed examination of the spent fuel, CRUD, and residual contamination contributions to the releasable source term.

The evaluation of the spent fuel contribution to the source term has been modeled fairly accurately using the STACE methodology. The structural model predicts the cask drop load history, the mechanical response of the fuel assembly, and the probability of cladding breach. These data are then used to predict the amount of fission gas, volatile species, and fuel fines that are releasable from the cask. There are some areas where data are sparse or lacking (e.g., the quantity and size distribution of fines released from fuel rod breaches) in which experimental validation is planned. The CRUD spallation fraction is the major area where no quantitative data has been found; therefore, this also requires experimental validation. In the interim, STACE conservatively assumes a 100% spallation fraction for computing the releasable activity. The source term methodology also conservatively assumes that there is 1 Ci of residual contamination available for release in the transport cask. However, residual contamination is still by far the smallest contributor to the source term activity.

Finally, the ANSI N14.5 recommendation that 3% and 100% of the fuel rods fail during normal and hypothetical accident conditions of transport, respectively, has been shown to be overly conservative by several orders of magnitude for these example analyses. Furthermore, the maximum permissible leakage rates for this example assembly under normal and hypothetical accident conditions, estimated to be 2.8×10^{-3} cm^3/s and 33 cm^3/s, respectively, are significantly higher than the leaktight requirement of 10^{-7} std cm^3/s. By relaxing the maximum permissible leakage rates, the source term methodology is expected to significantly improve cask economics and safety.

REFERENCES

American National Standards Institute, *American National Standards for Radioactive Materials Leakage Tests on Packages for Shipment*, ANSI Standard N14.5 (1987).

Barrett, P. R., I. Kurkchubasche, and K. D. Seager, *A Spacer Grid Hysteretic Model for the Structural Analysis of Spent Fuel Assemblies Under Impact, SAND91-2528C (TTC-1114)*, proceedings of the Third International High Level Radioactive Waste Management Conference, Las Vegas, NV, p. 2249 (1992).

Barsell, A. W., *Nonlinear Statistical Analysis of Zircaloy-2 Fracture Toughness Data*, internal correspondence, GA Technologies, San Diego, CA (1987).

Bauer, A. A., W. J. Gallagher, L. M. Lowery, and A. J. Markworth, *Evaluating Strength and Ductility of Irradiated Zircaloy, BMI-NUREG-1985*, Battelle-Columbus Laboratories, Columbus, OH (1977).

Burian, R. J., K. D. Kok, R. Di Salvo, M. E. Balmert, K. R. Freeman, and A. W. Pentiman, *Response of Spent LWR Fuel to Extreme Environments, SAND85-7213*, Sandia National Laboratories, Albuquerque, NM (1985).

Croff, A. G., *ORIGEN2: A Versatile Computer Code for Calculating the Nuclide Compositions and Characteristics of Nuclear Materials*, Nuclear Technology, 62 (1983).

Foadian, H., Y. R. Rashid, and K. D. Seager, *Probabilistic Assessment of Spent-Fuel Cladding Breach, SAND91-2527C (TTC-1113)*, proceedings of the Third International High Level Radioactive Waste Management Conference, Las Vegas, NV, p. 1018 (1992).

IAEA Safety Standards, *Safety Series 6*, International Atomic Energy Agency, Vienna, Austria (1990).

Lorenz, R. A., J. L. Collins, and A. P. Malinauskas, *Fission Product Release From Highly Irradiated LWR Fuel, NUREG/CR-0722*, Oak Ridge National Laboratory, Oak Ridge, TN (1980).

Lorenz, R. A., J. L. Collins, M. F. Osborne, R. L. Towns, and A. P. Malinauskas, *Fission Product Release From BWR Fuel Under LOCA Conditions, NUREG/CR-1773*, Oak Ridge National Laboratory, Oak Ridge, TN (1981).

Miyamoto, Y., Y. Komatsu, T. Kakuma, and N. Nagai, *Mechanical Behavior of Zircaloy-2 Tubing Under Biaxial Stresses*, Journal of Nuclear Materials, 61 (1976).

OCRWM, *Characteristics of Spent Fuel, High-Level Waste, and Other Radioactive Wastes Which May Require Long-Term Isolation, DOE/RW-0184*, Washington, D.C. (1987).

Sanders, T. L., V. Pasupathi, H. Jordan, W. J. Mings, and P. C. Reardon, *A Methodology for Estimating the Residual Contamination Contribution to the Source Term in a Spent-Fuel Transport Cask, SAND90-2407 (TTC-1020)*, Sandia National Laboratories, Albuquerque, NM (1991).

Sanders, T. L., K. D. Seager, Y. R. Rashid, P. R. Barrett, A. P. Malinauskas, R. E. Einziger, H. Jordan, T. A. Duffey, S. H. Sutherland, and P. C. Reardon, *A Method for Determining the Spent-Fuel Contribution to Transport Cask Containment Requirements, SAND90-2406 (TTC-1019)*, Sandia National Laboratories, Albuquerque, NM (1992).

Sandoval, R. P., R. E. Einziger, H. Jordan, A. P. Malinauskas, and W. J. Mings, *Estimate of CRUD Contribution to Shipping Cask Containment Requirements, SAND88-1358 (TTC-0811)*, Sandia National Laboratories, Albuquerque, NM (1991).

Seager, K. D., P. C. Reardon, and P. R. Barrett, *STACE: An Integrated Code for Evaluating Spent-Fuel Transport Cask Containment, SAND91-2526C (TTC-1112)*, proceedings of the Third International High Level Radioactive Waste Management Conference, Las Vegas, NV, p. 1765 (1992).

U.S. Nuclear Regulatory Commission, *Leakage Tests on Packages for Shipment of Radioactive Materials, Regulatory Guide 7.4*, U.S. Nuclear Regulatory Commission, Washington, D.C. (1975)

Title 10 Code of Federal Regulations, Part 71, Office of the Federal Registrar, Washington, DC (1990).

TRANSPORTATION CASK CONTAMINATION WEEPING: A PROGRAM LEADING TO PREVENTION*

P. C. Bennett, D. H. Doughty, W. B. Chambers

Sandia National Laboratories**, Albuquerque, New Mexico USA

INTRODUCTION

This paper describes the problem of cask contamination weeping, and efforts to understand the phenomenon and to eliminate its occurrence during spent nuclear fuel transport. The paper summarizes analyses of field experience and scoping experiments, and concentrates on current modelling and experimental validation efforts.

The "weeping" phenomenon associated with spent fuel transportation casks (also known as "sweating") is believed to be due to the conversion of fixed contamination on the external surface of the cask to a removable form. Spent fuel transportation casks are loaded under water at nuclear power plants in a spent fuel storage pool, exposing the cask surfaces to contamination by radionuclides present in the pool water including ^{137}Cs, ^{134}Cs, and ^{60}Co. The external surfaces of loaded casks are routinely surveyed for removable contamination and decontaminated to 1/10 of the U.S. and IAEA regulatory limits prior to being released for shipment (49CFR 1983, IAEA 1989). However, 3% to 8% of U.S. spent fuel casks have arrived at final destinations with removable surface contamination in excess of that allowed by regulation, though many pre-shipment surveys have shown contaminant levels to be within allowable limits (Grella 1987). Attempts to reduce the incidence of weeping have met with limited success and resulted in time-consuming operational constraints and procedures that significantly increase cask processing times and occupational exposures at loading facilities. As the U.S. Department of Energy (DOE) moves toward a high volume spent fuel transportation campaign beginning in 1998, the elimination of weeping occurrence and minimization of operational constraints has received increased attention.

A DOE program is underway at Sandia National Laboratories (SNL) to determine the physical and chemical processes involved in radionuclide contamination and release on transportation cask surfaces. These activities are being conducted in order to provide a basis for: 1) the development of more effective decontamination procedures; and 2) the development of contaminant blocking methods to prevent initial cask surface contamination.

The program follows the approach illustrated in Figure 1. In-service data was collected and analyzed for weeping conditions during fuel and irradiated hardware transport campaigns, as well as during cask storage periods. Scoping experiments were also conducted to help clarify observations in this phase.

Based on these observations and analysis, an initial model of the weeping phenomenon was developed. We have proposed that ion-exchange characteristics of the stainless steel cask surface are responsible, at least in part, for weeping (Chambers et al. 1991). Radionuclide contaminants present in the spent fuel storage pool

* This work performed at Sandia National Laboratories, Albuquerque, New Mexico, supported by the United States Department of Energy under Contract DE-AC04-76DP000789.

** A United States Department of Energy Facility

in a dissolved, ionic state, are likely sources of cask surface contamination. Once fixed, these ionic contaminants are likely to remain chemically bound until some change in surface chemistry releases them.

SNL is now in the Experimentation and Validation phases, where various aspects of the model are being tested and refined. A computer code is being adapted to predict surface chemistry reactions to guide experiments, recommendations for methods of preventing weeping and field trials of such methods.

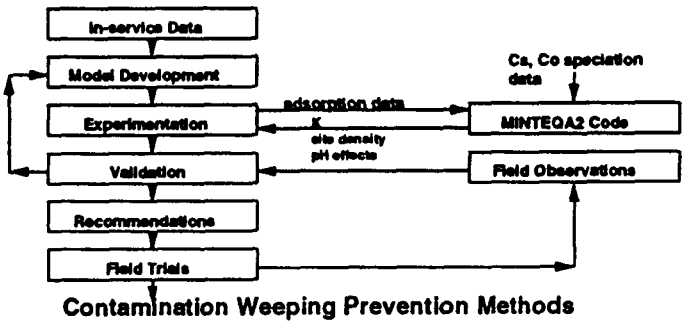

Figure 1. Contamination Weeping Project Flow

Initial recommendations will be made and field trials will begin within the next two years. Refinements to the weeping prevention methods will then be made with utility participation, and final recommendations on cask design and operational procedures will be made.

BACKGROUND

1. In-Service Data Analysis

In-service data analysis efforts focused on archival data and observation of on-going spent nuclear fuel and irradiated hardware transportation campaigns (176 cask movements), as well as cask storage conditions (Bennett et al. 1989). Weeping occurs as a transformation of apparently fixed surface contamination to a removable form. ^{137}Cs appears to be the primary contaminant in weeping, followed by ^{60}Co and ^{134}Cs. Weeping has been observed on a variety of cask surfaces and ages, both in transit and in storage, and on casks which were loaded and empty. A regression analysis conducted on transport data indicated a correlation of low ambient temperatures and high relative humidity with rises in removable contamination levels. This analysis also indicated more information is necessary to explain site-dependent factors. Reconstruction of previous shipments from archived data provided limited insights due to lack of detailed documentation. Cask pre-release surveys were of pass/fail nature, without mapped survey points or logged contamination values. Non-standardized instruments and swiping techniques were also used.

2. Scoping Experiments

To augment in-service observations and additional data regarding cask surface materials, finishes and environmental influences, scoping experiments were conducted at the University of Missouri. A surface area of 18.5 m^2 in the form of 122 stainless steel and titanium cylinders was contaminated in Union Electric's Callaway Plant spent fuel pool and subjected to environmental conditioning (Bennett et al. 1991). Contaminants involved in weeping on the test samples were identified as ^{137}Cs, ^{134}Cs, ^{60}Co and ^{54}Mn. The behavior of the main radioactive isotopes (Cs and Co) showed differences in the preferential rate at which they deposited onto the surfaces of the samples, and the rate at which they were removed by the swipes.

Rise in removable contamination occurred on the sample surfaces more often than not, and generally under a variety of conditions of changing temperatures. A source of potentially removable contamination approximately 100 times larger than what a health physicist can readily measure appears to be bound on the surface as "fixed" contamination. It has been demonstrated that a small portion (a few percent) of this initially fixed contamination will "weep" under certain conditions, becoming removable contamination. General indications of factors correlated to weeping were observed. Smoother cask surfaces, shorter pool exposures and protection from extreme temperature gradients correlate to lower rises in removable contamination.

The scoping experiment did not address the pool conditions or decontamination methods specifically. The parameters of a reactor spent fuel storage pool such as temperature, contaminant concentration and chemical form, and pH could conceivably affect reaction of contaminants with cask surfaces. The decontamination procedure could influence the percent of removable contamination is removed, and cause changes in the surface chemistry of the cask leading to increased rates of conversion to removable contamination.

3. Model Development: Adsorption of dissolved metals on oxide surfaces

Stainless steel is a chromium rich alloy that owes its corrosion resistance to a Cr-rich passive oxide layer (McCafferty and Brodd 1986). We have investigated the adsorption of dissolved metals on stainless steel surfaces using Cr_2O_3 powder as a model surface.

In order to recommend processes to prevent adsorption of Co^{2+} and Cs^{+} on a cask surface (or remove it by controlled desorption) it is necessary to understand the interaction between the dissolved metals and the oxide surface. Specifically, it is necessary to:

1. Determine the time required to achieve equilibrium.

2. Determine the distribution coefficient of metals such as cobalt, cesium, and other relevant species that will adsorb on oxide surfaces.

3. Develop a model of the storage pool chemistry and adsorption thermodynamics and apply the model to predict chemical methods that might be used to avoid contamination or remove contamination from surfaces of nuclear waste shipping casks.

Determining the time required to achieve equilibrium is necessary in order to accurately determine the distribution coefficient of metal ion adsorption. The approach described below is generally applicable to any species adsorbed on a surface (Allison et al. 1991). Using the adsorption of Co2+ on Cr2O3 as a model, the distribution coefficient is related to the equilibrium constant for the reaction of dissolved cobalt on a chromium oxide surface:

$$Co^{2+}(aq) + Cr_2O_3 \overset{K_{eq}}{<=========>} Co^{2+}(ads) - - Cr_2O_3$$

where:

$$K_{eq} = \frac{a(Co^{2+}(ads))}{a(Co^{2+})\,a(Cr_2O_3)}$$

In this expression, a(Co2+) is the activity of cobalt in solution and is described by:

$$a(Co^{2+}) = f(Co^{2+})\ [Co^{2+}]$$

where $[Co^{2+}]$ is the concentration of cobalt in solution as expressed in mol/L (M) and $f(Co^{2+})$ is the activity coefficient of cobalt in solution. Activity coefficients can be described by a variety of expressions. We have used the modified Debye-Huckel expression or the Davies equation for calculating activity coefficients.

There is no generally accepted method of computing activity coefficients for unreacted or reacted adsorption sites so we will define these coefficients as unity. Thus: $a(Co^{2+}(ads)\text{--}Cr_2O_3) = a(Co^{2+}(ads)) = [Co^{2+}(ads)]$.

Since the activity of a pure solid is unity, $a(Cr_2O_3) = 1$, therefore:

$$K_{eq} = \frac{[Co^{2+}(ads)]}{f(Co^{2+})\,[Co^{2+}(aq)]}$$

The equilibrium constant (K_{eq}) thus described is defined as the Activity Distribution Coefficient (Activity K_d) for adsorption of an ionic species onto an oxide surface. Variations of this model yield Activity Langmuir and Activity Freundlich expressions (Allison 1991). The distribution coefficient is directly related to the cask contamination model in that it describes how effectively a dissolved species is bound to a solid adsorbent. The larger the distribution coefficient, the more strongly the Co is adsorbed. The distribution coefficient for adsorption of other metal ions can also be measured to determine the potential for blocking the adsorption of Co^{2+} and other ionic radionuclides with more strongly bound metals. The addition of other chemicals, such as chelating agents, which bind Co^{2+} in the aqueous phase reduce the activity of Co^{2+} and therefore reduce the available concentration of Co^{2+} that can contaminate the oxide surface. These chemicals can be evaluated for use as decontamination agents.

EXPERIMENTAL METHODS

Modelling

We are applying an Environmental Protection Agency (USEPA) computer code, MINTEQA2, to the problem of adsorption of Co^{2+} and Cs^{+} on metal oxide surfaces. MINTEQA2 is a geochemical equilibrium speciation model capable of computing equilibria among the dissolved, adsorbed, solid and gas phases in an environmental setting. MINTEQA2 includes an extensive database of reliable thermodynamic data for these calculations.

Because the system that we are working with is not a common environmental situation, data needed to describe this system is not readily available in the data base. We are both generating thermodynamic data to allow the use of MINTEQA2 and exploring the seven different models that are available to describe adsorption phenomena to see which one(s) best model our system.

Adsorption studies:

The experimental methodology used in the studies described in this paper has previously been published (Chambers et al. 1991). In that earlier work, we described the reversible binding of Co^{2+} to Cr_2O_3. We noted that Cs^{+} binding had not been observed.

An experiment was designed to determine the kinetics for the adsorption reaction. A 20 wt% slurry of Cr_2O_3 in a solution containing 1.67 mM Co^{2+} was prepared. The concentration of Co^{2+} in this slurry was estimated to represent approximately 20% of the available adsorption sites on the Cr_2O_3 (assuming a surface binding site density of 2.5 sites/nm^2 as calculated previously (Chambers et al. 1991)). Less than 50% of the available sites were targeted for adsorption to avoid saturation effects in calculating the equilibrium distribution. The unadjusted, natural pH of the slurry was approximately 6.5, and remained relatively stable (i.e. slowly increased to 7.0) over the duration of the experiment. The slurry was sampled at various time intervals for up to 6 days, filtered, and the solution analyzed for cobalt concentration. This experiment was repeated in triplicate and the individual experiments are identified in the following discussion as: #SMI-26, #PWI-26, and #PWI-28.

Experiments were also performed to determine the distribution coefficient for Co adsorption on Cr_2O_3 as a function of pH. A slurry composed of 10 wt% Cr_2O_3 in 0.2 mM Co^{2+} was prepared and titrated from pH=7.52 to pH=3.09 (#PWI-36). In this case, the concentration of Co was estimated to represent 100% of the available adsorption sites. Samples were collected at intervals, filtered, and analyzed for Co concentration. The experiment was repeated with the addition of 0.1M tetramethylammonium chloride to the solution (#WSA-6). The tetramethylammonium ion provides for a constant ionic strength solution but does not compete for adsorption sites or sequester the Co^{2+}.

RESULTS AND DISCUSSION

Adsorption experiments:

The results of the three adsorption rate experiments described above for Co^{2+} on Cr_2O_3 are shown in Figure 2. These results show that equilibrium between Co^{2+}(aq) and Co(ads) on Cr_2O_3 is achieved slowly, although most (>90%) of the available cobalt was adsorbed within 60 minutes. The distribution coefficient at 98 hours was calculated to be:

$$K_d = [Co^{2+}(ads)] / [Co^{2+}(aq)] = 438$$

Graphs that show the dependence of K_d on pH as determined from the titration experiments are shown in Figures 3 and 4. Figure 3 is in agreement with data obtained from the equilibrium adsorption experiments (Fig. 2) as the extrapolated K_d at pH = 7 is very close to 438, the average value from the adsorption experiments. Figures 3 and 4 display the dependence of K_d for the first titration step (acidification). Previous experiments described in Chambers (1991) note hysteresis on cycling between acid and basic pH, which would affect K_d values. Note that agreement of Figure 3 and Figure 4 is poor. We presently ascribe the difference to the ionic strength effects of the tetramethylammonium ion. We plan to investigate these effects with the aid of the MINTEQA2 model and, if necessary, experimental studies.

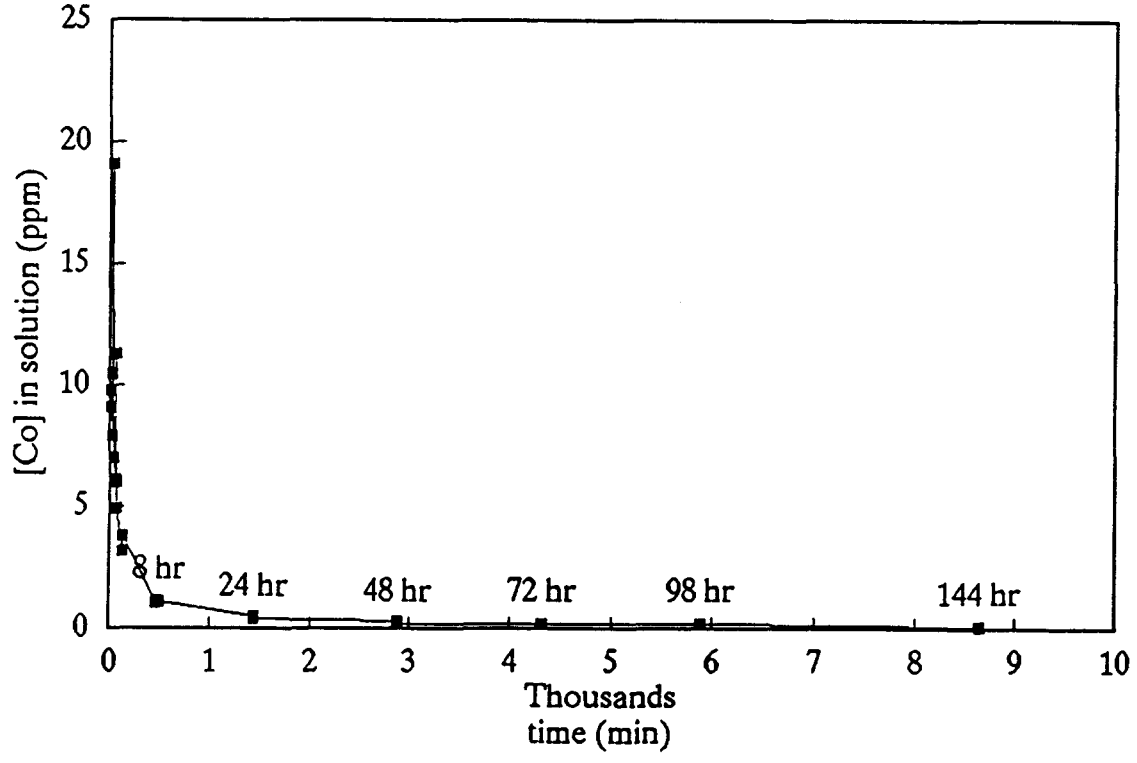

Figure 2. Equilibrium adsorption rate; Co^{2+} on Cr_2O_3

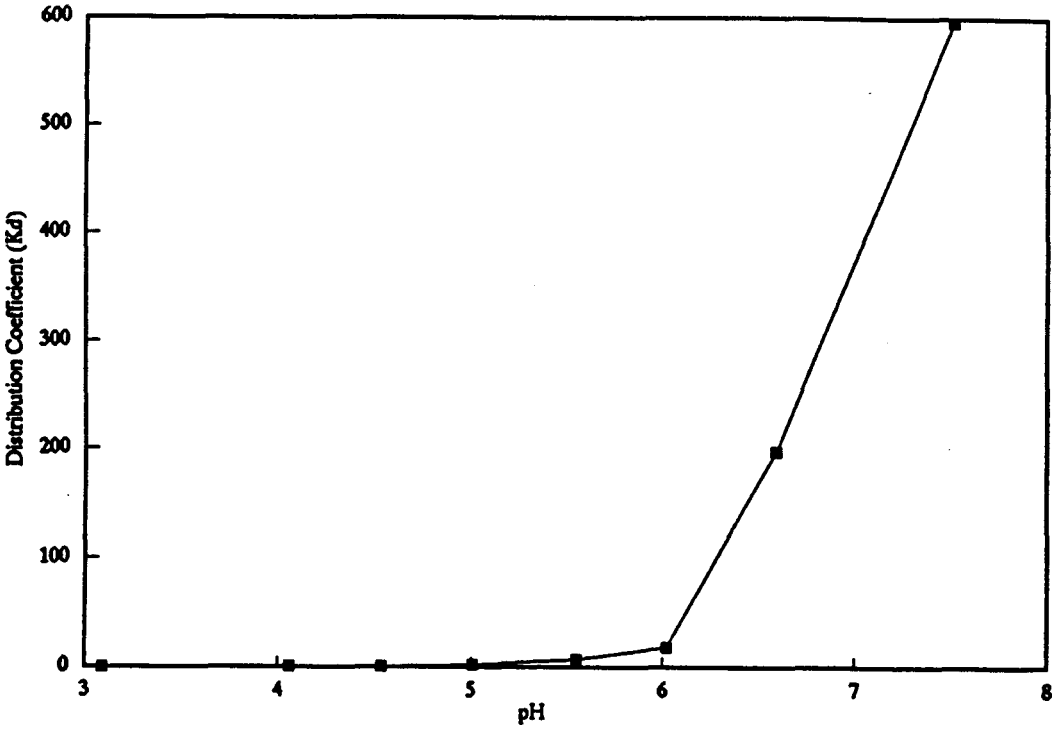

Figure 3. Distriubtion coefficient (K_d) vs. pH

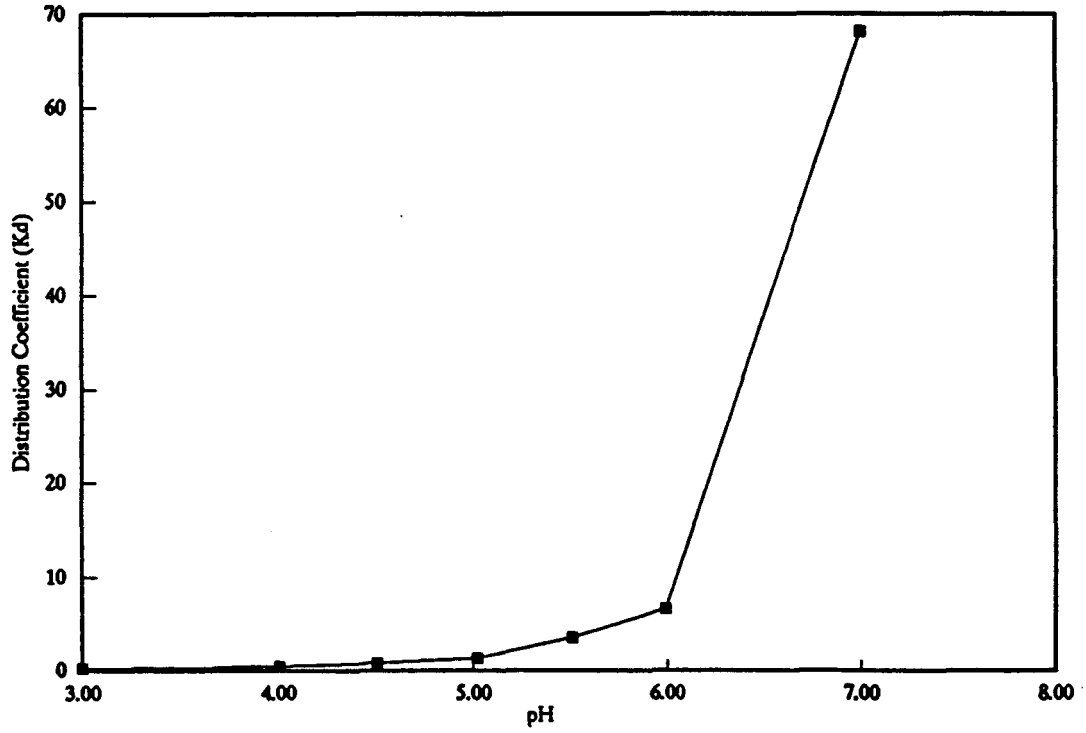

Figure 4. Distribution coefficient (K_d) vs. pH with ionic buffer

Adsorption modeling

We find that two of the adsorption models in the MINTEQA2 code yield promising results. These results are especially encouraging since several of the thermodynamic constants that are needed for accurate modeling are not currently available. The calculational runs described below are simulations substituting cadmium for cobalt as the solution species.

The first goal was to identify which of the seven adsorption models supported by MINTEQA2 most accurately describes our experiments. To date, three of the models have been used: the Activity K_d Adsorption model, the Activity Langmuir Adsorption model, and the Activity Freundlich model. The evaluation consists of using the K_d or K_L, total concentrations of species, and the total amount of adsorbate as input parameters for the code. The output (final concentration of metal adsorbed and dissolved) is calculated and compared to the actual measured concentrations. Table 1 gives the results using either the average Kd value of 438 or the average K_L of 33,710 obtained from the three Co^{2+} on Cr_2O_3 adsorption experiments (#PWI-26, #PWI-28 and #SMI-26).

Table 1

Comparison of Calculated and Measured Cobalt Adsorption on Cr_2O_3
(all concentrations expressed in mol/L)

	Measured	Calculated		
		Activity K_d	Activity Langmuir	Activity Freundlich
#PWI-26				
[Co]aq	3.74E-6	3.84E-6	2.21E-4	3.80E-6
[Co]ads	1.56E-3	1.66E-3	1.44E-3	1.66E-3
#PWI-28				
[Co]aq	3.57E-6	3.84E-6	2.21E-4	3.80E-6
[Co]ads	1.56E-3	1.55E-3	1.44E-3	1.66E-3
#SMI-26				
[Co]aq	3.40E-6	3.84E-6	2.21E-4	3.80E-6
[Co]ads	1.56E-3	1.66E-3	1.44E-3	1.66E-3

These data clearly show that the Activity K_d and the Activity Freundlich models are superior to the Activity Langmuir model and are in good agreement with the experimental data. Since the Activity Freundlich model is a special case of the Activity K_d model and since the results are comparable, we will continue evaluations at this stage using the Activity K_d model.

CONCLUSION AND FUTURE WORK

Several conclusions can be drawn from the results described in this report:

1. Adsorption of Co^{2+} onto Cr_2O_3 is close to equilibrium after several hours but takes a few days to achieve complete equilibrium.

2. K_d for adsorption of Co^{2+} onto Cr_2O_3 is dependant on pH and has a value of approximately 438 at pH = 7.

3. K_d for pH titration experiments agree with pH-static experiments as long as pH swings are not too extreme.

4. Distribution coefficients are dependant on ionic strength.

5. Activity K_d model describes our experimental results with sufficient accuracy.

From these experiments we have determined that adsorption of Co^{2+} on Cr_2O3 is kinetically favored in the pH range of a boric acid modified fuel storage pool. The value for K_d is higher at pH=7, the approximate pH of de-ionized H_2O. This suggests that a de-ionized water wash would have little effect in decontaminating these surfaces, whereas an acidic wash would be more effective.

We plan to continue our experiments and modelling efforts in order to define the chemical issues as completely as possible. While the data presented here supports the ion-exchange model for Co^{2+} adsorption on Cr_2O_3, scoping experiments have been performed that allow calculation of adsorption equilibria for other systems and which indicate that pure Cr_2O_3 is not the best model for adsorption on stainless steel. Experiments investigating the adsorption of Co^{2+} and Cs^+ on Fe_2O_3 and stainless steel powders are in progress.

We will continue to develop the MINTEQA2-based adsorption model with emphasis on incorporating appropriate thermodynamic constants. Furthermore, we will use the model to explore solution chemistry of storage pools and decontaminating solutions in order to gain insight into factors that will reduce initial surface contamination as well as remove contamination with more effective decontamination procedures. Recommendations based on the insights will be made, followed by field testing to evaluate the recommendations. Finally, the developed procedures will be available to prevent contamination weeping.

References:

Allison, J. D. et al., MINTEQA2/PRODEFA2, A Geochemical Assessment Model for Environmental Systems: Version 3.0 User's Manual. EPA/600/3-91/021, March 1991.

Bennett, P.C., et al., "In-Service Analysis of Cask Contamination Weeping," Proceedings of the 9th Annual Symposium on the Packaging and Transportation of Radioactive Materials, Washington, DC, June 1989, pp. 247-254.

Bennett, P.C., J.F. Kunze, and B.M. Rutherford, "Scoping Experimental Analysis Of Factors Affecting Cask Contamination Weeping," Proceedings of the 2nd Annual International Conference on High Level Radioactive Waste Management, Las Vegas, NV, April 1991, pp. 1248-1255.

Chambers, W. B. et al., RAMTRANS Vol. 2 No. 1/3 pp. 145-149 (1991).

Grella, A.W.. "Compliance Inspections by USNRC of Recent Spent Fuel Shipments," Proceedings of the Symposium on Waste Management, Tuscon, AZ, 1987, pp. 431-435.

IAEA Safety Series No. 6, International Atomic Energy Agency, Vienna, Austria, 1985.

McCafferty, E. and Brodd, R. J. (eds) "Surfaces, Inhibition and Passivation." Proceedings of the International Symposium of the Electrochemical Society Corrosion Division, 1986,pp.304-307.

U.S. Code of Federal Regulations, Title 49, part 173.443, Contamination Control, Washington, D.C., July 1983.

Burnup Verification Measurements for Spent Nuclear Fuel*

R. I. Ewing

Sandia National Laboratories, Albuquerque, New Mexico, United States of America**

INTRODUCTION

The U.S. Department of Energy is presently scheduled to begin transport of spent fuel from utility reactor sites to a federal storage facility in 1998, using casks certified by the U.S. Nuclear Regulatory Commission. Maximizing the capacity of transport casks now being designed is essential to reduce costs and to maintain public and occupational risks "as low as reasonably achievable." The spent fuel to be transported in the immediate future has been cooled for a decade or more, and its radiation output is greatly reduced due to natural radioactive decay. The reduced requirements for heat dissipation and radiation shielding allow more spent fuel to be loaded into a cask of a fixed gross weight. Conceptually, cask capacity can be increased to the point where, under certain conditions, nuclear criticality safety must be considered in the design of transport casks (Sanders and Westfall, 1990). The reduced reactivity of the "burned up" fuel permits about twice as many spent assemblies to be safely transported in each cask as could be accommodated if the assemblies were fresh, unburned fuel. The loaded casks are to be transported in a dry condition. Nuclear criticality becomes possible during the transport of spent fuel only if: (1) the cask is involved in an accident, (2) the accident is severe enough to breach the cask, (3) the cask is flooded with water that contains a low level of neutron absorbers, and (4) the fuel has unacceptably high reactivity.

The criticality of the loaded, flooded cask can be calculated from three parameters which are cataloged at the reactor for each assembly. The three factors are: initial enrichment, usually expressed as weight percent U235; burnup (gigawatt days per metric tonne of U metal); and the cooling time (years) (Brady and Sanders, 1991). Casks designed taking advantage of the reduced reactivity of the burned fuel to calculate criticality are called "burnup credit" casks. The characteristics of fuel acceptable for loading into a burnup credit cask can be specified by a loading curve as shown in the example of Figure 1. Acceptable assemblies are configured in the cask so that, under flooded conditions, the system is less than 95% of critical. The curve delineates the minimum burnup credit required for a particular initial enrichment. The use of burnup credit in cask design raises the possibility that a cask could be misloaded with unacceptable fuel, if such assemblies are present. Radiation measurements can be used to help prevent misloading of a cask by verifying that each assembly has the appropriate characteristics.

---

*This work was performed at Sandia National Laboratories, Albuquerque, New Mexico, supported by the United States Department of Energy under contract DE-AC04-76DP00789.

**A United States Department of Energy Facility.

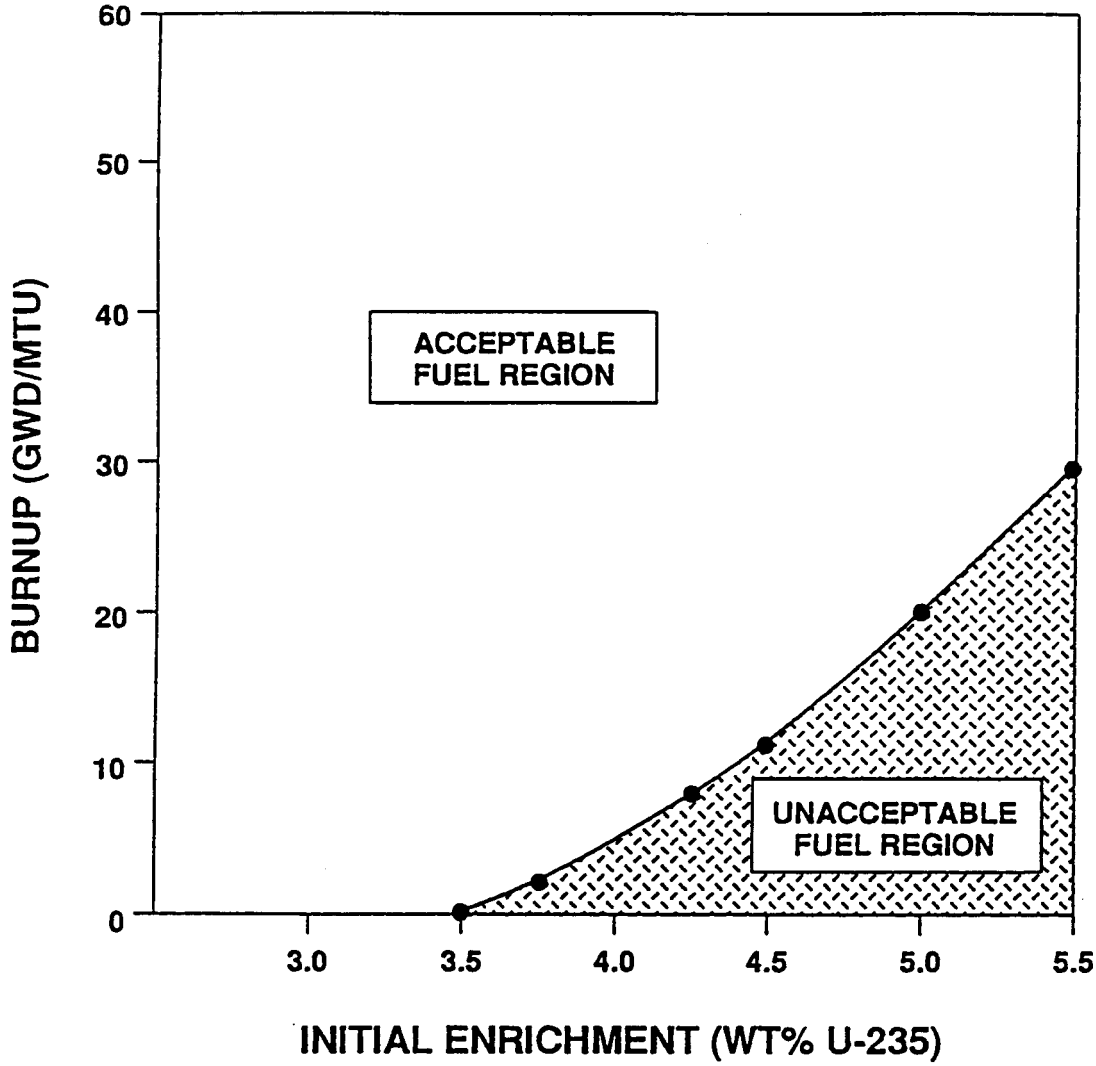

Figure 1. Loading Curve for a Burnup Credit Cask

RADIATION MEASUREMENTS

Studies have concluded that the utility-supplied data on burnup, cooling time, and initial enrichment is of greater accuracy and reliability than could be provided by additional radiation measurements on spent fuel assemblies (ORNL, 1988). However, radiation measurements can be used to help prevent misloading of casks with unacceptable fuel by screening assemblies to confirm reactor records and to detect accidental selection of overreactive assemblies. To confirm reactor records, it is sufficient to determine burnup and cooling time, since the initial enrichment is common to a large number of assemblies and generally is not in question. For purposes of screening fuel for burnup credit, it is necessary only to establish that burnup is greater than the burnup credit required for the cask at the initial enrichment of the assembly, and that the cooling time is greater than 5 years.

The FORK measurement system, designed by Los Alamos National Laboratory (LANL), has been used for many years by the International Atomic Energy Agency to verify reactor records worldwide by measuring neutron and gamma-ray emissions from spent fuel assemblies (Rinard

and Bosler, 1988). This technique has proved to be adequate to eliminate the need for more complex active or high-resolution measurement techniques (Phillips et al., 1983). The system appears to be particularly well-suited for application to spent fuel verification measurements at U.S. storage sites. The system is diagrammed in an operational arrangement in Figure 2. The detector head can be moved in the storage pool to the spent fuel assembly to be examined. The assembly is raised in the storage rack so that its midpoint is about 2 feet above the top of the rack. The detector head is positioned at the midpoint of the assembly for the measurement. The neutron measurements can be correlated with burnup, resulting in a power law relationship that is specific to each assembly design. The gamma-ray signal is proportional to the burnup. Analysis of the measurements is simplified by the fact that the fuel assemblies of immediate interest for transport have all been cooled for over 10 years, leaving only a few gamma and neutron sources that have well-defined half-lives. The detector must be calibrated with fuel assemblies of known and reliable burnup and cooling time in the range of values of interest. A burnup profile measurement can be performed by measuring along the length of the assembly as it is raised out of the storage rack. Burnup has been determined to an average accuracy of about 5%. The gamma-ray measurements have been consistent with operator-declared values for burnup and cooling time to about 10%. Fission chambers are used to measure neutrons from the assembly, and an ion chamber is used to measure gammas. A battery-powered electronics unit is used to supply all power to the detectors, collect and analyze the detector outputs, and perform necessary calculations and documentation. Data collection has required less than 60 seconds per measurement. A trained crew can assemble the system and check it out for operation in about 30 minutes.

TEST PROGRAM

A joint program involving SNL, LANL, and the Electric Power Research Institute is under way to evaluate the FORK system at U.S. utility storage sites. The objectives of the tests are to: (1) demonstrate that neutron and gamma-ray emission measurements are adequate to verify spent fuel assembly characteristics for burnup credit; (2) obtain calibrations of the instrument over the burnup, cooling time, and initial enrichment ranges of interest; (3) examine the axial distribution of burnup in some assemblies; and (4) develop operational procedures with utility input. The existing data taken with the FORK detector will be analyzed for its applicability to the proposed tests, and criteria will be specified for selecting the calibration assemblies before tests begin at the utility storage pools. The results of the tests will indicate if further development of the FORK detector is required for the burnup credit application. An important part of these tests is the development of operational procedures that meet the requirements of the utilities and the management of the spent fuel storage pools. It is imperative that any measurement system selected be as simple, inexpensive, quick, and nonintrusive as possible.

SUMMARY

The number of shipments of spent fuel could potentially be reduced by about one-half by the use of burnup credit casks, considerably enhancing public and occupational safety, and reducing costs. Radiation measurements can be used in burnup credit operations to help prevent misloading of fuel that does not meet the minimum specifications for a particular cask design. Neutron and gamma-ray yield measurements are proposed as a means of qualifying spent fuel assemblies. Plans are under way to evaluate the FORK measurement system at utility spent fuel storage pools.

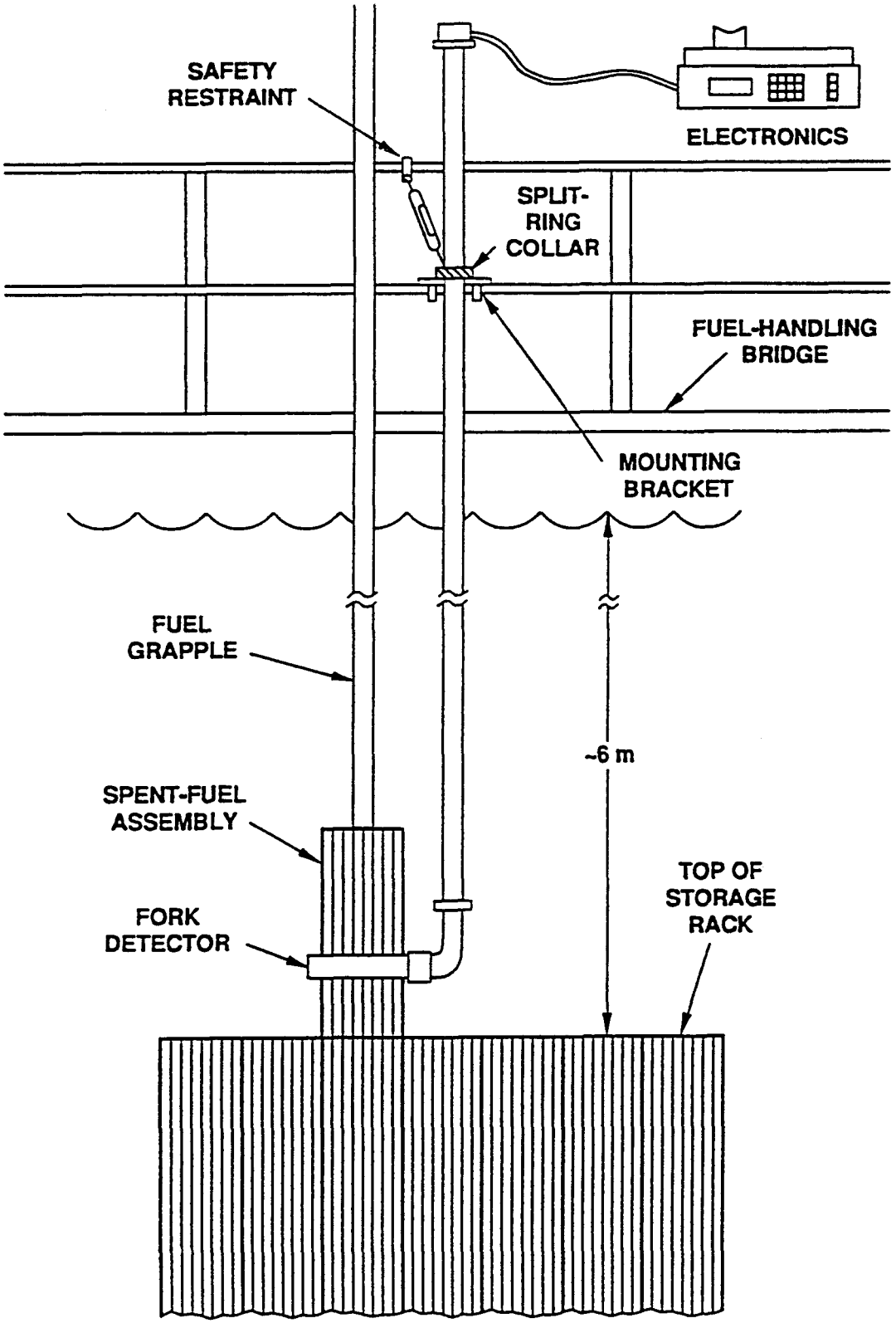

Figure 2. Sketch of a FORK Detector in Operation

REFERENCES

Brady, M. C. and Sanders, T. L., "A Validated Methodology for Evaluating Burnup Credit in Spent Fuel Casks," Proceedings of the International Conference on Nuclear Criticality Safety, p. II-68, Oxford, UK, September 1991.

ORNL, "The Incentives and Feasibility for Direct Measurement of Spent Nuclear Fuel Characteristics in the Federal Waste Management System," ORNL/Sub/86-SA094/3, JAI-296, report prepared by E. R. Johnson Assoc. for Oak Ridge National Laboratory, 1988.

Phillips, J. R., et al., "Experience Using a Spent-Fuel Measurement System," INMM Annual Meeting 1983, Vol. 12, p. 175, 1983.

Rinard, P. M. and Bosler, G. E.,"Safeguarding LWR Spent Fuel with the FORK Detector," LA-11096-MS, Los Alamos National Laboratory, Los Alamos, New Mexico, March 1988.

Sanders, T. L. and Westfall, R. M., "Feasibility and Incentives for Burnup Credit in Spent-Fuel Transport Casks," Nuclear Science and Engineering, Vol. 104, pp 66-77, 1990.

Incentives for the Use of Depleted Uranium Alloys as Transport Cask Containment Structure*

P. McConnell+, *R. Salzbrenner, G.W. Wellman, and K.B. Sorenson*

+GRAM, Inc., Albuquerque New Mexico 87112 USA
Sandia National Laboratories, Albuquerque New Mexico 87185 USA

INTRODUCTION

Radioactive material transport casks use either lead or depleted uranium (DU) as gamma-ray shielding material. Stainless steel is conventionally used for structural containment. If a DU alloy had sufficient properties to guarantee resistance to failure during both normal use and accident conditions to serve the dual-role of shielding and containment, the use of other structural materials (i.e., stainless steel) could be reduced. (It is recognized that lead can play no structural role.) Significant reductions in cask weight and dimensions could then be achieved perhaps allowing an increase in payload. The mechanical response of depleted uranium has previously not been included in calculations intended to show that DU-shielded transport casks will maintain their containment function during all conditions. This paper describes a two-part study of depleted uranium alloys: First, the mechanical behavior of DU alloys was determined in order to extend the limited set of mechanical properties reported in the literature (Eckelmeyer, 1991). The mechanical properties measured include the tensile behavior the impact energy. Fracture toughness testing was also performed to determine the sensitivity of DU alloys to brittle fracture. Fracture toughness is the inherent material property which quantifies the fracture resistance of a material. Tensile strength and ductility are significant in terms of other failure modes, however, as will be discussed. These mechanical properties were then input into finite element calculations of cask response to loading conditions to quantify the potential for claiming structural credit for DU. (The term "structural credit" describes whether a material has adequate properties to allow it to assume a positive role in withstanding structural loadings.)

DEPLETED URANIUM ALLOYS STUDIED

Because some DU alloys have limited ductility, it has been presumed that no DU alloy can be relied upon to provide a cask containment function (unalloyed DU is typically used for shielding). Mechanical properties were measured for a select group of DU alloys. The chemistry and processing history of these alloys were selected and controlled to produce a broad range of properties and microstructures. The materials matrix was chosen to include effects from intentional alloying additions (e.g., Mo, Nb) which increase the strength, unwanted trace elements (e.g., C, H) which are known to affect the tensile ductility, and heat treatments designed to alter the microstructure.

Table 1 summarizes the DU alloys which were produced for this program. All with the exception of Heat I were cast by Cameco Corporation using a conventional vacuum induction melting process. Heat I was produced by the Y-12 Plant, Martin Marietta Energy Systems, Inc. All of the as-cast materials underwent further processing at the Y-12 Plant which included heat treating to reduce the hydrogen content and/or to control crystal structure and

*Work supported by the United States Department of Energy under Contract DE-AC04-76DP00789.

Table 1. Depleted uranium alloys investigated.

Heat	Nominal Description	Meas. H (ppm)	Meas. C (ppm)
A	unalloyed casting with 200 ppm C	1.53	210
B	unalloyed casting with 200 ppm C +H outgas treatment @630°C/65 hr	0.44	210
C	unalloyed casting with 200 ppm C +H outgas treatment @720°C/35 hr +β cycle (2 times) for grain reduction	0.13	210
D	unalloyed casting with 200 ppm C (thicker casting than Heat A)	1.91	160
E	unalloyed plate with 200 ppm C +H outgas treatment @ 800°C/96 hr, followed by warm rolling at 300°C	0.10	---
F	unalloyed casting with 50 ppm C +H outgas treatment @ 720°C/35 hr	0.07	10
G	3% Mo alloy casting with 50 ppm C +H outgas treatment @ 800°C/24 hr	0.05	53
H	3% Mo alloy casting with 200 ppm C +H outgas treatment @ 800°C/24 hr	0.08	190
I	1.7% Nb alloy casting with 50 ppm C +H outgas treatment @ 800°C/24 hr	0.05	---

rolling to produce plate. The DU alloys were selected to quantify the effectiveness of the hydrogen outgassing treatment in improving ductility and toughness. In addition, the effect of increased additions of molybdenum and reduced levels of niobium, beyond the levels reported in the literature, was also to be characterized.

Metallographic characterization revealed an extremely large grain size (> 1 - 2 mm) in unalloyed DU Heats A, B, D, and F. This large grain size was found in alloys with very low impurity contents which were specially heat treated to remove hydrogen. The grain size of the other unalloyed DU heats (Heats C and E) was reduced to below 0.5 mm. The alloyed DU (Heats G, H, and I) possessed a fine grain size (< 0.1 mm).

MECHANICAL TEST RESULTS

Elastic moduli, tensile strength and ductility, and fracture toughness were measured in this study. The elastic moduli were determined by measuring the density and the ultrasonic velocities of longitudinal and shear waves and calculating the Young's and shear elastic constants. The tensile properties were measured on standard round

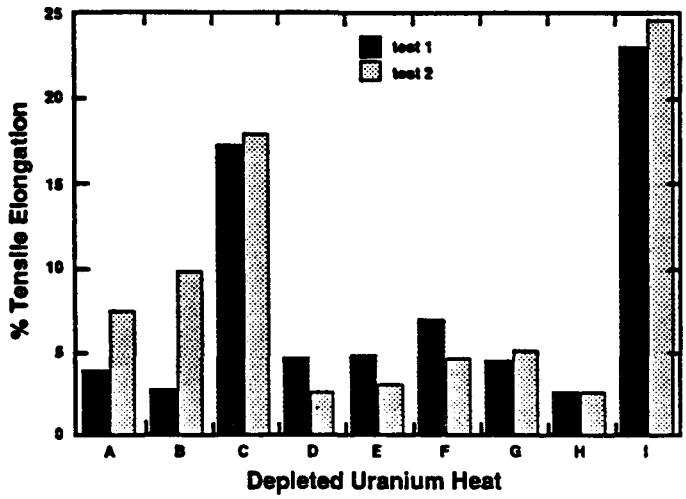

Figure 1. DU alloy tensile ductility test-to-test variation.

tensile specimens. The quasi-static-rate fracture toughness was measured by employing a single-specimen J-integral method, per ASTM E-813, on compact specimens with a net thickness of 22.9 mm. The fracture toughness of the majority of the alloys in this study were elastic-plastic values, J_{Ic}. Equivalent K_{Jc} values were estimated from the J_{Ic} values.

The room temperature mechanical properties for the DU alloys tested are shown in Table 2. Figure 1 is a plot of the tensile ductility measured in separate tests of the same alloy. There is substantial test-to-test variation for Heats A, B, D, E, and F. A sizable amount of test-to-test variation in replicate fracture toughness tests was exhibited for these same heats. The unalloyed Heats A, B, D, and F exhibited very large grain size. The large grain size apparently caused a significant amount of test-to-test variation in duplicate tensile and fracture toughness tests. The average grain size was a large fraction of the cross section of these test specimens, and thus the orientation of single grains could dominate in any particular test result.

The test results show that the fracture toughness of DU can be quite high even though the alloy may exhibit low ductility and/or low impact values. Most of the alloys examined retain elastic-plastic fracture behavior even at -40°C. Such elastic-plastic behavior indicates that failure will not likely occur via brittle fracture when applied stresses are below yield level.

Efforts to reduce impurities (C, H) also resulted in alloys with very large grain sizes (and collateral low ductility). The large grain size caused large variations of the mechanical property measurements within a heat, and thus the direct effect of different levels of C and H could not be accurately determined. Attention to alloy composition and casting process will allow adequately fine grain size to be maintained, along with a suitably high tensile ductility. This can no doubt be accomplished without introducing high levels of interstitial C and H.

The strength properties of DU alloys generally meet or exceed that of 304 stainless steel which is commonly used as the structural material in transport casks. Attempts to increase the strength through alloying often result in a considerable decrease in ductility and fracture toughness. When considered for cask structural applications, DU may be limited more by considerations of ductility and fracture toughness than by strength (i.e., even unalloyed DU may have adequate strength).

Table 2. Average room temperature quasi-static mechanical properties for the depleted uranium alloys.

DU Heat	yield strength (MPa)	ultimate tensile strength (MPa)	total elongation (%)	reduction in area (%)	Young's modulus (10^5 MPa)	shear modulus (10^5 MPa)	fracture toughness K_{Ic} or K_{Jc} MPa-$\sqrt{m}$	impact strength (J)
A	206	374	3.2	6.6	1.94	0.83	107	19
B	206	472	9.8	10.5	1.92	0.79	110	18
C	284	735	17.6	17.8	2.02	0.84	122	18
D	164	374	4.8	10.9	1.99	0.83	103	15
E	382	708	3.1	4.7	2.09	0.87	177	30
F	199	425	5.5	9.7	2.12	0.82	171	37
G	747	1174	4.7	3.9	1.92	0.89	51	4
H	647	1047	2.2	0.8	1.94	0.90	32	1
I	475	981	24.3	28.0	1.83	0.75	151	23

The mechanical properties generated in this study were subsequently used in calculations to determine the response of generic cask geometries to loading events simulating severe accident conditions. Two levels of DU materials properties were chosen. "Low" properties were based on the tensile and fracture toughness test results of unalloyed DU Heat F. This alloy exhibited low strength (yield strength of 199 MPa; ultimate tensile strength of 425 MPa) and low-to-moderate tensile ductility (total elongation of 5.5%; reduction in area of 9.7%). In spite of the limited ductility this alloy displayed a high fracture toughness (K_{Ic} = 171 MPa-$m^{1/2}$). The "high" DU properties were based on the behavior of the U-1.7Nb alloy (Heat I), which possessed both a high strength (yield strength of 475 MPa; ultimate tensile strength of 981 MPa) and a high ductility (total elongation of 24%; reduction in area of 28%). The measured fracture toughness for this material was also high (K_{Jc} = 151 MPa-$m^{1/2}$). The "low"

properties levels were chosen to underestimate the mechanical properties that should be readily available from unalloyed DU with no special processing controls. Representative stress-strain curves were used to provide the constants for the power-law model of the elastic-plastic materials model used in the finite element calculations.

FINITE ELEMENT ANALYSES

Calculations of the response to loading events simulating severe accident conditions were performed for two generic cask geometries, Figure 2. The "Case 1" geometry has a stainless steel thickness which was chosen to match that used in an actual cask (i.e., the General Atomics GA-4/9 cask, funded by the U.S. DOE Office of Civilian Radioactive Waste Management). In this cask the stainless steel serves as the primary structural support. Results were compared to those for a second geometry (Case 2) in which the stainless steel thickness was reduced, and the DU assumed the dominant structural role. For Case 1, the thick layer of stainless steel surrounding the DU was chosen by the cask designers to withstand the mechanical loadings from normal use and hypothetical accident conditions. The DU layer was sized to provide the requisite shielding (accounting for the stainless steel shielding). In Case 2, the thick stainless steel layer was reduced to a thin sheet; the thickness of the DU was appropriately increased over that used in Case 1 to provide for a constant amount of shielding between the two cases. The structural responsibilities of the DU increased in Case 2, since only thin stainless steel layers were present on either side of the DU.

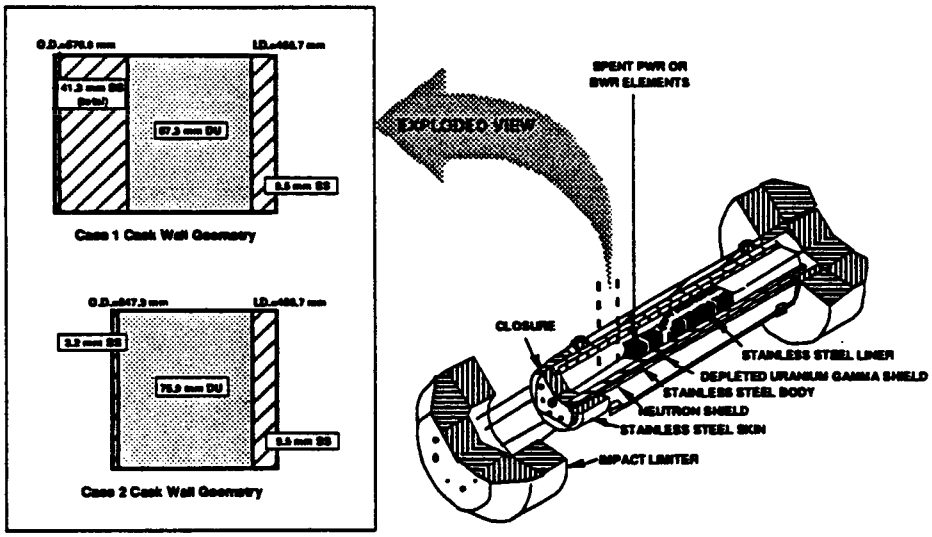

Figure 2. Schematics of the two cask designs for structural analyses.

The mechanical response of the DU layer was assessed in terms of three different failure criteria to determine whether DU assumed the increased structural responsibility required by changing the cask design from Case 1 to Case 2.

First, the maximum tensile stress in the DU layer was calculated as a function of applied acceleration ("g's") and then compared with U.S. Nuclear Regulatory Commission Regulatory Guide 7.6 stress allowable values. The NRC design guidance for transport casks (U.S. NRC 1978) imply that the cask should be able to elastically withstand all loads applied during normal use or hypothetical accident conditions. Specifically, it is generally assumed that application of such loads will not cause through-wall plasticity. If this condition is applied, the necessity of having a material capable of undergoing extreme plastic deformations is greatly diminished. Theoretically, only a limited tensile ductility might be required to withstand local plastic deformation (particularly when the fracture toughness is high). As a practical matter however, it is prudent to require sufficiently high ductility as a means of demonstrating a margin of safety against tearing failure. DU alloys which exhibit moderate tensile ductility (e.g., elongations >10%) may provide sufficient margin. In the analyses, the cask was treated as a simply supported beam subjected to multiple gravity loading. Elastic response of the cask materials was assumed. For the simulated side drop events, stresses were predominantly primary membrane. For such a loading condition, the Regulatory Guide allows a stress which is smaller than the lesser of 2.4 S_m or 0.7 S_u. The value of S_m is based on the ASME Design Stress Intensity, and is, for ferritic steels, the smaller of two-thirds of

the yield strength, S_y or one-fourth of the ultimate strength, S_u, of the alloy. DU is not listed as an ASME Code material, but for the purposes of this feasibility study was treated with the same restrictive rules as those which govern ferritic steels since DU alloys can, under certain conditions, fail in a brittle manner. For both the low and high property DU alloys, the allowed S_m is thus one-fourth S_u. The allowable stress ($=2.4\ S_m = 0.6\ S_u$) is therefore 255 MPa for the "low" property DU, and 589 MPa for the "high" property DU alloy. For comparison purposes, the ASME Design Stress Intensity for 304 stainless steel ($S_y = 207$ MPa) is 138 MPa and the maximum allowable stress is 331 MPa. The first stress-based failure criterion occurs therefore when:

$$2.4\ S_m / S_a < 1 \qquad \text{Equation 1}$$

where S_a is the maximum applied tensile stress.

Table 3 lists the factor of safety in terms of stress in the DU layer when the casks from Case 1 and Case 2 are subjected to an applied lateral g-load. The factor of safety, FS, is the ratio of the stress allowable to the maximum calculated stress in the DU layer (Eq. 1). When the FS ratio is less than unity, the DU fails this stress-based design criterion. Even the "low" property DU for both cask designs maintains its structural integrity at acceleration levels greater than the 50 g level expected for the nine-meter drop with impact limiters (Osborne et al. 1989). The "high" property DU alloy can withstand high levels of acceleration before the regulatory stress allowables are exceeded (103 and 74 gs for Case 1 and Case 2 geometries, respectively). As expected, the margin to failure is significantly reduced in moving from Case 1 to Case 2. This is primarily a geometric effect in moving from a larger to a smaller total wall thickness. A reduced margin of safety is precisely what is being traded for the lower mass which is associated with the decrease in thickness. Figure 3 shows a graphical presentation which demonstrates the effects of materials properties and geometry. Plotting the inverse of FS versus applied acceleration (g^s) allows the results to be viewed on a compressed scale. Failure is shown in Figure 3 if a value of one is exceeded. It is readily apparent from the figure that geometry dominates for this failure criterion: the effect of increasing the thickness of the structural layers is more significant than improving the materials properties.

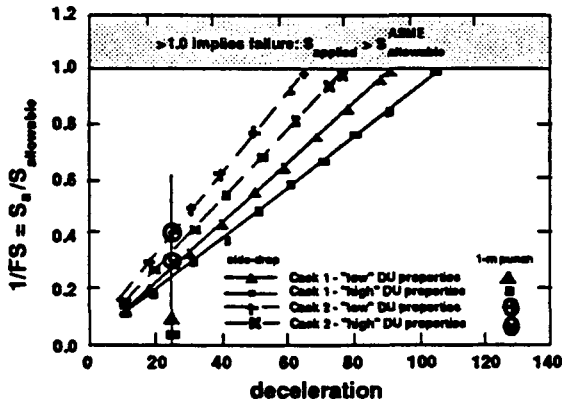

Figure 3. The inverse of the Factor of Safety for the ASME Design Stress Intensity failure criterion as a function of applied acceleration. (Case 1 is thick stainless steel layer, Case 2 is thin stainless steel.)

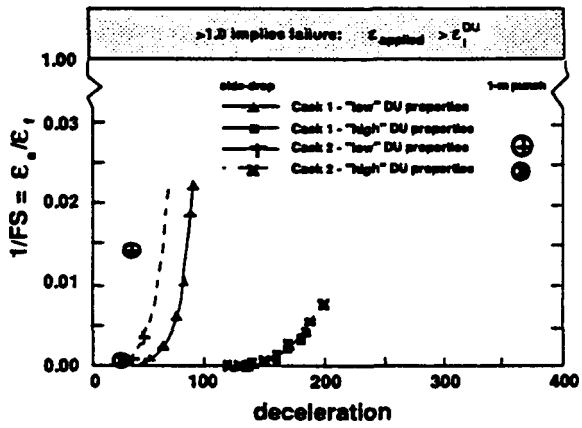

Figure 4. The inverse of the Factor of Safety for the True Strain-to-Failure failure criterion as a function of applied acceleration. (Case 1 is thick stainless steel layer, Case 2 is thin stainless steel.)

A second failure criterion is based on the strain-to-failure. This deformation failure criterion presents a more rational basis for determining the actual physical response of a structure than the NRC/ASME stress-based method described above. In applying this method, a finite element calculation of the strain in the DU layer was performed for the two geometries and the two levels of DU properties. The cask ends were constrained and a gravity load was applied. Nonlinear materials properties were used. The applied acceleration was increased until through-wall yielding of the cask was computed. A power-law constitutive model (JAC3D, a nonlinear, quasi-static, finite element computer program) was used for these calculations. This type of analysis is incapable of determining the

Table 3. The Factors of Safety (FS) calculated for the two cask designs using the ASME Design Stress Intensity and the True Strain-to-Failure Criteria.

	FS_σ* for ASME Design Stress Intensity				FS_ε** for True Strain Failure Criterion			
	Case 1		Case 2		Case 1		Case 2	
applied acceler.	"low" props.	"high" props.	"low" props.	"high" props.	"low" props.	"high" props.	"low" props.	"high" props.
(g's)								
10	9.4	10.4	6.7	7.4				
20	4.7	5.2	3.4	3.7				
30	3.1	3.5	2.2	2.5				
40	2.3	2.6	1.7	1.9			728	
50	1.9	2.1	1.3	1.5	31865		303	
60	1.6	1.7	1.1	1.2	1133			
70	1.3	1.5	0.9	1.1	418			
80	1.2	1.3		0.9	160			
90	1.0	1.2			53			
100	0.9	1.0						
110		0.9						
120								115438
130								9850
140						10579		2419
150						2253		1123
160						991		639
170						438		349
180						276		272
190						226		180
200								132

*FS_σ= ASME Sallowable/Sa **$FS_\varepsilon = \varepsilon_f / \varepsilon_a$

dynamic effects of an actual side drop and also ignores the behavior of impact limiters. Nonetheless, this analysis is very effective in providing the data required to assess the structural response of DU.

For every applied "g" the maximum true strain in the DU layer was calculated and compared to the true strain to failure determined from tensile test results. The failure criterion for this calculation is thus the true tensile strain to failure, ε_f, divided by the finite element calculation of the true applied plastic strain in the DU, ε_a.

$$\varepsilon_f / \varepsilon_a < 1 \qquad \text{Equation 2}$$

The strain-based FS at various applied g's are also presented in Table 3. Figure 4 is a graphical presentation of the data in which the inverse of FS is plotted as a function of applied acceleration. From the figure, it is apparent that the DU is far from failure as defined by the true strain to tensile failure. The calculations were terminated when through-wall yielding was found in the DU. This presents a high level of conservatism and provides agreement with the implied design requirements for a fully elastic response. In contrast to the results of the ASME method where the thickness of the various layers dominated the calculation of the FS, it is the materials properties which dominate the determination of the FS which is based on the strain-to-failure. Using a strain-based failure criterion provides the opportunity to judge the response of structures using a more fundamental understanding of actual materials behavior.

A third fracture mechanics failure analysis must be considered when using a material such as DU which can fail in a brittle manner under certain severe conditions. Fracture mechanics analyses are based on comparing the driving force for brittle fracture to the material's inherent resistance to fracture, a property known as fracture toughness. For brittle fracture the fracture toughness is measured in terms of the linear-elastic value designated as K_{Ic}. The fracture toughness of the majority of the alloys measured in this study were determined as ductile elastic-plastic values, J_{Ic}. Equivalent K_{Jc} values were estimated from the J_{Ic} values.

The linear elastic stress intensity in the region of a flaw provides a driving force for crack extension, and can be calculated from the following relationship:

$$K_I = S_e C (\pi a)^{1/2} \qquad \text{Equation 3}$$

where K_I is the applied stress intensity, C is a geometry factor ($\cong$1.2), and "a" is the flaw depth. When the K_I exceeds the fracture toughness (i.e., K_{Ic} or K_{Jc}), crack growth is predicted.

As a means of determining the sensitivity of the DU to brittle fracture for the casks in this study, Equation 3 can be rearranged as to calculate the critical flaw size for brittle fracture, a_c:

$$a_c = (1/\pi) [(K_{Jc})/(S_e{*}C)]^2 \qquad \text{Equation 4}$$

with K_{Jc} substituted for K_I. Thus the largest flaw that can be tolerated by the structure at a specific applied stress level can be computed. The overall cask system (which would include impact limiters) would be designed to prevent applied through-wall stresses which are above the yield strength level of each of the materials used. Equation 4 is only valid in the elastic regime, and thus the yield strength will be used for the calculation of the largest flaw size that can be tolerated. The "high" property DU has a lower fracture toughness (i.e., 151 MPa-$m^{1/2}$) than the "low" property DU and thus this value is used as an example. The "high" yield strength is 475 MPa. Substituting these values into Equation 4 produces a value for the critical flaw size, a_c, equal to 25.7 mm. Non-destructive evaluation (NDE) techniques are available which can locate all flaws which are even a small fraction of this value. The above calculation with improbable yield-level applied stress demonstrates flaw tolerance of DU. Proper design of the cask with impact limiters would reduce the applied stress significantly, and thus the allowed (i.e., non-critical) flaw size would be even greater. Potential for brittle fracture can be eliminated by: i) NDE inspection to assure that all flaws which are present are significantly smaller than $\cong$25 mm in depth, and/or ii) designing to guarantee that applied stress will always be below an appropriate value. Such requirements would result in a high level of conservatism against brittle fracture.

Further finite element analyses of the four cask geometry/materials combinations were conducted to model a one-meter side drop onto a 152 mm diameter puncture pin. The puncture event was analyzed as a non-linear dynamic impact event. The power-law hardening constitutive model in PRONTO 3D was used for these computations. Additional mass was assigned to the cask ends to represent the impact limiters which were not specifically modeled. The pin contacted the cask at mid-span on the transverse center line. This location causes the maximum stress in the cask wall. In applying the stress-based and strain-based failure criteria described above, the resulting stress and strain combinations from these calculations were so low that failure from a drop onto a pin does not present a credible failure potential for any of these geometry and material combinations. The values are plotted on Figures 3 and 4 at a nominal value of 25 g and indicate the large factor of safety inherent to the DU for the one-meter punch condition.

DISCUSSION

Results from the analyses described above indicate that certain DU alloys have sufficient strength, ductility, and toughness to be considered for structural applications in transport casks, particularly true when cask design response to various accident conditions precludes through-wall yielding. The data are not extensive enough however, to act as the basis for qualifying a particular material in this regard. For the structural analysis calculations shown, the room temperature properties were used as the basis of the materials model. If similar calculations are to be performed to support a claim for structural credit of DU in a specific design, the applicable mechanical properties must be determined at rates and temperatures which match those of the worst loading conditions. Further, the finite element calculations should be conducted for the specific cask design which includes all relevant features, including: cask bottom end, cask closure end, impact limiters, etc.

The most obvious benefit of qualifying DU as a structural component in transport casks results from a reduction of the thickness of the overall structure, while maintaining the necessary structural integrity. This allows a reduced cask body mass and an increased spent-fuel payload potential. In those casks which use a particularly expensive material (e.g., stainless steel or titanium) the ability to partially or completely eliminate such material may lead to an important reduction in the cost of fabrication through lower cost for raw materials. In addition, there is a cost reduction associated with the increased ease of fabricating (forming, welding, inspecting, etc.) and assembling

thinner sections. For cask designs which approach dimensional and/or mass limitations, the qualification of DU as a positive contributor to the structural integrity (thereby reducing the requirement for other materials) may provide a significant advantage. Potential mass reduction in the cask without sacrificing payload may provide the necessary margin if the gross cask mass becomes a certification issue. For the current example (i.e., Case 1 vs. Case 2), the mass savings from the reduction in the thickness of the stainless steel amounts to ≅1550 kg. This is ≅10% of the overall cask mass (or ≅ 6.3% for the fully loaded cask with impact limiters), and may be of significance for an actual cask which is near the maximum allowable mass, with scant margin for contingencies such as tie-downs, skids, or support cradles.

In any event, the use of DU in cask design may be more prudent than the use of lead for shielding due to such factors as lead melting or lead slump (Ammerman, 1992) which may affect the integrity of the stainless steel containment.

The DU in both cask geometries is surrounded by two layers of stainless steel. Stainless steel offers corrosion resistance and decontamination advantages, and even when present in only thin sections (i.e., Case 2) has an important effect on the structural response. The highly ductile and tear-resistant stainless steel provides additional conservatism against brittle fracture by spreading any locally applied stresses thus acting as a barrier to brittle fracture propagation.

Heat transfer characteristics would be enhanced if the thickness of the stainless steel could be reduced. A further heat transfer benefit would be gained if one or more interfaces could be eliminated by removing a stainless steel layer in designs in which DU can assume structural responsibility.

Problems which must be addressed to pursue structural credit for DU in cask design are not insignificant, however. Foremost may be the inherent regulatory reluctance to the use of any material for cask containment which may fail in a brittle manner, no matter how remote that possibility. Second are the procedural issues related to ASME Code acceptance of DU for structural applications and the standardization of candidate DU alloys through ASTM. Finally, there are the fabrication issues related to construction of a cylindrical body of DU for containment. DU shields are constructed of semi-circular rings which, for structural application, may require welding or linkage by means of axial tie-rods. Concerns over the properties of the welded regions or the bending strength of the segmented DU layer require analysis.

CONCLUSIONS

Materials properties of a broad range of DU alloys have been measured. These mechanical properties form the basis for finite element calculations that suggest that certain DU alloys can be assigned a structural role in specific transport cask designs. The effect of gaining structural credit for the DU allows the use of stainless steel to be reduced. In this example, a thick layer of stainless steel was eliminated, which resulted in a direct mass reduction of > 6% for the fully loaded cask. This is considered highly significant due to potential weight problems in cask design and in the potential for increase in payload.

REFERENCES

Ammerman, D. J., Wellman, G. W., and Heinstein, M. W., *Comparison of Elastic and Inelastic Analyses*, Proceedings of PATRAM '92, The 10th International Symposium on the Packaging and Transportation of Radioactive Materials, September 13-18, Yokahama, Japan (1992).

Eckelmeyer, K.H., *Uranium and Uranium Alloys*, in Metals Handbook, Volume 2, 10th Edition, ASM International, Materials Park, OH, USA (1991).

Osborne, D., Koploy, M., and Pickering, L., *Analysis of the Non-Cylindrical GA-4 and GA-9 Spent Fuel Casks*, Proceedings of PATRAM '89, The 9th International Symposium on the Packaging and Transportation of Radioactive Materials, June 11-16, Oak Ridge National Laboratory, Washington, DC, USA (1989).

Regulatory Guide 7.6: Design Criteria for the Structural Analysis of Shipping Cask Containment Vessels, U.S. Nuclear Regulatory Commission, Revision 1 (1978).